STRATEGIES TOWARDS THE HYDROGENATION OF CO$_2$ AND CARBOXYLIC ACID DERIVATIVES

by

Nomaan Mohammed Rezayee

A dissertation submitted in partial fulfillment
of the requirements for the degree of
Doctor of Philosophy
(Chemistry)
in the University of Michigan
2017

Doctoral Committee:

Professor Melanie S. Sanford, Chair
Professor Adam J. Matzger
Professor Nathaniel K. Szymczak
Professor Levi T. Thompson

Nomaan M. Rezayee

nomaanr@umich.edu

ORCID iD: 0000-0002-9622-6324

for Mom, Dad, Sulaiman, and Miral

ACKNOWLEDGEMENTS

what it's like to leave everyone and everything you know in Afghanistan to come to the United States in search of a better life. Your hard work and sacrifices have not gone unnoticed and I aspire to continue to work to make you both proud. Sul and Miral, I can't possibly put into words what you both mean to me. Big bro, you might not remember this, but you introduced me to what a Ph.D is. I remember in 3rd grade, you instilled the desire in me to seek a higher education. You've cultivated my curiosity and always pushed me to work harder and to never settle. Miral, you are the best thing that has happened to our family. You've shaped me into the person I am today. You are an inspiration and one of the strongest people I've ever met. You have taught me to be patient, diligent, and resilient. Though you are my sister-in-law, you are more of an older sister to me. I would be nowhere near where I am today without both of your unconditional support. I'm blessed to essentially have a second set of parents. I know you both are always there for me. Lastly, I'd like to thank Anne Ravn for supporting me through this last year. You've been there for me since Autumn school clear through my Dissertation defense. I'm lucky to have you in my life.

TABLE OF CONTENTS

CHAPTER 1. INTRODUCTION

CHAPTER 2. SYSTEMATIC INVESTIGATIONS FOR THE IN SITU HYDROGENATION OF ESTERS USING AMINOPHOSPHINE LIGANDS

LIST OF FIGURES

LIST OF TABLES

ABSTRACT

Increasing energy demands have been met with added combustion of fossil fuels. The massive quantities of carbon dioxide (CO_2) given off as a byproduct of these processes have led to environmental and economical ramifications. Consequently, great emphasis has been placed in remediating CO_2 emissions through Carbon Capture and Sequestration (CSS) technologies. A limitation of CSS is that it fails to productively use CO_2. A complementary approach is to utilize CO_2 as a C-1 source. This dissertation discusses several strategies for the valorization of CO_2 to methanol (CH_3OH) stemming from fundamental hydrogenation studies.

Chapter 2 outlines a facile approach for the *in situ* generation of ester hydrogenation catalysts. Treatment of *cis*-dihydridotetrakis(triphenylphosphine)ruthenium(II) with two equivalents of an aminophosphine ligand led to a series of active hydrogenation catalysts. Unlike traditional methods, this simple approach circumvents the use of sub-stoichiometric alkoxide base. Systematic studies of ligand and base effects on the hydrogenation of the esters, are disclosed. Generally, diphenylphosphinoethylamine, was found to form the most active catalyst for the hydrogenation of alkyl and aryl esters with >80% yield for select substrates. However, sterically bulky ligands such as ditertbutylphosphinoethylamine were found to yield the highest activity towards formate ester hydrogenation. Mechanistic studies elucidated the unproductive, base-catalyzed decarbonylation of the formate ester with traditional alkoxide bases. Consequently, alternatives were investigated and K_3PO_4 was found to be a viable and compatible substitute.

The improved insight from formate ester hydrogenation guided our studies for the one-pot hydrogenation of CO_2 to CH_3OH. Application of these catalysts and conditions

to the cascade hydrogenation of CO_2 identified incompatibility with Lewis acids. Chapter 3 focuses on this limitation and discloses a new class of ester hydrogenation catalysts that are compatible with Lewis acids. Application of these half-sandwich ester hydrogenation catalysts to the Lewis acidic cascade system led up to 8 turnovers of CH_3OH in a single-pot batch reactor. Further studies implicate labile ligands as a source of inhibition.

In Chapter 4, a conceptually novel approach is disclosed, wherein CO_2 is captured using an amine scrubbing agent ($NHMe_2$) as dimethylammonium dimethylcarbamate (DMC) and subsequently hydrogenated in a single pot to >500 turnovers of CH_3OH. Up to 96% of CO_2 was converted to a mixture of CH_3OH and *N,N*-dimethylformamide (DMF). Mechanistic studies of the pathway identify DMF as a key intermediate. This strategy of carbon capture and hydrogenation provides a complementary approach to many industrial carbon capture methods.

In an effort to develop an earth-abundant process for the hydrogenation of CO_2 to CH_3OH, iron pincer catalysts were investigated as potential surrogates to the ruthenium catalysts used in Chapter 4. These iron-catalysts demonstrated high activity for the hydrogenation of amides yielding C–N bond scission products with high selectivity. DMF, a key intermediate in the CO_2 to CH_3OH pathway developed in Chapter 4, was hydrogenated to yield >1000 turnovers of CH_3OH and $HNMe_2$. Kinetic studies were performed to compare the activity of the earth abundant iron catalyst to ruthenium. Remarkably, under otherwise identical conditions, the iron and ruthenium catalysts displayed rates within a factor of 2. Application of these catalysts to the CO_2 capture and hydrogenation pathway is also discussed.

Finally, with the development of hydrogenation methodologies for C–N bond scission of formamides to yield CH_3OH, complementary methods have been disclosed to yield the methylated amine through deoxy-hydrogenation. Fundamental studies were undertaken in Chapter 6 to explore the origin of selectivity for the hydrogenation of amides (C–N vs. C–O bond cleavage). Through these fundamental studies, a proton responsive catalyst was identified that enabled selective access to each product (C–N or C–O bond cleavage).

CHAPTER 1: INTRODUCTION

This dissertation describes the development of strategies and, ultimately, catalysts for the hydrogenation of CO_2 and carboxylic acid derivatives. The intent of these investigations is to gain insight into fundamental hydrogenation principles. Initial studies honed on the development of effective ester hydrogenation catalysts and their subsequent adaptation for the cascade hydrogenation of CO_2 to CH_3OH through a formate ester intermediate (Chapters 2 and 3). Successive strategies employed a novel route for the one-pot CO_2 capture and hydrogenation to CH_3OH (Chapter 4). Further refinement into the hydrogenation of the key formamide intermediate sheds light into vital features of catalyst design (Chapter 5 and 6).

1.1 CO_2: The Stretch and Bends of Controversial Bonds

CO_2 can be produced from naturally occurring and anthropogenic processes.[1] Natural sources such as plant and animal respiration, volcanic eruptions, and thawing of permafrost have contributed in making CO_2 an essential component of Earth's atmosphere. Among N_2, O_2, Ar, and other gases, CO_2 composes less than 0.05% of the Earth's atmosphere.[1] Though seeming of benign consequence, the concentration of CO_2 plays an essential role in regulating environmental temperatures through the greenhouse effect.[1] This effect describes the insulation of infrared radiation emitted by the sun in the atmosphere. Aside from CO_2, many other gases have been identified to display this phenomenon in the Earth's atmosphere including water vapor, methane, ozone, nitrous oxide, and chlorofluorocarbons (CFCs).[1] Just as low levels of greenhouse gases would

lead to a detrimental cooling effect, elevated concentrations also result in adverse environmental conditions, namely climate change.

Modernization has placed a great demand on energy.[1] Readily accessible sources of energy have come in the form of fossil fuels. Upon combustion, the chemically stored energy can be harnessed as thermal and mechanical energy with concomitant evolution of CO_2 and H_2O (subsequent transformation can lead to other forms of energy). Due to the ubiquity of this process, the key anthropogenic source of CO_2 results from the combustion of fossil fuels.[2] This is most evident in the comparison of atmospheric CO_2 levels. Since the beginning of the industrial era, atmospheric concentrations of CO_2 have increased from an annual average of 280 ppm in the later 1700s to 401 ppm in 2015.[1] As such, CO_2 has become the iconic greenhouse gas and a key climate change contributor. Unfortunately, anthropogenic climate change in the U.S. has become marred in political controversy despite general acceptance in the global scientific community.
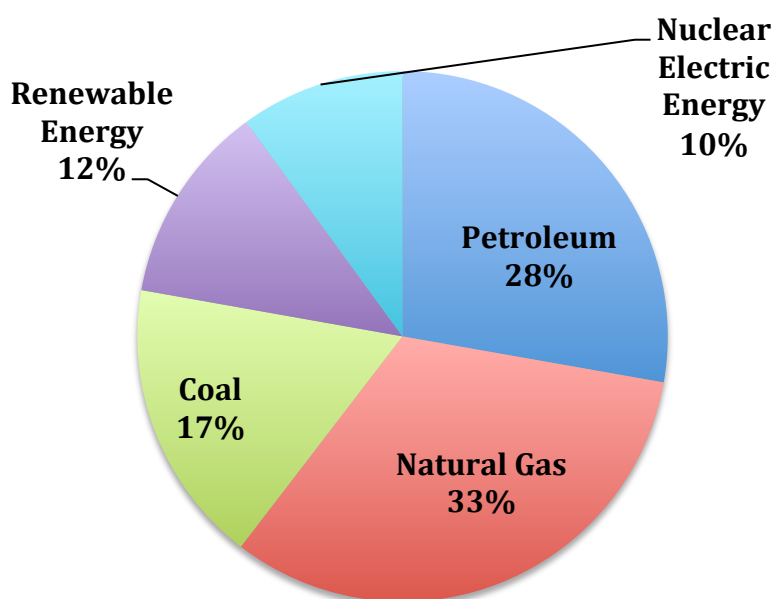
Source: U.S. Energy Information Administration (2016)

Figure 1.1. U.S. Energy Production by Source (2016).[1]

In the modern day, increased environmental awareness and improved technologies have led to 78% of the energy being derived from fossil fuels (Figure 1.1; coal, natural gas, and petroleum). This results in an annual emission of 5,157 million metric tons of CO_2. An analysis of energy usage by sector, shown in Figure 1.2, indicates the electrical power division as the major consumer of energy followed closely by the

industrial and transportation districts. Development of more efficient processes within these sectors will play a role in the mitigation of CO_2, however greater measures must be placed to reduce atmospheric CO_2 levels. Two leading methods to achieve this are: 1) CO_2 Capture and Sequestration (CCS), and 2) Carbon-neutral energy technologies.
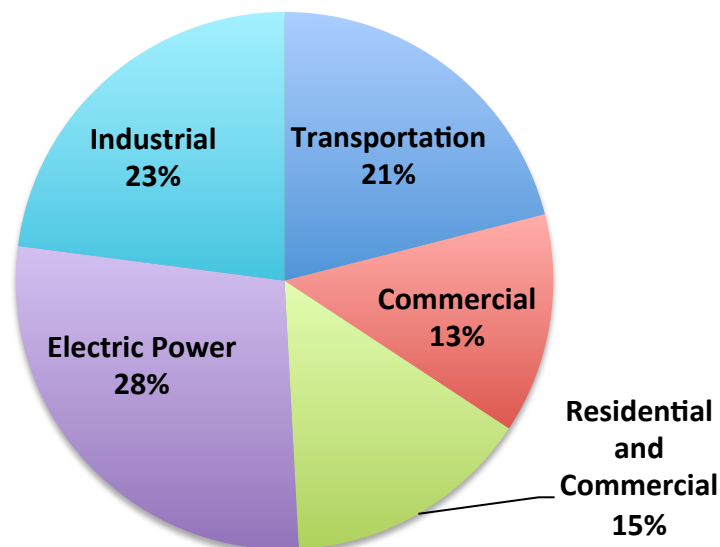
Source: U.S. Energy Information Administration (2016)

Figure 1.2. U.S. Energy Consumption by Sector (2016).[1]

1.2 Carbon Capture and Sequestration

As shown in Figure 1.1, the production of energy typically results from the combustion of fossil fuels. CCS is a process that is coupled with these large power plants in an effort to minimize the output of CO_2. In conjunction with the typical combustion of fossil fuels, procedures are implemented to chemically capture and store the CO_2 into geological formations.[2] Shown in Figure 1.3, after combustion, the resulting CO_2 is exposed to a solution of aqueous alkaline amines. These amines chemically trap CO_2 as the carbamate salt under ambient conditions. Following the capture, the solution is transferred to a heating chamber at 100–150 ºC to release the CO_2 and regenerate the alkaline amine solution. Finally, the released CO_2 is compressed and injected deep into brine-saturated geological formations, for permanent storage. Over time, the brine reacts with the sequestered CO_2 to form solid calcium carbonate.[2] This process adds several steps and requires an updated infrastructure to implement.
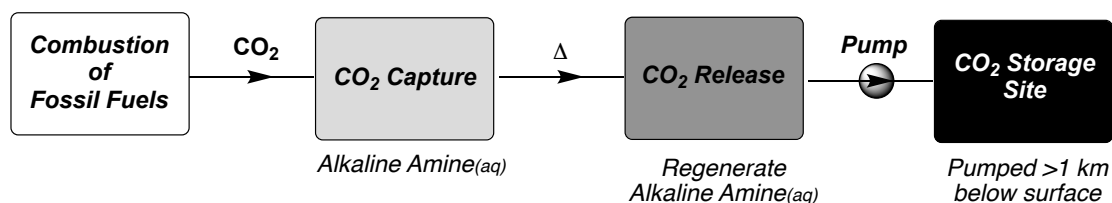
Figure 1.3. Carbon Capture and Sequestration process.

Though efficient for the removal of CO_2, critics of this strategy highlight the unfeasible cost of this process. Aside from added infrastructure, the amine scrubbers used consume roughly 20–30% of the energy produced by the power plant to capture and store its CO_2 emission.[2] A majority of this energy is expended to heat the aqueous carbamate solution to release CO_2. Despite the added costs, several CCS projects have been applied. Over a dozen CCS operations have been implemented as a profit-making process for enhanced oil-recovery. While the long-term geological effects remain to be studied, as long as fossil fuels remain as the main source of energy, some form of CCS must be implemented to combat climate change.

1.3 Conversion of CO_2

A major limitation of CCS is its failure to productively utilize CO_2. Due to its sheer abundance, CO_2 provides an economical C_1 feedstock. Fundamental studies have been conducted for the valorization of CO_2.[3] A key challenge associated with this strategy is the use of economically viable reagents. CO_2 is a thermodynamically stable compound necessitating the use of highly reactive reagents.[4]

Reduction of CO_2
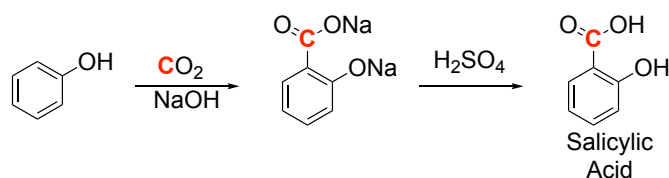
Figure 1.4. Production of salicylic acid through the Kolbe-Schmitt reaction.

Use of CO_2 as a C-1 source can lead to several different products. A seemingly simple transformation is the installation of a carboxylate group to yield carboxylic acids.[5] An industrial example of CO_2 usage is shown in Figure 1.4.[5] The production of salicylic acid, an exfoliator and precursor to aspirin, is manufactured from the

carboxylation of phenol using CO_2 and NaOH. Furthermore, chemical and electrochemical methods have also been developed for transition metal-catalyzed carboxylation of olefins and alkyl/aryl-halides (Figure 1.5).[5]
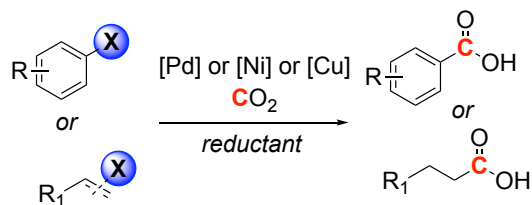
Figure 1.5. Carboxylation of alkyl- and aryl-halides.

Direct reduction of CO_2 has also been reported using highly reactive reducing agents such as silanes and boranes (Figure 1.6).[6, 7, 8, 9, 10, 11, 12, 13, 14, 15, 16, 17, 18] Depending on the stoichiometry and catalyst/reductant combination used, CO, formaldehyde, CH_3OH, or methane can be formed from the reduction of CO_2. These products are vital chemical feedstock for several applications such as fuel, solvents, polymers, pharmaceuticals etc. However, a major limitation of the methods shown in Figure 1.6 is the reductant used. Aside from their high cost, silanes and boranes are not derived from renewable resources. Moreover, the use of these stoichiometric reagents produces undesirable stoichiometric waste.
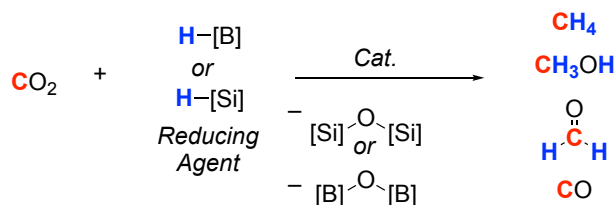
Figure 1.6. Reduction of CO_2 to a variety of products generating stoichiometric waste.

Heterogeneous Hydrogenation of CO_2
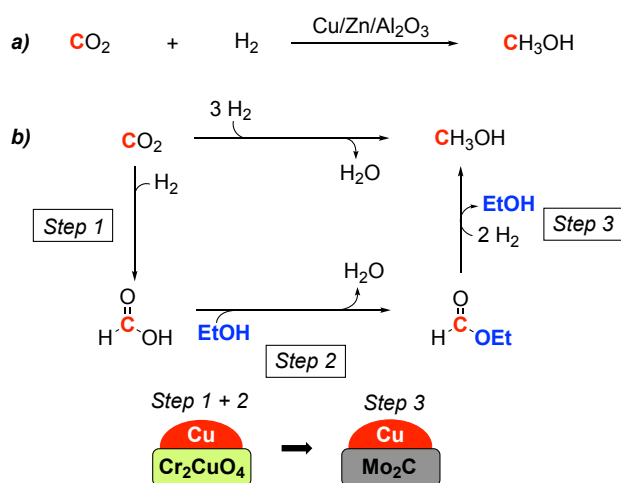
Figure 1.7. Heterogeneous hydrogenation of CO_2 to CH_3OH. *a)* CZA-catalyzed hydrogenation. *b)* Cascade hydrogenation.

Heterogeneous catalysts have been used for the hydrogenation of CO_2 to CH_3OH for many decades.[19] $Cu/Zn/Al_2O_3$ (CZA), shown in Figure 1.7a, has been industrially applied for the hydrogenation of CO_2 to CH_3OH. However, these catalysts operate at elevated temperatures (>200 °C) and necessitate high pressures of CO_2 and CH_3OH.[20] Furthermore, CZA was shown to be very sensitive to Lewis bases, such as those used for carbon capture.

Recently, a heterogeneous cascade process has been disclosed that operates through a similar pathway as the homogeneous catalysts described above (Figure 1.7b). The cooperative combination of Cu/Cr_2CuO_4 and Cu/Mo_2C provided a turnover frequency of $4.7 \times 10^{-4}\,s^{-1}$ under relatively mild conditions.[21]

Homogeneous Hydrogenation of CO_2

While heterogeneous catalysts are capable of hydrogenating CO_2 to CH_3OH, they typically require elevated temperatures and pressure. An attractive alternative is to use homogeneous catalysts that operate at lower temperature. Shown in Figure 1.8 is the hydrogenation of CO_2 to formate using the homogeneous catalysts **1** and **2**. These catalysts are among the most active yielding turnovers as high as 32,000 and 3,500,000, respectively.[22, 23] Furthermore, the addition of an alcohol or amine has been reported to

yield the corresponding formate ester/formamide. Several earth-abundant catalysts have also been developed to perform this transformation.[24, 25, 26]
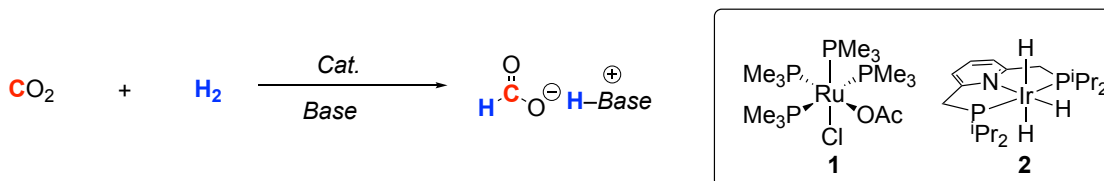
Figure 1.8. Homogeneous hydrogenation of CO_2 to formate.

Aside from the hydrogenation of CO_2 to products in the +2 oxidation state, further reduction using H_2 has been rare.[27] Despite great efforts in catalyst development, to date, only 4 examples of the homogeneous hydrogenation of CO_2 to CH_3OH have been reported. These processes typically employ the use of either cascade or tandem catalysis. Generally, CO_2 is hydrogenated to formic acid followed by an esterifcation or amidation. Subsequent hydrogenation yields CH_3OH. These strategies are more thoroughly described in Chapters 3 and 4.

1.4 Outlook on CO_2 Capture and Hydrogenation

Ideally, the valorization of CO_2 provides a carbon neutral and economically profitable approach for the mitigation of CO_2. Companies such as Audi and BASF have placed great effort in the development of processes for the utilization of CO_2. Unfortunately, even under circumstances where all manufactured products were made from CO_2, it would only consume about 20% of all the CO_2 currently produced.[2] Thus underscoring the need for the advancements of both CO_2 capture and CO_2 utilization technologies.

1.5 References

(1) U.S. Environmental Protection Agency. 2016. Climate change indicators in the United States, 2016. Fourth edition. EPA 430-R-16-004.

(2) Pelley, J. *ACS Central Science* **2015**, *1*, 412.

(3) Sakakura, T.; Choi, J.-C.; Yasuda, H. *Chem. Rev.* **2007**, *107*, 2365.

(4) Natte, K.; Neumann, H.; Beller, M.; Jagadeesh, R. V. *Angew. Chem. Int. Ed.* **2017**, *56*, 6384.

(5) Aresta, M.; Dibenedetto, A.; Angelini, A. *Chem. Rev.* **2014**, *114*, 1709.

(6) Eisenschmid, T. C.; Eisenberg, R. *Organometallics* **1989**, *8*, 1822.

(7) Riduan, S. N.; Zhang, Y.; Ying, J. Y. *Angew. Chem. Int. Ed.* **2009**, *48*, 3322.

(8) Chakraborty, S.; Zhang, J.; Krause, J. A.; Guan, H. *J. Am. Chem. Soc.* **2010**, *132*, 8872.

(9)Huang, F.; Lu, G.; Zhao, L.; Li, H.; Wang, Z. X. *J. Am. Chem. Soc.* **2010,** *132*, 12388.

(10) Huang, F.; Zhang, C.; Jiang, J.; Wang, Z.-X.; Guan, H. *Inorg. Chem.* **2011**, *50*, 3816.

(11) Riduan, S. N.; Ying, J. Y.; Zhang, Y. G. *ChemCatChem* **2013**, *5*, 1490.

(12) Wang, B. J.; Cao, Z. X. *R. Soc. Chem. Adv.* **2013**, *3*, 14007.

(13) Ménard, G.; Stephan, D. W. *J. Am. Chem. Soc.* **2010**, *132*, 1796.

(14) Stephan, D. W.; Erker, G. *Angew. Chem. Int. Ed.* **2010**, *49*, 46.

(15) Sgro, M. J.; Stephan, D. W. *Angew. Chem. Int. Ed.* **2012**, *51*, 11343.

(16) Zhu, J.; An, K. *Chem. Asian J.* **2013**, *8*, 3147.

(17) Courtemanche, M. A.; Legare, M. A.; Maron, L.; Fontaine, F. G. *J. Am. Chem. Soc.* **2013**, *135*, 9326.

(18) Anker, M. D.; Arrowsmith, M.; Bellham, P.; Hill, M. S.; Kociok-Kohn, G.; Liptrot, D. J.; Mahon, M. F.; Weetman, C. *Chem. Sci.* **2014**, *5*, 2826.

(19) Leitner, W. *Angew. Chem. Int. Ed.* **1995**, *34*, 2207.

(20) Grabow, L. C.; Mavrikakis, M. *ACS Catal.* **2011**, *1*, 365.

(21) Chen, Y.; Choi, S.; Thompson, L. T. *ACS Catal.* **2015**, *5*, 1717.

(22) Jessop, P. G. In *The Handbook of Homogeneous Hydrogenation*; Wiley-VCH Verlag GmbH: 2006, p 489.

(23) Tanaka, R.; Yamashita, M.; Nozaki, K. *J. Am. Chem. Soc.* **2009**, *131*, 14168.

(24) Mérel, D. S.; Do, M. L. T.; Gaillard, S.; Dupau, P.; Renaud, J.-L. *Coord. Chem. Rev.* **2015**, *288*, 50.

(25) Bertini, F.; Gorgas, N.; Stöger, B.; Peruzzini, M.; Veiros, L. F.; Kirchner, K.; Gonsalvi, L. *ACS Catal.* **2016**, 2889.

(26) Zhang, Y.; MacIntosh, A. D.; Wong, J. L.; Bielinski, E. A.; Williard, P. G.; Mercado, B. Q.; Hazari, N.; Bernskoetter, W. H. *Chem. Sci.* **2015**, *6*, 4291.

(27) Wang, W.-H.; Himeda, Y.; Muckerman, J. T.; Manbeck, G. F.; Fujita, E. *Chem. Rev.* **2015**, *115*, 12936.

CHAPTER 2: SYSTEMATIC INVESTIGATIONS FOR THE *IN SITU* HYDROGENATION OF ESTERS USING AMINOPHOSPHINE LIGANDS

The chemistry detailed in this chapter has been made possible with Dr. Chelsea A. Huff and Prof. Melanie S. Sanford. This chemistry was performed as a part of the Center for Enabling New Technologies Through Catalysis.

2.1 Introduction

Resonance-stabilized carbonyl containing compounds, such as esters, pose an intrinsic challenge towards reduction due to decreased electrophilicity of the carbonyl carbon.[1,2] Classical methodologies for reduction of these compounds typically necessitate the use of highly reactive stoichiometric reagents, such as lithium aluminum hydride (LAH), [3] yielding stoichiometric waste. Alternatively, a more synthetically and environmentally attractive route towards the reduction of esters is the transition metal-catalyzed hydrogenation.

Several homogeneous pre-catalysts have been reported to perform this transformation. These pre-catalysts typically employ polydentate ligands bearing phosphines and amines.[4,5,6] The basic site of the ligands shown in Figure 2.1a, is critical for catalytic activity and is proposed to play a bifunctional role *via* ligand-metal cooperativity.[7,8] First, it is intimately involved in the generation of the active catalyst through the heterolytic cleave of H_2 (Figure 2.1b), and second, shown in Figure 2.1c, is the

facilitation and activation of the carbonyl carbon by hydrogen bond directed hydride transfer.[9]
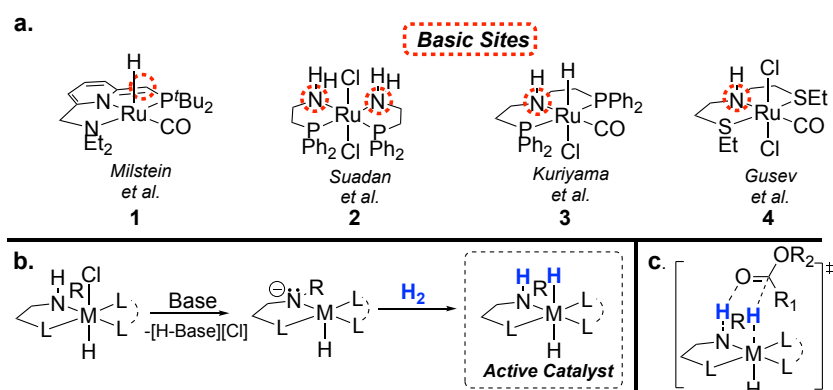
Figure 2.1. a.) Reported Ester Hydrogenation Precatalysts. b.) Plausible pathway for the Formation of the Active Catalyst. c.) Activation of Substrate by Ligand.

Saudan *et al.* have reported a suite of active ruthenium complexes that bear a pair of aminophosphine (N,P) ligands.[10] Among those evaluated, the *trans*-(N,P)$_2$RuCl$_2$ precatalyst, **2**, was found to be highly active for the hydrogenation of alkyl and aryl esters. However, two primary limitations restrict the synthetic utility of this class of pre-catalysts. First, the complexes surveyed are not commercially available and require synthesis under an inert atmosphere. Secondly, activation of **2** requires the addition of strong alkoxide bases to generate the active dihydride species.

This chapter describes our preliminary attempts to address these limitations through the base-free *in situ* generation of an active catalyst based on **2** (Figure 2.2c).[11] We find that this strategy enables the base-free hydrogenation of esters with a conveniently handled precatalyst. Our studies show that while base is not necessary, alkoxide bases do enhance catalyst activity for most substrates with the exception of formate esters. Mechanistic investigations reveal that alkoxide bases initiate the autocatalytic decomposition of formate esters (Figure 2.2a) and that this mode of substrate decomposition can be avoided using weaker inorganic bases.
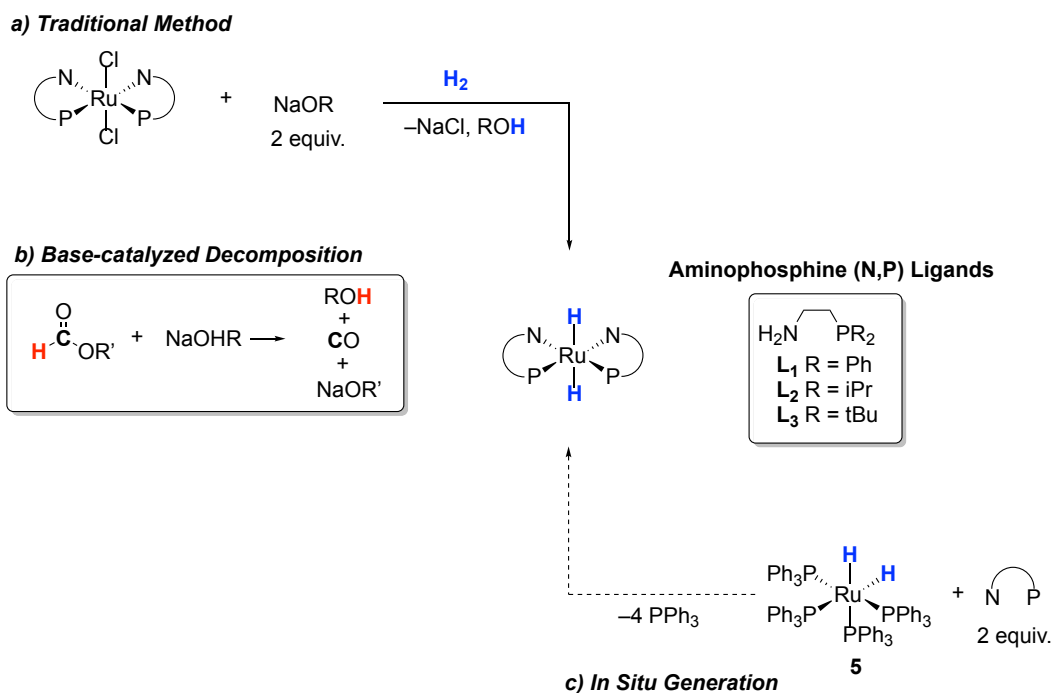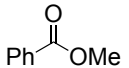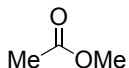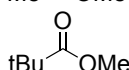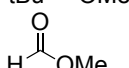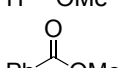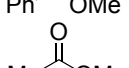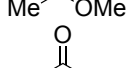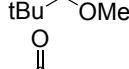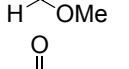
Figure 2.2. a.) Tradition Method for the Formation of the Active Catalyst. b.) Incompatibility Among Formate Esters and Alkoxide Bases. c.) *In Situ* Generation of Active Catalyst.

2.2 Results and Discussion

Base-free hydrogenation.

Our studies were inspired by the remarkable activity of **1** *in the absence of base*.[12] We hypothesized that similarly active catalysts of general structure shown in Figure 2.1c could be accessed without the need of base activators through the *in situ* ligation of a N,P ligand to a presynthesized Ru(II) dihydride, **5**. Importantly, this strategy allows for the rapid investigation of a wide range of ligands, as direct synthesis of the active catalyst is not necessary. We chose three ligands, **L₁₋₃**, with varying steric profiles to evaluate for the hydrogenation of a series of methyl esters listed in Table 2.1. We were delighted to observe modest conversion of several methyl esters over a 16 h period, providing an exciting proof of principle. The yield and turnover number (TON) for these reactions were based on the reduction of the carbonyl to the corresponding alcohol (e.g. benzyl alcohol for the reduction of methyl benzoate).

Table 2.1. *In Situ* Hydrogenation of Esters Under Base-free Conditions.[a]

$$\underset{\substack{2\ mmol}}{\overset{\displaystyle O}{R{\Large\|}OMe}} \xrightarrow[\substack{50\ bar\ H_2 \\ THF,\ 100\ ^\circ C \\ 16\ h}]{\substack{0.25\ mol\ \%\ \textbf{5} \\ 0.50\ mol\ \%\ Ligand}} \underset{\displaystyle R}{\overset{\displaystyle H\ H}{OH}} + MeOH$$

Entry	Substrate	Ligand	Yield [%]	TON
1	Ph—C(=O)—OMe	L₁	33	133
2	Me—C(=O)—OMe	L₁	29	114
3	tBu—C(=O)—OMe	L₁	32	127
4	H—C(=O)—OMe	L₁	<3	11
5	Ph—C(=O)—OMe	L₃	0	0
6	Me—C(=O)—OMe	L₃	0	0
7	tBu—C(=O)—OMe	L₃	0	0
8	H—C(=O)—OMe	L₃	22	87
9	H—C(=O)—OEt	L₃	19	76

[a]Conditions: Ester (2 mmol, 400 equiv.), **5** (5 μmol, 1 equiv.), **L₁₋₃** (10 μmol, 2 equiv.), H₂ (50 bar), THF (1 mL), 100 °C, 16 h.
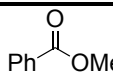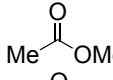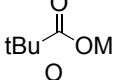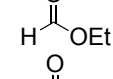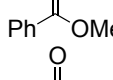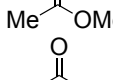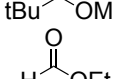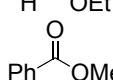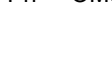
The active species formed from **L₁** yielded the most active hydrogenation catalyst for aryl and alkyl esters (entries 1-3). However, the hydrogenation of formate esters remained challenging (entry 4). The catalyst formed from **L₃** was surprisingly inactive for alkyl and aryl esters. We propose this may be due to the added sterics of the ᵗBu groups disrupting hydride transfer. To our surprise, however, the active catalyst formed from **L₃** yielded the highest activity for the reduction of methyl formate (entry 8). In order to insure the methanol detected resulted from hydrogenation of methyl formate and not hydrolysis, ethyl formate was also hydrogenated to yield methanol (entry 9). Interestingly, these data delineate from typical ester reduction trends in which either increased electrophilicity or sterics govern the competency of the catalyst.

Hydrogenation using NaOMe as base.

Typically sub-stoichiometric inorganic base is used to: form the active *trans*-dihydride Ru species from a dichloro precatalyst, facilitate and labilize intermediates, and serve as a proton shuttle to intermediates.[9,11,13] While we have developed a base-free approach, this *in situ* method also allows for the addition of base. To probe the effect of the inorganic base on the hydrogenation of esters, NaOMe was added in conjunction with our *in situ* method. A dramatic increase in the rate of hydrogenation was observed for all substrates but formate esters. Compared to the 16 h base-free conditions, reactions yielded nearly quantitative yields in just 1 h. For example, the hydrogenation of methyl benzoate with **L₁** increased from 33 % over a 16 h time period (Table 2.1, entry 1) to 98 % in 1 h (Table 2.2, entry 1). Enhanced rate and activity was seen for all substrates however no new reactivity was observed. This is consistent with the perceived role of base to facilitate the liberation of the alkoxide intermediates.

Table 2.2. *In Situ* Hydrogenation of Esters With NaOMe Added.[a]

Entry	Substrate	Ligand	Yield [%]	TON
1	Ph–C(=O)–OMe	L₁	96	382
2	Me–C(=O)–OMe	L₁	98	393
3	tBu–C(=O)–OMe	L₁	48	193
4	H–C(=O)–OEt	L₁	<3	5
5	Ph–C(=O)–OMe	L₂	53	213
6	Me–C(=O)–OMe	L₂	63	250
7	tBu–C(=O)–OMe	L₂	5	21
8	H–C(=O)–OEt	L₂	<3	9
9	Ph–C(=O)–OMe	L₃	0	0

10	Me–C(=O)–OMe	L_3	0	0
11	tBu–C(=O)–OMe	L_3	0	0
12	H–C(=O)–OEt	L_3	<3	5

With ligands L_1 and L_2, a general trend across the substrates was observed. Methyl acetate yielded the highest turnovers followed by methyl benzoate, methyl pivalate and finally, ethyl formate. Despite similar electrophilicity among methyl acetate and methyl pivalate, activity towards reduction varied dramatically. For example, shown in entries 2 and 3 using L_1, a 98% yield of the reduced methyl acetate product was observed compared to only 48% with methyl pivalate. We propose the decline in activity is a result the of bulky tBu group hampering the hydride transfer.

In order to examine the influence of the ligand on the reduction of these esters, we benchmarked each ligands activity to a single substrate. By assessing the activity of L_1, L_2, and L_3 towards the reduction of methyl benzoate, we observed a decrease in TON with the increase in the cone angle. This trend was also observed for hydrogenation of methyl acetate, and methyl pivalate. We hypothesize that the increased steric bulk limits the accessibility of the hydride to the substrate consequently decreasing the activity of the catalyst.
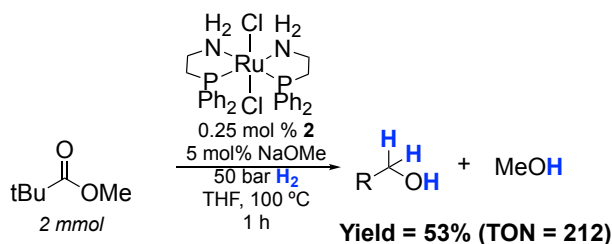
Figure 2.3. 2-Catalyzed Hydrogenation of Methyl Pivalate.

Notably, comparison of the *in situ* method (Table 2.2, entry 3) of hydrogenation to the traditional discrete complex (Figure 2.3) led to minimal difference in activity. Addition of four equivalents of PPh_3 does not appear to significantly inhibit the hydrogenation of these substrates. Furthermore, there was no evidence of catalyst deactivation by methanol as reported by Saudan *et al*.[10]

Studies of Formate Ester Decomposition

Given that formate esters are generally considered to be more electrophilic than alkyl or aryl esters, the low yielding hydrogenation of ethyl formate under basic conditions is particularly surprising. This observation is especially unexpected given that formate esters were well tolerated under base-free conditions. We hypothesized that the formate esters were undergoing a previously unrecognized autocatalytic decomposition in the presence of the base.

To test this hypothesis, we examined the compatibility of methyl formate with KOtBu, shown in Figure 2.4. Addition of KOtBu to a mixture of methyl formate in THF immediately resulted in gas evolution at room temperature. Analysis by ^{13}C NMR spectroscopy confirmed the formation of CO. Under catalytic conditions, we anticipate this incompatibility to lead to poor mass balance and catalyst poisoning.
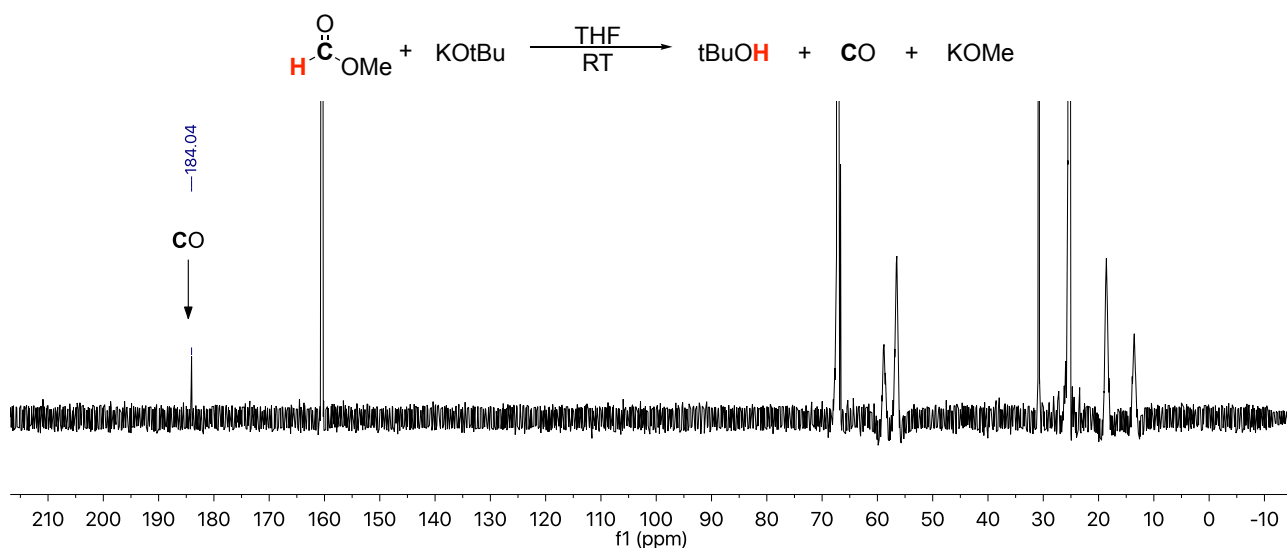
Figure 2.4. ^{13}C NMR of Methyl Formate Treated With KOtBu.

Hydrogenation with K₃PO₄ as base.

Our decomposition studies suggested that weaker bases may confer the same enhanced reactivity as traditional alkoxide bases. After a variety of different bases were evaluated for the reaction shown in Figure 2.5, K_3PO_4 was identified as a viable and compatible inorganic base under these conditions shown in Table 2.3.
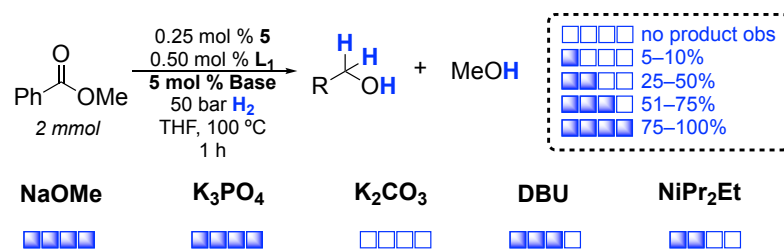
Figure 2.5. Base-screen for Methyl Benzoate Hydrogenation.

Table 2.3. *In Situ* Hydrogenation of Esters with K_3PO_4.[a]

Entry	Substrate	Ligand	Yield [%]	TON
1	Ph—C(=O)—OMe	L_1	80	320
2	Me—C(=O)—OMe	L_1	87	346
3	tBu—C(=O)—OMe	L_1	16	63
4	H—C(=O)—OEt	L_1	3	12
5	Ph—C(=O)—OMe	L_2	15	61
6	Me—C(=O)—OMe	L_2	35	141
7	tBu—C(=O)—OMe	L_2	<3	10
8	H—C(=O)—OEt	L_2	6	25
9	Ph—C(=O)—OMe	L_3	0	0
10	Me—C(=O)—OMe	L_3	0	0
11	tBu—C(=O)—OMe	L_3	0	0
12	H—C(=O)—OMe	L_3	16	63
12	H—C(=O)—OEt	L_3	20	79

[a]Conditions: Ester (2 mmol, 400 equiv.), **5** (5 μmol, 1 equiv.), **L$_{1-3}$** (10 μmol, 2 equiv.), K_3PO_4 (100 μmol, 20 equiv.), H_2 (50 bar), THF (1 mL), 100 °C, 1 h.

The trends identified previously with the use of NaOMe remain consistent with K_3PO_4, however, the reduction of formate esters can now be examined. Interestingly, **L$_3$**

(19%, 76 TON) yielded the highest activity towards the reduction of ethyl formate while L_1 demonstrated the lowest (Entry 4, 3 % Yield, 12 TON). From these data we can observe a trend opposite of the alkyl- and aryl- esters where the reduction of ethyl formate increased with cone angle. Furthermore, to our surprise, the addition of K_3PO_4 had no influence on the reduction of ethyl formate.

Competition Experiment.

In order to improve our understanding for the reduction of formate esters, we conducted a competition experiment in which methyl formate and methyl acetate were both subjected to the active catalyst at equal concentrations (Table 2.4).

Table 2.4. Competition Experiment Between Methyl Formate and Methyl Acetate.[a]
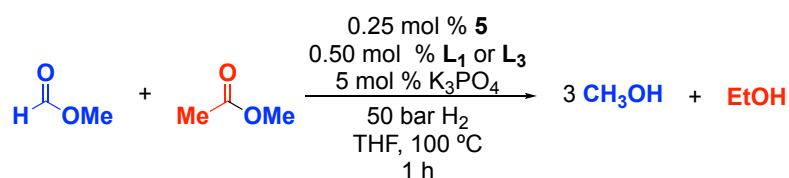
Entry	Ligand	CH$_3$OH Yield[a] [%]	TON[a]	EtOH Yield[b] [%]	TON[b]
1	L_1	3	10	0	0
2	L_3	23	93	0	0

[a]Conditions: Methyl formate (2 mmol, 400 equiv.), methyl acetate (2 mmol, 400 equiv.), **5** (5 μmol, 1 equiv.), L_1 or L_2 (10 μmol, 2 equiv.), K_3PO_4 (100 μmol, 20 equiv.), H$_2$ (50 bar), THF (1 mL), 100 °C, 1 h.

As shown in Table 2.4, ethanol was not detected in the reaction. This is somewhat surprising since methyl acetate was found to be a highly active substrate. Specifically in the case of entry 1, we have previously shown the efficient reduction of methyl acetate under similar conditions (Table 2.3, entry 2, 346 TON). These data suggest inhibition of the catalyst by methyl formate. Importantly, this study also suggests the preferential interaction of the active catalyst with methyl formate over methyl acetate. Furthermore entry 2 suggests that the active catalyst formed from using L_3 chemoselectively hydrogenates the formate ester. This is a rare example of chemoselectivity among esters.
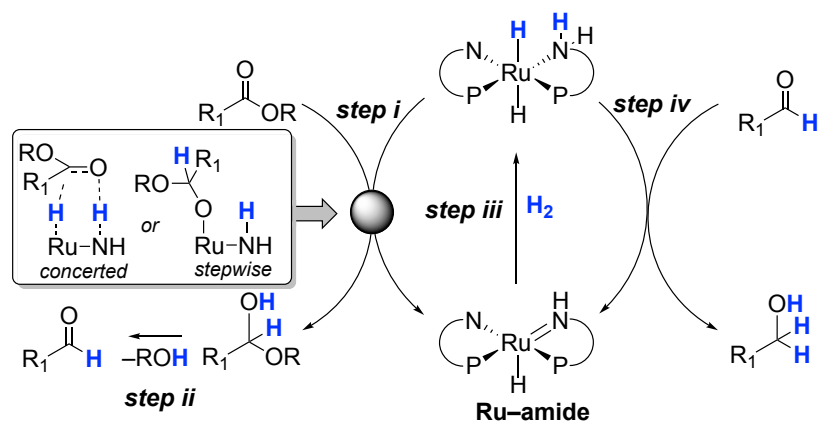
Figure 2.6. Plausible Pathway for the Hydrogenation of Esters.

Proposed catalytic cycle.

By analogy to traditional Noyori-type hydrogenations of carbonyl-containing substrates, a plausible catalytic cycle for the hydrogenation of esters to primary alcohols is proposed in Figure 2.6.[14] The initial step (step i) involves a ligand-assisted hydride transfer to the carbonyl carbon of the ester with subsequent formation of the hemiacetal and the ruthenium–amide species. This can occur via a concerted outer-sphere process or a step-wise inner sphere pathway. The resulting hemiacetal undergoes elimination to extrude an alcohol and aldehyde shown in step ii. Heterolytic cleavage of H_2 across the Ru–amide bond (step iii) regenerates the active hydrogenation species. Finally, in step iv, the resulting aldehyde is reduced to the corresponding primary alcohol. Step i of the proposed catalytic cycle and the Ru–amide species has been documented by Bergens *et al*. to form through a stepwise process.[9,13]

2.3 Conclusions

In this chapter, a novel *in situ* method for the hydrogenation of esters was disclosed. This process facilitated the systematically study of ligand effects and bases on the hydrogenation of esters. Generally, diphenylphosphinoethylamine, **L₁**, was found to form the most active catalyst for the hydrogenation of alkyl and aryl esters. However, sterically bulky ligands such as **L₃** were found to yield the highest activity towards formate esters. The active species formed from **L₃** and **5** was found to be chemoselective for formate esters. Furthermore, key incompatibilities among alkoxide bases and formate esters were identified ultimately leading to the identification of the compatible base K_3PO_4.

Chapter 2 divulges key findings that greatly influenced further worked described in the following chapters.

2.4 Experimental

General Procedures

All manipulations were carried out under a nitrogen atmosphere using standard Schlenk line or glove box techniques unless otherwise noted. All high-pressure reactions were carried out using a Parr Model 5000 Multiple Reactor system that includes six 45 mL vessels equipped with flat-gaskets and head mounting valves. The system was operated by a 4871 process controller and SpecView version 2.5 software. All pressures are reported from the SpecView interface at room temperature. NMR spectra were obtained on Varian VNMRs: 400 MHz (400 MHz for ^{1}H; 100 MHz for ^{13}C) or 700 MHz (700 MHz for ^{1}H; 176 MHz for ^{13}C). Chemical shifts are reported in parts per million (ppm) and are referenced to an internal standard. Unless otherwise noted, the NMR yields were based on the alcohol formed from carbonyl reduction and were quantified using benzene or DMF as an internal standard in Acetonitrile-d_3 (MeCN-d_3).

Reactor Descriptions

Each vessel used has an internal volume of 45 mL and is composed of a well (in which the solid and liquid reagents are charged) and a head, which contains various attachments as described below.

Reactors of type A variety are made of Hastelloy C, and the wells are 7.5 cm tall and 3 cm in diameter. The heads consist of a pressure transducer and two inlet/outlet valves that can connect to a Parr Model 5000 Multiple Reactor system described above, a safety release valve, and a well for a thermocouple (Figure 2.7).
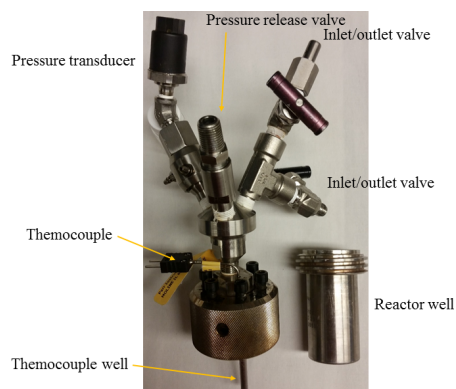
Figure 2.7. Picture of reactor type A with the parts of the reactor labeled.

Materials and Methods

The ligands **L₁₋₃** were purchased from Aldrich. Complexes **2**,[15] and **5**[16] were synthesized according to literature. Anhydrous K_2CO_3 (Acros, 99%), sublimed KOtBu (Oakwood, 99%), NaOMe (Fluka, 95%), $NaBH_4$ (Aldrich, Venpure SF), and anhydrous K_3PO_4 (Aldrich, 98%) were ground with a mortar and pestle before use. DBU (Acros, 95%), NEt_3 (Fisher), methyl benzoate (Acros), methyl acetate (Fisher), methyl pivalate (Oakwood), methyl formate (Acros) and ethyl formate (Acros) were dried and degassed prior to use. Ultra-high purity hydrogen (99.999%) was purchased from Metro Welding. All catalytic experiments were set up under an oxygen-free atmosphere in a glovebox. All catalytic experiments were conducted in triplicate, and the reported results represent an average of three runs (NMR yields). Tetrahydrofuran (THF), dichloromethane (DCM), toluene, and pentane, were purified using an Innovative Technologies (IT) solvent purification system consisting of a copper catalyst, activated alumina, and molecular sieves. Anhydrous ethanol (EtOH, Aldrich), dimethylsulfoxide-d_6 (DMSO-d_6, Cambridge Isotope Laboratories), benzene (C_6D_6, Cambridge Isotope Laboratories), Acetonitrile-d_3 (MeCN-d_3, Cambridge Isotope Laboratories) and chloroform (CDCl₃, Cambridge Isotope Laboratories) were purchased from the respective supplier and used as received.

I. General *In Situ* Hydrogenation Method: In a N_2-atmosphere dry box, **5** (5.8 mg, 5 μmol, 0.25 mol %) was dissolved in 1 mL THF and **L₁₋₃** (10 μmol, 0.5 mol %), and this solution was added to the metal well of a pressure vessel containing the appropriate quanitiy of base (100 μmol, 5 mol %, 20 equiv relative to Ru) and a micro magnetic stirbar (3 x 10 mm). The ester substrate (2.0 mmol, 400 equiv relative to Ru) was then added, and the vessel was sealed and removed from the dry box. The vessel was connected to

the Parr Multiple Reactor System, and the manifold was thoroughly purged with ultra-high purity hydrogen (99.999%). The vessel was then pressurized with 50 bar of ultra-high purity H_2, and the reaction was heated to 100 ºC with a stir rate of 800 RPM. The heating was conducted using Specview software. After 16 h or 1h of heating, the reaction mixture was allowed to cool to room temperature. The pressure vessel was placed in a –84 °C bath (ethyl acetate/LN_2) for 15 min and then carefully vented using a metering valve. Benzene or DMF (NMR standard) was added to the reaction mixture and analyzed by ^{1}H NMR Spectroscopy.

II. Hydrogenation of Methyl Pivalate with 2 (Figure 2.3): In a N_2-atmosphere dry box, **2** (2.8 mg, 5 μmol, 0.25 mol %) was dissolved in 1 mL THF, and this solution was added to the metal well of a pressure vessel containing NaOMe (5.4 mg, 100 μmol, 5 mol %, 20 equiv relative to Ru) and a micro magnetic stirbar (3 x 10 mm). The methyl pivalate (266 μL, 232.32 mg, 4.0 mmol, 400 equiv relative to Ru) was then added, and the vessel was sealed and removed from the dry box. The vessel was connected to the Parr Multiple Reactor System, and the manifold was thoroughly purged with ultra-high purity hydrogen (99.999%). The vessel was then pressurized with 50 bar of ultra-high purity H_2, and the reaction was heated to 100 ºC with a stir rate of 800 RPM. The heating was conducted using Specview software. After 1h of heating, the reaction mixture was allowed to cool to room temperature. The pressure vessel was placed in a –84 °C bath (ethyl acetate/LN_2) for 15 min and then carefully vented using a metering valve. DMF (NMR standard) was added to the reaction mixture and analyzed by ^{1}H NMR Spectroscopy.

III. Formate Ester Compatibility With KOtBu (Figure 2.4): In a N_2-atmosphere dry box, KOtBu (5 mg, 44.5 μmol) was added to an NMR tube charged with methyl formate (100 μL) and anhydrous THF (400 μL). The NMR tube was capped and shaken. The mixture was analyzed by ^{13}C NMR Spectroscopy.

IV. Competition Experiment (Table 2.4): In a N_2-atmosphere dry box, **5** (5.8 mg, 5 μmol, 0.25 mol %) was dissolved in 1 mL THF and **L$_1$** or **L$_2$** (10 μmol, 0.5 mol %), and this solution was added to the metal well of a pressure vessel containing K_3PO_4(21.2 mg, 100 μmol, 5 mol %, 20 equiv relative to Ru) and a micro magnetic stirbar (3 x 10 mm). Methyl

acetate (159 μL, 2.0 mmol, 400 equiv relative to Ru) and methyl formate (123 μL, 2.0 mmol, 400 equiv relative to Ru) was then added, and the vessel was sealed and removed from the dry box. The vessel was connected to the Parr Multiple Reactor System, and the manifold was thoroughly purged with ultra-high purity hydrogen (99.999%). The vessel was then pressurized with 50 bar of ultra-high purity H_2, and the reaction was heated to 100 °C with a stir rate of 800 RPM. The heating was conducted using Specview software. After 16 h or 1h of heating, the reaction mixture was allowed to cool to room temperature. The pressure vessel was placed in a –84 °C bath (ethyl acetate/LN_2) for 15 min and then carefully vented using a metering valve. Benzene or DMF (NMR standard) was added to the reaction mixture and analyzed by ^{1}H NMR Spectroscopy.

2.4 References

(1) Dub, P. A.; Ikariya, T. *ACS Catal.* **2012**, *2*, 1718.

(2) Saudan, L. A. In *Sustainable Catalysis*; John Wiley & Sons, Inc.: 2013, p 37.

(3) Brewster, T. P.; Rezayee, N. M.; Culakova, Z.; Sanford, M. S.; Goldberg, K. I. *ACS Catal.* **2016**, 3113.

(4) Kuriyama, W.; Matsumoto, T.; Ogata, O.; Ino, Y.; Aoki, K.; Tanaka, S.; Ishida, K.; Kobayashi, T.; Sayo, N.; Saito, T. *Org. Process Res. Dev.* **2012**, *16*, 166.

(5) Chakraborty, S.; Dai, H.; Bhattacharya, P.; Fairweather, N. T.; Gibson, M. S.; Krause, J. A.; Guan, H. *J. Am. Chem. Soc.* **2014**, *136*, 7869.

(6) Spasyuk, D.; Smith, S.; Gusev, D. G. *Angew. Chem. Int. Ed.* **2013**, *52*, 2538.

(7) Ohkuma, T.; Ooka, H.; Ikariya, T.; Noyori, R. *J. Am. Chem. Soc.* **1995**, *117*, 10417.

(8) Werkmeister, S.; Junge, K.; Wendt, B.; Alberico, E.; Jiao, H.; Baumann, W.; Junge, H.; Gallou, F.; Beller, M. *Angew. Chem. Int. Ed.* **2014**, *53*, 8722.

(9) John, J. M.; Bergens, S. H. *Angew. Chem. Int. Ed.* **2011**, *50*, 10377.

(10) Saudan, L. A.; Saudan, C. M.; Debieux, C.; Wyss, P. *Angew. Chem. Int. Ed.* **2007**, *46*, 7473.

(11) Zuo, W.; Prokopchuk, D. E.; Lough, A. J.; Morris, R. H. *ACS Catal.* **2015**, 301.

(12) Balaraman, E.; Gunanathan, C.; Zhang, J.; Shimon, L. J. W.; Milstein, D. *Nat. Chem.* **2011**, *3*, 609.

(13) John, J. M.; Takebayashi, S.; Dabral, N.; Miskolzie, M.; Bergens, S. H. *J. Am. Chem. Soc.* **2013**, *135*, 8578.

(14) Elangovan, S.; Wendt, B.; Topf, C.; Bachmann, S.; Scalone, M.; Spannenberg, A.; Jiao, H.; Baumann, W.; Junge, K.; Beller, M. *Adv. Synth. Catal.* **2016**, *358*, 820.

(15) Jia, W.; Chen, X.; Guo, R.; Sui-Seng, C.; Amoroso, D.; Lough, A. J.; Abdur-Rashid, K. *Dalton Trans.* **2009**, 8301.

(16) Young, R.; Wilkinson, G.; Komiya, S.; Yamamoto, A. In *Inorganic Syntheses*; John Wiley & Sons, Inc.: 1990, p 337.

CHAPTER 3: DEVELOPMENT OF LEWIS ACID TOLERANT ESTER HYDROGENATION CATALYSTS

The chemistry detailed in this chapter has been made possible with Dr. Chelsea A. Huff, Prof. Melanie S. Sanford, and in close collaboration with Prof. Karen I. Goldberg's lab at the University of Washington. This collaboration was performed in part of the Center for Enabling New Technologies Through Catalysis. Portions of this work have been published with Dr. Timothy P. Brewster, Zuzana Culakova, and Prof. Karen I. Goldberg.[1]

3.1 Introduction

Motivated by both environmental and economic concerns, a large amount of effort has been placed into identifying practical methods to reduce CO_2.[2] However, the reduction of CO_2 (4+) can lead to several distinct products (Figure 3.1), including carboxylic acids (3+),[3] formic acid (2+),[4, 5] formate esters (2+),[6] formamides (2+),[7] and methanol (2-).[8, 9, 10, 11, 12] A challenge associated with the reduction of CO_2 is the development of a practical and selective method. CO_2 is a relatively inert molecule deriving from its thermodynamic stability, and this necessitates the use of higher energy reductants. Classical reductants such as boranes[13] and silanes[14] have been used to perform these transformations. However, these reductants are often expensive and result in undesirable stoichiometric byproducts. An attractive alternative would be the use of dihydrogen (H_2) as the terminal reductant. H_2, in conjunction with a catalyst, provides access to an atom economical and potentially renewable route for the reduction of CO_2.[15] Efforts in our lab have placed emphasis in developing methods for the selective hydrogenation of CO_2 to methanol (CH_3OH).

CH$_3$OH is a commodity chemical that has an annual production exceeding 65 million tons and continues to grow by 4-5% per year.[16] Aside from the use of CH$_3$OH as a solvent in academic settings, industrially, CH$_3$OH is a precursor to bulk chemicals such as formaldehyde, acetic acid, methyl esters, methyl amines, methyl ethers, and lower olefins.16 Furthermore, methanol is considered an ideal energy storage material (high H$_2$ density) and has garnered interest as a drop-in liquid fuel alternative.[17] Current manufacturing processes derive from syngas (mixture of H$_2$ and carbon monoxide) in combination with various heterogeneous catalysts.[18] Alternative methods also derive from fossil fuel sources such as natural gas, and coal. While these methods have been thoroughly developed and optimized, producing CH$_3$OH from CO$_2$ and H$_2$ can potentially provide an avenue for a cheap, carbon-neutral process that is independent of fossil fuels.
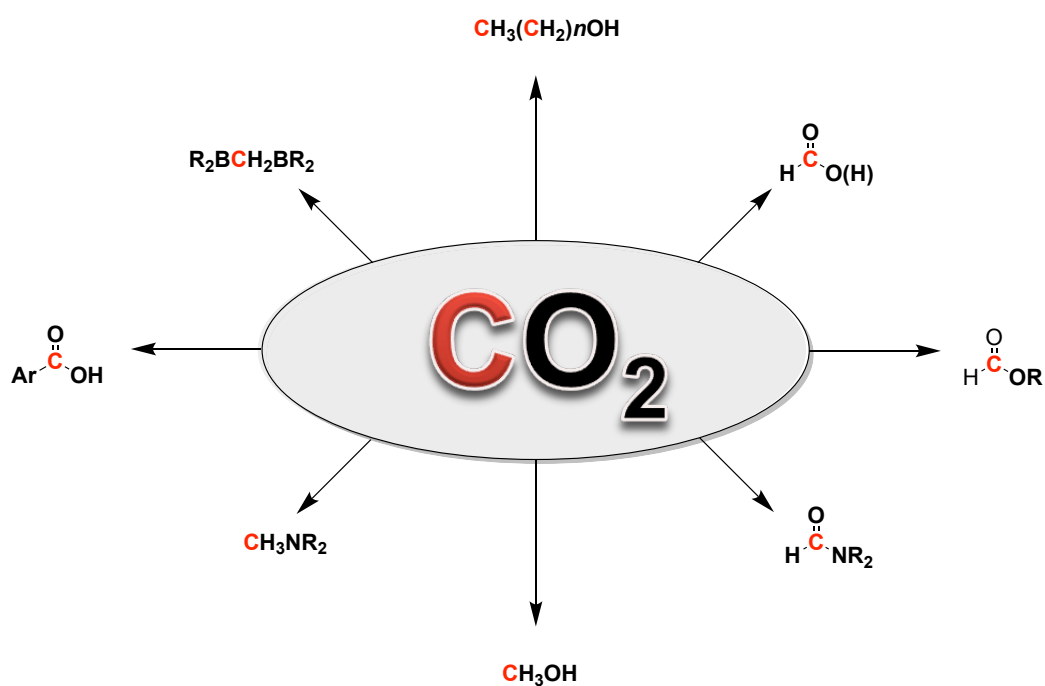
Figure 3.1. Survey of compounds derived from CO$_2$ reduction.

While the hydrogenation of CO$_2$ to CH$_3$OH remains a desirable transformation, homogeneous catalysts and/or methods to achieve this have been rare.[15] Conversely, the hydrogenation of CO$_2$ to compounds in the 2+ oxidation state (*e.g.* formate, formate ester, formamides, etc.) have been extensively studied.[19] This discrepancy in precedent has been attributed to the challenge associated with designing a single-site catalyst capable of a series of proton-coupled electron transfers on different C-1 intermediates. These challenges are further compounded by the entropically disfavorable nature of the hydrogenation reaction. Thermodynamically, the hydrogenation of CO$_2$ to

CH₃OH is feasible (Figure 3.2).[19] Despite the overall exergonic thermodynamics, limited examples for reduction of CO_2 to CH_3OH suggest a large activation barrier.

							ΔH° (kcal/mol)	ΔS° (cal/mol·K)	ΔG° (kcal/mol)
(*i*)	$CO_{2(g)}$	+	$H_{2(g)}$	⇌	$\text{HCOOH}_{(l)}$		−7.5	−51.6	7.8
(*ii*)	$CO_{2(g)}$	+	$H_{2(g)}$	⇌	$CH_3OH_{(l)}$ + $H_2O_{(l)}$		−31.3	−97.8	−2.3

Figure 3.2. *(i)* Thermodynamic data for the hydrogenation of CO_2 to formic acid under standard conditions. *(ii)* Thermodynamic data for the hydrogenation of CO_2 to CH_3OH under standard conditions.

Cascade CO_2 to CH_3OH Pathway

Various strategies have been employed to develop methods for the hydrogenation of CO_2 to CH_3OH. Heterogeneous catalysts are applied under flow conditions to generate two thousand tons of CH_3OH from CO_2 and H_2 (from electrolysis) annually at the George Olah plant.[16] However, elevated temperatures (>250 °C) are required, which hampers the yield due to entropic factors. In an effort to mitigate these high temperatures, homogeneous catalysts, which typically operate at lower temperatures, have recently been evaluated. Initial attempts at reducing CO_2 to CH_3OH using homogeneous catalysis led to exclusively 2+ products. In an effort to facilitate hydrogenation to CH_3OH, a new strategy was developed in our lab, leading to the seminal work on the homogeneous hydrogenation of CO_2.[8] Rather than applying a single catalyst to perform the 6e⁻ reduction, a combination of three catalysts in series were implemented to achieve a cascade sequence for the hydrogenation of CO_2 to CH_3OH.[8]
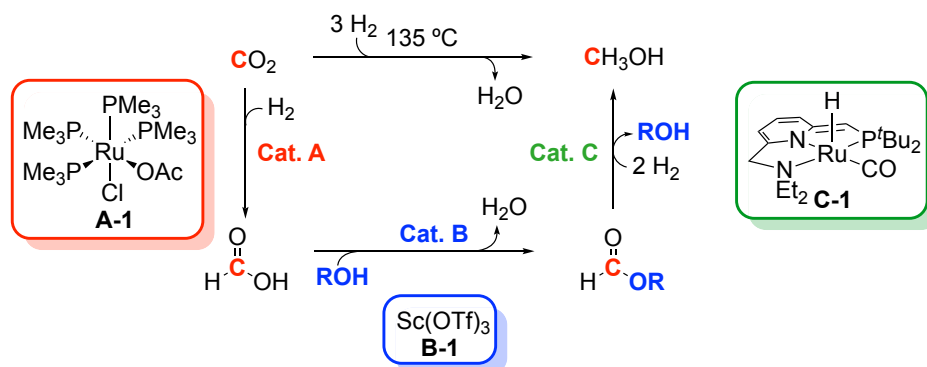
Figure 3.3. 1ˢᵗ Generation CO_2 to CH_3OH Cascade Pathway.

In this system, CO_2 is first hydrogenated to formic acid using **A-1** in an alcohol solvent. This initial step in thermodynamically unfavorable, but is driven forward by

subsequent esterification using **B-1** and solvent, to yield the corresponding formate ester. Finally, the formate ester is hydrogenated using **C-1** to produce CH_3OH and alcohol, seen in Figure 3.3. The cascade strategy is particularly advantageous because it allows for: 1) lower operating temperatures than heterogeneous catalysts, 2) formation of stable intermediates, 3) rational catalyst design, and 4) a modular framework such that each step of the process can be optimized independent of the others. Excitingly, this was the first reported homogeneous hydrogenation of CO_2 to CH_3OH yielding 3 turnovers of CH_3OH in a single batch reactor.
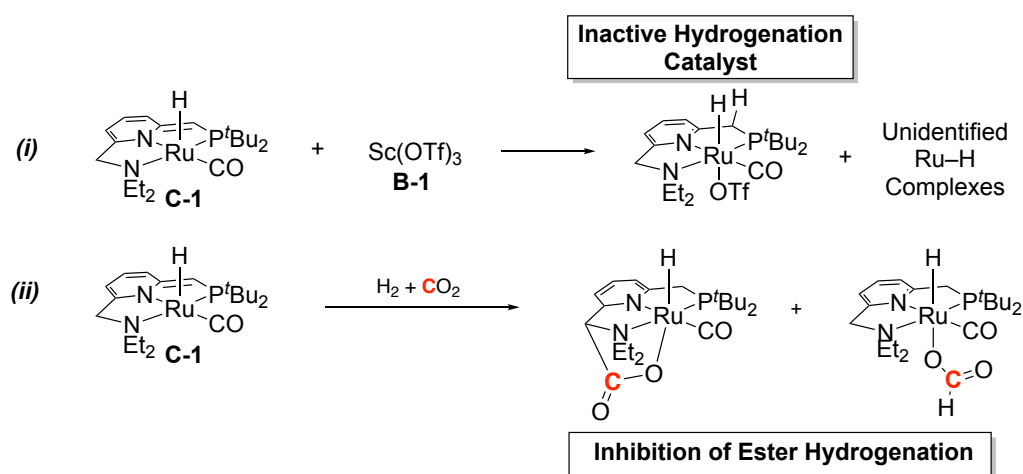
Figure 3.4. *(i)* Inhibition by $Sc(OTf)_3$ and advantageous H_2O. *(ii)* Inhibition by CO_2.

Upon closer examination, our group has found two limitations to the pathways outlined in Figure 3.4: The first is incompatibility between **B-1** and **C-1**, such that the activity of **C-1** is significantly hampered by **B-1**. This is due to the Lewis acidic **B-1** quenching the basic sites of **C-1**, effectively inhibiting the ligand-metal cooperativity of **C-1**. Indeed, separating **A-1** and **B-1** from **C-1** led to an increase in activity with up to 25 turnovers of CH_3OH. Secondly, an inherent challenge associated with this strategy is that CO_2 is in higher concentration and is more electrophilic than the intermediate formate ester. This leads to an unproductive, off-cycle formate bound catalyst **C-1** species.[20] Furthermore, CO_2 has been shown to directly interact with the ligand of **C-1** potentially leading to inhibition.[21] This inhibition is a consequence of the nucleophilic site of the ligand forming a reversible (at elevated temperatures) adduct with CO_2.
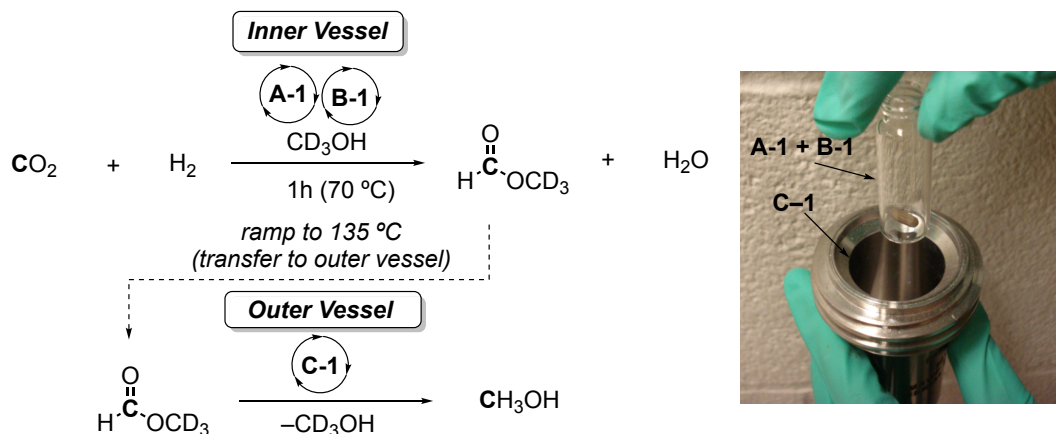
Figure 3.5. Two-pot Cascade Hydrogenation.

Klankermayer and Leitner reported a subsequent improvement to this strategy by using a single hydrogenation catalyst and a Brønsted acid for converting carbon dioxide to methanol (Figure 3.6).[9] This combination circumvented the challenge of compatibility and led to an overall improved system with turnovers as high as 221. It should be noted that their hydrogenation catalysts, Ru(Triphos), is unusual in that it is compatible with acids and does not depend on ligand-metal cooperativity for activity. Further investigation of Ru(Triphos) by Cantat *et al.* revealed that the catalyst, under similar conditions, could directly reduce formic acid to CH_3OH.[22] These results suggest an alternative pathway for the hydrogenation of CO_2 to CH_3OH that circumvents the formate ester intermediate. Indeed, detailed follow-up work by Klankermayer and Leitner revealed that an alcohol is not necessary to hydrogenate CO_2 to CH_3OH with Ru(Triphos), further supporting a pathway involving initial hydrogenation to formic acid and direct reduction to CH_3OH.[10] However, this does not exclude the possible formation of a formate ester intermediate during the progression of the reaction. While this set-up was found to afford up to 442 turnovers in a single batch reactor, further development necessitates the daunting task of designing and developing a superior single-site catalyst capable of performing 6 proton-coupled electron transfers.
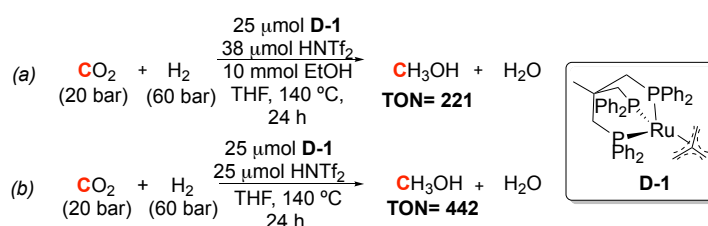
Figure 3.6. *(a)* Hydrogenation of CO_2 to CH_3OH with Ethanol additive. *(b)* Hydrogenation of CO_2 to CH_3OH *via* Formic Acid.

An attractive approach has been to revisit our initial work on the cascade system. While this strategy has the inherent challenge of compatibility, it has the potential to surpass the current state-of-the-art systems. Since our studies revealed inhibition of **C-1** by **B-1**, initial efforts focused on evaluating a series of ester hydrogenation catalysts as suitable substitutes.

3.2 Results and Discussion

Evaluation of Reported Homogeneous Ester Hydrogenation Catalysts
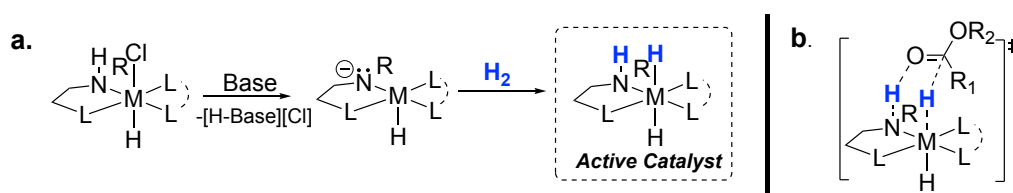
Figure 3.7. a. Deprotonation and heterolytic cleavage of H_2 to generate active catalyst. b. activation of substrate *via* hydrogen-bonding.

Several homogeneous pre-catalysts have been reported to perform this transformation (Figure 3.8).[23,24, 25] However, these pre-catalysts are typically utilized in conjunction with sub-stoichiometric alkoxide base to generate the active *trans*-dihydride species (Figure 3.7a).[26] However, alkoxide bases are incompatible with formate esters, leading to deprotonation of the aldehydic proton and decarbonylation (Figure 2.3). Evidence for carbon monoxide formation under these conditions was obtained via ^{13}C NMR spectroscopy. In an effort to minimize substrate decomposition and potential catalyst poisoning from carbon monoxide, alternative bases were evaluated. Potassium phosphate was found to a suitable surrogate. These catalysts were then evaluated for the hydrogenation of ethyl formate, a key intermediate, with potassium phosphate.
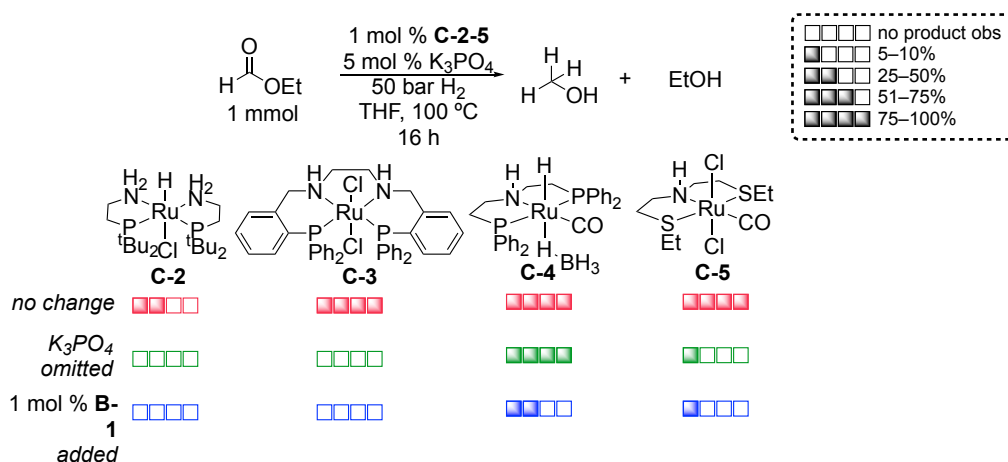
Figure 3.8. Ethyl formate hydrogenation with **C-2-5.**

Pre-catalysts **C-2**, and **C-3**, were found to be poor catalysts for the hydrogenation of ethyl formate. This is presumed to be due to incompatibility with CH_3OH,[27] as reported. In contrast, pre-catalysts **C-4** and **C-5**, bearing a carbon monoxide ligand along with a tridentate pincer ligand, afforded quantitative conversion to CH_3OH. The carbon monoxide ligand has been proposed to minimize decomposition by exogenous carbon monoxide formed during the course of the reaction.[28] In the absence of K_3PO_4, pre-catalyst **C-4** was found to remain active, quantitatively leading to CH_3OH, which is vital for application to the cascade pathway. However, the addition of the Lewis acidic **B-1**, $Sc(OTf)_3$, to the reaction mixture of **C-4** or **C-5** led to significant inhibition of the hydrogenation of ethyl formate.

Since modification of the ester hydrogenation catalysts did not lead to improved compatibility with the esterification catalyst ($Sc(OTf)_3$), a different approach was undertaken. Alternate esterification catalysts of varying Lewis acidities were investigated in Table 3.1. Zinc dichloride ($ZnCl_2$), yttrium triflate ($Y(OTf)_3$), and lanthanum triflate ($La(OTf)_3$) were found to yield comparable or improved reactivity to $Sc(OTf)_3$. However, like $Sc(OTf)_3$, these catalysts led to inhibition of the ester hydrogenation catalyst shown in Figure 3.9.

Table 3.1. Evaluation of Esterification Catalysts with the Hydrogenation of CO_2.[a]

Entry	Lewis Acid	Methyl Formate (TON)
1	**B-1**	25
2	$ZnCl_2$	35
3	$Y(OTf)_3$	35
4	$La(OTf)_3$	25

[a]10 bar CO_2, 30 bar H_2, 25 µmol **A-1,** 25 µmol Lewis Acid, 2 mL CH_3OH, 135 °C, 16 h. Yields represent an average of 3 trials
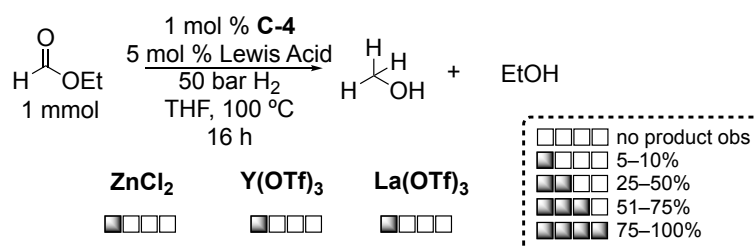
Figure 3.9. Evaluation of **C-4**-catalyzed Ethyl Formate Hydrogenation with Lewis Acids.

Identification of Lewis Acid Compatible General Hydrogenation Catalysts
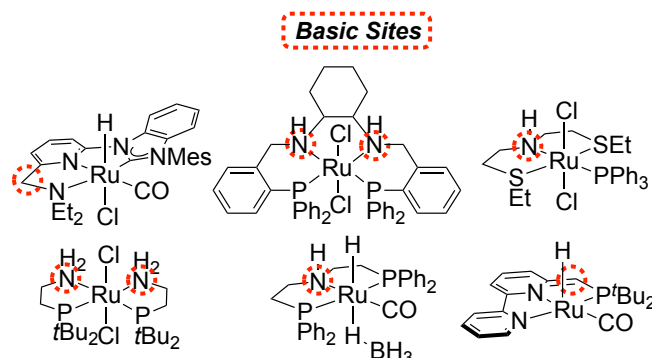
Figure 3.10. Survey of Ester Hydrogenation Catalysts with Basic Sites Identified.

A closer look into the catalyst design for ester hydrogenation sheds light into the nature of incompatibility. These pre-catalysts include a basic site (highlighted in red in Figure 3.10), which is either preformed using a strong alkoxide base (Milstein *et al.*)[29] or deprotonated *in situ*. This basic site is critical for catalytic hydrogenation and is proposed to play a bifunctional role in ligand-metal cooperativity.[30] First, it is intimately involved in the generation of the active catalyst by heterolytically cleaving H_2 (Figure 3.7a).[31] Second, as shown in Figure 3.7b, it activates the carbonyl carbon to hydride attack *via* directed hydrogen bonding.[32] As a consequence, many methodologies developed for the catalytic hydrogenolysis of esters are intolerant towards Brønsted and Lewis acids.

Rather than continued evaluation of a variety of ester hydrogenation pre-catalysts, reported carboxylic acid hydrogenation catalysts were investigated, as these require compatibility with acidic conditions. The Goldberg lab at the University of Washington has had extensive experience in the development of these hydrogenation catalysts.[33] After initial discussion, Dr. Tim Brewster provided several catalysts for initial evaluation. These seminal results initiated a collaboration between our two groups in order to develop a general ester hydrogenation catalyst that is compatible with Lewis acids.

Initial studies focused on the use of catalyst **C-6** for the hydrogenation of ethyl acetate. Heating a 2 mM solution of **C-6** in neat ethyl acetate under 60 bar H_2 for 18 h in the absence of any additives afforded ethanol with a TON of 363 ± 46 (Table 3.2). Catalysts **C-7** and **C-8**, which are sterically similar to **C-6**, but contain different 4,4'-substituents on the bipyridine ligands (Figure 3.11) were also examined. The highest turnover numbers were obtained using **C-6**, which contains electron-donating methoxy

substituents. An analogous trend was observed in the hydrogenation of carboxylic acids with this series of catalysts, suggesting that the reactions may be mechanistically similar.[33]
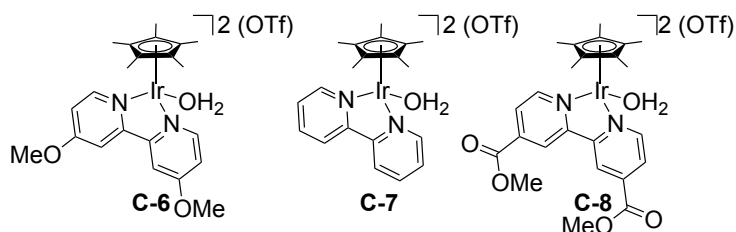
Figure 3.11. New Class of Ester Hydrogenation Catalysts.

Table 3.2. Evaluation of Catalysts for Ethyl Acetate Hydrogenation.[a]

Entry	Catalyst	TON
1	**C-6**	363 ± 46
2	**C-7**	309 ± 47
3	**C-8**	116 ± 7

[a]4 μmol catalyst in 2 mL ethyl acetate (20.4 mmol), 60 bar H_2, 18 h at 120 °C. Average of 3 trials with standard deviation. Theoretical Maximum TON under these conditions = 5100. Small amounts of diethyl ether (~10%) are also observed.

Mechanistic investigations of the hydrogenation of ethyl acetate with catalyst **C-6** were next undertaken. The reactions were conducted in neat ethyl acetate, and the % conversion and TON were determined after 18 h of heating at 120 °C. The rate of hydrogenation of ethyl acetate exhibits a linear dependence on catalyst concentration (Figure 3.12A), while saturation behavior is observed with respect to hydrogen pressure (Figure 3.12B). Saturation is reached at approximately 50 bar H_2, and a linear dependence on H_2 pressure is observed up to approximately 17 bar (Figure 3.12B). The dependence on substrate concentration was determined utilizing hexyl formate as the substrate (for ease in measurement of the concentrations of reactant and products) in 1,2-dimethoxyethane (DME). The reactions were run for 4 h at 100 °C under 60 bar H_2. Under these conditions, a linear dependence on substrate concentration was observed (Figure 3.12C).
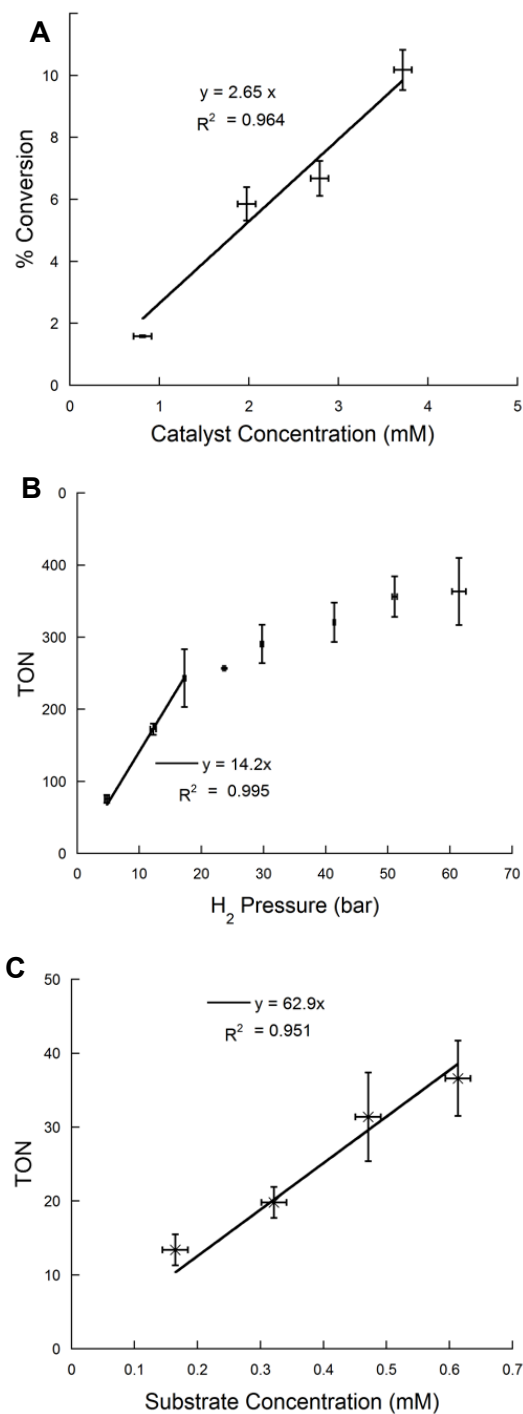
Figure 3.12. Dependence of **C-6**-catalyzed Hydrogenation of Esters on: **A.** Catalyst Concentration, **B.** H_2 Pressure, and **C.** Substrate Concentration. **A.** 2 mL (20.4 mmol), 30 bar H_2, 120 °C, 18h. **B.** 4 μmol of **C-6** in 2 mL Ethyl Acetate (20.4 mmol), 120 °C, 18h. **C.** Substrate: hexyl formate, 4 μmol of **C-6** in DME, 60 bar H_2, 100 °C, 4h.

These data are consistent with the ionic hydrogenation mechanism proposed in Figure 3.13. Initial addition of H_2 to the aquo complex Cp*Ir(bpy)(H$_2$O)$^{2+}$ reversibly forms the iridium dihydrogen complex (**I**). In neat reactions, the H_2 complex is then deprotonated

by substrate to generate the corresponding iridium hydride (**II**) along with the protonated ester. This hydride attacks the protonated substrate to generate a hemiacetal intermediate, which then eliminates one equivalent of alcohol to generate a transient aldehyde. The aldehyde is significantly more electrophilic than the parent ester and undergoes rapid hydrogenation to form the alcohol product. When the reactions are run in DME, the solvent likely acts as a proton shuttle to protonate the ester substrate prior to nucleophilic attack.
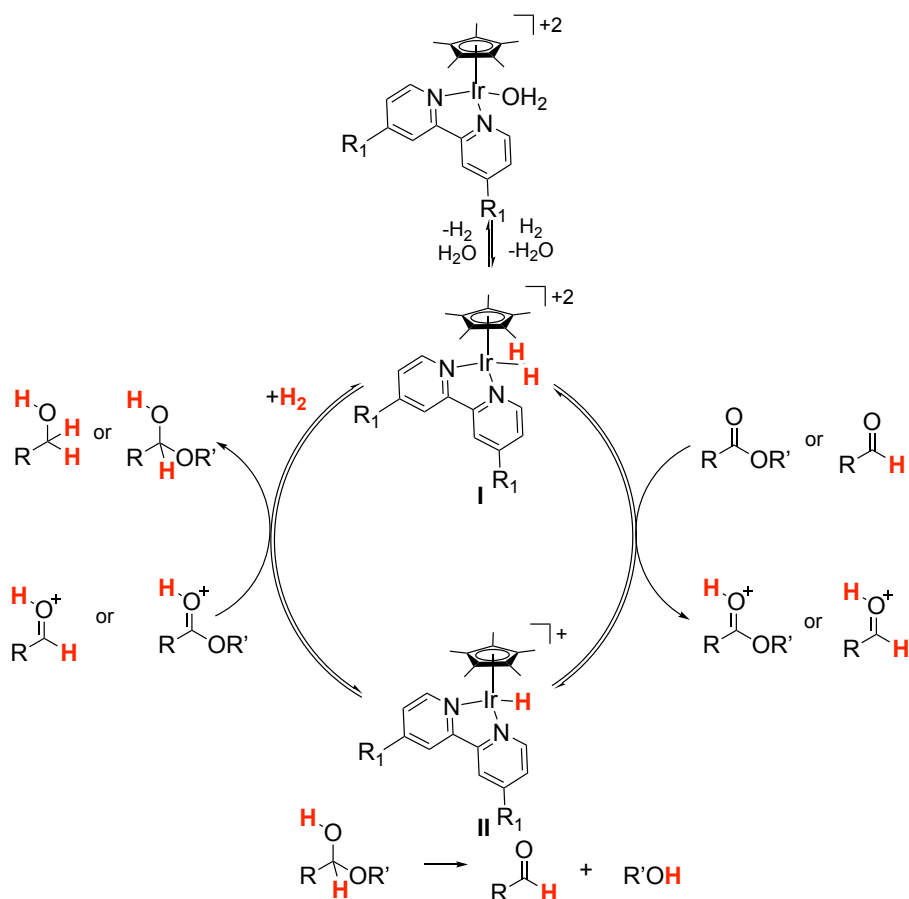
Figure 3.13. Proposed Mechanism for Ester Hydrogenation.

The 1st order dependence on H_2 pressure below 17 bar is consistent with turnover-limiting formation of the dihydrogen complex (**I**). The saturation observed at higher hydrogen pressures suggests a change to turnover-limiting hydride transfer. Notably, a similar mechanism (and change in turnover limiting step) was proposed previously for the **C-6**-catalyzed hydrogenation of carboxylic acids.

The scope of this transformation was next investigated. A series of esters and lactones were evaluated using catalyst **C-6** and 30 bar of H_2 in both neat substrate and in DME solvent. Quantitative analysis of TON was carried out using either ^{1}H NMR
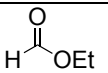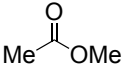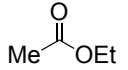
spectroscopy or gas chromatography. Under neat conditions, the reaction was examined in the presence and absence of the Lewis acid **B-1**. Based on the mechanism proposed in Figure 3.13, we hypothesized that a Lewis acid should accelerate the hydrogenation reaction by activating the ester substrate for nucleophilic attack, as seen previously in the hydrogenation of carboxylic acids catalyzed by **C-6.**

The hydrogenation of esters **E1**-**E3** was first conducted under neat conditions using 2 mM **C-6** and 30 bar H_2 at 100 °C for 16 h. In all cases, significant quantities of hydrogenation products were observed, with the TON ranging from 106 to 341 (Table 3.3). The addition of 20 mM **B-1** resulted in a marked improvement in TON. This effect is most dramatic with ethyl formate (**E1**), where the TON increases from 341 to 1317 upon the addition of **B-1**.

Table 3.3. Ester Hydrogenation Under Neat Conditions.[a]

Entry	Substrate	TON	TON with B-1[b]
E1	H–C(=O)–OEt	341 ± 25	1317 ± 37
E2	Me–C(=O)–OMe	305 ± 38	346 ± 28
E3	Me–C(=O)–OEt	106 ± 16	200 ± 23

[a]Average of at least 3 trials with standard deviation. 4 μmol of **C-6** in 2 mL substrate (**E1**, 24.8 mmol; **E2**, 24.4 mmol; **E3**, 20.4 mmol), 30 bar H_2, 100 °C, 16 h. [b]with 40 μmol **B-1**. Theoretical Maximum TON under these conditions = **E1**, 6200; **E2**, 6300; **E3**, 5100.

The hydrogenation of ester substrates **E1-E11** was next evaluated in DME (Table 3.4). These reactions were conducted using 1 mmol of substrate in 1 mL of solvent under 30 bar H_2 at 100 ºC for 16 h using 0.5 mol % of **C–6**. These conditions enabled a comparison between different substrates, since the reactions generally proceeded to moderate conversion. The reactivity was found to be strongly sensitive to the size of the carbonyl substituent. For example, ethyl formate afforded nearly quantitative conversion (TON = 173), while the more sterically encumbered substrate ethyl acetate showed much lower reactivity (TON = 27). Substrates bearing even larger carbonyl substituents such as *tert*-butyl and phenyl (**E4, E5**) afforded very low conversion under these conditions.

Hydride transfer is likely prohibitively slow in these systems due to the steric demands of the substrate.

Based on the high reactivity off ethyl formate, the reactions of a series of other formate esters were examined. Formate esters bearing alkyl ester substituents (**E6-E11**) afforded methanol with TONs ranging from 89-115. Interestingly, these reactions were relatively insensitive to the size and functionality of the alkoxy component of the ester substrate. For example, *t*-butylformate (**E8**) and the FMOC-protected amine **E11** underwent hydrogenation with comparable TON and no apparent deprotection of the amine functionality (115 and 107, respectively).
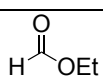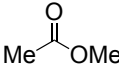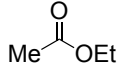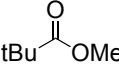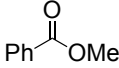
A variety of lactones (Figure 3.5) were also examined as substrates for hydrogenation with catalyst **C–6**. As shown in Figure 3.6, the initial product of lactone hydrogenation is a diol. However, in the presence of catalyst **C-6**, this diol intermediate undergoes rapid dehydration to afford cyclic ethers as the major product. This is noticeably different from the previously reported Ru/Triphos catalyst system for lactone hydrogenation, which affords the diol as the final product in the absence of added acid.[34]

The results for the hydrogenation of the 5-membered lactones γ-butyrolacone (**L1**) and γ-valerolactone (**L2**) are shown in Table 3.5. In neat lactone, the addition of Sc(OTf)$_3$ was found to enhance reactivity. In contrast, in DME solvent, the Lewis acid co-catalyst had minimal impact on TON. This may be due to competitive coordination of the Lewis acid to DME.

Table 3.4 Ester Hydrogenation in DME Solvent.[a]

$$R\overset{O}{\underset{OR'}{\|}} \xrightarrow[\substack{30 \text{ bar } H_2, \text{ DME} \\ 100 °C, 16 \text{ h}}]{0.5 \text{ mol\% C-6}} R\diagup OH + R'OH$$

1 mmol

Entry	Substrate	TON
E1	H‑C(=O)‑OEt	173 ± 30
E2	Me‑C(=O)‑OMe	24 ± 6
E3	Me‑C(=O)‑OEt	27 ± 5
E4	tBu‑C(=O)‑OMe	0 ± 0
E5	Ph‑C(=O)‑OMe	2 ± 1

E6	H–C(=O)–O–(CH2)5–Me	89 ± 5
E7	H–C(=O)–OiPr	94 ± 15
E8	H–C(=O)–OtBu	115 ± 5
E9	H–C(=O)–OBn	101 ± 12
E10	H–C(=O)–O–CH2–C6H4–OMe	114 ± 2
E11	H–C(=O)–O–CH2CH2–NH–C(=O)–O–CH2–Fmoc	107 ± 14[b]
E12	H–C(=O)–OEt	173 ± 30

[a]1 mmol substrate, 0.5 mol % **C-6**, 1 mL DME, 30 bar H_2, 100 ºC, 16 h. Yields represent an average of 3 trials ± standard deviation. [b]Reaction run in 2 mL DME. Average of 2 trials.

L1   **L2**   **L3**   **L4**   **L5**
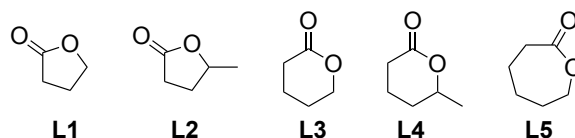
Figure 3.14. Lactone Substrate Scope.

.
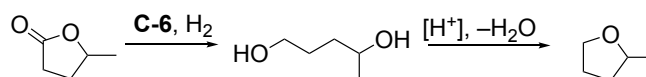
Figure 3.15. Hydrogenation of **L2**.

Table 3.5. Hydrogenation of **L1** and **L2** with **C-6**.[a]

			TON[a]	
Solvent	**Time (h)**	**Additive**	**L1**	**L2**
neat[b]	16	none	291 ± 7	76 ± 5
neat[b]	16	Sc(OTf)3[c]	410 ± 53	200 ± 19
neat[b]	65	none	487 ± 16	166 ± 54
DME[d]	16	none	33 ± 4	27 ± 5
DME[d]	16	Sc(OTf)3[e]	23 ± 6	19 ± 3
DME[d]	65	none	69 ± 4	78 ± 6

[a]TON for cyclic ether product, average of three trials, standard deviation in parentheses. [b]2 mL substrate, 4 mmol **C-6**, 30 bar H_2, 100 °C. [c]40 mmol Sc(OTf)3. [d]1 mmol substrate, 0.5 mol % **C-6**, 1 mL DME, 30 bar H_2, 100 ºC. [e]0.5 mol % Sc(OTf)3

The presence of the methyl group in **L2** led to significantly diminished TON in the neat reactions. This is consistent with the observation that steric bulk around the carbonyl component of the ester diminishes reactivity under neat conditions (**E2** vs **E3**, Table 3.3).

For the 6- and 7-membered ring lactones **L3-L5**, we observe rapid conversion of starting material to a mixture of products by NMR spectroscopy. However, only traces of the expected diol and cyclic ether products were detected (as confirmed by independent synthesis). Instead, ESI-MS revealed product masses consistent with the formation of oligoesters. This suggests that ring-opening polymerization occurs more rapidly than hydrogenation for these substrates.

These results demonstrate that **C-6** catalyzes the base-free hydrogenation of a variety of esters and lactones. This catalyst is particularly effective for the hydrogenation of formate esters, a substrate class that is an intermediate along the acid-assisted path for the CO_2 to methanol cascade system. Notably, the presence of the Lewis acid $Sc(OTf)_3$ was not detrimental to catalyst activity. Indeed, for reactions carried out in neat substrate, this additive led to enhanced TONs. Mechanistic investigations are consistent with a reaction pathway involving turnover-limiting hydride transfer at high pressures of H_2.

Application of Lewis Acid Tolerant Hydrogenation Catalyst to Cascade System
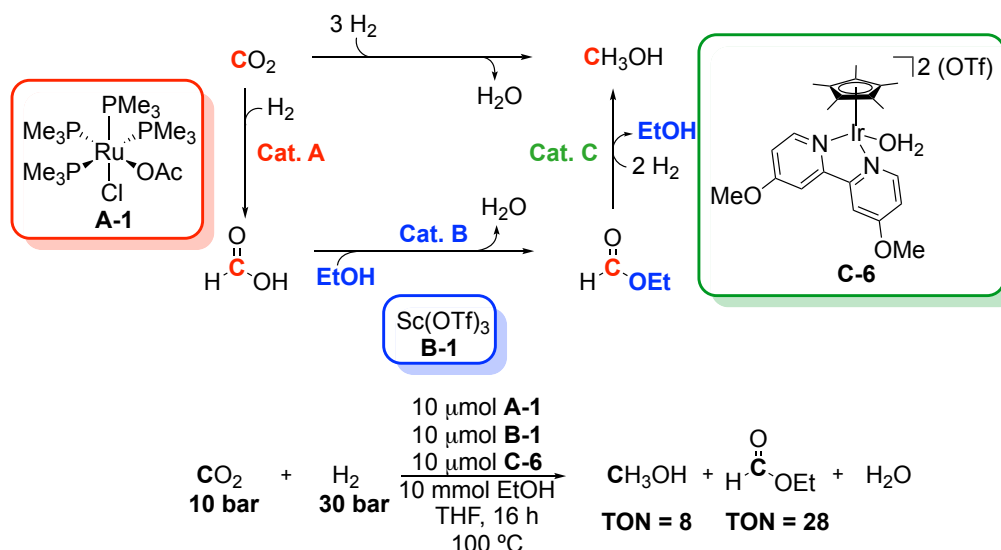
Figure 3.16. 2nd Generation Cascade Pathway.

The modular platform of the cascade system allows for the addition or substitution of catalysts throughout the three-component pathway. The identification of an

acid-tolerant ester hydrogenation catalyst allowed for the potential of an improved cascade process, since incompatibility among the Lewis acidic esterification catalyst and the previously used ester hydrogenation catalyst was found to be detrimental. Substituting catalyst **C-1** for **C-6** in the cascade system was thus investigated.

This next generation cascade pathway is shown in Figure 3.16. It should be noted that a key difference in this system compared to the previous iteration is the use of sub-stoichiometric ethanol in tetrahydrofuran (THF) as solvent. This would lead to an ethyl formate intermediate. These changes were made to solubilize all three components of the system as well as for the unambiguous analysis of the hydrogenation of CO_2 to CH_3OH. Application of the newly identified catalyst led to only modest improvement in the yield of CH_3OH. The quantity of ethyl formate remaining suggested challenges associated with ester hydrogenation. While encouraged by the increased yield, the marginal improvement despite increased compatibility was surprising.

Table 3.6. Systematic Hydrogenation of Ethyl Formate With **C-6** Under Cascade Conditions.[a]

$$ \underset{\text{1 mmol}}{\underset{\text{H}}{\overset{\text{O}}{\|}}\text{OEt}} \quad \xrightarrow[\substack{\text{30 bar H}_2\text{, THF} \\ \text{100 °C, 16 h}}]{\text{1 mol\% \textbf{C-6}}} \quad CH_3OH \quad + \quad EtOH $$
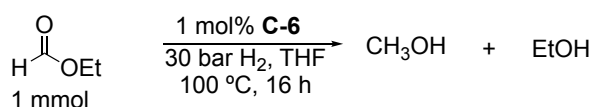
Entry	Conditions	CH$_3$OH (TON)
1	Standard	100
2	EtOH, 10 bar CO$_2$, 30 bar H$_2$	24
3	**B-1**, EtOH, 10 bar CO$_2$, 30 bar H$_2$	65
4	**A-1**, **B-1**, EtOH, 10 bar CO$_2$, 30 bar H$_2$	8
5	NBu$_4$Cl, **B-1**, 10 bar CO$_2$, 30 bar H$_2$	0
6	PPh$_3$, **B-1**, 10 bar CO$_2$, 30 bar H$_2$	0
7	**A-1**, AgOTf, **B-1**, 10 bar CO$_2$, 30 bar H$_2$	0

[a]1 mmol substrate, 0.5 mol % **C-6**, 1 mL THF, 30 bar H$_2$, 100 °C, 16 h. Yields represent an average of 3 trials

To better understand the limitations of the 2nd generation ester hydrogenation catalyst, a systematic investigation of the hydrogenation of ethyl formate by **C-6** was undertaken. In this study, shown in Table 3.6, hydrogenation of ethyl formate in THF led quantitatively to CH_3OH. However, the addition of 10 bar CO_2 significantly inhibited this reaction, leading to only a 24 % yield (24 turnovers). It should be noted that these values were determined at the conclusion of 16-hour period. While cursory evaluation suggests only a 76% inhibition, the rate of hydrogenation is more dramatically decreased since the

reaction goes to completion in just a few hours in the absence of CO_2. Presumably, **C-6** is inhibited by an off-cycle formate bound species similar to **C-1**. This reversible off-cycle species has been characterized in several CO_2-containing reactions. Strategies applied to mitigate this inhibition have been to promote the dissociation of the formate species either thermally or by the addition of Lewis acids. However, in the current system, the use of elevated temperature (>120 °C) led to diminished yields, suggesting thermal decomposition. Fortunately, **C-6** is compatible with Lewis acids, and the esterification catalyst, **B-1**, appears to be sufficiently acidic to promote CO_2 dissociation, resulting in a yield of 65% (entry 3). These reactions suggest that these components were compatible with **C-6** within the cascade system. However, the addition of **A-1**, led to diminished yields of methanol. It should be noted that under these conditions more than one mmol of ethyl formate was recovered due to the hydrogenation and subsequent esterification by catalyst **A-1** and **B-1**. These results suggest that the hydrogenation of the ester remains as a key challenge of the cascade system.

Despite the improved compatibility of the catalyst **C-6** and catalyst **B-1**, the cascade system had shown only a marginal improvement. The systematic compatibility study performed in Table 3.6 identified new incompatibility issues, this time between catalysts **A-1** and **C-6**. These incompatibilities may arise from **C-6**'s sensitivity towards Lewis bases. Indeed, the addition of 1 equivalent of chloride or PPh_3 relative to **C-6**, leads to diminished yields of CH_3OH (entries 5 and 6). The postulated nature of this incompatibility arises from the substitution of the labile aqua ligand preventing the formation of the H_2 adduct shown in Figure 3.13. Treatment of catalyst **A-1** with AgOTf to abstract the Cl ligand *in situ* and subsequent addition to a mixture of **C-6**, H_2, and ethyl formate did not lead to improved yields, suggesting inhibition by PMe_3 (entry 7).
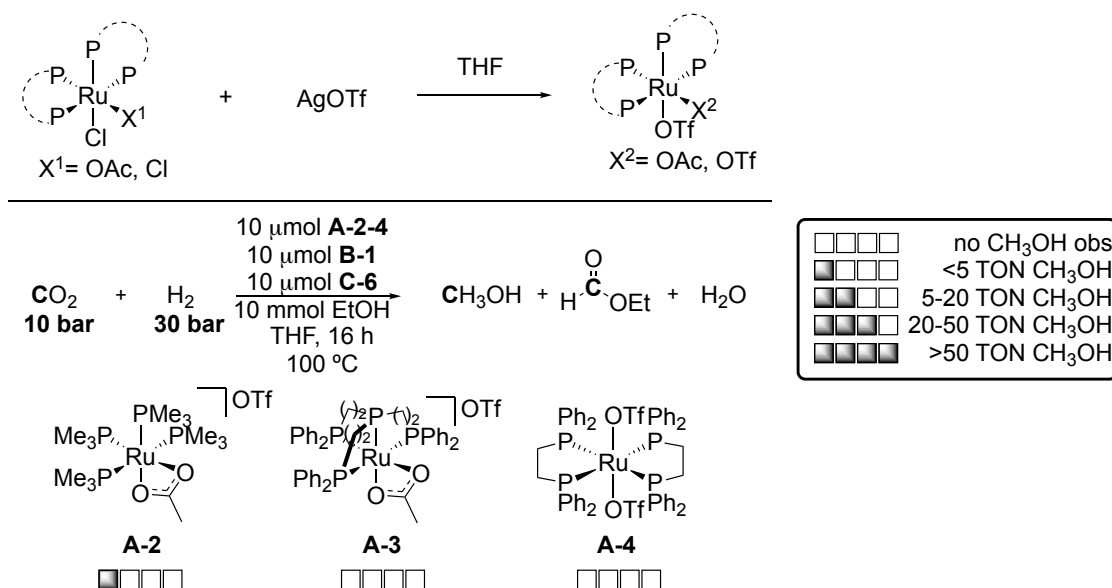
Figure 3.17. Halide Abstraction and Application to Cascade CO_2 Hydrogenation.

In order to minimize the poisoning of **C-6** by labile monodentate ligands, multidentate phosphine ligands were evaluated as a means of minimizing substitution by the chelation effect. Alternative catalysts bearing either bidentate or tridentate ligands were evaluated in the cascade pathway, shown in Figure 3.17. These catalysts (**A-2**-**A-4**) also avoided the use of the Cl ligand. While these catalysts were reported to be active for CO_2 hydrogenation, they did not work in cooperation with **B-1** and **C-6** to hydrogenate CO_2 to CH_3OH.

Table 3.7. Cascade Hydrogenation of CO_2 to CH_3OH at 100 ºC.[a]

Entry	Conditions	CH₃OH (TON)
1	Standard	81
2	Omission of **B-1** and **C-6**	trace
3	Omission of **C-6**	124

[a]10 bar CO₂, 30 bar H₂, 25 μmol **D-1,** 25 μmol HNTf₂, 25 μmol **B-1**, 25 μmol **C-6**, 10 mmol EtOH, 1.5 mL THF, 100 ºC, 16 h. Yields represent an average of 3 trials

Finally, in Table 3.7, the Ru(Triphos)(TMM) (**D-1**) catalyst developed by Klankermayer and Leitner was evaluated as a potential catalyst A. While Ru(Triphos) has been shown to independently hydrogenate CO_2 to CH_3OH, at low temperatures (100 ºC)

CO_2 is only hydrogenated to the formate ester. Application of Ru(Triphos)(TMM) (**D-1**) to the developed cascade system with **B-1** and **C-6**, led to 81 turnovers of CH_3OH. While exciting, experiments omitting **C-6** elucidate cooperation only between **D-1** and **B-1** (Table 3.7, Entry 3). In this case, **B-1** both facilitates esterification while also activating the formate ester towards hydrogenation. These results mark the lowest temperatures for the hydrogenation of CO_2 to CH_3OH.

3.3 Conclusions

This chapter describes the challenges and strategies employed to hydrogenate CO_2 to CH_3OH through an ester cascade system. These studies have identified several key challenges regarding reaction components that inhibit ester hydrogenation catalysts. The original ester hydrogenation catalyst (**C-1**) was incompatible with Lewis acids. This provides an inherent challenge, as conventional ester hydrogenation catalysts operate using ligand-metal cooperativity, thereby necessitating a Lewis basic site. This chapter discusses a new class of ester hydrogenation catalysts. These half-sandwich complexes are compatible with Lewis acids and operate *via* an alternative ionic hydrogenation mechanism. A thorough evaluation of substrates is reported, highlighting advantages and limitations. Furthermore, the optimal ester hydrogenation catalyst, **C-6**, was applied to the cascade system. However, despite improved compatibility with the esterification catalyst, only a modest improvement in overall yield of CH_3OH was observed. Through a systematic evaluation of **C-6**, incompatibility with halides and labile ligands was identified as the source of poor conversion. Attempts to circumvent these challenges with alternative catalysts proved unsuccessful. However, these studies provided enhanced insight into the key features necessary for an improved catalyst. Future work both in the Sanford lab and the Goldberg lab will focus on the development and identification of new catalysts that will overcome these challenges.

3.4 Experimental

General Procedures

All manipulations were carried out under a nitrogen atmosphere using standard Schlenk line or glove box techniques unless otherwise noted. All high-pressure reactions were carried out using a Parr Model 5000 Multiple Reactor system that includes

six 45 mL vessels equipped with flat-gaskets and head mounting valves. The system was operated by a 4871 process controller and SpecView version 2.5 software. All pressures are reported from the SpecView interface at room temperature. NMR spectra were obtained on Varian VNMRs: 400 MHz (400 MHz for ^{1}H; 100 MHz for ^{13}C) or 700 MHz (700 MHz for ^{1}H; 176 MHz for ^{13}C). Chemical shifts are reported in parts per million (ppm) and are referenced to an internal standard. Unless otherwise noted, the NMR yields with formamide substrates were based on methanol (δ = 3.16 ppm, T_1 = 7.2 s) and were quantified using 1,3,5-trimethoxybenzene (δ = 6.02 ppm, T_1 = 2.8 s) as an internal standard in dimethylsulfoxide-d_6 (DMSO-d_6). For each NMR experiment, 4 scans were collected, a 35 s relaxation delay was used, and a pulse angle of 90° was applied.

Materials and Methods

Catalysts **A-1**[35], **A-2**,[36] **A-3**,[37] **A-4**,[38] **C-2**,[39] **C-3**,[40] **C-4**,[28] **C-5**,[41] **C-6**,[42] **C-7**,[43] **C-8**,[33] and **D-1** were prepared according to the corresponding literature procedures All catalytic experiments were conducted in duplicate at minimum, and the reported results represent an average of all the runs. Catalytic experiments were set up under an oxygen-free atmosphere in either a glovebox or using standard Schlenk techniques. Research grade carbon dioxide (99.999%) and ultra high purity hydrogen (99.999%) were purchased from Metro Welding. Anhydrous K_3PO_4 (Aldrich, 98%) was ground with a mortar and pestle before use. **B-1** (Oakwood), $ZnCl_2$ (Strem), Y(OTf)$_3$ (Aldrich), La(OTf)$_3$ (Aldrich), AgOTf (Oakwood) and 1,3,5-trimethoxybenzene (Acros) were used without further purification. Tetrahydrofuran (THF) was purified using an Innovative Technologies (IT) solvent purification system consisting of a copper catalyst, activated alumina, and molecular sieves. Deuterated solvents (CDCl$_3$, CD$_2$Cl$_2$, and CD$_3$CN) were obtained from Cambridge Isotope Laboratories and used as-received. Authentic samples of the cyclic ethers tetrahydropyran,[44] 2-methyl tetrahydropyran[45] and oxepane[46] were synthesized by dehydration of the corresponding diol in the presence of Nafion-H.[47] Ethyl acetate, ethyl formate, methyl acetate, methyl benzoate, anhydrous methanol, anhydrous dimethoxyethane, and methyl pivalate were obtained from commercial sources and dried according to literature procedures prior to use.[48] Products were verified by comparison with literature spectra.

Reactor Descriptions

Each vessel is 45 mL in volume and are composed of a well (in which the solid and liquid reagents are charged) and a head, which contains various attachments as described below.

The reactors are made of Hastelloy C, and the wells are 7.5 cm tall and 3 cm in diameter. The heads consist of a pressure transducer and two inlet/outlet valves that can connect to a Parr Model 5000 Multiple Reactor system described above, a safety release valve, and a well for a thermocouple (Figure 4.17).
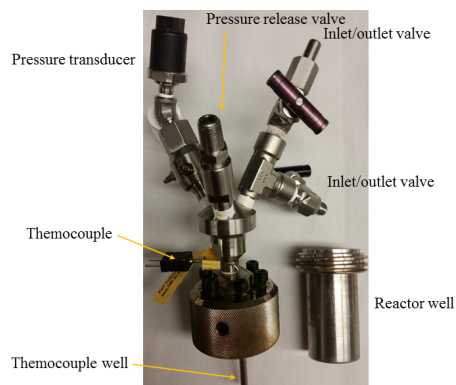
Figure 3.18. Picture of reactor type A with the parts of the reactor labeled.

Synthesis of 2-(N-fmoc-amino)ethyl formate (E12)
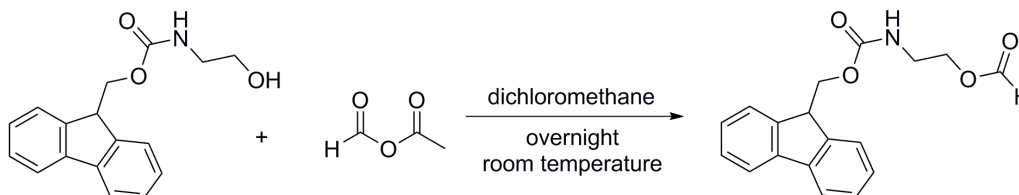
Acetic-formic anhydride[49] was synthesized by the addition of 2.7 mL formic acid (97%) to 5.9 mL of acetic anhydride under inert atmosphere. This material was stored in a Schlenk flask under N_2 and was used without further purification. 2-(N-Fmoc-amino)ethanol was synthesized as described in the literature.[50] In a round-bottom flask, 1.507 g (5.32 mmol) of 2-(N-fmoc-amino)ethanol was dissolved in 60 mL dichloromethane. Formic-acetic anhydride (3 mL, large excess) was added via syringe. The reaction was stirred under air overnight at room temperature. The resulting solution was then extracted with 3 x 60 mL saturated Na_2CO_3. The organic layer was dried over Na_2SO_4, and the volatiles were removed. The crude product was then purified by flash chromatography and isolated as a white powder (silica gel, 70:30 hexanes:ethyl acetate, R_f = 0.4). ^{1}H NMR (300 MHz, CD_2Cl_2) δ 8.06 (s, 1H), 7.78 (d, J = 7.5 Hz, 2H), 7.60 (d, J = 7.4 Hz, 2H), 7.41 (t, J = 7.4 Hz, 2H), 7.32 (td, J = 7.4, 1.3 Hz, 2H), 5.07 (s, 1H), 4.41 (d, J = 6.8 Hz, 2H), 4.22 (m, 3H),

3.46 (q, J = 5.7 Hz, 2H). 60 s relaxation delay employed to obtain proper integration of formate proton. ^{13}C NMR (126 MHz, CD$_2$Cl$_2$) δ 161.13, 156.56, 144.40, 141.68, 128.04, 127.41, 125.38, 120.32, 66.98, 63.17, 47.65, 40.30. Elemental Analysis: Calculated C 69.44, H 5.50, N 4.50. Measured C 69.18 H 5.58 N 4.45. Yield: 874 mg (53.0%). Melting point: 111.7-113.0°C.

General Procedure for Hydrogenation Reactions
I. Ethyl Formate Hydrogenation with C-2-5 (Table 3.1)

In a N$_2$-atmosphere dry box, [Ru] (10 μmol, 1 mol %) was dissolved in 2 mL of THF, and this solution was added to the metal well of a pressure vessel containing K$_3$PO$_4$ (10.6 mg, 50 μmol, 5 mol %) or omitted, Sc(OTf)$_3$ (4.9 mg, 10 μmol, 1 mol %) or omitted, and a micro magnetic stirbar (3 x 10 mm). Ethyl formate (81 μL, 1.0 mmol, 100 equiv relative to Ru) was then added, and the vessel (Reactor-type A) was sealed and removed from the dry box. The vessel was connected to the Parr Multiple Reactor System, and the manifold was thoroughly purged with ultra-high purity grade H$_2$ (99.999%). The vessel was then pressurized with H$_2$ (50 bar) at room temperature, and the reaction was heated at 100 ºC with a stir rate of 800 RPM. The heating was conducted using Specview software. After 16 h of heating, the reaction mixture was allowed to cool to room temperature. The pressure vessel was placed in a –84 °C bath (ethyl acetate/LN$_2$) for 15 min and then carefully vented using a metering valve. THF (0.5 mL) was added through the venting valve of the pressure vessel to wash any residual liquids/solids into the vessel. The vessel was then opened, 1,3,5-trimethoxybenzene (0.178 mmol, 300 μL of 0.593 M solution in DMSO-d_6) was added as a ^{1}H NMR standard, and the contents of the vessel were diluted with DMSO-d_6. Approximately 50 μL of the resulting solution was added to an NMR tube, diluted further with DMSO-d_6. The sample was then analyzed by ^{1}H NMR spectroscopy.

II. Hydrogenation of CO$_2$ to Methyl Formate Catalyzed by A-1 (Figure 3.9)

In a N$_2$-atmosphere dry box, **A-1** (12.5 mg, 25 μmol) was dissolved in 1.5 mL of anhdyrous CH$_3$OH, and this solution was added to the metal well of a pressure vessel containing the appropriate Lewis Acid (25 μmol) and a micro magnetic stirbar (3 x 10 mm). The vessel (Reactor-type A) was sealed and removed from the dry box. The vessel was connected to the Parr Multiple Reactor System, and the manifold was thoroughly purged with CO$_2$ and

pressurized (10 bar). The vessel was then pressurized with H_2 (30 bar, 40 total pressure) at room temperature, and the reaction was heated at 135 °C with a stir rate of 800 RPM. The heating was conducted using Specview software. After 16 h of heating, the reaction mixture was allowed to cool to room temperature. The pressure vessel was placed in a – 84 °C bath (ethyl acetate/LN_2) for 15 min and then carefully vented using a metering valve. Methanol (0.5 mL) was added through the venting valve of the pressure vessel to wash any residual liquids/solids into the vessel. The vessel was then opened, 1,3,5-trimethoxybenzene (0.178 mmol, 300 µL of 0.593 M solution in DMSO-d_6) was added as a ^{1}H NMR standard, and the contents of the vessel were diluted with DMSO-d_6. Approximately 50 µL of the resulting solution was added to an NMR tube, diluted further with DMSO-d_6. The sample was then analyzed by ^{1}H NMR spectroscopy.

III. Ethyl Formate Hydrogenation with C-4 (Figure 3.9)

In a N_2-atmosphere dry box, **C-4** (5.8 mg ,10 µmol, 1 mol %) was dissolved in 2 mL of THF, and this solution was added to the metal well of a pressure vessel with the appropriate Lewis acid (10 µmol, 1 mol %), and a micro magnetic stirbar (3 x 10 mm). Ethyl formate (81 µL, 1.0 mmol, 100 equiv relative to Ru) was then added, and the vessel (Reactor-type A) was sealed and removed from the dry box. The vessel was connected to the Parr Multiple Reactor System, and the manifold was thoroughly purged with ultra-high purity grade H_2 (99.999%). The vessel was then pressurized with H_2 (50 bar) at room temperature, and the reaction was heated at 100 °C with a stir rate of 800 RPM. The heating was conducted using Specview software. After 16 h of heating, the reaction mixture was allowed to cool to room temperature. The pressure vessel was placed in a – 84 °C bath (ethyl acetate/LN_2) for 15 min and then carefully vented using a metering valve. THF (0.5 mL) was added through the venting valve of the pressure vessel to wash any residual liquids/solids into the vessel. The vessel was then opened, 1,3,5-trimethoxybenzene (0.178 mmol, 300 µL of 0.593 M solution in DMSO-d_6) was added as a ^{1}H NMR standard, and the contents of the vessel were diluted with DMSO-d_6. Approximately 50 µL of the resulting solution was added to an NMR tube, diluted further with DMSO-d_6. The sample was then analyzed by ^{1}H NMR spectroscopy.

IV. Neat Ethyl Acetate Hydrogenations with C-6-8 (Table 3.2)

In a N_2-atmosphere dry box, [Ir] (4 μmol) was dissolved in 2 mL of ethyl acetate, and this solution was added to the metal well of a pressure equipped with a micro magnetic stirbar (3 x 10 mm). The vessel (Reactor-type A) was sealed and removed from the dry box. The vessel was connected to the Parr Multiple Reactor System, and the manifold was thoroughly purged with ultra-high purity grade H_2 (99.999%). The vessel was then pressurized with H_2 (60 bar) at room temperature, and the reaction was heated at 120 ºC with a stir rate of 800 RPM. The heating was conducted using Specview software. After 18 h of heating, the reaction mixture was allowed to cool to room temperature. The pressure vessel was placed in a –84 °C bath (ethyl acetate/LN_2) for 15 min and then carefully vented using a metering valve. THF (0.5 mL) was added through the venting valve of the pressure vessel to wash any residual liquids/solids into the vessel. The vessel was then opened, 1,3,5-trimethoxybenzene (0.178 mmol, 300 µL of 0.593 M solution in DMSO-d_6) was added as a ^{1}H NMR standard, and the contents of the vessel were diluted with DMSO-d_6. Approximately 50 µL of the resulting solution was added to an NMR tube, diluted further with DMSO-d_6. The sample was then analyzed by ^{1}H NMR spectroscopy.

IV. Neat Ester Hydrogenations with C-6-8 and B-1 (Table 3.3)

In a N_2-atmosphere dry box, **C-6** (3.4 mg, 4 μmol) was dissolved in 2 mL of the appropriate ester, and this solution was added to the metal well of a pressure vessel equipped with the appropriate quantity of **B-1** (40 μmol or 0 mmol), and a micro magnetic stirbar (3 x 10 mm). The vessel (Reactor-type A) was sealed and removed from the dry box. The vessel was connected to the Parr Multiple Reactor System, and the manifold was thoroughly purged with ultra-high purity grade H_2 (99.999%). The vessel was then pressurized with H_2 (30 bar) at room temperature, and the reaction was heated at 100 ºC with a stir rate of 800 RPM. The heating was conducted using Specview software. After 16 h of heating, the reaction mixture was allowed to cool to room temperature. The pressure vessel was placed in a –84 °C bath (ethyl acetate/LN_2) for 15 min and then carefully vented using a metering valve. THF (0.5 mL) was added through the venting valve of the pressure vessel to wash any residual liquids/solids into the vessel. The vessel was then opened, 1,3,5-trimethoxybenzene (0.178 mmol, 300 µL of 0.593 M solution in DMSO-d_6) was added as a ^{1}H NMR standard, and the contents of the vessel were diluted with

DMSO-d_6. Approximately 50 µL of the resulting solution was added to an NMR tube, diluted further with DMSO-d_6. The sample was then analyzed by ^{1}H NMR spectroscopy.

V. Ester Hydrogenation In DME With C-6 (Table 3.4)

In a N$_2$-atmosphere dry box, **C-6** (8.6 mg, 10 µmol) was dissolved in 1 mL DME and this solution was added to the metal well of a pressure equipped with a micro magnetic stirbar (3 x 10 mm). Ester (1.0 mmol, 100 equiv relative to Ir) was then added, and the the vessel (Reactor-type A) was sealed and removed from the dry box. The vessel was connected to the Parr Multiple Reactor System, and the manifold was thoroughly purged with ultra-high purity grade H$_2$ (99.999%). The vessel was then pressurized with H$_2$ (30 bar) at room temperature, and the reaction was heated at 100 ºC with a stir rate of 800 RPM. The heating was conducted using Specview software. After 16 h of heating, the reaction mixture was allowed to cool to room temperature. The pressure vessel was placed in a –84 °C bath (ethyl acetate/LN$_2$) for 15 min and then carefully vented using a metering valve. THF (0.5 mL) was added through the venting valve of the pressure vessel to wash any residual liquids/solids into the vessel. The vessel was then opened, 1,3,5-trimethoxybenzene (0.178 mmol, 300 µL of 0.593 M solution in DMSO-d_6) was added as a ^{1}H NMR standard, and the contents of the vessel were diluted with DMSO-d_6. Approximately 50 µL of the resulting solution was added to an NMR tube, diluted further with DMSO-d_6. The sample was then analyzed by ^{1}H NMR spectroscopy.

VI. Hydrogenations of L1 and L2 with C-6 and B-1 (Table 3.5)

In a N$_2$-atmosphere dry box, **C-6** (3.4 mg, 4 µmol) was dissolved in the appropriate quantity of **L1** or **L2** (2 mL or 1 mmol), DME (1 mL or 0 mL), and this solution was added to the metal well of a pressure vessel equipped with the appropriate quantity of **B-1** (40 µmol or 0 mmol), and a micro magnetic stirbar (3 x 10 mm). The vessel (Reactor-type A) was sealed and removed from the dry box. The vessel was connected to the Parr Multiple Reactor System, and the manifold was thoroughly purged with ultra-high purity grade H$_2$ (99.999%). The vessel was then pressurized with H$_2$ (30 bar) at room temperature, and the reaction was heated at 100 ºC with a stir rate of 800 RPM. The heating was conducted using Specview software. After 16 h of heating, the reaction mixture was allowed to cool to room temperature. The pressure vessel was placed in a –84 °C bath (ethyl acetate/LN$_2$)

for 15 min and then carefully vented using a metering valve. THF (0.5 mL) was added through the venting valve of the pressure vessel to wash any residual liquids/solids into the vessel. The vessel was then opened, 1,3,5-trimethoxybenzene (0.178 mmol, 300 μL of 0.593 M solution in DMSO-d_6) was added as a ^{1}H NMR standard, and the contents of the vessel were diluted with DMSO-d_6. Approximately 50 μL of the resulting solution was added to an NMR tube, diluted further with DMSO-d_6. The sample was then analyzed by ^{1}H NMR spectroscopy and ESI-MS.

VII. 2nd Generation Cascade Pathway (Figure 3.16)

In a N_2-atmosphere dry box, **A-1** (4.9 mg, 10 μmol), **B-1** (4.9 mg, 10 μmol), and **C-6** (8.6 mg, 10 μmol) were dissolved in 1.5 mL of THF and EtOH (10 mmol), and this solution was added to a pressure vessel equipped with an octagonal magnetic stirbar (5/16 x 1/2 in). The vessel was then sealed and removed from the dry box. The vessel was pressurized with CO_2 (10 bar) and H_2 (30 bar) at room temperature, and the reaction was heated at 100 ºC with a stir rate of 800 RPM. The heating was conducted using Specview software. After 18 h of heating, the reaction mixture was allowed to cool to room temperature. The pressure vessel was placed in a –84 °C bath (ethyl acetate/LN$_2$) for 15 min and then carefully vented using a metering valve. THF (0.5 mL) was added through the venting valve of the pressure vessel to wash any residual liquids/solids into the vessel. The vessel was then opened, 1,3,5-trimethoxybenzene (0.178 mmol, 300 μL of 0.593 M solution in DMSO-d_6) was added as a ^{1}H NMR standard, and the contents of the vessel were diluted with DMSO-d_6. 50 μL of the resulting solution was added to an NMR tube, diluted further with DMSO-d_6. The sample was then analyzed by ^{1}H NMR spectroscopy.

VIII. Systematic Ethyl Formate Hydrogenation with C-6. (Table 3.6)

In a N_2-atmosphere dry box, **C-6** (8.6 mg, 10 μmol, 1 mol %) was dissolved in 1.5 mL of THF and EtOH (10 mmol or 0 mmol), this solution was added to the metal well of a pressure vessel containing **A-1** (4.9 mg, 10 μmol) or omitted, **B-1** (4.9 mg, 10 μmol) or omitted, NBu$_4$Cl (10 μmol or 0 mmol), PPh$_3$ (10 μmol or 0 mmol), and AgOTf (10 μmol or 0 mmol) and a micro magnetic stirbar (3 x 10 mm). Ethyl formate (81 μL, 1.0 mmol, 100 equiv relative to Ir) was then added, and the vessel (Reactor-type A) was sealed and removed from the dry box. The vessel was connected to the Parr Multiple Reactor System,

and the manifold was thoroughly purged with ultra-high purity grade H_2 (99.999%). The vessel was then pressurized with CO_2 (10 bar or 0 bar) and H_2 (30 bar) at room temperature, and the reaction was heated at 100 ºC with a stir rate of 800 RPM. The heating was conducted using Specview software. After 16 h of heating, the reaction mixture was allowed to cool to room temperature. The pressure vessel was placed in a –84 °C bath (ethyl acetate/LN$_2$) for 15 min and then carefully vented using a metering valve. THF (0.5 mL) was added through the venting valve of the pressure vessel to wash any residual liquids/solids into the vessel. The vessel was then opened, 1,3,5-trimethoxybenzene (0.178 mmol, 300 µL of 0.593 M solution in DMSO-d_6) was added as a ^{1}H NMR standard, and the contents of the vessel were diluted with DMSO-d_6. Approximately 50 µL of the resulting solution was added to an NMR tube, diluted further with DMSO-d_6. The sample was then analyzed by ^{1}H NMR spectroscopy.

IX. Halide Abstracted A Catalysts and Application to Cascade (Figure 3.17)

In a N_2-atmosphere dry box, **A-2-4-Cl** (10 µmo) was pre-stirred in 1.5 mL THF containing AgOTf (10 µmol or 20 µmol). **C-6** (8.6 mg, 10 µmol) and EtOH (10 mmol) were added to this solution and transferred to a pressure vessel equipped with an octagonal magnetic stirbar (5/16 x 1/2 in). The vessel was then sealed and removed from the dry box. The vessel was pressurized with CO_2 (10 bar) and H_2 (30 bar) at room temperature, and the reaction was heated at 100 ºC with a stir rate of 800 RPM. The heating was conducted using Specview software. After 18 h of heating, the reaction mixture was allowed to cool to room temperature. The pressure vessel was placed in a –84 °C bath (ethyl acetate/LN$_2$) for 15 min and then carefully vented using a metering valve. THF (0.5 mL) was added through the venting valve of the pressure vessel to wash any residual liquids/solids into the vessel. The vessel was then opened, 1,3,5-trimethoxybenzene (0.178 mmol, 300 µL of 0.593 M solution in DMSO-d_6) was added as a ^{1}H NMR standard, and the contents of the vessel were diluted with DMSO-d_6. 50 µL of the resulting solution was added to an NMR tube, diluted further with DMSO-d_6. The sample was then analyzed by ^{1}H NMR spectroscopy.

X. Cascade Hydrogenation with D-1 (Table 3.7)

In a N_2-atmosphere dry box, **D-1** (25 µmol), **B-1** (25 µmol or 0 mmol), and **C-6** (25 µmol or 0 mmol) were dissolved in 1.5 mL of THF and EtOH (10 mmol), and this solution was added to a pressure vessel equipped with an octagonal magnetic stirbar (5/16 x 1/2 in). The vessel was then sealed and removed from the dry box. The vessel was pressurized with CO_2 (10 bar) and H_2 (30 bar) at room temperature, and the reaction was heated at 100 ºC with a stir rate of 800 RPM. The heating was conducted using Specview software. After 18 h of heating, the reaction mixture was allowed to cool to room temperature. The pressure vessel was placed in a –84 °C bath (ethyl acetate/LN_2) for 15 min and then carefully vented using a metering valve. THF (0.5 mL) was added through the venting valve of the pressure vessel to wash any residual liquids/solids into the vessel. The vessel was then opened, 1,3,5-trimethoxybenzene (0.178 mmol, 300 µL of 0.593 M solution in DMSO-d_6) was added as a ^{1}H NMR standard, and the contents of the vessel were diluted with DMSO-d_6. 50 µL of the resulting solution was added to an NMR tube, diluted further with DMSO-d_6. The sample was then analyzed by ^{1}H NMR spectroscopy.

3.5 References

(1) Brewster, T. P.; Rezayee, N. M.; Culakova, Z.; Sanford, M. S.; Goldberg, K. I. *ACS Catal.* **2016**, 3113.

(2) Appel, A. M.; Bercaw, J. E.; Bocarsly, A. B.; Dobbek, H.; DuBois, D. L.; Dupuis, M.; Ferry, J. G.; Fujita, E.; Hille, R.; Kenis, P. J.; Kerfeld, C. A.; Morris, R. H.; Peden, C. H.; Portis, A. R.; Ragsdale, S. W.; Rauchfuss, T. B.; Reek, J. N.; Seefeldt, L. C.; Thauer, R. K.; Waldrop, G. L. *Chem Rev* **2013**, *113*, 6621.

(3) León, T.; Correa, A.; Martin, R. *J. Am. Chem. Soc.* **2013**, *135*, 1221.

(4) Munshi, P.; Main, A. D.; Linehan, J. C.; Tai, C. C.; Jessop, P. G. *J. Am. Chem. Soc.* **2002**, *124*, 7963.

(5) Rohmann, K.; Kothe, J.; Haenel, M. W.; Englert, U.; Hölscher, M.; Leitner, W. *Angew. Chem. Int. Ed.* **2016**, *55*, 8966.

(6) Lau, C. P.; Chen, Y. Z. *J. Chem. Mol. Catal. A: Chem.* **1995**, *101*, 33.

(7) Jessop, P. G.; Hsiao, Y.; Ikariya, T.; Noyori, R. *J. Am. Chem. Soc.* **1994**, *116*, 8851.

(8) Huff, C. A.; Sanford, M. S. *J. Am. Chem. Soc.* **2011**, *133*, 18122.

(9) Wesselbaum, S.; Vom Stein, T.; Klankermayer, J.; Leitner, W. *Angew. Chem. Int. Ed.* **2012**, *51*, 7499.

(10) Wesselbaum, S.; Moha, V.; Meuresch, M.; Brosinski, S.; Thenert, K. M.; Kothe, J.; Stein, T. v.; Englert, U.; Holscher, M.; Klankermayer, J.; Leitner, W. *Chem. Sci.* **2015**, *6*, 693.

(11) Chen, Y.; Choi, S.; Thompson, L. T. *ACS Catal.* **2015**, *5*, 1717.

(12) Schneidewind, J.; Adam, R.; Baumann, W.; Jackstell, R.; Beller, M. *Angew. Chem. Int. Ed.* **2017**, *56*, 1890.

(13) Courtemanche, M. A.; Legare, M. A.; Maron, L.; Fontaine, F. G. *J. Am. Chem. Soc.* **2013**, *135*, 9326.

(14) Riduan, S. N.; Zhang, Y.; Ying, J. Y. *Angew. Chem. Int. Ed.* **2009**, *48*, 3322.

(15) Klankermayer, J.; Wesselbaum, S.; Beydoun, K.; Leitner, W. *Angew. Chem. Int. Ed.* **2016**, *55*, 7296.

(16) Natte, K.; Neumann, H.; Beller, M.; Jagadeesh, R. V. *Angew. Chem. Int. Ed.* **2017**, *56*, 6384.

(17) Olah, G. A.; Goeppert, A.; Prakash, G. K. S.; Wiley-VCH Verlag GmbH & Co. KGaA, 2009.

(18) Palo, D. R.; Dagle, R. A.; Holladay, J. D. *Chem. Rev.* **2007**, *107*, 3992.

(19) Jessop, P. G. In *The Handbook of Homogeneous Hydrogenation*; Wiley-VCH Verlag GmbH: 2006, p 489.

(20) Huff, C. A.; Sanford, M. S. *ACS Catal.* **2013**, *3*, 2412.

(21) Huff, C. A.; Kampf, J. W.; Sanford, M. S. *Organometallics* **2012**, *31*, 4643.

(22) Savourey, S.; Lefevre, G.; Berthet, J. C.; Thuery, P.; Genre, C.; Cantat, T. *Angew. Chem. Int. Ed.* **2014**, *53*, 10466.

(23) Dub, P. A.; Ikariya, T. *ACS Catal.* **2012**, *2*, 1718.

(24) Yuwen, J.; Chakraborty, S.; Brennessel, W. W.; Jones, W. D. *ACS Catal.* **2017**, *7*, 3735.

(25) Korstanje, T. J.; Ivar van der Vlugt, J.; Elsevier, C. J.; de Bruin, B. *Science* **2015**, *350*, 298.

(26) Sandoval, C. A.; Ohkuma, T.; Muñiz, K.; Noyori, R. *J. Am. Chem. Soc.* **2003**, *125*, 13490.

(27) Saudan, L. A.; Saudan, C. M.; Debieux, C.; Wyss, P. *Angew. Chem. Int. Ed.* **2007**, *46*, 7473.

(28) Kuriyama, W.; Matsumoto, T.; Ogata, O.; Ino, Y.; Aoki, K.; Tanaka, S.; Ishida, K.; Kobayashi, T.; Sayo, N.; Saito, T. *Org. Process Res. Dev.* **2012**, *16*, 166.

(29) Balaraman, E.; Gunanathan, C.; Zhang, J.; Shimon, L. J. W.; Milstein, D. *Nat. Chem.* **2011**, *3*, 609.

(30) Werkmeister, S.; Junge, K.; Beller, M. *Org. Process Res. Dev.* **2014**, *18*, 289.

(31) Morris, R. H. *Acc. Chem. Res.* **2015**, *48*, 1494.

(32) Ohkuma, T.; Ooka, H.; Ikariya, T.; Noyori, R. *J. Am. Chem. Soc.* **1995**, *117*, 10417.

(33) Brewster, T. P.; Miller, A. J. M.; Heinekey, D. M.; Goldberg, K. I. *J. Am. Chem. Soc.* **2013**, *135*, 16022.

(34) Geilen, F. M. A.; Engendahl, B.; Harwardt, A.; Marquardt, W.; Klankermayer, J.; Leitner, W. *Angew. Chem. Int. Ed.* **2010**, *49*, 5510.

(35) Mainz, V. V.; Andersen, R. A. *Organometallics* **1984**, *3*, 675.

(36) Synthesized from **A-1** and AgOTf

(37) Bianchini, C.; Perez, P. J.; Peruzzini, M.; Zanobini, F.; Vacca, A. *Inorg. Chem.* **1991**, *30*, 279.

(38) Mason, R.; Meek, D. W.; Scollary, G. R. *Inorg. Chim. Acta.* **1976**, *16*, L11.

(39) Jia, W.; Chen, X.; Guo, R.; Sui-Seng, C.; Amoroso, D.; Lough, A. J.; Abdur-Rashid, K. *Dalton Trans.* **2009**, 8301.

(40) Jing-Xing, G.; Hui-Lin, W.; Wai-Kwok, W.; Man-Chung, T.; Wing-Tak, W. *Polyhedron* **1996**, *15*, 1241.

(41) Spasyuk, D.; Smith, S.; Gusev, D. G. *Angew. Chem. Int. Ed.* **2013**, *52*, 2538.

(42) Ogo, S.; Kabe, R.; Hayashi, H.; Harada, R.; Fukuzumi, S. *Dalton Trans.* **2006**, 4657.

(43) Ogo, S.; Makihara, N.; Kaneko, Y.; Watanabe, Y. *Organometallics* **2001**, *20*, 4903.

(44) *Williams, D. E.; Peters, M. B.; Wang, B.; Roitberg, A. E.; Merz, K. M. J. Phys. Chem. A* **2009***, 113, 11550.*

(45) Dzudza, A.; Marks, T. J. *Org. Lett.* **2009**, *11*, 1523.

(46) Spectral Database for Organic Compounds (SDBS); 1H NMR spectrum; SDBS No.: 10291; RN 592-90-5; http://riodb01.ibase.aist.go.jp/sdbs/ (July 1, 2014).

(47) Olah, G. A.; Fung, A. P.; Malhotra, R. *Synthesis* **1981** 474.

(48) In *Purification of Laboratory Chemicals (Fifth Edition)*; (Eds: Armarego, W.L.F.; Chai, C.L.) Butterworth-Heinemann: Burlington, 2003, p 80.

(49) Elders, N.; Schmitz, R. F.; de Kanter, F. J. J.; Ruitjer, E.; Groen, M. B.; Orru, R. U. A. *J. Org. Chem.* **2007**, *72*, 6135.

(50) Porcheddu, A.; Giacomelli, G.; Piredda, M.; Carta, M.; Nieddu, G. *Eur. J. Org. Chem.* **2008**, 5786.

Chapter 4: CO$_2$ Capture and Hydrogenation- Strategies for the Tandem Amine- and Ruthenium- catalyzed Capture and Reduction of CO$_2$ to CH$_3$OH

The chemistry detailed in this chapter has been made possible with Dr. Chelsea A. Huff, Prof. Melanie S. Sanford. This collaboration was performed in part of the Center for Enabling New Technologies Through Catalysis. Portions of this work have been published.[1]

4.1 Introduction

Increases in anthropogenic CO$_2$ emissions have resulted in a rising interest in mitigating atmospheric concentrations.[2,3] One strategy to address this problem involves remediating CO$_2$ emissions via capture at a point source, with concomitant sequestration in underground geological formations.[4] This approach, termed carbon capture and sequestration (CCS), has been the subject of extensive research and commercialization efforts.[5,6,7] However, CCS suffers from the fundamental limitation that it fails to productively utilize CO$_2$.[8,9,10,11,12]

An attractive and complementary approach would be to use captured CO$_2$ as a C$_1$ source for the synthesis of fuels and/or chemicals such as CH$_3$OH.[13,14,15,16,17] Over the past 40 years, there has been significant work on the development of Cu/ZnO/Al$_2$O$_3$ (CZA) and other heterogeneous catalysts for the conversion of CO$_2$ to CH$_3$OH.[13,18,19] These processes have been combined with other renewable technologies (electrolysis of water) and implemented on an industrial scale at the George Olah Plant in Reykjavik, Iceland producing 5 million liters of CH$_3$OH per year. Despite these improved methodologies,

these processes generally operate at high temperatures (>200 ºC), which limits conversion in this entropically unfavorable reduction reaction.[20] Additionally, it remains challenging to rationally tune the reactivity and selectivity of such heterogeneous catalysts. Furthermore, these catalysts are acutely susceptible to poisoning from Lewis bases, which is problematic since Lewis bases are currently one of the most prevalent technologies used for carbon capture. Single-site homogeneous catalysts could potentially offer an attractive alternative, since they generally operate at lower temperatures and have easily tunable ligand environments that may be tuned to enable compatibility with Lewis bases.

Despite many years of effort,[21][22][23,24,25,26,27,28,29] homogeneous catalysts capable of selectively converting CO_2 and H_2 to CH_3OH[30,31,32,33,34,35,36,37,38,39] have only recently been disclosed.[40,41,42,43,44,45] In 2011, our group reported a combination of three homogenous catalysts that operate in tandem to sequentially convert CO_2 to formic acid, methyl formate, and ultimately CH_3OH (Figure 4.).[40] More recently, several reports by Leitner and Klankermayer have demonstrated that the combination of the ruthenium(triphos) complex and $NHTf_2$ catalyze the conversion of CO_2 to CH_3OH *via* either a formic acid or methyl formate intermediate.[44] However, both of these systems operate under acidic conditions, and are thus incompatible with the bases typically utilized for CO_2 capture.[5]
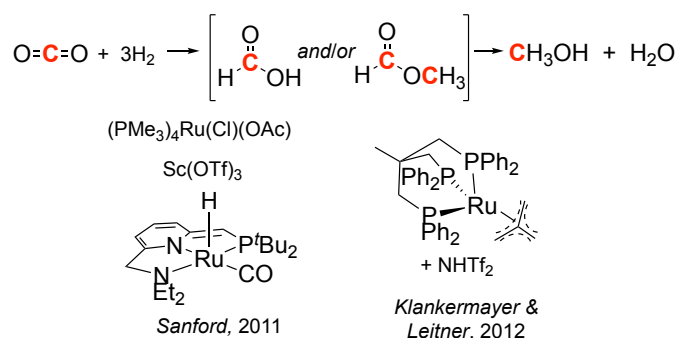
Figure 4.1. Homogeneous Catalysts for the Hydrogenation of CO_2 to CH_3OH.

Inspired by the efficiency of amines to sequester CO_2 as a carbamate salt, we sought an alternative strategy that would combine CO_2 capture to form a carbamate salt (**A**) (Figure 4.2a) with hydrogenation to generate CH_3OH (Figure 4.2b).[46] Conceptually, this approach is very different than those in Figure 4.1, as it involves catalysis under basic, rather than acidic conditions. Thus, it should be compatible with CO_2 capture processes. This chapter focuses on the development of a CO_2-capture and hydrogenation process using a tandem amine and ruthenium system to ultimately yield CH_3OH.
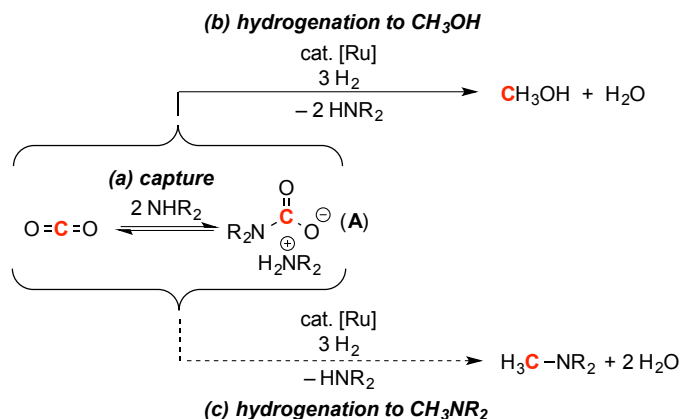
Figure 4.2. Tandem CO_2 Capture/Hydrogenation Sequence.

4.2 Results and Discussion

CO_2 Capture

The use of amines as a CO_2 scrubbing agent is a practice employed across a multitude of processes from methane production to the food and beverage industry.[47] The mechanism of CO_2–amine capture under anhydrous conditions necessitates two amines per CO_2 molecule. As such, many polyamine sorbents have been developed and applied to these CO_2 scrubbing systems. While efficient for CO_2 trapping, the polyamine–CO_2 adducts are poorly defined at the molecular level. Furthermore, these adducts often suffer from insolubility in organic solvents under ambient conditions. Development of new amine-containing materials to overcome these limitations is an area of study outside the scope of our CO_2 capture and hydrogenation approach. To serve as a proof of concept, simple amines were studied to trap CO_2 to form well-defined CO_2–amine adducts as the carbamate salt.

Two main considerations guided our selection in a CO_2-capturing agent. The first consideration focused on the solubility of the amine and the captured species in THF. The second criterion was the compatibility of the CO_2 capturing agent and the reduction catalyst shown in Figure 4.3. Aniline, **A-1**, though soluble in THF, was found to be a poor CO_2 capturing agent under ambient conditions presumably due to the poor nucleophilicity. More electron rich substrates were evaluated ranging from primary amines to secondary alkyl amines, **A-2-A-7.** After an evaluation of several potential amines, we found that dimethyl amine ($NHMe_2$, **A-7**) and the corresponding CO_2-sequestered species, dimethylammonium dimethylcarbamate (DMC), were both soluble in THF. DMC was found to be a miscible ionic liquid, making **A-7** an ideal CO_2 captured agent. Furthermore, DMC

is commercially available, which allows for convenient hydrogenation studies without the need to synthesis the carbamate substrate.
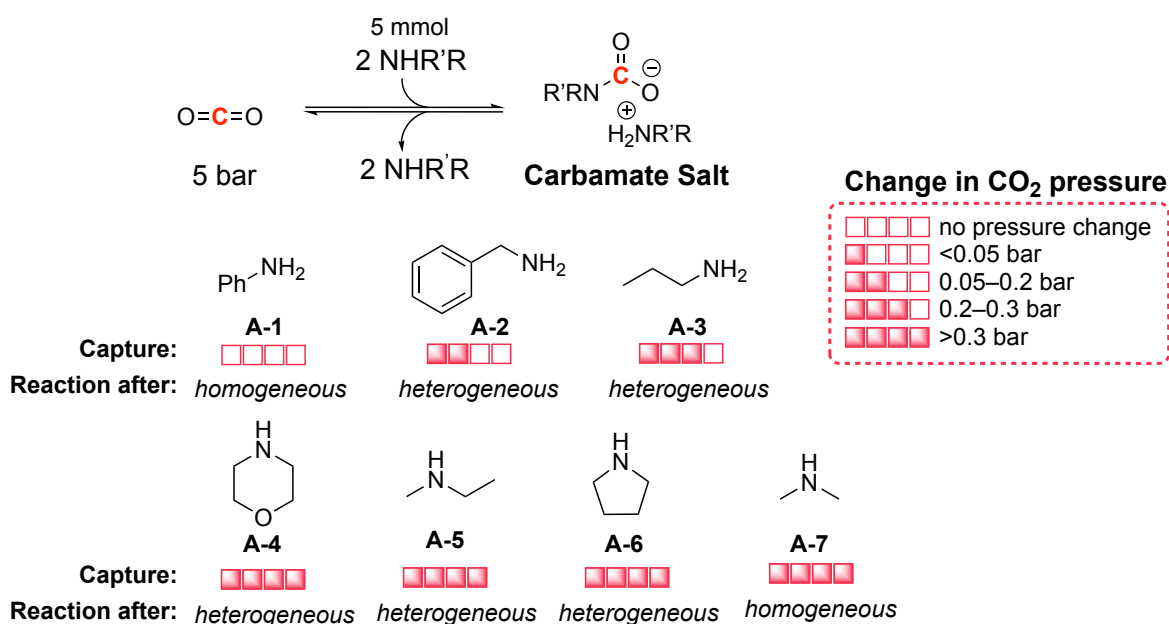
Figure 4.3. CO_2 Capture to Form Carbamate Salt.

Direct Hydrogenation of Carbamate Salt

DMC, which is formed by the reaction of CO_2 with $NHMe_2$, was selected as a representative example of the CO_2 capture intermediate. Our initial studies focused on identifying homogeneous catalysts capable of hydrogenating DMC to CH_3OH. We anticipated several key challenges associated with this transformation. First, the carbonyl functionality in DMC is very weakly electrophilic; thus, the ideal catalyst should be highly reactive towards C=O hydrogenation. Second, $NHMe_2$, a Brønsted base and potential ligand will be released over the course of the reaction requiring that the catalyst must be stable under basic conditions and must not be inhibited by $NHMe_2$. Third, the formation of trimethylamine is a possible competing side reaction (Figure 4.2c)[48,49,50,51,52] such that the catalyst must be selective for hydrogenation with C–N cleavage (to produce CH_3OH) over hydrogenation with C–O cleavage (to yield NMe_3).[53] These requirements led us to examine ruthenium pincer complexes **1**, **2**, and **3** as catalysts for this reaction. These complexes are known to catalyze the hydrogenation of weakly electrophilic ester,[43, 54] amide,[55,56] and/or neutral carbonate[43] substrates. Additionally, catalysts **1**, **2,** and **3** have all been demonstrated to be compatible with amines.[43,55] Finally, Milstein recently demonstrated that **2** catalyzes the hydrogenation of *N*-formylmorpholine to selectively

generate CH_3OH rather than the tertiary amine, *N*-methylmorpholine.[55] The latter result suggests that selective hydrogenation with C–N cleavage to generate CH_3OH is feasible with this class of pincer catalysts.

Table 4.1. Direct Hydrogenation of DMC to CH_3OH and DMF.[a]
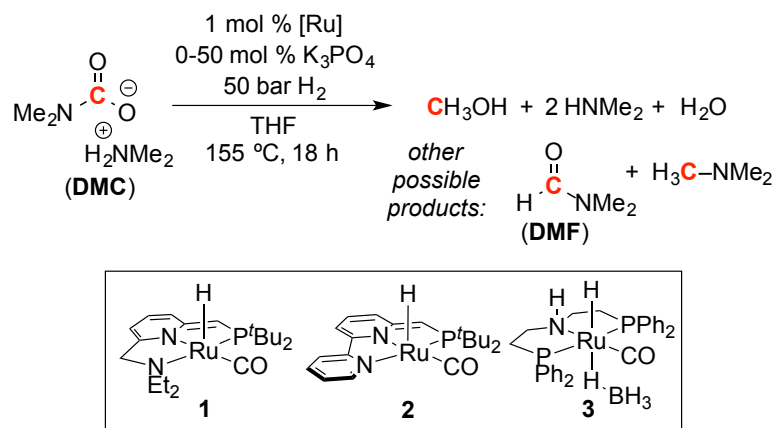
Entry	catalyst	base	TON CH_3OH	TON DMF	TON NMe_3
1	**1**	none	0	0	<1
2	**2**	none	3	0	<1
3	**3**	none	3	2	<1
4	**1**	K_3PO_4	0	3	<1
5	**2**	K_3PO_4	4	3	<1
6	**3**	K_3PO_4	19	3	<1
7[b]	**3**	K_3PO_4	20	0	<1

[a] Conditions: 50 bar H_2, 0.5 mmol of DMC (0.33 M in THF), 5 μmol of catalysts, 0.25 mmol of K_3PO_4, 18 h. [b] Reaction time of 30 h.

We first examined the hydrogenation of DMC with 1 mol % of catalysts **1**, **2**, or **3** at 155 ºC in THF under 50 bar of H_2. As shown in Table 4.1, very low turnover numbers (between 0 and 3) were observed in all cases (entries 1-3). We noted that exogenous bases have been reported to enhance the reactivity of ruthenium carbonyl hydrogenation catalysts.[57,58,59,60,61,62] An evaluation of different base/catalyst combinations revealed that the combination of commercially available catalyst **3** and K_3PO_4 was particularly effective for our system. The addition of 50 equiv of K_3PO_4 relative to **3** resulted in up to 19 turnovers of CH_3OH at 155 ºC (TON determined relative to the loading of **3**, entry 6). Importantly, this reaction was highly selective for CH_3OH over NMe_3 (<1 turnover of NMe_3 was detected). Small quantities of dimethylformamide (DMF, 3 turnovers) were also formed under these conditions.

The **3**-catalyzed conversion of DMC to CH_3OH (Table 4.1, entry 6) provides exciting proof-of-principle for our approach. However, there is still major room for improvement, as this result represents just 22% conversion of DMC to hydrogenated products over 18 h. Notably, increasing the reaction time to 30 h had minimal impact on conversion (entry 7). This result suggests that catalyst decomposition is competitive with DMC hydrogenation at 155 ºC.

Pathways for Carbamate Hydrogenation

In order to develop a rational strategy to improve this reaction further, we analyzed possible pathways from DMC to CH_3OH. Literature precedent suggests that there are at least two possible routes for the conversion of DMC to CH_3OH in this system. The most direct is shown in Figure 4.4, Path A, and involves initial hydrogenation of DMC to DMF (step i) followed by hydrogenation of DMF with C–N bond cleavage to produce CH_3OH (step ii). Milstein has demonstrated the ruthenium-catalyzed hydrogenation of related carbonates,[43] carbamates,[43] and amides,[55a] suggesting the viability of both steps i and ii. Alternatively, DMC could reversibly release CO_2 and 2 equiv of $NHMe_2$ (step iii, Path B). This would be followed by hydrogenation of CO_2 to formic acid (FA, step iv), a thermodynamically unfavorable reaction that would be driven to the right by deprotonation of FA to yield dimethylammonium formate (DMFA, step v). Subsequent amidation of FA to afford DMF (step vi) and selective hydrogenation of DMF (step ii) would then release CH_3OH. Notably, Jessop had previously demonstrated the ruthenium-catalyzed conversion of DMC to DMF via steps iii-vi.[63,64,65]
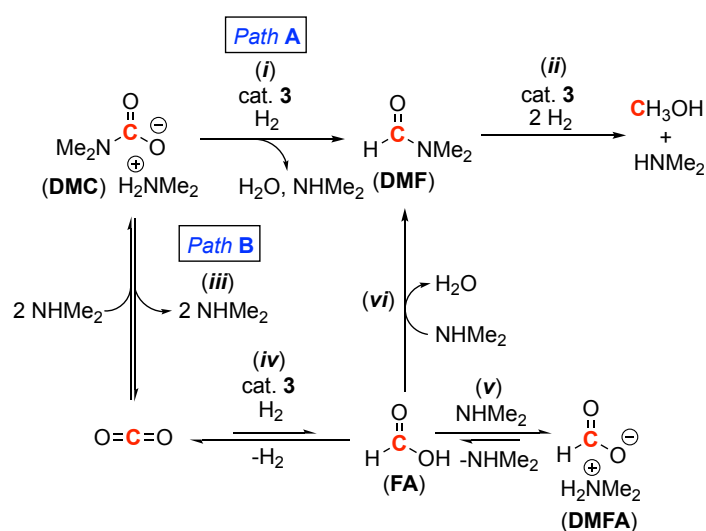
Figure 4.4. Possible Paths for Hydrogenation of DMC to CH_3OH.

Both of the paths in Figure 4.4 involve DMF as a key intermediate. We conducted independent experiments that confirm that **3** is a competent and selective catalyst for the hydrogenation of DMF to CH_3OH (Figure 4.5a). Furthermore, the addition of 0.5 mmol of DMF at the onset of the **3**-catalyzed hydrogenation of DMC results in a 4-fold increase in the quantity of CH_3OH produced (Figure 4.5b). Both of these results are consistent with the proposed intermediacy of DMF in this transformation.
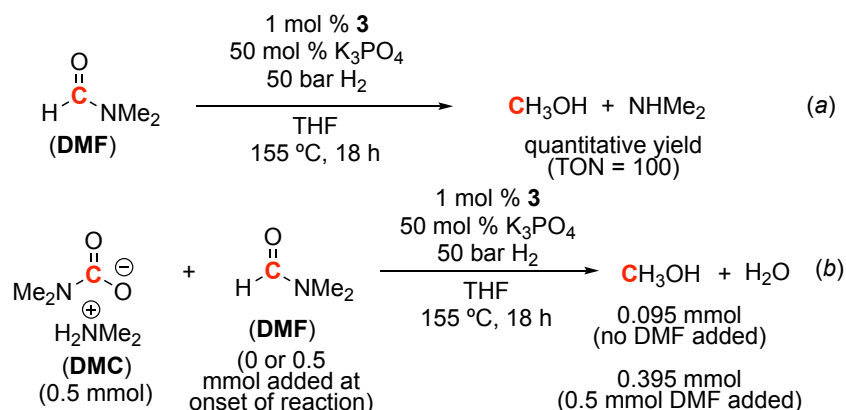
Figure 4.5. (*a*) Hydrogenation of DMF with **3**. (*b*) Hydrogenation of DMC and DMF.

We next sought to utilize the proposed pathways in Figure 4.4 and Figure 4.5 to further optimize the **3**-catalyzed hydrogenation of DMC. Since catalyst decomposition appears to be problematic at 155 °C, we focused on strategies for lowering the reaction temperature. Figure 4.6 implicates four different carbonyl-containing intermediates that could accumulate under the reaction conditions: DMC, DMFA, DMF, and CO_2. Among these possible substrates, DMC is expected to be the most difficult to hydrogenate (since it is the least electrophilic) while CO_2 should be the most reactive towards hydrogenation (since it is the most electrophilic) (Figure 4.6). Thus, assuming that there is some equilibrium between DMC and CO_2 during the reaction, this analysis suggests that Path B should be accessible under much milder conditions than Path A.
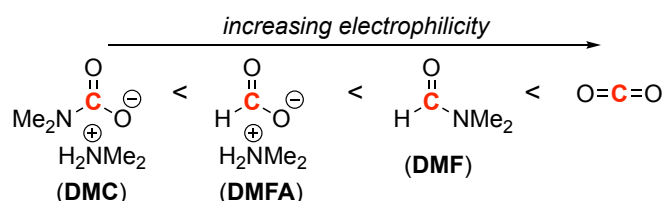
Figure 4.6. Potential carbonyl-containing intermediates.

Hydrogenation of Carbamate to CH_3OH Using A Temperature Ramp

To test this hypothesis, we lowered the temperature for the DMC hydrogenation reaction to 95 °C (Table 4.2). At this temperature, the **3**-catalyzed hydrogenation of DMF is extremely slow (<1% conversion over 18 h). Instead, the sole detectable hydrogenation products were DMF and DMFA (10 conversion of DMC, TON = 10 entry 2). Path B is expected to be the only accessible route to these products at this temperature. We next hypothesized that increasing the initial concentration of DMC would further accelerate Path B by increasing the equilibrium concentration of the reactive electrophile, CO_2. As predicted, moving from 0.32 M (entry 2) to 1.89 M DMC (entry 3) resulted in a significant increase in conversion of DMC (39% conversion, TON (DMF + DMFA) = 385). Finally, we reasoned that the addition of exogenous $NHMe_2$ would further drive Path B by accelerating trapping of the FA generated in step iv. Indeed, the addition of 7.6 mmol of **A-7** ($NHMe_2$) at the onset of the reaction resulted in >75% conversion of DMC over 18 h at 95 °C to form a mixture of DMF and DMFA (800 turnovers).

Table 4.2. Optimization of **3**/**A-7**-Catalyzed Hydrogenation of DMC.[a]
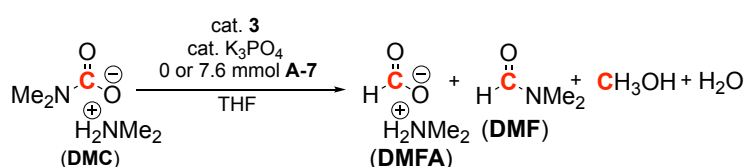
Entry	Temp. (°C)	[DMC] (M)	added NHMe₂ (mmol)	% conv. DMC	TON CH₃OH	TON DMF + DMFA
1	155	0.32	none	22	19	3
2	95	0.32	none	10	<1	10
3	95	1.89	none	39	<1	385
4	95	1.89	7.6	87	<1	872
5[b]	95⇨155	1.89	7.6	58	306	270

[a] Conditions: 50 bar H_2, 5 μmol of **6**, 0.25 mmol of K_3PO_4, 18 h. [b] 95 °C for 18 h then 155 °C for 18 h.

The results in Table 4.2, entries 2-4 led us to examine a single pot, temperature ramp strategy for hydrogenating DMC to CH_3OH. This approach involves initial hydrogenation of DMC at 95 °C to build up a high concentration of DMF followed by

an increase in reaction temperature to enable the **3**-catalyzed conversion of DMF to CH_3OH. Gratifyingly, a ramp of 95 ºC for 18 h followed by 155 ºC for 18 h afforded a mixture of CH_3OH (31% yield, TON = 306) and DMF/DMFA (27%, TON = 270).

CO$_2$ Hydrogenation to DMF

With the development of a method for the hydrogenation of DMC to CH_3OH, we next placed emphasis in adapting the system to CO_2. Initial studies evaluated the reduction of CO_2 to DMF using a suite of catalysts. This transformation is well precedented, and provides an opportunity to benchmark several CO_2 hydrogenation catalysts. To evaluate each catalyst for its ability to hydrogenate CO_2, 1 bar CO_2 (2 mmol) and 50 bar H_2 were used as shown in Table 4.3.

Table 4.3. Hydrogenation of CO_2 in the presence of **A-7** to DMF.[a]
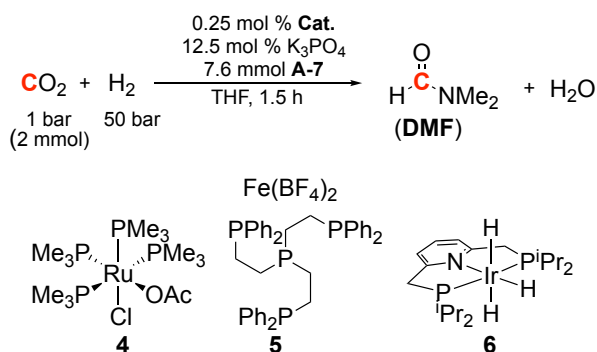
Entry	Catalyst	Temp. (ºC)	% Conv. of CO$_2$	DMF TON
1	**3**	30	1	3
2	**3**	50	11	45
3	**3**	65	32	129
4	**3**	80	57	227
5	**3**	95	87	348
6	**3**	110	52	207
7	**3**	125	47	186
8	**1**	95	78	312
9	**2**	95	86	344
10	**4**	95	64	255
11	**5**	95	6	23
12	**6**	95	14	55
13	**6**	155	16	62

[a] Conditions: 1 bar CO_2 (2 mmol), 50 bar H_2, 5 μmol of **1-6**, 0.25 mmol of K_3PO_4, 7.6 mmol **A-7**, 1.5 h.

The evaluation of temperature on CO_2 hydrogenation was first evaluated using **3** since it was found to be the most effective catalyst for DMC hydrogenation. Starting at 30 ºC (entry 1), only 3 turnovers of DMF was detected over a 1.5 h time period. Increasing the temperature led to increased formation of DMF with a turnover number of 348 at 95 ºC (entry 5). Temperatures exceeding 95 ºC led to lower yields of DMF, presumably due to the reaction being entropically disfavorable. With the optimized temperature in hand, other catalysts were evaluated. Catalysts **1** and **2**, which are also active for DMF hydrogenation, showed comparable activity to **3** with turnover numbers of 312 and 344 of DMF, respectively. Importantly CH_3OH was not detected under any of these conditions. Catalysts **4-6,** which exclusively hydrogenate CO_2, yielded turnover numbers ranging from 23-255, with **4** being the most active. Hydrogenation of CO_2 with **3** at 125 ºC led to 186 turnovers of DMF, with no CH_3OH detected. These results were somewhat surprising since amide hydrogenation has been precedented to occur at temperatures as low as 110 ºC.

Isothermal CO_2 Hydrogenation to CH_3OH

Ideally, conditions would be identified where CO_2 could be hydrogenated to CH_3OH through DMF at a single temperature. In effort to investigate this, the isothermal hydrogenation of CO_2 was evaluated in Table 4.4.

Table 4.4. Isothermal Capture and Hydrogenation of CO_2 to CH_3OH with **A-7**.[a]

$$CO_2 + H_2 \xrightarrow[\text{THF, 18 h}]{\substack{5\ \mu\text{mol 1-3}\\ 0.25\ \text{mmol } K_3PO_4\\ 7.6\ \text{mmol A-7}}} \underset{(\textbf{DMF})}{H-\overset{\overset{\displaystyle O}{\|}}{C}-NMe_2} + CH_3OH + H_2O$$
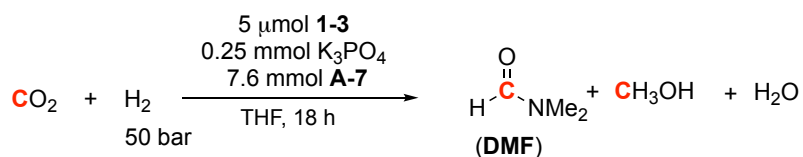
Entry	Catalyst	CO_2 (bar)	Temp. (ºC)	% Conv. of CO_2	DMF TON	CH_3OH TON
1	3	1	135	27	97	9
2	1	1	145	6	24	<1
3	2	1	145	11	33	10
4	3	1	145	10	23	18
5	3	2	145	10	53	29
6	3	2	155	9	32	36
7	3	3	145	5	34	22
8	3	5	145	4	57	25
9	3	10	145	5	210	2
10	3	20	145	4	297	<1

[a] Conditions: 50 bar H_2, 5 μmol of **1-3**, 0.25 mmol of K_3PO_4, 7.6 mmol **A-7**, 18 h.

Increasing the temperature of the **3**-catalyzed CO_2 hydrogenation from 125 °C (shown in Table 4.2, entry 7) to 135 °C (Table 4.3, entry 1) led to lower overall conversion of CO_2; however, 9 turnovers of CH_3OH were detected. Further increasing the temperature to 145 °C doubles the overall yield of CH_3OH (18 turnovers) despite a dramatic decrease in yield of DMF with only 23 turnovers (entry 4). The decreased yield of DMF at elevated temperatures is consistent with the entropically disfavorable nature of CO_2 hydrogenation. Further evaluation of catalysts **1-3** identified **3** as the superior catalyst for this transformation. Increasing the concentration of CO_2 from 1 to 5 bar shown in entries 5-8, led to increased concentrations of DMF (up to 57 turnovers of DMF). Unfortunately, only a modest improvement in CH_3OH was observed. Dramatically increasing the quantity of CO_2 to 10 and 20 bar, led to high turnover numbers of DMF (210 and 297, respectively), with trace quantities of CH_3OH. These results suggest inhibition of DMF hydrogenation by CO_2.

Indeed, introducing a single bar of CO_2 at 145 °C dramatically affected the activity of the catalysts towards DMF reduction, summarized in Table 4.5.

Table 4.5. Evaluation of catalysts **1-3** towards DMF reduction to CH_3OH.[a]
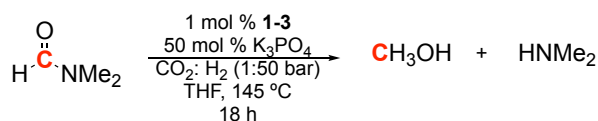
Entry	Catalyst	CH_3OH TON
1	**1**	7
2	**2**	48
3	**3**	67

[a]Conditions: 0.5 mmol DMF, 1 bar CO_2, 50 bar H_2, 5 μmol of catalysts, 0.25 mmol of K_3PO_4, 50 bar H_2, 1.5 mL of THF, 18 h.

These data are consistent with our previous work where we found that, in the case of **1**, the hydrogenation of esters was inhibited by CO_2. Based on this result, Dr. Chelsea Huff examined the effect of CO_2 on catalysts **1** and **2** under reducing conditions. We have shown that **1** reacts directly with CO_2 and CO_2/H_2 to form the products shown in Figure 4.7. Treating **1** with H_2 and CO_2 at 120 °C yielded Ru-CO_2 adduct **1-CO$_2$** in 95% yield after 15 min. where the Ru-formate complex, **1-HCOO**, can also be detected in low yields.
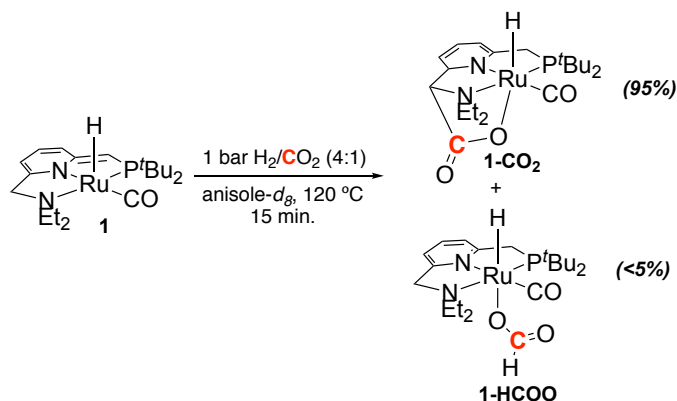
Figure 4.7. Potential pathways for inhibition by CO_2.

Conversely, **2** is blocked at the "N-side" of the pincer arm where CO_2 binding occurs at **1**. In this case, only the Ru-formate complex, **2-HCOO**, is detected at 45 °C (Figure 4.8). This difference in ligand design provides a potential explanation for the variation in yields shown in Table 4.5 entries 1 and 2. Furthermore, the modest improvement from **2** to **3** may result from the absence of a benzylic basic-site on the supporting ligand leading to formation of the formate complex. This highlights a key challenge in the system, where CO_2 concentration needs to be sufficiently high to build an appreciable quantity of DMF, however low enough to prevent catalyst inhibition. The inhibition of DMF hydrogenation by CO_2 makes the isothermal hydrogenation of CO_2 to CH_3OH particularly challenging.
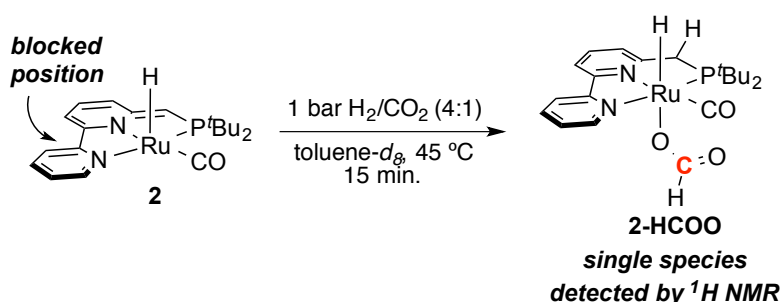
Figure 4.8. Blocked position to prevent formation of CO_2-adduct.

In an effort to improve the hydrogenation of DMF to CH_3OH, we postulated that decreasing the concentration of CO_2 would lead to higher yields of CH_3OH. Inspired by our previous work in cascade hydrogenation (Chapter 3), we envisioned adding a CO_2 hydrogenation catalyst in addition to **3** (catalysts **4-6**) would aid in converting CO_2 to formic acid (step 1) and, consequently, DMF (step 2). Concurrently, **3** reduces CO_2 to DMF and hydrogenates DMF to CH_3OH (step 3). This cascade system (Figure 4.9) is intended to

maximize conversion of CO_2 to DMF to ultimately allow for the unimpeded hydrogenation of DMF to CH_3OH.
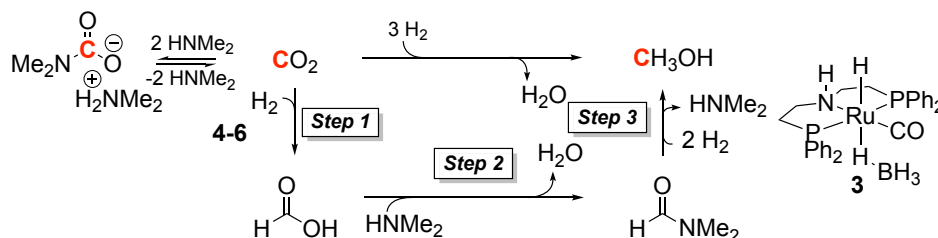
Figure 4.9. Cascade pathway for the hydrogenation of CO_2 to CH_3OH with **4-6** and **3**.

Application of the CO_2 hydrogenation catalysts (**4-6**) to the isothermal CO_2-capture and hydrogenation system is summarized in Table 4.6. Out of the evaluated catalysts, **4** was found to work cooperatively with **3** to convert 88% of CO_2 to a mixture of DMF and CH_3OH (entry 1); however, we remained surprised at the marginal conversion of DMF to CH_3OH despite the decreased concentration of CO_2. Though encouraged by these results, we remained focused on developing an improved method for the hydrogenation of CO_2 to CH_3OH.

Table 4.6. Isothermal cascade hydrogenation of CO_2 to CH_3OH: Combining CO_2 hydrogenation with **3**.
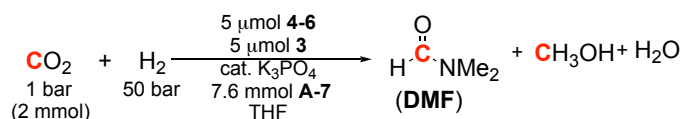
Entry	Catalyst	% Conv. of CO_2	DMF TON	CH_3OH TON
1	**4**	88	315	35
2	**5**	38	151	2
3	**6**	7	20	8

[a] Conditions: 1 bar CO_2 (2 mmol), 50 bar H_2, 5 μmol of **4-6**, 5 μmol of **3**, 0.25 mmol of K_3PO_4, 7.6 mmol of **A-7**, 145 °C.

CO_2 Capture and Hydrogenation to CH_3OH

In facing the challenges of CO_2 reduction isothermally, we next sought to apply the temperature ramp strategy invoked in DMC hydrogenation. These reactions were conducted with 2.5 bar CO_2 and 50 bar H_2 using the same temperature ramp described in Table 4.2, entry 5 (95 °C for 18 h ramping to 155 °C for 18 h). As shown in Table 4.7, entry 1, these conditions resulted in 84% conversion of CO_2 to a mixture of DMF/DMFA (TON = 520) and CH_3OH (TON = 220). Notably, the percent conversion of CO_2 is comparable to the isothermal cascade strategy (Table 4.6, entry 1); however, the

quantity of CH_3OH using the ramp is dramatically higher (35 TONs isothermal vs. 220 with ramp). Extending the time at 155 ºC to 48 h yielded slight increases in conversion (to 92%) and CH_3OH yield (TON = 310) (entry 2). This is consistent with catalyst decomposition at this elevated temperature. Finally, decreasing the loading of **3** to 0.03 mol % resulted in a further increase in the TON of CH_3OH (TON = 567). Overall, these results demonstrate that the combination of an amine, **A-7**, and a ruthenium pincer catalyst, **3**, can be used to convert both CO_2 and CO_2-capture intermediates such as DMC to CH_3OH.

Table 4.7. Catalyst **3/A-7**-Catalyzed Hydrogenation of CO_2 to CH_3OH.[a]

$$CO_2 \ (2.5 \ bar) + H_2 \ (50 \ bar) \xrightarrow[\substack{THF \\ 95\,°C \Rightarrow 155\,°C}]{\substack{cat.\ 3 \\ cat.\ K_3PO_4 \\ 7.6\ mmol\ A\text{-}7}} \underset{\substack{H_2NMe_2 \ (\textbf{DMFA})}}{H\text{-}\overset{O}{C}\text{-}O^{\ominus}} + H\text{-}\overset{O}{C}\text{-}NMe_2 \ (\textbf{DMF}) + CH_3OH + H_2O$$
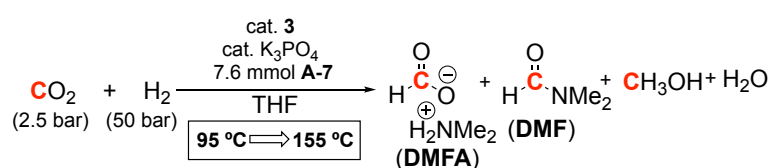
Entry	Loading of **3** (mol %)	Time at 95 ºC (h)	Time at 155 ºC (h)	% conv CO_2	TON CH_3OH	TON DMF + DMFA
1	0.10	18	18	84	220	740
2	0.10	18	36	92	267	623
3	0.03	18	36	86	550	1870

[a] Conditions: 2.5 bar CO_2 (5 mmol), 50 bar H_2, 5 μmol of **3**, 0.25 mmol of K_3PO_4.

Shown in Figure 4.10, substitution of CO_2 with isotopically enriched $^{13}CO_2$ under otherwise identical conditions led to the labeled products of ^{13}C-DMF and $^{13}CH_3OH$. Analysis by ^1H NMR in DMSO-d_6, Figure 4.10, exhibits a doublet at 7.93 ppm with a coupling constant of 190 Hz, consistent with $^{13}C(sp^2)$-H, and another doublet at 3.14 with a coupling constant of 140 Hz, indicative of $^{13}C(sp^3)$-H. These chemical shifts are consistent with ^{13}C-DMF and $^{13}CH_3OH$. Carbon (^{13}C) NMR, Figure 4.11, further verifies a mixture of DMF, CH_3OH, and CO_2. Taken together, this information confirms the origin of DMF and CH_3OH to be derived from CO_2 reduction.
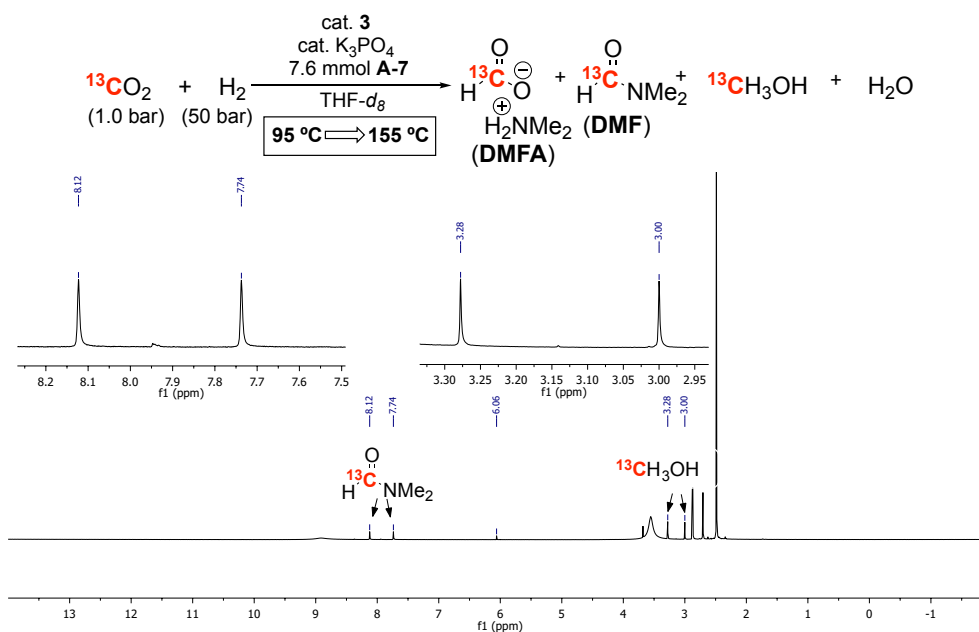
Figure 4.10. Product Analysis for the Hydrogenation of $^{13}CO_2$ to $^{13}CH_3OH$ using Ramp: Representative ^1H NMR Spectrum. Coupling constants for DMF (J = 190 Hz) and CH_3OH (J = 140 Hz) were consistent with $^{13}C(sp^2)$-H and $^{13}C(sp^3)$-H, respectively.
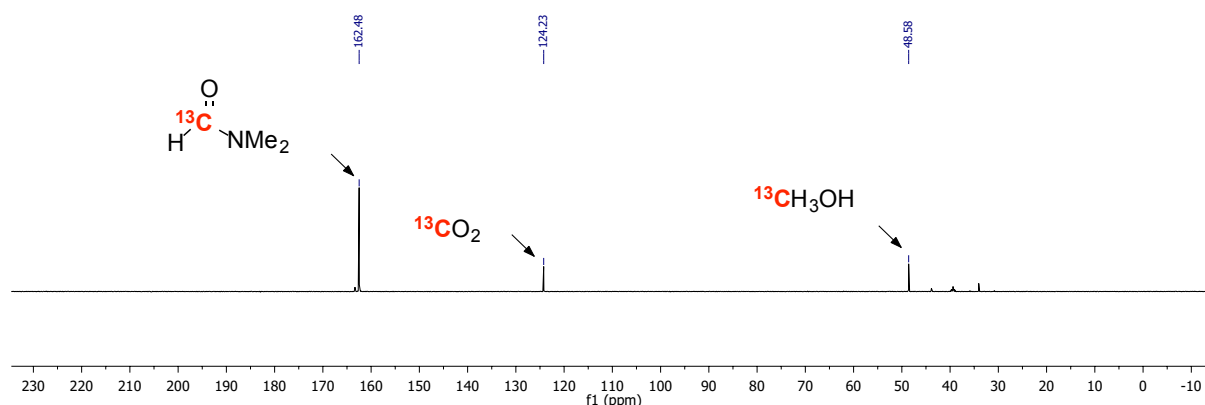
Figure 4.11. Product Analysis for the Hydrogenation of $^{13}CO_2$ to $^{13}CH_3OH$ using Ramp: Representative ^{13}C NMR Spectrum.

With the development of the CO_2 capture and hydrogenation strategy we next sought to elucidate the pathway(s) of reduction. Analysis of the pathway for carbamate hydrogenation (*vide supra*) implicated Path B which contained 4 different carbonyl containing compounds shown in Figure 4.6. We have previously shown that the direct hydrogenation of DMC to CH_3OH was not a viable pathway (Table 4.1, entry 7), and that DMF and CO_2 could be reduced with great efficiency. Up to this point, we were unable to definitively rule out direct hydrogenation of DMFA to CH_3OH. Attempts at discrete hydrogenation of DMFA leads to ambiguous results since DMFA can rapidly undergo

amidation under reaction conditions to yield DMF. To directly evaluate the viability of the hydrogenation of the formate salt, we conducted the experiment outlined in Figure 4.12. Treatment of formic acid with the tertiary amine, triethylamine (NEt_3), yields the triethylammonium formate salt. This salt is unable to undergo amidation to the corresponding formamide, thus providing an excellent substrate for this analysis. Hydrogenation of this salt with **3**, yielded only 8 turnovers of CH_3OH, with no intermediates detected. Based on these results, hydrogenation of DMFA to CH_3OH was not considered a major contributing pathway for CO_2 reduction.
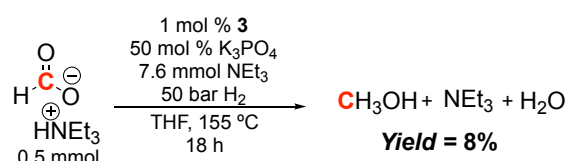
Figure 4.12. Evaluation of the hydrogenation of triethylammonium formate salt by **3**.

Independent analysis of each of the carbonyl containing compounds in pathways A and B allowed for the elucidation of the mechanism. We anticipate that the pathway for CO_2 hydrogenation under the developed conditions would operate under the same mechanism as DMC shown in Figure 4.13. Initially, at room temperature, $NHMe_2$ (**A-7**) sequesters CO_2 as the carbamate salt, DMC. Upon heating to 95 °C, DMC slowly releases CO_2 and two equivalents of $HNMe_2$. At these temperatures CO_2 is hydrogenated by **3** to yield FA. However, this step is thermodynamically unfavorable and requires the off-cycle deprotonation or amidation by $HNMe_2$ to drive the reaction forward. Ultimately, FA and DMFA undergo amidation to DMF. Upon formation of an appreciable quantity of DMF, the temperature is elevated from 95 °C to 155 °C to promote the hydrogenation of DMF to CH_3OH by **3**.
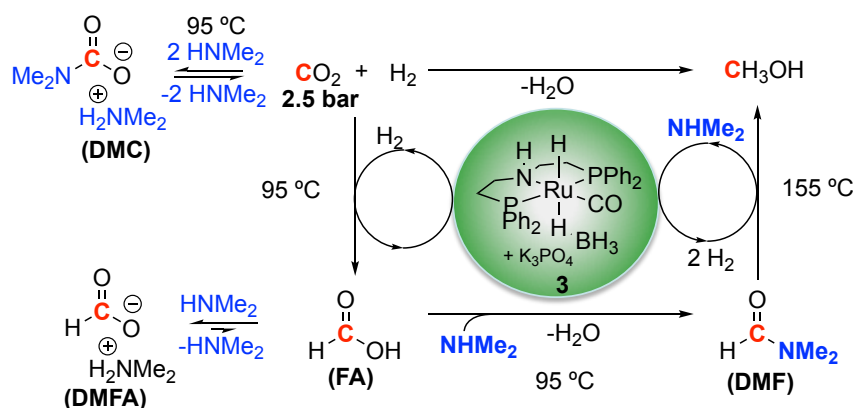
Figure 4.13. Pathway for the **3**- and **A-7**-catalyzed hydrogenation of CO_2 to CH_3OH using temperature ramp strategy.

4.3 Follow-up Studies

Since the publication of our seminal work on CO_2-capture and hydrogenation, this area of research has garnered much interest. Milstein and co-workers utilized an industrially relevant alkanolamine, valinol, to sequester CO_2 as the oxazolidinone shown in Figure 4.14.[66] Subsequent filtration and addition of reagents (**2-Cl**, KOtBu, and H_2) led to the hydrogenation product of CH_3OH and valinol with 53% yield (TON 21) over a 72 h period. Unfortunately, high-loadings of **2-Cl** and KOtBu were necessary to generate modest yields of CH_3OH. Incompatibilities of **2-Cl** with CO_2, necessitated a step-wise pathway wherein CO_2 is captured, the atmosphere of the reactor is vented to release any CO_2 that is not sequestered, and finally, introduction of the catalyst and hydrogen allowed for the formation of methanol.
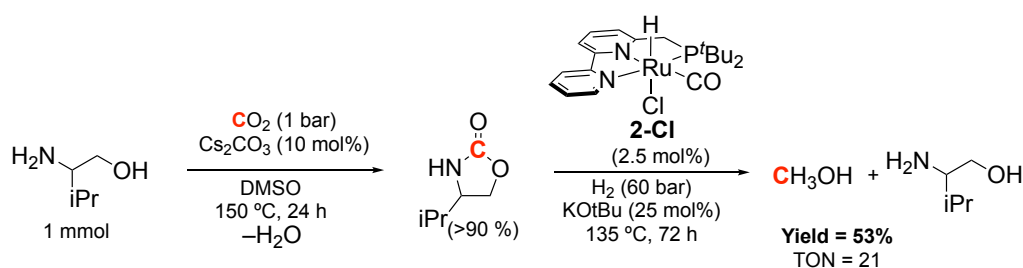
Figure 4.14. Two-step CO_2-capture and hydrogenation strategy by Milstein *et al.*

Ding *et al.*, shown in Figure 4.15, highlight a conceptually similar approach for the *N*-formylation of amines and subsequent hydrogenation to CH_3OH.[67] After a thorough analysis of pincer complexes, Ding and co-workers identified **3-Cl**, the parent complex of **3**, as the optimal catalyst for CO_2 hydrogenation. A variety of primary and secondary amines were *N*-formylated using CO_2 and H_2 with turnover numbers approaching 2,000,000. A one-pot CO_2 to CH_3OH sequential strategy was also employed using morpholine as the amine to yield a formamide intermediate. Subsequent removal of CO_2 and pressurization with H_2 ultimately led to high yields of CH_3OH (36%, 3600 turnovers). Interestingly, discussion of carbamate formation was neglected in this work.
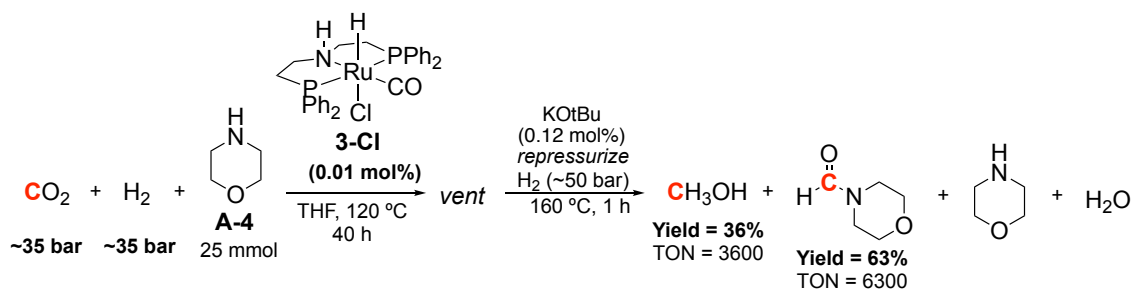
Figure 4.15. Two-step hydrogenation of CO_2 to CH_3OH through a formamide intermediate by Ding *et al*.

A seemingly consistent theme for the CO_2-capture and hydrogenation strategy has been to either vent excess CO_2 after sequestration or chemically consume the residual CO_2. For example, we adopted a temperature ramp to convert large quantities of CO_2 to formamide prior to formamide hydrogenation. In overcoming this limitation, Prakash and Olah identified the use of the polyamine pentaethylenehexamine (PEHA) as an improved CO_2 capturing agent that circumvents the need for a temperature ramp shown in Figure 4.16.[68] Using the parent compound of **3**, **3-Cl**, 3.4 mmol of PEHA (20.4 mmol of accessible CO_2 capturing nitrogens), and 75 bar of CO_2/H_2 (1:4), 10.4 mmol of CH_3OH (520 turnovers) was obtained under isothermal conditions. While the discrete intermediates of the polyamine were not characterized, the hydrogenation of CO_2 CH_3OH is proposed to operate through an analogous mechanism as shown in Figure 4.13.
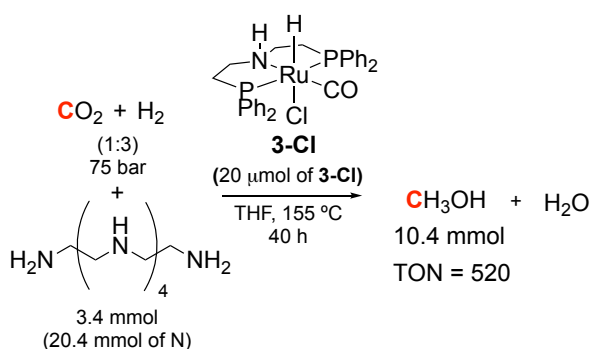
Figure 4.16. Isothermal CO_2-capture and hydrogenation to CH_3OH by Prakash and Olah.

4.4 Conclusions

In summary, this chapter describes the development of a catalytic homogeneous method that enables the capture and reduction of CO_2 to CH_3OH with $NHMe_2$, **A-7**, and ruthenium catalyst **3**. Unlike previous examples of homogeneously catalyzed CO_2 reduction, this process proceeds under basic conditions. The amine is

proposed to play a dual role in this system, directly reacting with CO_2 to produce DMC and also intercepting formate and formic acid intermediates to form DMF. Overall, the current process proceeds with high carbon efficiency, leading to up to 92% conversion of CO_2 to a mixture of DMF and CH_3OH. This process can likely be improved further through the identification of more stable hydrogenation catalysts as well as through advances in reaction/reactor engineering.

4.4 Experimental

General Procedures

All high-pressure reactions were carried out using a Parr Model 5000 Multiple Reactor system that includes six 50 mL vessels equipped with flat-gaskets and head mounting valves. The system was operated by a 4871 process controller and SpecView version 2.5 software. All pressures are reported from the SpecView interface at room temperature. NMR spectra were obtained on a Varian VNMR 500 MHz (500 MHz for ^1H; 126 MHz for ^{13}C). Chemical shifts are reported in parts per million (ppm) and are referenced to an internal standard. The yield of methanol (δ = 3.16 ppm, T_1 = 7.2 s) was quantified by NMR using 1,3,5-trimethoxybenzene (δ = 6.02 ppm, T_1 = 2.8 s) as an internal standard. Peaks at δ = 8.96 (dimethyl ammonium salt), 3.99 (dimethyl ammonium salt), 3.86 (dimethyl ammonium salt), 3.58 (THF), 2.49 (DMSO), and 1.74 (THF) ppm were suppressed (10 Hz) for improved resolution. For each NMR experiment, 4 scans were collected, a 35 s recycle delay was used, and a tip angle of 90° was applied. In several cases, the yield of methanol was also independently determined by gas chromatography using a Shimadzu 17A GC-FID with a Restek Rt®-U-BOND column (divinylbenzene ethylene glycol/dimethylacrylate; 30 m, 0.32 mm ID, 0.10 µm df). The method used was as follows: hold for 10 min at 150 °C, then ramp to 170 °C at 5 °C/min, then hold for an additional 13 min at 170 °C. The retention time of CH_3OH was 3.9 min using this method.

Materials and Methods

Catalysts **1**[1], **2**[2], **4**[69], and **6**[70] were prepared according to the corresponding literature procedures. Carbonylchlorohydrido[bis(2-(diphenylphosphinoethyl)amino] ruthenium(II) (**3**) was purchased from Strem and used as received. All catalytic experiments were conducted in duplicate at minimum, and the reported results represent an average of all the runs. Catalytic experiments were set up under an oxygen-free atmosphere in either a

glovebox or using standard Schlenk techniques. Research grade carbon dioxide (99.999%) and ultra high purity hydrogen (99.999%) were purchased from Metro Welding. $^{13}CO_2$ (^{13}C, 99%, <1% ^{18}O) was purchased from Cambridge Isotope Laboratories. Anhydrous K_3PO_4 (Aldrich, 98%) was ground with a mortar and pestle before use. *N,N*-Dimethylformamide (DMF, Alfa Aesar, 99.8%), nitroethane (Aldrich), tris[2-(diphenylphosphino)ethyl]phosphine (Aldrich), Fe(BF_4) 6H_2O (Aldrich), and 1,3,5-trimethoxybenzene (Acros) were used without further purification. Tetrahydrofuran (THF) was purified using an Innovative Technologies (IT) solvent purification system consisting of a copper catalyst, activated alumina, and molecular sieves. Dimethylamine (**A-7**, Aldrich, anhydrous >99%) was condensed in dry THF using standard Schlenk line techniques to yield a 3.8 M solution of $NHMe_2$ in THF. Dimethylammonium dimethylcarbamate (DMC) was purchased from Aldrich, degassed, and used without further purification. Dimethylsulfoxide-d_6 (DMSO-d_6) and THF-d_8 were purchased from Cambridge Isotope Laboratories and used as received.

Reactor Descriptions

Each vessel is 45 mL in volume and is composed of a well (in which the solid and liquid reagents are charged) and a head, which contains various attachments as described below.

The reactors are made of Hastelloy C, and the wells are 7.5 cm tall and 3 cm in diameter. The heads consist of a pressure transducer and two inlet/outlet valves that can connect to a Parr Model 5000 Multiple Reactor system described above, a safety release valve, and a well for a thermocouple (Figure 4.17).
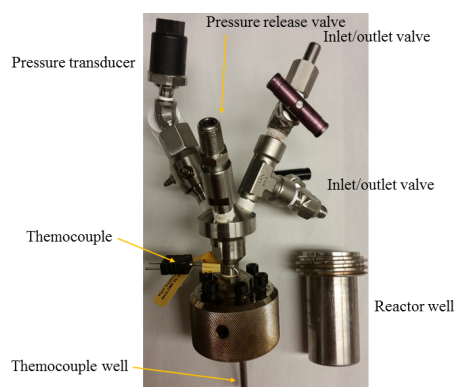
Figure 4.17. Picture of reactor type A with the parts of the reactor labeled.

General Procedure for Hydrogenation Reactions

I. CO$_2$ capture (Figure 4.3)

In a N$_2$-atmosphere dry box, the appropriate amine (5 mmol) was dissolved in 1.5 mL THF, and this solution was added to the metal well of a pressure vessel and an octagonal magnetic stirbar (5/16 x 1/2 in). The vessel was sealed and removed from the dry box. The vessel was pressurized with CO$_2$ (5 bar) at room temperature, and the reaction was stirred with a rate of 800 RPM for 1 hour. The pressure was monitored using the pressure transducer and Specview software.

II. Hydrogenation of DMC (Table 4.1)
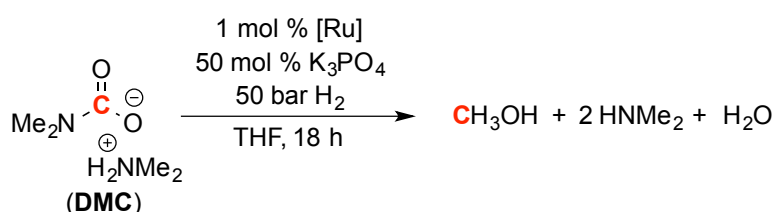
In a N$_2$-atmosphere dry box, the appropriate [Ru] catalyst (2.3 mg of **1**, 2.2 mg of **2,** or 2.9 mg of **3**, 5 μmol, 1 mol %) was dissolved in 1.5 mL THF, and this solution was added to the metal well of a pressure vessel containing K$_3$PO$_4$ (53 mg, 0.250 mmol, 50 mol %) and an octagonal magnetic stirbar (5/16 x 1/2 in). DMC was then added (64 μL, 0.5 mmol, 1 equiv), and the vessel was sealed and removed from the dry box. The vessel was pressurized with H$_2$ at room temperature (50 bar), and the reaction was heated at 155 ºC with a stir rate of 800 RPM. The heating was conducted using Specview software; the temperature was initially set to 115 ºC and then raised to 155 ºC in order to avoid over-shooting the desired temperature. After 18 h of heating, the reaction mixture was allowed to cool to room temperature. The pressure vessel was placed in a –84 °C bath (ethyl acetate/LN$_2$) for 15 min and then carefully vented using a metering valve. THF (0.5 mL) was added through the venting valve of the pressure vessel to wash any residual liquids/solids into the vessel. The vessel was then opened, 1,3,5-trimethoxybenzene (0.178 mmol, 300 μL of 0.593 M solution in DMSO-d_6) was added as a ^{1}H NMR standard, and the contents of the vessel were diluted with DMSO-d_6. 50 μL of the resulting solution was added to an NMR tube, diluted further with DMSO-d_6, and acidified using 12 M HCl to a pH of 2. The sample was then analyzed by ^{1}H NMR spectroscopy with solvent suppression (see Figure 4.18 for a representative ^{1}H NMR spectrum).
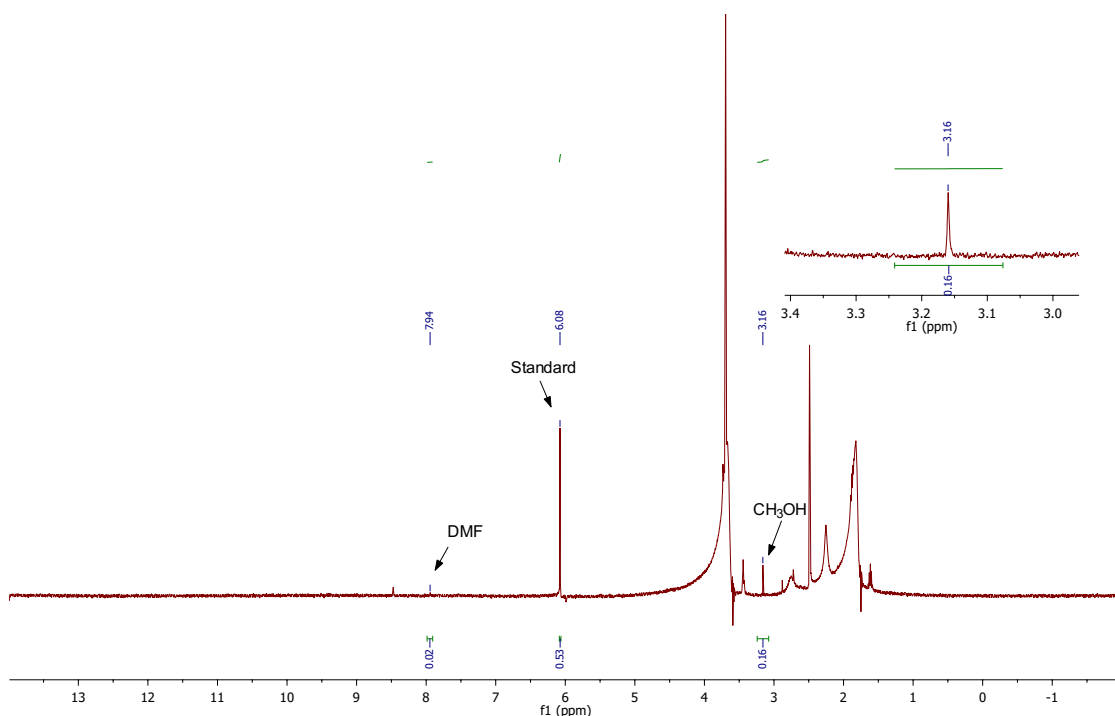
Figure 4.18. Product Analysis for the Hydrogenation of DMC to CH$_3$OH: Representative
^{1}H NMR Spectrum (Table 4.1, entry 6).

III. Hydrogenation of DMF (Figure 4.5a)
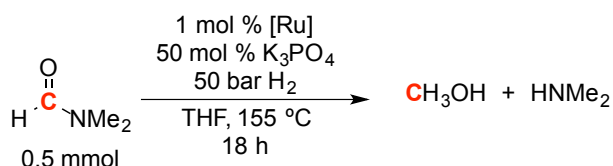
In a N$_2$-atmosphere dry box, **3** (2.9 mg, 5 μmol, 1 mol %) was dissolved in 1.5 mL of THF, and this solution was added to a pressure vessel containing K$_3$PO$_4$ (53 mg, 0.250 mmol, 50 mol %) and an octagonal magnetic stirbar (5/16 x 1/2 in). DMF (40 μL, 0.5 mmol, 100 equiv relative to Ru) was added, and the vessel was then sealed and removed from the dry box. The vessel was pressurized with H$_2$ at room temperature (50 bar), and the reaction was heated at 155 ºC with a stir rate of 800 RPM. The heating was conducted using Specview software; the temperature was initially set to 115 ºC and then raised to 155 ºC in order to avoid over-shooting the desired temperature. After 18 h of heating, the reaction mixture was allowed to cool to room temperature. The pressure vessel was placed in a –84 °C bath (ethyl acetate/LN$_2$) for 15 min and then carefully vented using a metering valve. THF (0.5 mL) was added through the venting valve of the pressure vessel

77

to wash any residual liquids/solids into the vessel. The vessel was then opened, 1,3,5-trimethoxybenzene (0.178 mmol, 300 µL of 0.593 M solution in DMSO-d_6) was added as a ^{1}H NMR standard, and the contents of the vessel were diluted with DMSO-d_6. 50 µL of the resulting solution was added to an NMR tube, diluted further with DMSO-d_6. The sample was then analyzed by ^{1}H NMR spectroscopy with solvent suppression (see Figure 4.19 for a representative spectrum).
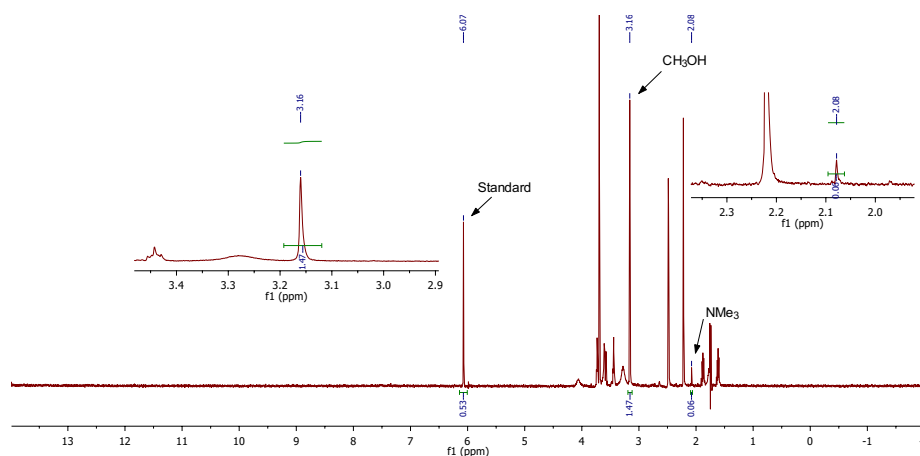
Figure 4.19. Product Analysis for the Hydrogenation of DMF to CH$_3$OH: Representative ^{1}H NMR Spectrum.

IV. Optimization of 3/NHMe$_2$-Catalyzed Hydrogenation of DMC (Table 4.2)
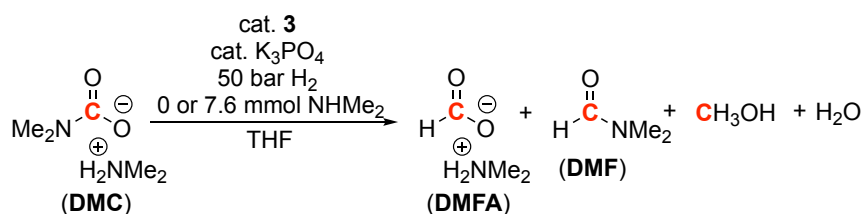
In a N$_2$-atmosphere dry box, catalyst **6** (2.9 mg, 5 µmol) was dissolved in 1.5 mL THF or in 2 mL of a THF and NHMe$_2$ (3.8 M, 7.6 mmol, 1520 equiv relative to Ru) solution. This solution was added to a pre-chilled (in the dry box freezer at –33 °C) metal well of a pressure vessel containing K$_3$PO$_4$ (53 mg, 0.250 mmol, 50 equiv relative to Ru) and an octagonal magnetic stirbar (5/16 x 1/2 in). DMC (64 µL, 0.5 mmol, 100 equiv relative to Ru or 640 µL, 5.0 mmol, 1000 equiv relative to Ru) was added, and the vessel was sealed and removed from the dry box. The vessel was pressurized with H$_2$ at room temperature (50 bar), and the reaction was heated at the desired temperature(s) (95 °C or 95 °C ⇨ 155 °C) with a stir rate of 800 RPM. After the appropriate reaction time (18 h or 36 h), the reaction mixture was allowed to cool to room temperature. The pressure vessel was

placed in a –84 °C bath (ethyl acetate/LN$_2$) for 15 min and then carefully vented using a metering valve. THF (0.5 mL) was added through the venting valve of the pressure vessel to wash any residual liquids/solids into the vessel.

Preparation of samples for NMR analysis: The vessel was opened, 1,3,5-trimethoxybenzene (0.178 mmol, 300 µL of 0.593 M solution in DMSO-d_6) was added as a ^{1}H NMR standard, and the contents of the vessel were diluted with DMSO-d_6. 50 µL of the resulting solution was added to an NMR tube, diluted further with DMSO-d_6, and acidified using 12 M HCl to a pH of 2. The sample was then analyzed by ^{1}H NMR spectroscopy with solvent suppression (see Figure 4.20 for a representative spectrum). The FA observed arises from the protonation of DMFA upon acidic workup.

Preparation of samples for GC-FID analysis: The vessel was opened, nitroethane (1.97 mmol, 140 µL) was added as a GC standard, and the contents of the vessel were diluted with THF. 800 µL of the resulting solution was added to a 2 mL vial and diluted with THF (~ 1 mL). The sample was then analyzed by gas chromatography.
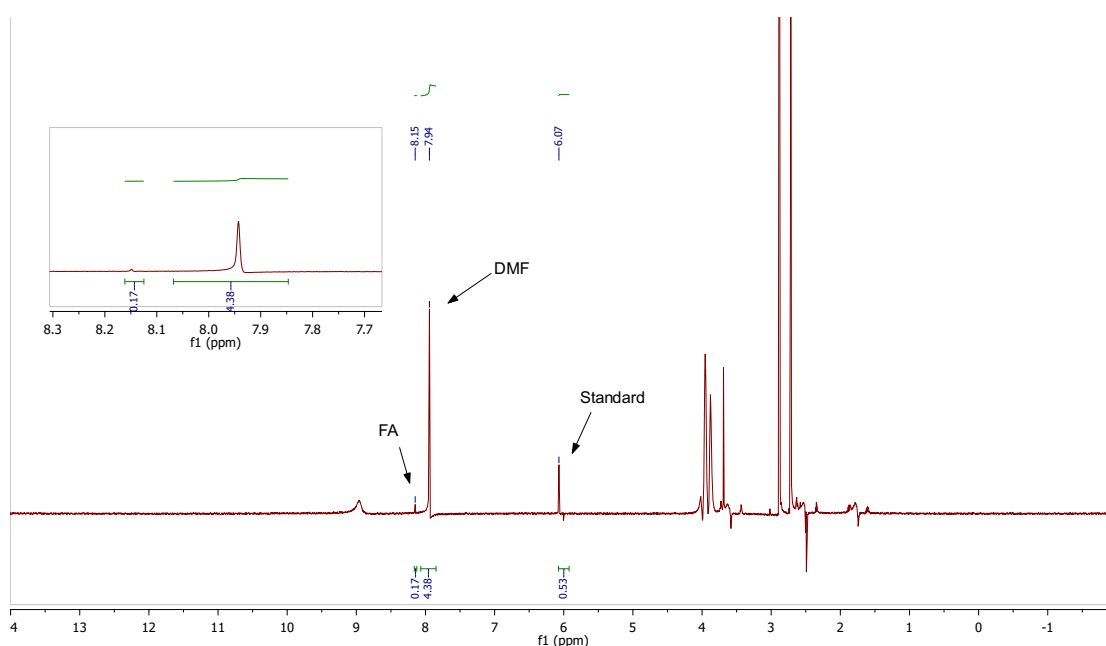
Figure 4.20. Product Analysis for the Hydrogenation of DMC to DMF and CH$_3$OH: Representative ^{1}H NMR Spectrum (Table 4.2, entry 4).

V. Exploration of Isothermal Hydrogenation of CO$_2$ to DMF (Table 4.3)

$$\text{CO}_2 + \text{H}_2 \xrightarrow[\text{THF, 1.5 h}]{\substack{0.25 \text{ mol \% } \textbf{1-6} \\ 12.5 \text{ mol \% K}_3\text{PO}_4 \\ 7.6 \text{ mmol NHMe}_2}} \underset{\substack{\oplus \\ \text{H}_2\text{NMe}_2 \\ (\textbf{DMFA})}}{\text{H}-\overset{\text{O}}{\underset{\ominus}{\overset{\|}{\text{C}}}}\text{O}} + \underset{(\textbf{DMF})}{\text{H}-\overset{\text{O}}{\overset{\|}{\text{C}}}\text{NMe}_2} + \text{H}_2\text{O}$$

1 bar   50 bar

In a N_2-atmosphere dry box, catalyst **1-6** (5 μmol, 0.25 mol %) was dissolved in 2 mL of a THF and NHMe_2 (3.8 M, 7.6 mmol, 1520 equiv relative to Ru) solution. The resulting solution was added to a pre-chilled (in the dry box freezer at –33 ºC) metal well of a pressure vessel containing K_3PO_4 (53 mg, 0.250 mmol, 12.5 mol %) and an octagonal magnetic stirbar (5/16 x 1/2 in). The vessel was sealed and removed from the dry box. The vessel was pressurized with CO_2 (1 bar, approx. 2 mmol, 400 equiv relative to Ru) and then immediately with H_2 (50 bar) at room temperature. The reaction was then heated at the appropriate temperature with a stir rate of 800 RPM. After 1.5 h of heating, the reaction mixture was allowed to cool to room temperature. The pressure vessel was placed in a –84 °C bath (ethyl acetate/LN_2) for 15 min and then carefully vented using a metering valve. THF (0.5 mL) was added through the venting valve of the pressure vessel to wash any residual liquids/solids into the vessel. The vessel was then opened, 1,3,5-trimethoxybenzene (0.178 mmol, 300 µL of 0.593 M solution in DMSO-d_6) was added as a ^{1}H NMR standard, and the contents of the vessel were diluted with DMSO-d_6. 50 µL of the resulting solution was added to an NMR tube, diluted further with DMSO-d_6, and acidified using 12 M HCl to a pH of 2. The sample was then analyzed by ^{1}H NMR spectroscopy with solvent suppression (Figure 4.21) No methanol was detected under these conditions. The FA observed arises from the protonation of DMFA upon acidic workup.
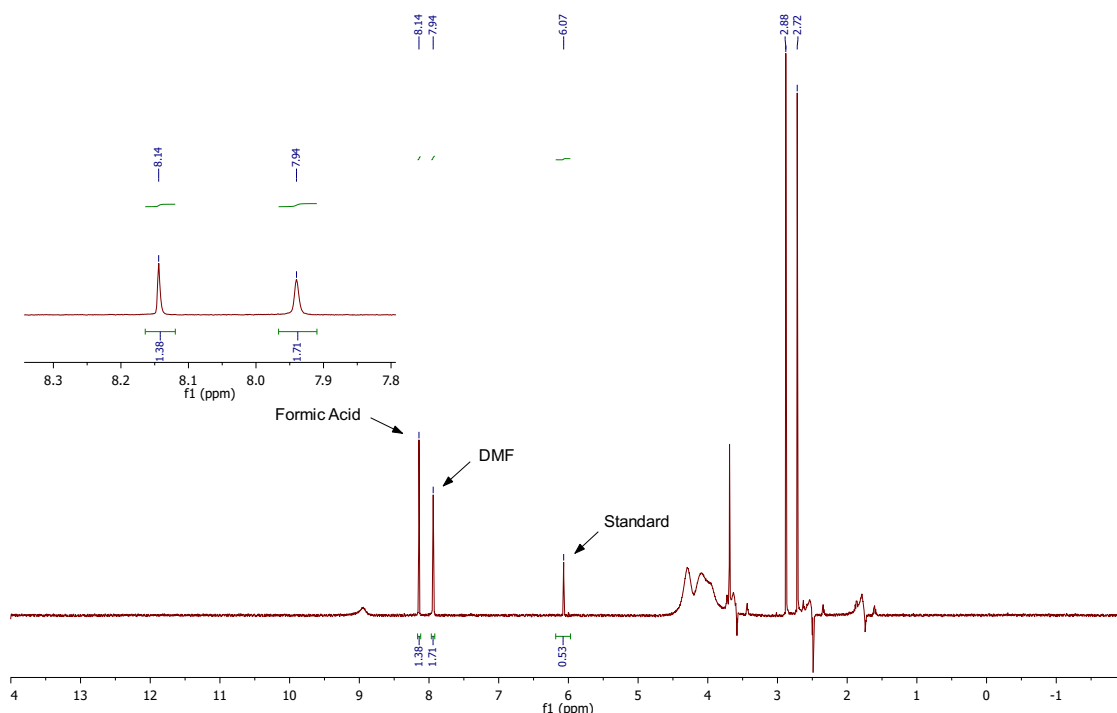
Figure 4.21. Product Analysis for the Hydrogenation of CO_2 to DMF: Representative ^1H NMR Spectrum (Table 4.3, entry 5).

VI. Isothermal Capture and Hydrogenation (Table 4.4)

$$CO_2 \ + \ H_2 \xrightarrow[\text{THF, 18 h}]{\substack{5 \ \mu mol \ \textbf{1-3} \\ 0.25 \ mmol \ K_3PO_4 \\ 7.6 \ mmol \ \textbf{A-7}}} \quad \underset{\textbf{(DMF)}}{H-\overset{\overset{\textstyle O}{\|}}{C}-NMe_2} \ + \ \textbf{C}H_3OH \ + \ H_2O$$

(50 bar)
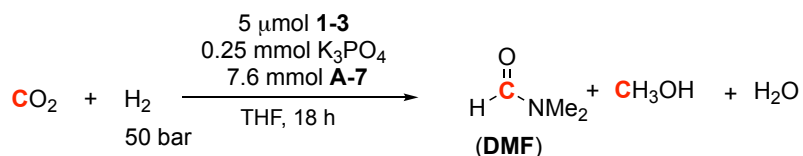
In a N_2-atmosphere dry box, Ru catalyst **1-3** (5 μmol) was dissolved in 2 mL of a THF and NHMe$_2$ (3.8 M, 7.6 mmol, 1520 equiv relative to Ru) solution. The resulting solution was added to a pre-chilled (in the dry box freezer at –33 °C) metal well of the pressure vessel containing K$_3$PO$_4$ (0.250 mmol and an octagonal magnetic stirbar (5/16 x 1/2 in). The vessel was sealed and removed from the dry box. The vessel was pressurized with the appropiate quantity of CO_2 and then immediately with H$_2$ (50 bar) at room temperature. The reaction was then heated to the desired temperature with a stir rate of 800 RPM. After the appropriate reaction time, the reaction mixture was allowed to cool to room temperature. The pressure vessel was placed in a –84 °C bath (ethyl acetate/LN$_2$) for 15 min and then carefully vented using a metering valve. THF (0.5 mL) was added through the venting valve of the pressure vessel to wash any residual liquids/solids into the vessel.

The vessel was then opened, 1,3,5-trimethoxybenzene (0.178 mmol, 300 μL of 0.593 M solution in DMSO-d_6) was added as a ^{1}H NMR standard, and the contents of the vessel were diluted with DMSO-d_6. 50 μL of the resulting solution was added to an NMR tube, diluted further with DMSO-d_6, and acidified using 12 M HCl to a pH of 2. The sample was then analyzed by ^{1}H NMR spectroscopy with solvent suppression. The FA observed arises from the protonation of DMFA upon acidic workup.

VII. Hydrogenation of DMF in the Presence of CO_2 (Table 4.5)

In a N_2-atmosphere dry box, the appropriate catalyst **1-3** (5 μmol, 1 mol %) was dissolved in 1.5 mL of THF, and this solution was added to a pressure vessel containing K_3PO_4 (53 mg, 0.250 mmol, 50 mol %) and an octagonal magnetic stirbar (5/16 x 1/2 in). DMF (40 μL, 0.5 mmol, 100 equiv relative to Ru) was added, and the vessel was then sealed and removed from the dry box. The vessel was pressurized with CO_2 (1 bar) and H_2 (50 bar) at room temperature, and the reaction was heated at 145 ºC with a stir rate of 800 RPM. The heating was conducted using Specview software; the temperature was initially set to 115 ºC and then raised to 155 ºC in order to avoid over-shooting the desired temperature. After 18 h of heating, the reaction mixture was allowed to cool to room temperature. The pressure vessel was placed in a –84 °C bath (ethyl acetate/LN_2) for 15 min and then carefully vented using a metering valve. THF (0.5 mL) was added through the venting valve of the pressure vessel to wash any residual liquids/solids into the vessel. The vessel was then opened, 1,3,5-trimethoxybenzene (0.178 mmol, 300 μL of 0.593 M solution in DMSO-d_6) was added as a ^{1}H NMR standard, and the contents of the vessel were diluted with DMSO-d_6. 50 μL of the resulting solution was added to an NMR tube, diluted further with DMSO-d_6. The sample was then analyzed by ^{1}H NMR spectroscopy with solvent suppression.

VIII. Isothermal cascade hydrogenation of CO_2 to CH_3OH (Table 4.6)
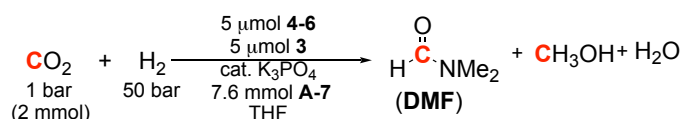
In a N_2-atmosphere dry box, the appropriate catalyst **3** (5 μmol) and catalyst **4-6** (5 μmol) was dissolved in 1.5 mL of THF, and this solution was added to a pressure vessel containing K_3PO_4 (53 mg, 0.250 mmol, 50 mol %) and an octagonal magnetic stirbar (5/16 x 1/2 in). The vessel was then sealed and removed from the dry box. The vessel was pressurized with CO_2 (1 bar) and H_2 (50 bar) at room temperature, and the reaction was heated at 145 ºC with a stir rate of 800 RPM. The heating was conducted using Specview software. After 18 h of heating, the reaction mixture was allowed to cool to room temperature. The pressure vessel was placed in a –84 °C bath (ethyl acetate/LN_2) for 15 min and then carefully vented using a metering valve. THF (0.5 mL) was added through the venting valve of the pressure vessel to wash any residual liquids/solids into the vessel. The vessel was then opened, 1,3,5-trimethoxybenzene (0.178 mmol, 300 μL of 0.593 M solution in DMSO-d_6) was added as a ^{1}H NMR standard, and the contents of the vessel were diluted with DMSO-d_6. 50 μL of the resulting solution was added to an NMR tube, diluted further with DMSO-d_6. The sample was then analyzed by ^{1}H NMR spectroscopy with solvent suppression.

IX. Hydrogenation of CO_2 to CH_3OH with Temperature Ramp (Table 4.7)
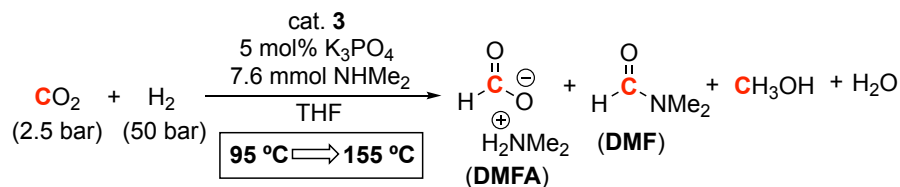
Table 4.8. Comparison of the Yield of CH_3OH in Table 4.7 by NMR and GC-FID.

Entry	Solvent	Analysis Conditions	CH_3OH TON
1	THF	NMR- Solvent Suppression	220 ± 31
2	THF-d_8	NMR - No Solvent Suppression	155 ± 16
3	THF	GC-FID	180 ± 23

In a N_2-atmosphere dry box, Ru catalyst **6** (2.9 mg, 5 μmol, 0.10 mol % or 1.0 mg, 1.7 μmol, 0.03 mol %) was dissolved in 2 mL of a THF (or THF-d_8) and NHMe$_2$ (3.8 M, 7.6 mmol, 1520 equiv relative to Ru or 4470 equiv relative to Ru) solution. The resulting solution was added to a pre-chilled (in the dry box freezer at –33 ºC) metal well of the

pressure vessel containing K_3PO_4 (0.250 mmol, 5 mol %) and an octagonal magnetic stirbar (5/16 x 1/2 in). The vessel was sealed and removed from the dry box. The vessel was pressurized with CO_2 (2.5 bar, approx. 5 mmol, 1000 equiv relative to Ru or 2941 equiv relative to Ru) and then immediately with H_2 (50 bar) at room temperature. The reaction was then heated using the temperature ramp (95 °C ⇨ 155 °C) with a stir rate of 800 RPM. After the appropriate reaction time, the reaction mixture was allowed to cool to room temperature. The pressure vessel was placed in a –84 °C bath (ethyl acetate/LN_2) for 15 min and then carefully vented using a metering valve. THF (0.5 mL) was added through the venting valve of the pressure vessel to wash any residual liquids/solids into the vessel. The vessel was then opened, 1,3,5-trimethoxybenzene (0.178 mmol, 300 µL of 0.593 M solution in DMSO-d_6) was added as a ^{1}H NMR standard, and the contents of the vessel were diluted with DMSO-d_6. 50 µL of the resulting solution was added to an NMR tube, diluted further with DMSO-d_6, and acidified using 12 M HCl to a pH of 2. The sample was then analyzed by ^{1}H NMR spectroscopy with solvent suppression (Figure 4.22 or Figure 4.23). The FA observed arises from the protonation of DMFA upon acidic workup.

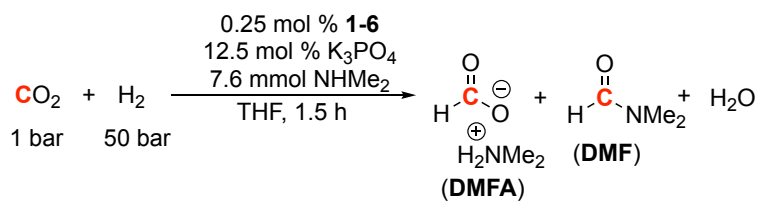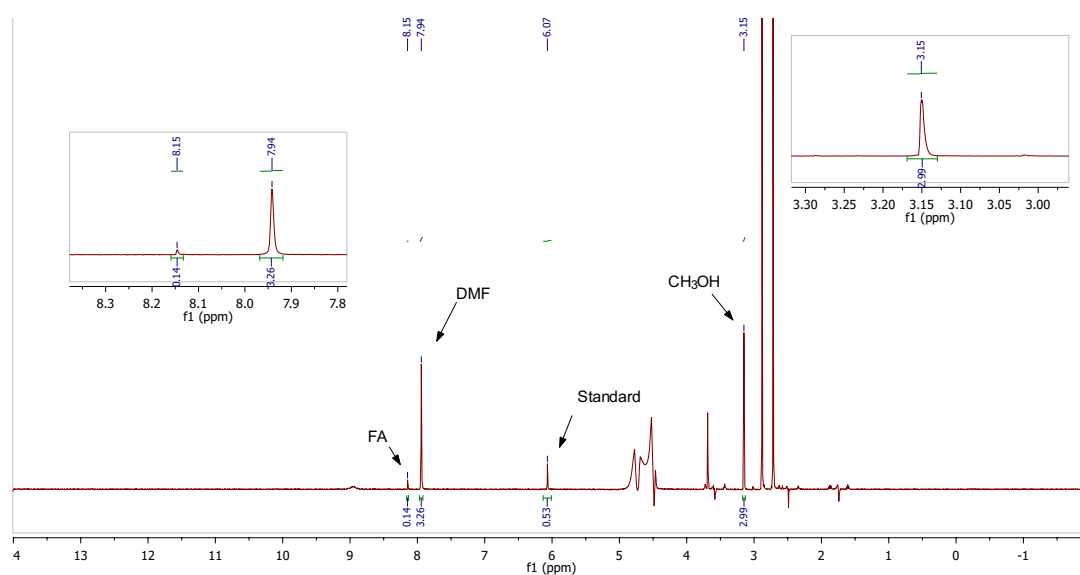**Figure 4.22.** Product Analysis for the Hydrogenation of CO_2 to CH_3OH using Ramp: Representative ^{1}H NMR Spectrum (Table 4.7, entry 3).
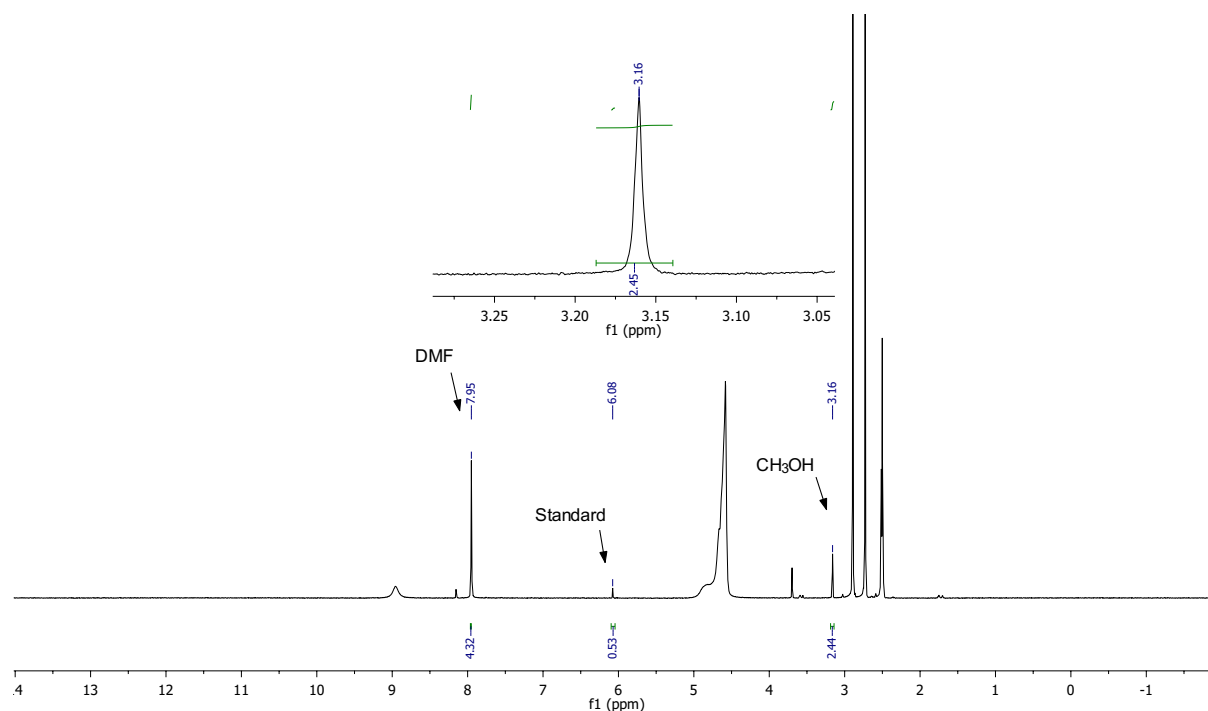
Figure 4.23. Product Analysis for the Hydrogenation of CO_2 to CH_3OH in THF-d_8 using Ramp: Representative ^{1}H NMR Spectrum (Table 4.8, entry 2).

X. Hydrogenation of [13]CO_2 to [13]CH_3OH with Temperature Ramp
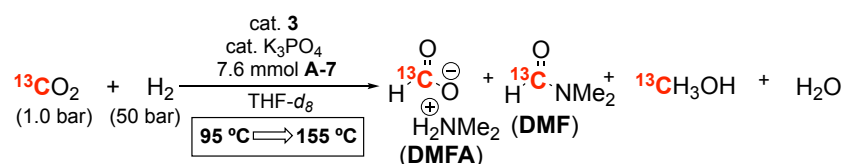
In a N_2-atmosphere dry box, Ru catalyst **6** (2.9 mg, 5 μmol, 0.10 mol %) was dissolved in 2 mL of a THF-d_8 solution of $NHMe_2$ (3.8 M, 7.6 mmol, 1520 equiv relative to Ru or 4470 equiv relative to Ru). The resulting solution was added to a pre-chilled (in the dry box freezer at –33 ºC) metal well of the pressure vessel containing K_3PO_4 (0.250 mmol, 5 mol %) and an octagonal magnetic stirbar (5/16 x 1/2 in). The vessel was sealed and removed from the dry box. The vessel was pressurized with [13]CO_2 (1 bar, approx. 2 mmol, 1000 equiv relative to Ru) and then immediately with H_2 (50 bar) at room temperature. The reaction was then heated using the temperature ramp (95 ºC ⇨ 155 ºC) with a stir rate of 800 RPM. After the appropriate reaction time (36 h), the reaction mixture was allowed to cool to room temperature. The pressure vessel was placed in a –84 °C bath (ethyl acetate/LN_2) for 15 min and then carefully vented using a metering valve. DMSO-d_6 (0.5 mL) was added through the venting valve of the pressure vessel to wash any residual liquids/solids into the vessel. The vessel was then opened, 1,3,5-trimethoxybenzene

(0.178 mmol, 300 µL of 0.593 M solution in DMSO-d_6) was added as a ^{1}H NMR standard, and the contents of the vessel were diluted with DMSO-d_6. 50 µL of the resulting solution was added to an NMR tube, diluted further with DMSO-d_6, and acidified using 12 M HCl to a pH of 2. The sample was then analyzed by ^{1}H NMR spectroscopy.

VII. Exploration of the Hydrogenation of $HCO_2^-NEt_3H^+$
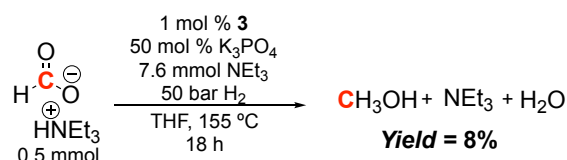
In a N_2-atmosphere dry box, formic acid (19 µL, 0.5 mmol, 100 equiv) was added to a solution of NEt_3 (70 µL, 0.5 mmol, 100 equiv) in 1.5 mL of THF. The resulting solution was used to dissolve **6** (2.9 mg, 5 µmol, 1 mol %) and was added to a pressure vessel containing K_3PO_4 (53 mg, 0.250 mmol, 50 mol %) and an octagonal magnetic stirbar (5/16 x 1/2 in). NEt_3 (1.06 mL, 7.6 mmol, 1520 equiv relative to Ru) was added, and the vessel was then sealed and removed from the dry box. The vessel was pressurized with H_2 at room temperature (50 bar), and the reaction was heated at 155 ºC with a stir rate of 800 RPM. The heating was conducted using Specview software; the temperature was initially set to 115 ºC and then raised to 155 ºC in order to avoid over-shooting the desired temperature. After 18 h of heating, the reaction mixture was allowed to cool to room temperature. The pressure vessel was placed in a –84 °C bath (ethyl acetate/LN_2) for 15 min and then carefully vented using a metering valve. THF (0.5 mL) was added through the venting valve of the pressure vessel to wash any residual liquids/solids into the vessel. The vessel was then opened, 1,3,5-trimethoxybenzene (0.178 mmol, 300 µL of 0.593 M solution in DMSO-d_6) was added as a ^{1}H NMR standard, and the contents of the vessel were diluted with DMSO-d_6. 50 µL of the resulting solution was added to an NMR tube, diluted further with DMSO-d_6. The sample was then analyzed by ^{1}H NMR spectroscopy with solvent suppression (see Figure 4.24 for a representative spectrum).
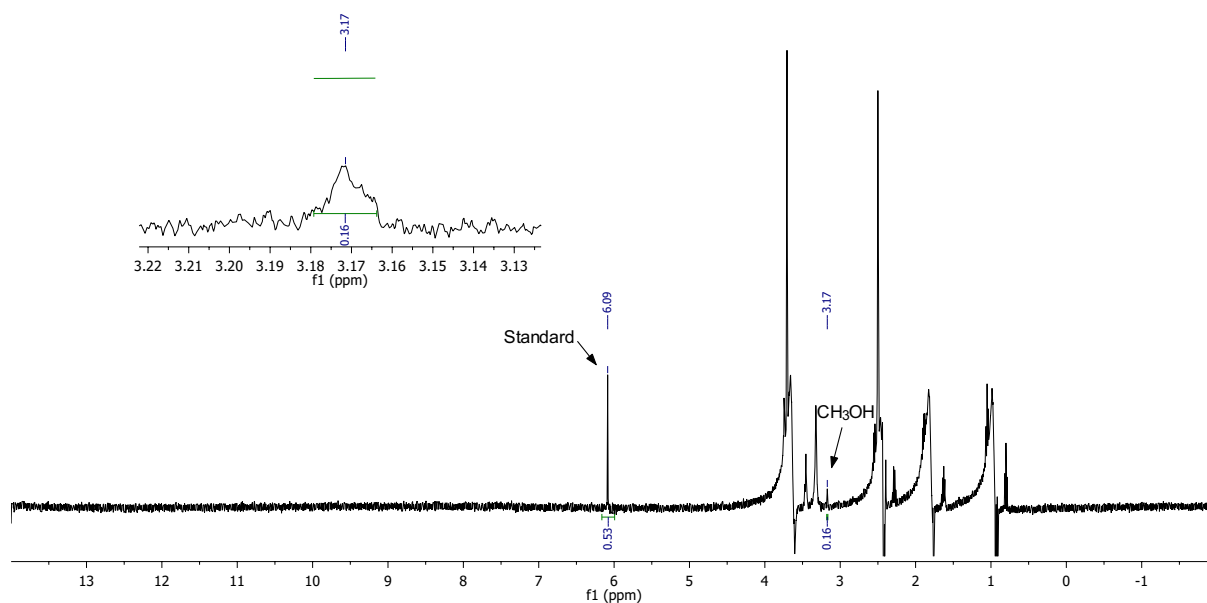
Figure 4.24. Product Analysis for the Hydrogenation of $HCO_2^-NEt_3H^+$ at 155 °C: Representative ^1H NMR Spectrum.

4.5 References

(1) Rezayee, N. M.; Huff, C. A.; Sanford, M. S. *J. Am. Chem. Soc.* **2015**, *137*, 1028.

(2) Kamijo, T.; Sorimachi, Y.; Shimada, D.; Miyamoto, O.; Endo, T.; Nagayasu, H.; Mangiaracina, A. *Energy Procedia* **2013**, *37*, 813.

(3) Pera-Titus, M. *Chem. Rev.* **2013**, *114*, 1413.

(4) *Inventory of U.S. Greenhouse Gas Emissions and Sinks: 1990–2012* **2014**.

(5) Figueroa, J. D.; Fout, T.; Plasynski, S.; McIlvried, H.; Srivastava, R. D. *Int. J. Greenh. Gas Control* **2008**, *2*, 9.

(6) Yang, H.; Xu, Z.; Fan, M.; Gupta, R.; Slimane, R. B.; Bland, A. E.; Wright, I. *J. Environ. Sci.* **2008**, *20*, 14.

(7) Macdowell, N.; Florin, N.; Buchard, A.; Hallett, J.; Galindo, A.; Jackson, G.; Adjiman, C. S; Williams, C. K.; Shah, N.; Fennell, P. *Energy Environ. Sci.* **2010**, *3*, 1645.

(8) Corsten, M.; Ramírez, A.; Shen, L.; Koornneef, J.; Faaij, A. *Int. J. Greenh. Gas Control* **2013**, *13*, 59.

(9) Appel, A. M.; Bercaw, J. E.; Bocarsly, A. B.; Dobbek, H.; DuBois, D. L.; Dupuis, M.; Ferry, J. G.; Fujita, E.; Hille, R.; Kenis, P. J. A.; Kerfeld, C. A.; Morris, R. H.; Peden, C. H.

F.; Portis, A. R.; Ragsdale, S. W.; Rauchfuss, T. B.; Reek, J. N. H.; Seefeldt, L. C.; Thauer, R. K.; Waldrop, G. L. *Chem. Rev.* **2013**, *113*, 6621.

(10) Darensbourg, D. J. *Inorg. Chem.* **2010**, *49*, 10765.

(11) Riduan, S. N.; Zhang, Y. G. *Dalton Trans.* **2010**, *39*, 3347.

(12) Dibenedetto, A.; Angelini, A.; Stufano, P. *J. Chem. Technol. Biot.* **2014**, *89*, 334.

(13) Leitner, W. *Angew. Chem. Int. Ed.* **1995**, *34*, 2207.

(14) Grabow, L. C.; Mavrikakis, M. *ACS Catal.* **2011**, *1*, 365.

(15) Choudhury, J. *ChemCatChem* **2012**, *4*, 609.

(16) Li, Y. H.; Junge, K.; Beller, M. *ChemCatChem* **2013**, *5*, 1072.

(17) Li, Y. N.; Ma, R.; He, L. N.; Diao, Z. F. *Catal. Sci. Tech.* **2014**, *4*, 1498.

(18) Waller, D.; Stirling, D.; Stone, F. S.; Spencer, M. S. *Faraday Discuss. Chem. Soc.* **1989**, *87*, 107.

(19) Spencer, M. S. *Top. Catal.* **1999**, *8*, 259.

(20) Martino, G.; Courty, P.; Marcilly, C.; Kochloefl, K.; Lunsford, J. H. In *Handbook of Heterogeneous Catalysis*; Wiley-VCH Verlag GmbH: 1997, p 1801.

(21) Eisenschmid, T. C.; Eisenberg, R. *Organometallics* **1989**, *8*, 1822.

(22) Riduan, S. N.; Zhang, Y.; Ying, J. Y. *Angew. Chem. Int. Ed.* **2009**, *48*, 3322.

(23) Chakraborty, S.; Zhang, J.; Krause, J. A.; Guan, H. *J. Am. Chem. Soc.* **2010**, *132*, 8872.

(24) Huang, F.; Lu, G.; Zhao, L.; Li, H.; Wang, Z. X. *J. Am. Chem. Soc.* **2010,** *132*, 12388.

(25) Huang, F.; Zhang, C.; Jiang, J.; Wang, Z.-X.; Guan, H. *Inorg. Chem.* **2011**, *50*, 3816.

(26) Riduan, S. N.; Ying, J. Y.; Zhang, Y. G. *ChemCatChem* **2013**, *5*, 1490.

(27) Wang, B. J.; Cao, Z. X. *R. Soc. Chem. Adv.* **2013**, *3*, 14007.

(28) LeBlanc, F. A.; Piers, W. E.; Parvez, M. *Angew. Chem. Int. Ed.* **2014**, *53*, 789.

(29) Anker, M. D.; Arrowsmith, M.; Bellham, P.; Hill, M. S.; Kociok-Kohn, G.; Liptrot, D. J.; Mahon, M. F.; Weetman, C. *Chem. Sci.* **2014**, *5*, 2826.

(30) Ashley, A. E.; Thompson, A. L.; O'Hare, D. *Angew. Chem. Int. Ed.* **2009**, *48*, 9839.

(31) Ménard, G.; Stephan, D. W. *J. Am. Chem. Soc.* **2010**, *132*, 1796.

(32) Stephan, D. W.; Erker, G. *Angew. Chem. Int. Ed.* **2010**, *49*, 46.

(33) Sgro, M. J.; Stephan, D. W. *Angew. Chem. Int. Ed.* **2012**, *51*, 11343.

(34) Zhu, J.; An, K. *Chem. Asian J.* **2013**, *8*, 3147.

(35) Courtemanche, M. A.; Legare, M. A.; Maron, L.; Fontaine, F. G. *J. Am. Chem. Soc.* **2013**, *135*, 9326.

(36) Courtemanche, M. A.; Legare, M. A.; Maron, L.; Fontaine F. G. *J. Am. Chem. Soc.* **2014**, *136*, 10708.

(37) Wang, T.; Stephan, D. W. *Chem. Commun.* **2014**, *50*, 7007.

(38) Anker, M. D.; Arrowsmith, M.; Bellham, P.; Hill, M. S.; Kociok-Kohn, G.; Liptrot, D. J.; Mahon, M. F.; Weetman, C. *Chem. Sci.* **2014**, *5*, 2826.

(39) Fontaine, F. G.; Courtemanche, M. A.; Legare, M. A. *Chem. Eur. J.* **2014**, *20*, 2990.

(40) Tominaga, K.; Sasaki, Y.; Kawai, M.; Watanabe, T.; Saito, M. *J. Chem. Soc., Chem. Commun.* **1993**, 629.

(41) Tominaga, K.; Sasaki, Y.; Watanabe, T.; Saito, M. *Bull. Chem. Soc. Jpn.* **1995**, *68*, 2837.

(42) Huff, C. A.; Sanford, M. S. *J. Am. Chem. Soc.* **2011**, *133*, 18122.

(43) Balaraman, E.; Gunanathan, C.; Zhang, J.; Shimon, L. J. W.; Milstein, D. *Nat. Chem.* **2011**, *3*, 609.

(44) Wesselbaum, S.; vom Stein, T.; Klankermeyer, J.; Leitner, W. *Angew. Chem. Int. Ed.* **2012**, *51*, 7499.

(45) Wesselbaum, S.; Moha, V.; Meuresch, M.; Brosinski, S.; Thenert, K. M.; Kothe, J.; Stein, T. v.; Englert, U.; Holscher, M.; Klankermayer, J.; Leitner, W. *Chem. Sci.* **2015**, *6*, 693.

(46) Yadav, M.; Linehan, J. C.; Karkamkar, A. J.; van der Eide, E.; Heldebrant, D. J. *Inorg. Chem.* **2014**, *53*, 9849.

(47) Rochelle, G. T. *Science* **2009**, *325*, 1652.

(48) Jacquet, O.; Frogneux, X.; Das Neves Gomes, C.; Cantat, T. *Chem. Sci.* **2013**, *4*, 2127.

(49) Beydoun, K.; Vom Stein, T.; Klankermayer, J.; Leitner, W. *Angew. Chem. Int. Ed.* **2013**, *52*, 9554.

(50) Li, Y.; Sorribes, I.; Yan, T.; Junge, K.; Beller, M. *Angew. Chem. Int. Ed.* **2013**, *52*, 12156.

(51) Beydoun, K.; Ghattas, G.; Thenert, K.; Klankermayer, J.; Leitner, W. *Angew. Chem. Int. Ed.* **2014**, *53*, 11010.

(52) Sorribes, I.; Junge, K.; Beller, M. *Chem. Eur. J.* **2014**, *20*, 7878.

(53) John, J. M.; Bergens, S. H. *Angew. Chem. Int. Ed.* **2011**, *50*, 10377.

(54) Kuriyama, W.; Matsumoto, T.; Ogata, O.; Ino, Y.; Aoki, K.; Tanaka, S.; Ishida, K.; Kobayashi, T.; Sayo, N.; Saito, T. *Org. Process Res. Dev.* **2012**, *16*, 166.

(55) Balaraman, E.; Gnanaprakasam, B.; Shimon, L. J. W.; Milstein, D. *J. Am. Chem. Soc.* **2010**, *132*, 16756.

(56) Oldenhuis, N. J.; Dong, V. M.; Guan, Z. *Tetrahedron* **2014**, *70*, 4213.

(57) Noyori, R.; Ohkuma, T. *Angew. Chem. Int. Ed.* **2001**, *40*, 40.

(58) Hamilton, R. J.; Bergens, S. H. *J. Am. Chem. Soc.* **2006**, *128*, 13700.

(59) Clarke, M. L.; Diaz-Valenzuela, M. B.; Slawin, A. M. Z. *Organometallics* **2007**, *26*, 16.

(60) Saudan, L. A.; Saudan, C. M.; Debieux, C.; Wyss, P. *Angew. Chem. Int. Ed.* **2007**, *46*, 7473.

(61) Huff, C. A.; Sanford, M. S. *ACS Catal.* **2013**, *3*, 2412.

(62) Dub, P. A.; Henson, N. J.; Martin, R. L.; Gordon, J. C. *J. Am. Chem. Soc.* **2014**, *136*, 3505.

(63) Jessop, P. G.; Hsiao, Y.; Ikariya, T.; Noyori, R. *J. Am. Chem. Soc.* **1994**, *116*, 8851.

(64) Jessop, P. G.; Hsiao, Y.; Ikariya, T.; Noyori, R. *J. Am. Chem. Soc.* **1996**, *118*, 344.

(65) Jessop, P. G. In *The Handbook of Homogeneous Hydrogenation*; Wiley-VCH Verlag GmbH: 2008, p 489.

(66) Khusnutdinova, J. R.; Garg, J. A.; Milstein, D. *ACS Catal.* **2015**, *5*, 2416.

(67) Zhang, L.; Han, Z.; Zhao, X.; Wang, Z.; Ding, K. *Angew. Chem. Int. Ed.* **2015**, *54*, 6186.

(68) Kothandaraman, J.; Goeppert, A.; Czaun, M.; Olah, G. A.; Prakash, G. K. S. *J. Am. Chem. Soc.* **2016**, *138*, 778.

(69) Mainz, V. V.; Andersen, R. A. *Organometallics* **1984**, *3*, 675.

(70) Tanaka, R.; Yamashita, M.; Nozaki, K. *J. Am. Chem. Soc.* **2009**, *131*, 14168.

CHAPTER 5: DEVELOPMENT OF AN IRON-BASED AMIDE HYDROGENATION CATALYST AND APPLICATION FOR THE CONVERSION OF CO$_2$ TO CH$_3$OH

The chemistry detailed in this chapter has been made possible with Danielle C. Samblanet and Prof. Melanie S. Sanford. The work described was performed in part of the Center for Enabling New Technologies Through Catalysis. Portions of this work have been published.[83]

5.1 INTRODUCTION

The hydrogenation of carboxylic acid derivatives represents an atom-economical reduction process with potential applications in both industrial and academic settings.[1,2] The vast majority of homogeneous catalysts for these transformations involve 2nd or 3rd row transition metals (e.g., Ru, Rh, Pd, Pt).[3,4,5] In contrast, there are fewer examples of the hydrogenation of carboxylic acid derivatives using earth-abundant first row metal catalysts.[6,7] Recent efforts towards this goal have focused on Fe-based catalysts for the hydrogenation of aldehydes,[8,9,10,11] ketones,[8, 9, 10, 11,12,13,14,15,16] and esters.[17,18,19,20,21] However, analogous Fe-catalyzed hydrogenations of less electrophilic amide derivatives remain largely unexplored.[22,23] These weakly electrophilic substrates are expected to be particularly challenging for Fe catalysts due to the anticipated lower hydricity of first row metal-hydrides compared to their second- and third-row counterparts.[24,25]

Classical methods for amide hydrogenation require the use of stoichiometric reductants such as lithium aluminum hydride (LAH) or samarium iodide (SmI$_2$).[3] These

reductions occur with either C–O or C–N bond scission to yield distinct sets of products (Figure 5.1).[3] Typically, LAH yields the C–O bond cleavage product,[26,27] while SmI_2 is selective for C–N bond scission.[28]
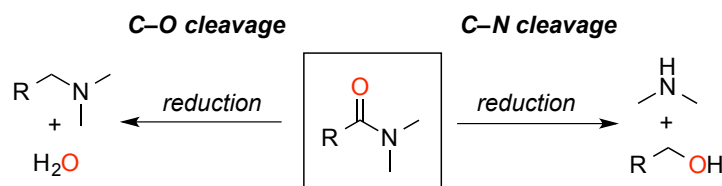
Figure 5.1. Pathways for amide reduction.

The transition metal-catalyzed hydrogenation of amides represents a mild alterative to LAH or SmI_2-mediated processes. Recent reports have described homogeneous Ru catalysts for this transformation[29,30,31,32,33,34,35,36,37,38,39,40,41,42,43] and have demonstrated that selective C–N cleavage can be achieved by appropriate choice of supporting ligands. Figure 5.2a shows one of the mildest and most general reported examples involving catalyst Ru-**1**.[29] First reported by Milstein *et al.*, **Ru-1** catalyzes the hydrogenolysis of a series of 3º and 2º amides to their corresponding alcohols and amines. The basic-site of the dearomatized bipyridine in **Ru-1** participates cooperatively with the Ru center to heterolytically cleave H_2 and generate a metal hydride[44,45,46,47] that then reacts with amide electrophiles. Remarkably, this catalyst is effective under relatively mild conditions (10 bar H_2 at 110 ºC). Recently, Milstein *et al.*, have disclosed the first catalyst derived from an earth-abundant metal (**Fe-1**) that, in combination with KHMDS (potassium hexamethyldisilazide), hydrogenates activated amides to the corresponding amine and alcohol using 60 bar H_2 at 140 ºC (Figure 5.2b).[22] In stark contrast with the Ru analog, **Fe-1** is unreactive towards unactivated substrates such as *N*-phenylacetamide. This highlights the dramatic reduction in hydricity of first-row complexes compared to their second-row counterparts resulting from decreased electron density at the metal centers.[24, 25]

We sought to develop an analogous Fe-catalyzed hydrogenation of unactivated amides and to conduct a detailed investigation of catalysts, conditions, and scope. Furthermore, we sought to benchmark the best Fe-catalyst to its 2nd-row congener. At the start of our investigation, there were no reported examples of homogeneous Fe-catalyzed amide hydrogenation reactions. Two very recent papers have described amide hydrogenation to yield C–N bond scission products using catalysts Fe-**1**[22] and Fe-**2c**.[23]

However, these methods suffer from a limited substrate scope,[22,23] modest TONs (up to 50),[22,23] and/or forcing conditions (140 °C, 60 bar H_2, Figure 5.2b).[22] This chapter discloses the development of Fe-PNP^{Cy}-BH$_4$ (Fe-**2a**) as an effective catalyst for the hydrogenation of unactivated amides (Figure 5.2c). These transformations selectively afford C–N cleavage products, and many substrates can be hydrogenated within 3 h at 110 °C. Further, we demonstrate that Fe-**2a** catalyzes this reaction with an initial rate that is within a factor of 2 of its Ru analogue (Ru-**2a**), under otherwise identical conditions. Finally, catalysts Fe-**2a** and Fe-**2b** were applied in the CO_2 capture and hydrogenation pathway described in Chapter 4.
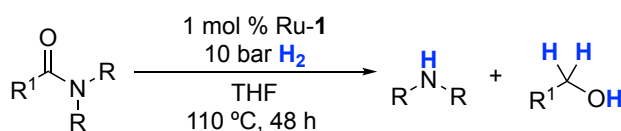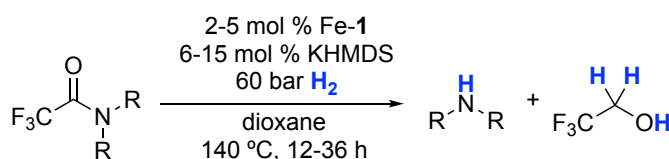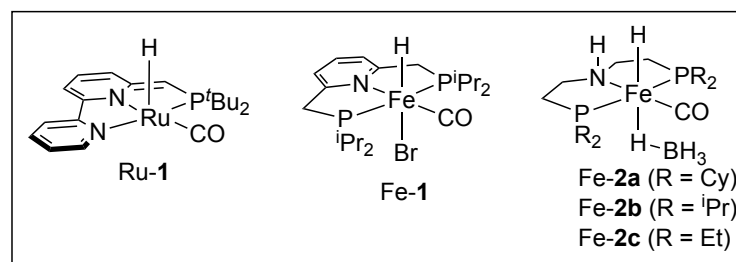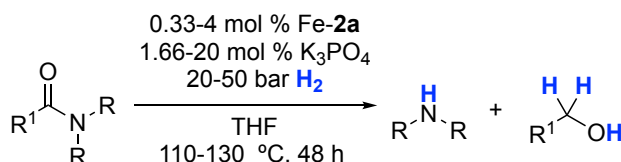
Figure 5.2. Examples of Ru- and Fe-catalyzed amide hydrogenation.

5.2 RESULTS AND DISCUSSION

Development of an Fe-based Amide Hydrogenation Catalyst

Based on our ongoing interest in the reduction of C_1 starting materials,[48, 49, 50, 51] we initially focused on the Fe-catalyzed hydrogenation of *N,N*-dimethylformamide (DMF). Fe-**2** derivatives were selected as catalysts based on literature precedent for the use of related Ru and Fe complexes for various C=O hydrogenation reactions.[17, 18, 21, 50, 52, 53, 54, 55, 56, 57] The aminodiphosphine (PNP^R) ligand provides a modular template that can be varied to tune electron density at the metal center based on the substituents on the phosphorus atoms. Furthermore, the presence of the secondary amine allows for substrate activation *via* hydrogen bonding, potentially allowing for more facile reductions. Due to the decreased electron density at Fe relative to Ru, we pursued complexes Fe-**2a-c** bearing electron donating PNP^R ligands (Figure 5.3).

The catalysts were synthesized by stirring the appropriate PNP^R ligand with a suspension of anhydrous iron(II) bromide (FeBr$_2$) in THF. Over 5 min, a white precipitate formed, indicating coordination of the ligand to FeBr$_2$. The solution containing the paramagnetic species in THF was submerged in LN$_2$, and the headspace was evacuated. Next, an atmosphere of carbon monoxide (CO) was introduced, and the reaction mixture was allowed to warm to RT. Coordination of the CO ligand resulted in a diamagnetic blue complex. After 3 h, the solvent was removed, and the solid was washed with pentanes. Finally, treatment of the blue complex with NaBH$_4$ in an ethanol/toluene mixture resulted in complexes Fe-**2a-c**.
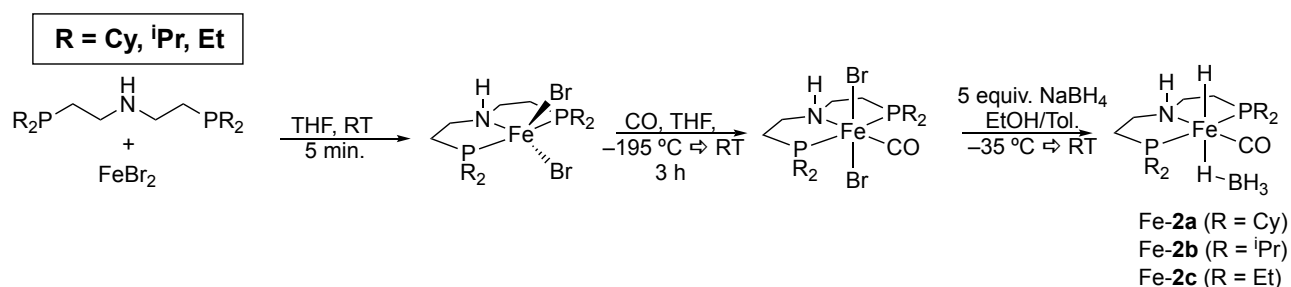
Figure 5.3. Preparation of Fe-**2** complexes.

With these complexes in hand, we first examined the hydrogenation of DMF and *N*-formylmorpholine using 1 mol % Fe-**2a**, 25 mol% K$_3$PO$_4$, and 50 bar of H$_2$ at 130 °C (Table 5.1).[58] In our initial trials, this reaction proved to be highly irreproducible, with yields fluctuating between 0 and 99% over >10 runs (entries 1-20). After an exhaustive

investigation, we identified the purity of the H_2 as the origin of the poor reproducibility. This issue was resolved by changing from ultra-high purity H_2 (99.999%) to research grade H_2 (99.9999%), which resulted in consistent and reproducible results (entries 20-25).

Table 5.1. Reproducibility studies with Fe-**2a**.[a]
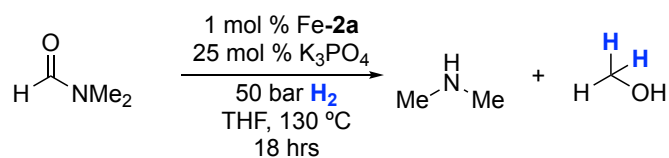
Entry	H$_2$ Grade	Date	NMR Yield (%)	TON
1	Ultra-high Purity	12-29-14	62	62
2	Ultra-high Purity	03-02-15	0	0
3	Ultra-high Purity	03-31-15	5	5
4	Ultra-high Purity	03-31-15	7	7
5	Ultra-high Purity	04-01-15	76	76
6	Ultra-high Purity	04-11-15	28	28
7	Ultra-high Purity	04-11-15	7	7
8	Ultra-high Purity	04-15-15	0	0
9	Ultra-high Purity	04-15-15	0	0
10	Ultra-high Purity	04-18-15	73	73
11	Ultra-high Purity	04-22-15	14	14
12	Ultra-high Purity	04-22-15	10	10
13	Ultra-high Purity	05-11-15	52	52
14	Ultra-high Purity	05-14-15	24	24
15	Ultra-high Purity	05-18-15	>99	100
16	Ultra-high Purity	05-18-15	23	23
17	Ultra-high Purity	05-18-15	49	49
18	Ultra-high Purity	08-30-15	0	0
19	Ultra-high Purity	08-30-15	0	0
20	Research Grade	09-15-15	>99	100
21	Research Grade	12-19-15	97	97
22	Research Grade	12-20-15	>99	100
23	Research Grade	01-30-16	>99	100
24	Research Grade	01-30-16	>99	100

| 25 | Research Grade | **01-30-16** | >99 | 100 |

[a]Conditions: 1.0 mmol DMF, 10 μmol [Fe], 2 mL THF, 3 h in a 45-mL high-pressure Parr vessel with H_2. Yield and TON based on CH_3OH and determined by ^{1}H NMR spectroscopy.

Using research grade H_2 (50 bar) and 0.33 mol % Fe-**2a** at 130 ºC, we obtained 63% yield of CH_3OH after 3 h, with high (>99%) selectivity for C–N cleavage (Table 5.2, entry 1). The addition of base is known to promote metal-catalyzed hydrogenation,[59,60,61,62] and K_3PO_4 proved particularly effective in a related Ru-catalyzed hydrogenation of DMF.[50] Similarly, the addition of K_3PO_4 (25 equiv relative to Fe) to the Fe-**2a**-catalyzed hydrogenation of DMF under otherwise identical conditions boosted the yield to >99% (entry 2). Further optimization revealed that the base loading, temperature, and H_2 pressure can be decreased while maintaining similar yield (entries 3-7). A survey of organic and inorganic bases revealed K_3PO_4 as the optimal base for DMF hydrogenation.[63] Overall, under the optimized conditions (0.33 mol % of Fe-**2a**, 1.66 mol % of K_3PO_4, 20 bar H_2, 110 ºC, 3 h), the reaction proceeded in 96% yield (288 turnovers, entry 7).

Table 5.2. Optimization of Fe-**2**-catalyzed DMF hydrogenation.[a]
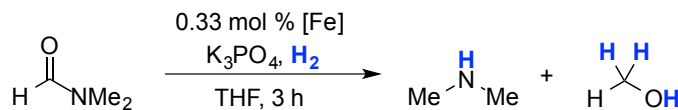
Entry	[Fe]	Base (mol %)	Temp (ºC)	H₂ (bar)	Yield (%)	TON
1	Fe-**2a**	none	130	50	63	189
2	Fe-**2a**	K_3PO_4 (8.33)	130	50	>99	300
3	Fe-**2a**	K_3PO_4 (1.66)	130	50	>99	300
4	Fe-**2a**	K_3PO_4 (1.66)	110	50	>99	300
5	Fe-**2a**	K_3PO_4 (1.66)	150	50	23	69
6	Fe-**2a**	none	110	20	59	17
7	Fe-**2a**	K_3PO_4 (1.66)	110	20	96	288
8	Fe-**2a**	NEt_3 (1.66)	110	20	78	244
9	Fe-**2a**	K_2CO_3 (1.66)	110	20	47	140
10	Fe-**2a**	NaOEt (1.66)	110	20	8	23

11	Fe-**2a**	KO^{t}Bu (1.66)	110	20	7	20
12	Fe-**2a**	KHMDS (1.66)	110	20	4	11
13	Fe-**2b**	K$_3$PO$_4$ (1.66)	110	20	63	189
14	Fe-**2c**	K$_3$PO$_4$ (1.66)	110	20	2	7

^{a}Conditions: 3.0 mmol DMF, 10 μmol [Fe], 2 mL THF, 3 h in a 45-mL high-pressure Parr vessel with research grade H$_2$. Yield and TON based on CH$_3$OH and determined by ^{1}H NMR spectroscopy.

Alternative Fe catalysts, Fe-**2b** (entry 13) and Fe-**2c** (entry 14) afforded significantly lower yields under otherwise identical conditions (63% and 2%, respectively). These results are particularly noteworthy since Beller has shown that Fe-**2c** has higher activity than Fe-**2a** for ester hydrogenation.[21,64] Furthermore, Fe-**2c** has recently been disclosed as a catalyst for the hydrogenation for other amide substrates (but not DMF).[23] Finally, by decreasing the catalyst loading of Fe-**2a** to 0.038 mol % and increasing the H$_2$ pressure to 60 bar, we obtained 1080 turnover numbers over 12 h (Figure 5.4).
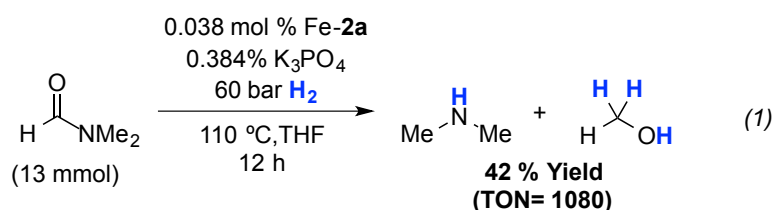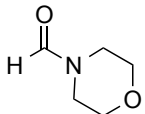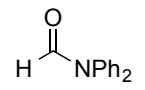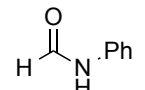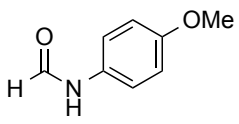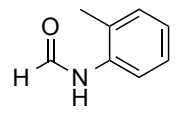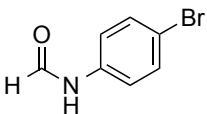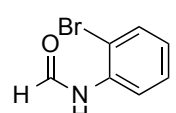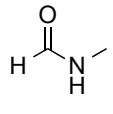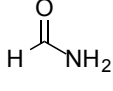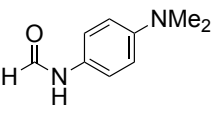
Figure 5.4. Fe-**2a**-catalyzed Hydrogenation of DMF.

We next examined the scope of the Fe-**2a**-catalyzed hydrogenation of formamides (Table 5.3). The tertiary alkyl and aryl formamides, *N*-formylmorpholine and *N,N*-diphenylformamide, underwent hydrogenation in quantitative yield and with >95% selectivity for C–N cleavage (entries 1 and 2). Secondary aryl formamides were also viable substrates, affording 57-95% yield of the C–N cleavage products under the standard conditions (entries 3-7). The highest yields were obtained with substrates bearing electron-neutral or -withdrawing substituents on the aromatic ring (compare entry 4 to entries 3 and 6). Substitution at *ortho* sites on the arene ring was well-tolerated (entries 5 and 7). Aryl bromides were compatible with the reaction conditions, and no hydrodehalogenation products were detected. Lower yields were observed with 2°-alkyl and 1°-formamides (entries 8 and 9). These reactivity trends are comparable to those reported in related Ru-catalyzed amide hydrogenation reactions.[37, 38, 65]

Table 5.3. Scope of formamide substrates.[a]

0.33 mol % Fe-**2a**
1.66 mol % K_3PO_4
20 bar H_2
THF, 110 °C
3 h

Entry	Substrate	Conversion (%)	Yield (%)	TON
1		>99	>99[b]	300
2		>99	99	300
3		>99	95	300
4		69	57	207
5		>99	94	300
6		>99	96	300
7		>99	97	300
8		12	12[b]	36
9		1	1[b]	3
10		0	0	0
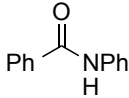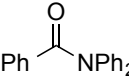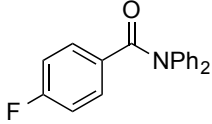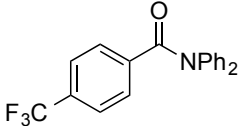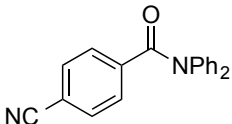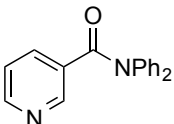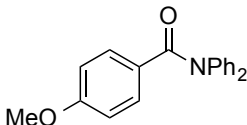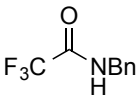
[a]Conditions: 3 mmol amide, 10 μmol Fe-**2a**, 50 μmol K_3PO_4, 2 mL THF, 20 bar H_2, 110 °C, 3 h. Yields are isolated yields of the amine product. Conversion (based on DMF) and TON (based on CH_3OH) were determined by ^{1}H NMR spectroscopy. [b]Yield determined by ^{1}H NMR spectroscopy based on CH_3OH.

Alkyl- and aryl-substituted amides often required more forcing conditions than the formamides; however, after some reoptimization, they also underwent selective reduction in modest to high yields (Table 5.4). For example, *N*-phenyl- and *N,N*-diphenylacetamide both afforded quantitative conversion and high yields of ethanol and the corresponding amine at 110 °C with 30 bar H_2 and 2 mol % of Fe-**2a** (entries 1, 2). Notably, *N*-phenylacetamide was reported to be unreactive with catalyst Fe-**1**.[22] Substituted benzamides also underwent high-yielding hydrogenation (entries 3-8), albeit at elevated temperature (130 °C), pressure (50 bar), and catalyst loading (4 mol %). Benzamides bearing electron-withdrawing *p*-F, *p*-CF$_3$, and *p*-CN substituents exhibited the highest reactivity (entries 6-8), while derivatives with electron donating *p*-OMe or NMe$_2$ groups afforded <1% yield (Table 5.3 entry 10 and Table 5.2 entry 11). In the case of *p*-CN-*N,N*-diphenylbenzamide (entry 8), both the amide and the cyano functional group underwent hydrogenation.[66] Fe-**2a** is also compatible with potentially coordinating pyridine functional groups (entry 9), and catalyzes the hydrogenation of trifluoromethyl amides under significantly milder conditions than those reported with Fe-**1** (entry 10).[22] Overall, the substrate scope, catalyst loading, and TONs obtained with Fe-**2a** rival those of many Ru catalysts.[33,37]

Table 5.4. Scope of amide substrates.[a]

Entry	Substrate	Conversion (%)	Yield (%)	TON
1[b]		>99	88	50
2[b]		>99	96	50
3		38	36	9

Entry	Substrate	Conversion	Yield	TON
4	Ph—C(=O)—NPh H (N-phenylbenzamide)	>99	95	25
5	Ph—C(=O)—NPh₂	>99	99	25
6	4-F-C₆H₄—C(=O)—NPh₂	>99	93	25
7	4-F₃C-C₆H₄—C(=O)—NPh₂	>99	94	25
8[c]	4-NC-C₆H₄—C(=O)—NPh₂	>99	94	25
9	pyridin-3-yl—C(=O)—NPh₂	>99	95	25
10	4-MeO-C₆H₄—C(=O)—NPh₂	<1	<1	<1
11[d]	F₃C—C(=O)—NBn H	44[d]	44[d]	120

[a]Conditions: 0.25 mmol amide, 10 μmol Fe-**2a**, 50 μmol K₃PO₄, 2 mL THF, 50 bar H₂, 130 °C, 3 h. Yields are isolated yields of the amine product. Conversion (based on amide substrate) and TON (based on ROH) were determined by ¹H NMR spectroscopy. [b]Conditions: 0.50 mmol amide, 10 μmol Fe-**2a**, 50 μmol K₃PO₄, 2 mL THF, 30 bar H₂, 110 °C, 3 h. [c]Nitrile functional group was also hydrogenated. [d]Conditions: 3 mmol amide, 10 μmol Fe-**2a**, 50 μmol K₃PO₄, 2 mL THF, 20 bar H₂, 110 °C, 3 h. Conversion determined by ¹⁹F NMR spectroscopy and yield by ¹H NMR spectroscopy based on 2,2,2-trifluoroethanol.

Comparison of Fe and Ru

We next sought to compare the rate of amide hydrogenation with Fe-**2a** to that of its Ru analogue Ru-**2a**. This comparison was conducted by monitoring the hydrogenation of DMF via *in situ* Raman spectroscopy.[67,68,69] As shown in Figure 5.5, the complete consumption of DMF required ~5.5 h with Fe-**2a**, while with Ru-**2a** DMF was fully converted within ~3 h. Comparison of the initial reaction rates show that the Ru catalyst is approximately 1.7-fold faster than the Fe catalyst. This result is consistent with very recent

computational studies that compared the hydrogenation of methyl benzoate with M^{II}-PNP catalysts (M = Fe and Ru). In these studies, the barriers for hydride transfer from *trans*-Fe-PNP-$(H)_2$ and *trans*-Ru-PNP-$(H)_2$ to the ester were calculated to be within 3 kcal/mol of one another, and the relative magnitudes showed a large dependence on basis set.[25,70] Our experimental results confirm the similar barriers for hydrogenation catalyzed by Fe-**2a** and Ru-**2a**, and are particularly noteworthy considering that previous studies have demonstrated orders of magnitude differences in the kinetic hydricity of 1st-row transition metal hydrides versus their 2nd/3rd-row counterparts.[71]
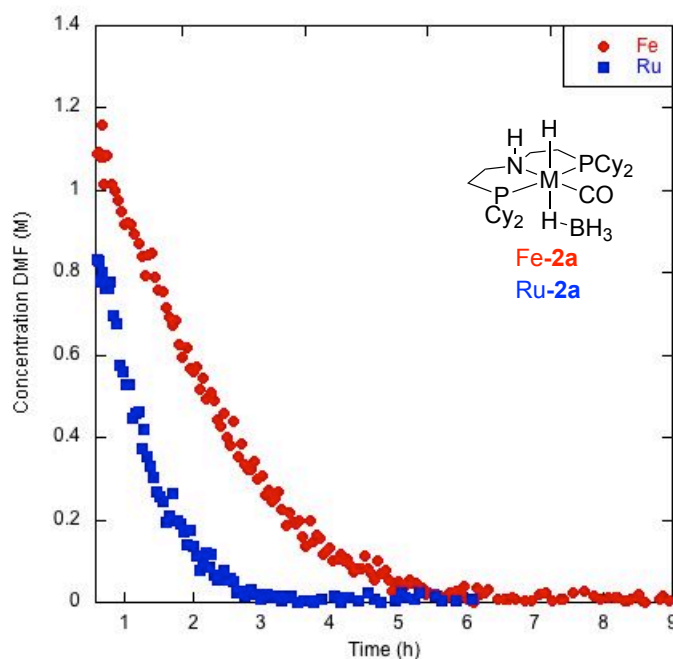
Figure 5.5. Reaction progress of the hydrogenation of DMF with **Fe-2a** vs **Ru-2a**. Conditions: 10.5 mmol amide, 35 μmol **Fe-2a**, 175 μmol K_3PO_4, 7 mL THF, 70 bar H_2. Disappearance of DMF monitored via Raman peak at 865 cm^{-1}. Reactions were conducted in a high pressure reactor fitted with a Raman probe, and temperature was equilibrated to 110 ºC (internal temperature) prior to data collection.

Mechanism of Hydrogenation
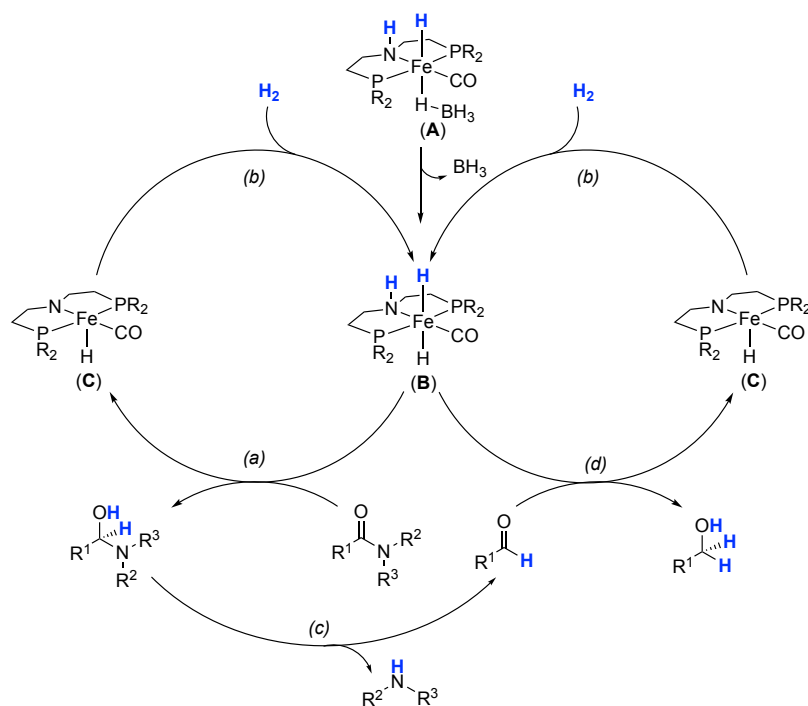
Figure 5.6. Proposed mechanism for the Fe-catalyzed hydrogenation of amides.

A plausible catalytic cycle for Fe-catalyzed amide hydrogenation is shown in Figure 5.6. This mechanism is similar to those reported in the literature for carbonyl hydrogenation with related Ru and Fe catalysts.[25] In a catalyst initiation step, the loss of BH_3 from **A** leads to the active *trans*-dihydride complex, **B**. The BH_3 is presumably captured by a Lewis base in solution (e.g., solvent, PO_4^{3-}, etc). Complex **B** then transfers a hydride and a proton to the amide substrate (step *a*) to yield a hemiaminal intermediate and **C**. Heterolytic cleavage of H_2 by **C** regenerates **B** (step *b*), while the hemiaminal intermediate extrudes the amine and concomitantly generates the aldehyde (step *c*). Finally, hydrogenation of the aldehyde by **B** (step *d*) yields the primary alcohol and reforms **C**. Importantly, an exogeneous base is not necessary for this cycle to proceed, and our results show that added base is not necessary to achieve efficient catalysis (Table 5.2, entry 1. We hypothesize that the enhanced TON in the presence of relatively weak bases such as K_3PO_4 and NEt_3 is likely due to either base-promoted catalyst initiation (via sequestration of BH_3) and/or the base acting as a proton shuttle during the hydrogenation step and/or in the conversion of the aminal to the aldehyde. The ineffectiveness of strong bases (e.g., KO^{t}Bu, KHMDS, KOEt; Table 5.2, entries 10-12) appears to be a result of their incompatibility with the substrate, DMF.[72]
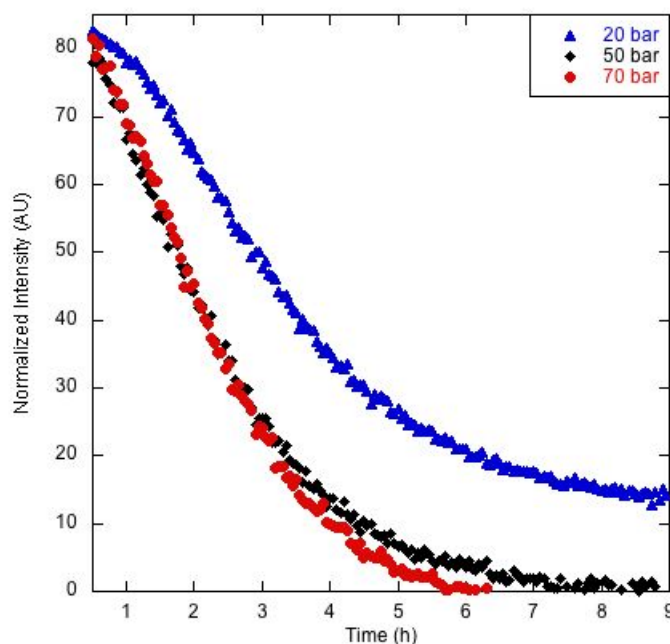
Figure 5.7. Reaction progress of the hydrogenation of DMF with Fe-**2a** at 20, 50, and 70 bar H_2. Conditions: 10.5 mmol amide, 35 μmol Fe-2a, 175 μmol K_3PO_4, 7 mL THF. Disappearance of DMF monitored via Raman peak at 865 cm^{-1}. Reactions were conducted in a high pressure reactor fitted with a Raman probe, and temperature was equilibrated to 110 ºC (internal temperature) prior to data collection.

To gain additional mechanistic insights into this transformation, we monitored the reaction progress of Fe-**2a**-catalyzed DMF hydrogenation as a function of H_2 pressure via Raman spectroscopy. As shown in Figure 5.7, the reaction progress curves are nearly identical at 50 and 70 bar H_2. In contrast, the reaction is significantly slower at 20 bar H_2, and there appears to be an induction period at this lower pressure. While more detailed studies will be necessary to fully interpret these data, the preliminary results suggest that the turnover limiting step and/or initiation rate change as a function of H_2 pressure.

Next, we sought to evaluate the resting state of the catalyst. While the pressure and temperature (20-50 bar H_2 and 110-130 ºC) of the reaction precludes direct adaption to typical NMR studies, we analyzed the reaction under the modified reaction conditions shown in Figure 5.8. A J-Young NMR tube was charged with Fe-**2a**, K_3PO_4, and C_6D_6 under an atmosphere of H_2. An initial ^{1}H NMR spectrum was acquired, and it showed no change in Fe-**2a** at room temperature. The hydride region was evaluated as a diagnostic tool for new, potentially catalytically relevant, intermediates (Figure 5.8, 0 h). The sealed J-Young NMR tube was heated in an oil bath at 100 ºC. The vibrant yellow heterogeneous mixture rapidly changed color to a deep red solution; however, the K_3PO_4,

remained insoluble through the course of the reaction. After 0.5 h of heating, the J-Young tube was removed from the oil bath and allowed to cool for 10 min prior to analysis via ^{1}H NMR spectroscopy. As shown in Figure 5.8 (0.5 h), Fe-**2a** (triplet at −19.6 ppm) was completely consumed with the concomitant appearance of 2 new peaks. broad singlet at −11.2 ppm and triplet at −14.5 ppm). Continued heating led to a persistent red solution. Further analysis showed the presence of a new hydride signal at–9.4 ppm (Figure 5.8, 3 h). The multiplicities of this new signal (doublet of triplets) is consistent with the formation complex H$_2$-Fe-**2a**. The H$_2$-Fe-**2** species has been implicated as the active hydrogenation species for substrates such as CO_2, nitriles, and esters.[21, 66]
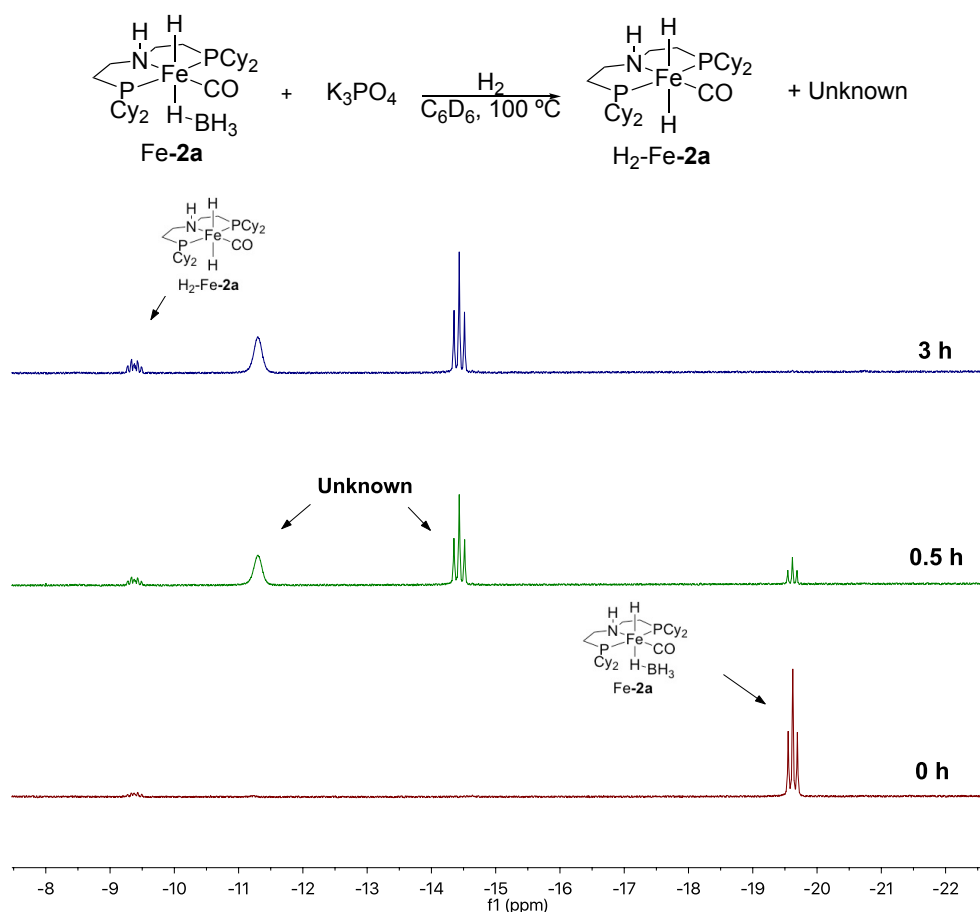
Figure 5.8. ^{1}H NMR time study of hydride region of Fe-**2a** with K$_3$PO$_4$ and H$_2$.

While H$_2$-Fe-**2a** is anticipated to be the active hydrogenation species, we were interested in identifying the unknown species.[17] Several *cis*-H$_2$-Fe-**2** complexes have been reported in the literature, and comparison of the ^{1}H NMR spectra shows that they are

inconsistent with the observed species. Conducting the analogous reaction in the absence of H_2 led to selective formation of the unknown species. Omission of base led to a mixture of H_2-Fe-**2a** and Fe-**2a.** Based on these results, we propose that the unidentified species is linked to the interaction of Fe-**2a** and base. Substitution of K_3PO_4 for the homogeneous base morpholine confirmed this hypothesis. As shown in Figure 5.9, this reaction led to the appearance of a broad singlet at–11.2 ppm, suggesting a dynamic process. Low temperature ^{1}H NMR studies were unsuccessful in identifying a coalescence point. Interestingly, the unknown species is pentane soluble and could be isolated. As shown in Figure 5.10, this species is an active amide hydrogenation catalyst Crystallization attempts from a myriad of solvent combinations proved unfruitful. Based on these studies a putative structure is proposed in Figure 5.9. An analogous complex containing aniline has recently been reported by Langer and co-workers.[23] Interestingly, the addition of Lewis bases to Fe-**2** has been shown by Guan *et al.* to lead to a 2-fold improvement in yields of ester hydrogenation.[19] However, their computational studies suggest that the role of base is to promote the activation of Fe-**2** to H_2-Fe-**2**.[19] Based on these results, Fe-**2a**–Morph is expected to be an off-cycle intermediate in amide hydrogenation catalysis.
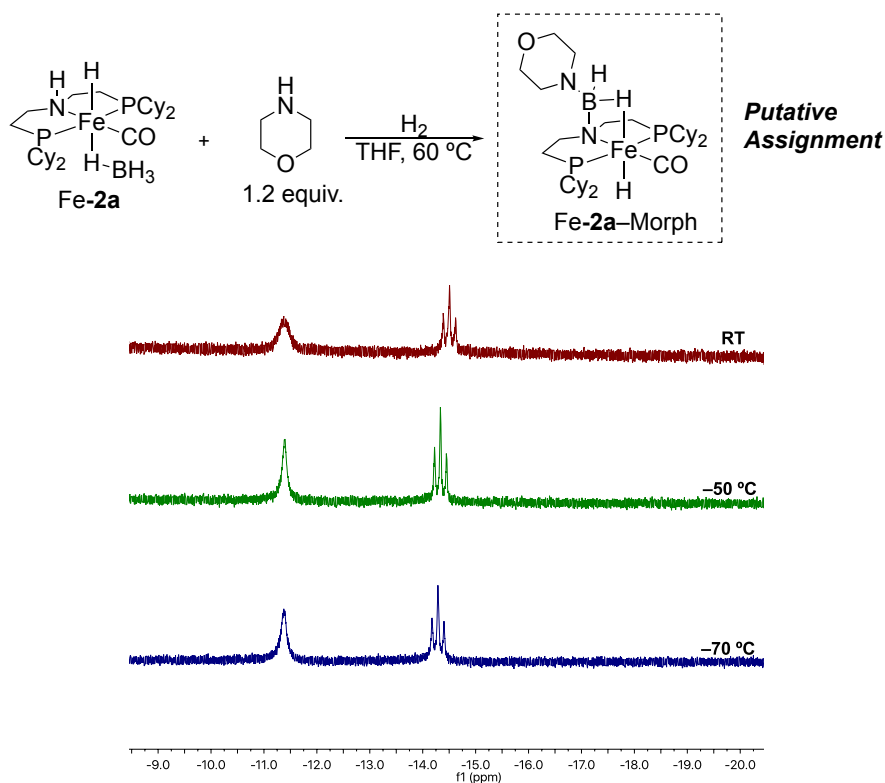
Figure 5.9. Low temperature ^{1}H NMR studies of hydride region of Fe-**2a**–Morph.
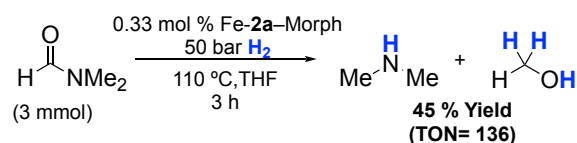
Figure 5.10. Hydrogenation of DMF with Fe-**2a**–Morph.

Application of Fe-2 Catalysts for the CO$_2$ Capture and Hydrogenation Process

We next sought to apply these iron hydrogenation catalysts to the CO$_2$ capture and hydrogenation system developed in the previous chapter (Chapter 4). As shown in Figure 5.11, this pathway sequesters CO$_2$ as the carbamate salt using two equivalents of amine. Upon heating, the sequestered CO$_2$ is slowly released and hydrogenated to formic acid (step 1). Formic acid subsequently undergoes amidation (step 2) by an amine to yield the corresponding amide. Finally, the amide is hydrogenated to yield CH$_3$OH and regenerate the amine (step 3). Several Fe-based catalysts have been reported to perform steps 1 and 2 with high efficiency. However, until now, the hydrogenation of amides (step 3) with an Fe-based catalyst was unprecedented.
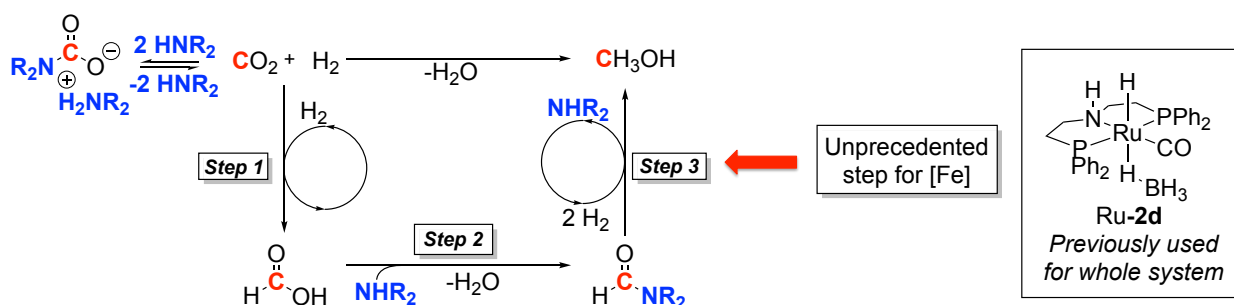
Figure 5.11. CO$_2$ capture and hydrogenation pathway.

Previous studies have found a single ruthenium catalyst (Ru-**2d**) capable of performing each step of the pathway.[50] The developed Fe-based catalysts (Fe-**2**) were modeled after the optimal ruthenium catalyst. Thus, we explored these catalysts for the hydrogenation of CO$_2$. While NHMe$_2$ was used in the original pathway, reactions with high concentrations of NHMe$_2$ were difficult to conduct due to the high volatility of this amine. Morpholine provided a less volatile surrogate. As a result, evaluation of these catalysts for CO$_2$ hydrogenation was conducted in conjunction with either NHMe$_2$ or morpholine, and the results are summarized in Table 5.5.

Table 5.5. Hydrogenation of CO_2 to formamide with Fe-**2**.[a]

$$CO_2 \quad + \quad H_2 \quad + \quad \text{(morpholine)} \quad \xrightarrow[\substack{\text{THF, 10 h} \\ 95\ °C}]{10\ \mu\text{mol Fe-}\mathbf{2}} \quad \text{(N-formylmorpholine)} \quad + \quad H_2O$$
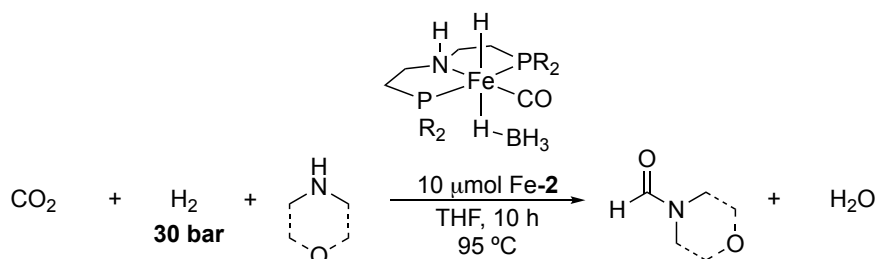
Entry	Catalyst	CO_2 (bar)	Amine	Amine (mmol)	Formamide TON	Notes
1	Fe-**2b**	0.5	$NHMe_2$	3.8	14	
2	Fe-**2b**	0.5	Morph	5.7	35	
3	Fe-**2b**	30	$NHMe_2$	4	29	
4	Fe-**2b**	30	$NHMe_2$	7.6	682	
5	Fe-**2b**	30	Morph.	19.9	436	
6[b]	Fe-**2b**	30	Morph.	19.9	142	Pentafluorophenol
7[b]	Fe-**2b**	30	Morph.	10	72	Pentafluorophenol
8	Fe-**2a**	30	$NHMe_2$	7.6	642	

[a]Conditions: CO_2, 10 μmol Fe-**2**, 50 μmol K_3PO_4, 2 mL THF, 50 bar H_2, 95 °C, 10 h. TON (based on formamide) were determined by ^{1}H NMR spectroscopy. [b]330 μmol of was added pentafluorophenol.

Beginning with 0.5 bar CO_2 (1 mmol) (entries 1 and 2), Fe-**2b** yielded 14 and 35 turnovers of DMF and *N*-formylmorpholine using $NHMe_2$ and morpholine, respectively. Higher pressures of CO_2 (entry 3) resulted in marginal improvements in the turnover of formamide (29 turnovers) with 4 mmol of $NHMe_2$ added. Increasing the amount of $NHMe_2$ from 4 mmol to 7.6 mmol dramatically enhanced the activity of Fe-**2b** to 682 turnovers of DMF (entry 4). A similar trend was observed with the morpholine, where 19.9 mmol of morpholine yielded 436 turnovers of *N*-formylmorpholine (entry 5). In this case, the resulting solution contained large of quantities of the insoluble carbamate salt, effectively minimizing the concentration of CO_2 and morpholine. Previous studies by Jessop *et al.* found that the addition of pentafluorophenol promoted the conversion of less volatile amines to the corresponding formamide. However, in this system, the addition of pentafluorophenol to the reaction mixture led to diminished activity (entries 6 and 7). Presumably, pentafluorophenol reacts unproductively with Fe-**2b** precluding enhanced activity. Finally, subjecting Fe-**2a** to similar conditions as Fe-**2b** led to a slightly lower turnover number of 642 (entry 8).
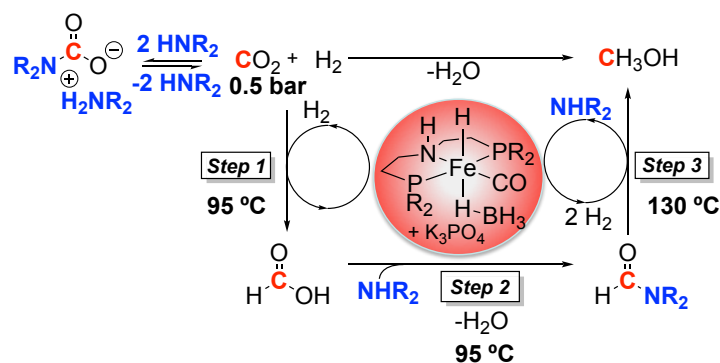
Figure 5.12. One-pot CO_2 capture and hydrogenation.

Prior investigations with Ru-**2d** found that amide hydrogenation was dramatically inhibited by CO_2 (Chapter 4). As a result, high conversion of CO_2 to the corresponding formamide was crucial for the one-pot hydrogenation of CO_2 to CH_3OH. This was accomplished by initial heating of the reaction mixture to 95 °C to convert CO_2 to formamide (steps 1 and 2), followed by subsequent hydrogenation of formamide to CH_3OH at 155 °C (step 3). Catalysts Fe-**2a** and Fe-**2b** are active for each step of the pathway; however, temperatures >130 °C lead to diminished yields in these systems (Table 5.2, entry 5). Therefore, an adapted one-pot strategy was applied where 0.5 bar CO_2 was used with an initial temperature of 95 °C and a final temperature of 130 °C (Figure 5.12). Application of these catalysts to the ramp strategy described for the hydrogenation of CO_2 to CH_3OH is shown in Table 5.6.

The Fe-catalyzed one-pot CO_2 capture and hydrogenation process proved challenging to adopt. Use of $HNMe_2$ as the sequestration amine led to 23% conversion of CO_2 (entry 1) with Fe-**2a**. The primary product under these conditions was the corresponding formamide. Only a traces of CH_3OH was observed by ^{1}H NMR spectroscopic analysis of the reaction mixture. Substitution of $HNMe_2$ to morpholine (entry 2) or pentaethylenehexamaine (PEHA) (entry 3) did not lead to improved yields of CH_3OH. Finally, the use of Fe-**2b** with morpholine led to a 38% conversion of CO_2, with 3 turnovers of CH_3OH detected (entry 4). At the end of these latter reactions large quantities of the solid carbamate salt were observed. This, in combination with the low pressure of CO_2, may contribute to the low conversion of CO_2 to formamide and ultimately CH_3OH. As a result, strategies were implemented to increase the concentration of the formamide intermediate.

Table 5.6. One-pot tandem Fe/Amine-catalyzed hydrogenation of CO_2 to CH_3OH.[a]
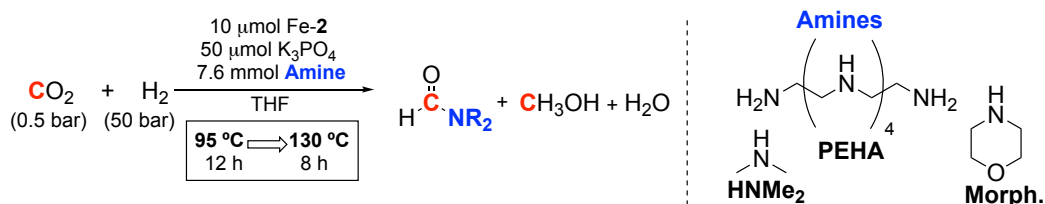
Entry	Catalyst	Amine	Conv. CO_2 (%)	CH_3OH (TON)	Formamide (TON)
1	Fe-**2a**	HNMe$_2$	23	<1	23
2	Fe-**2a**	Morph.	32	<1	32
3	Fe-**2a**	PEHA	nd	0	nd
4	Fe-**2b**	Morph.	38	3	35

[a]Conditions: 0.5 bar CO_2, 10 μmol Fe-**2**, 50 μmol K$_3$PO$_4$, 7.6 mmol of amine, 2 mL THF, 50 bar H$_2$, 95 °C for 12 h ⇨ 130 °C for 8 h. TONs were determined by ^{1}H NMR spectroscopy.

Increased pressure of CO_2 can lead to higher quantities of the formamide being produced; however, unreacted CO_2 has been shown to be detrimental to amide hydrogenation. This challenge was overcome in Chapter 4 by using Ru-**2d** over an extended time period (18 h) to convert >80% of the CO_2 to the formamide. Unfortunately, catalysts Fe-**2a** and Fe-**2b** were not as active for CO_2 hydrogenation as Ru-**2d**. Consequently, a different strategy was applied, as shown in Table 5.7. This approach is inspired by work performed by Ding *et al.*[54] In this strategy, CO_2 is hydrogenated to formamide at 95 °C, the reactor is vented, and then the reactor is repressurized with H$_2$ and heated to 110 °C. Due to the higher pressure of CO_2, the two-step, sequential hydrogenation strategy was anticipated to yield higher concentrations of the key formamide intermediate. The vent prior to amide hydrogenation is applied to remove unreacted CO_2 from the reaction. Results for this approach using Fe-**2a** is summarized in Table 5.7.

Utilization of Fe-**2a** in the 2-step process primarily yielded DMF (5 turnovers) (entry 1). While this approach improved the concentration of DMF, the inhibition of the Fe-catalyzed amide hydrogenation remained a key challenge. Ruthenium catalysts (Ru-**3-5**) were added to facilitate the first step. Importantly, catalysts Ru-**3-5** are inactive for amide hydrogenation. While these catalysts greatly enhanced the conversion of CO_2 to DMF, the second step of the reaction did not proceed under these conditions.

Table 5.7. Two-step hydrogenation of CO_2 to CH_3OH with Fe-**2a** and $NHMe_2$.
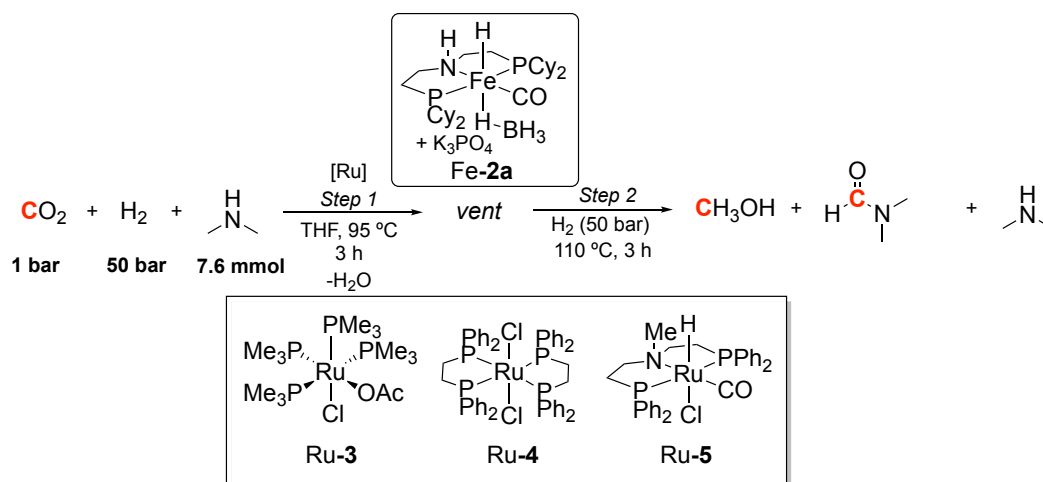
Entry	Ru-Catalyst	CH_3OH (TON)	DMF (TON)
1	none	0	5
2	Ru-**3**	0	34
3	Ru-**4**	<1	70
4	Ru-**5**	<1	50

Since Fe-**2a** has been shown to quantitatively hydrogenate DMF to CH_3OH and $NHMe_2$ under similar reaction conditions (Table 5.2, entry 3), the presence of CO_2 is presumed to be the major contributor of inhibition. Indeed, Hazari and Bernskoetter have investigated the nature of this inhibition with Fe-**2b** in the context of CO_2 hydrogenation, (Figure 5.13).[55] Upon initial exposure of H_2-Fe-**2b** to an atmosphere of CO_2 and H_2, two new species were detected. The major product was the formate-bound species, HCO_2-Fe-**2b**, and small quantities of CO_2-Fe-**2b** were also generated. CO_2-Fe-**2b** arises from the formal addition of CO_2 across the Fe-NR_2 bound of Fe-**2b'**. Over 5 h at room temperature, CO_2-Fe-**2b** cleanly converted to HCO_2-Fe-**2b**, suggesting that CO_2-Fe-**2b** is a minor contributor to the inhibition. HCO_2-Fe-**2b**, however, was found to be highly stable, and extrusion of the formate bound species was determined to be rate determining. Combining these results with our attempts at amide hydrogenation in the presence of CO_2, we anticipate HCO_2-Fe-**2a** is a major contributor to the inhibition of amide hydrogenation.
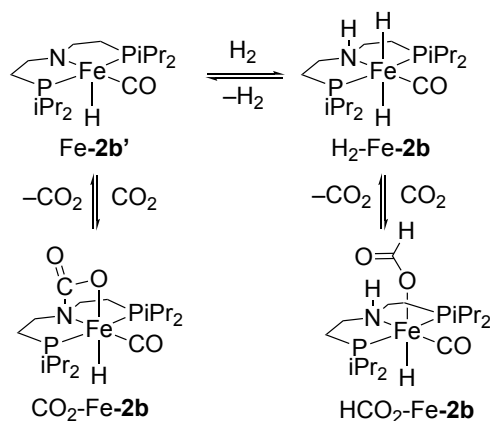
Figure 5.13. Potential routes for inhibition of formamide hydrogenation by CO_2.

5.3 CONCLUSIONS

In summary, this chapter describes the development of an Fe-catalyzed hydrogenation of unactivated amides to generate alcohols and amines. Prior to this work, this reaction was only possible using with noble metal catalysts. Under optimized conditions, this transformation affords TONs ranging from 25 to 300 and exhibits a broad scope. Turnover numbers as high as 1000 were observed for *N,N*-dimethylformamide hydrogenation. Kinetic experiments using *in situ* Raman spectroscopy demonstrate that the rate of amide hydrogenation with Fe-**2a** approaches that of its noble metal Ru counterpart. Efforts to detect intermediates implicate H_2-Fe-**2a** as the active hydrogenation species and Fe-**2a**–Amine (Morph) as an off-cycle species. Application of Fe-**2a** and Fe-**2b** for CO_2 capture and hydrogenation pathways led primarily to formamides. Further studies support that CO_2 greatly impedes the hydrogenation of formamides to CH_3OH and amine.

5.4 Experimental

General Procedures

All manipulations were carried out under a nitrogen atmosphere using standard Schlenk line or glove box techniques unless otherwise noted. All high-pressure reactions were carried out using a Parr Model 5000 Multiple Reactor system that includes six 45 mL vessels equipped with flat-gaskets and head mounting valves. The system was operated by a 4871 process controller and SpecView version 2.5 software. All pressures are reported from the SpecView interface at room temperature. NMR spectra were

obtained on Varian VNMRs: 400 MHz (400 MHz for ^{1}H; 100 MHz for ^{13}C) or 700 MHz (700 MHz for ^{1}H; 176 MHz for ^{13}C). Chemical shifts are reported in parts per million (ppm) and are referenced to an internal standard. Unless otherwise noted, the NMR yields with formamide substrates were based on methanol (δ = 3.16 ppm, T_1 = 7.2 s) and were quantified using 1,3,5-trimethoxybenzene (δ = 6.02 ppm, T_1 = 2.8 s) as an internal standard in dimethylsulfoxide-d_6 (DMSO-d_6). For each NMR experiment, 4 scans were collected, a 35 s relaxation delay was used, and a pulse angle of 90° was applied.

High pressure Raman data were collected using a Kaiser Optical Systems, Inc. RamanRxn1 system. *In situ* Raman analysis was performed with a NIR Immersion Sampling Optic Probe with a sapphire window and alloy C276 body (6 inch length and 0.25 inch diameter) attached to the MR Filtered Probe Head of the RamanRxn1 system. The laser source was a 400 mW Invictus operating at 785 nm. The high pressure experiments were performed in a 45 mL Parr cylinder containing a 0.3 inch center port hole with a 0.25 inch Swagelock fitting at the top. The probe was swaged into a 0.25 inch Swagelok fitting, which was then attached to the top center port hole of the reactor. Calibration was performed using cyclohexane as a wavelength standard and a white light correction for spectral intensity. Spectra were collected via the NIR Immersion Sampling Optic Probe with a range of 0-3450 cm^{-1}. Spectra were analyzed using ACD Spectrus Processer 2015 Pack 2 software.

Reactor Descriptions

Two different types of reaction vessels were used. All are 45 mL and are composed of a well (in which the solid and liquid reagents are charged) and a head, which contains various attachments as described below.

Reactors of type A variety are made of Hastelloy C, and the wells are 7.5 cm tall and 3 cm in diameter. The heads consist of a pressure transducer and two inlet/outlet valves that can connect to a Parr Model 5000 Multiple Reactor system described above, a safety release valve, and a well for a thermocouple (Figure 5.14).
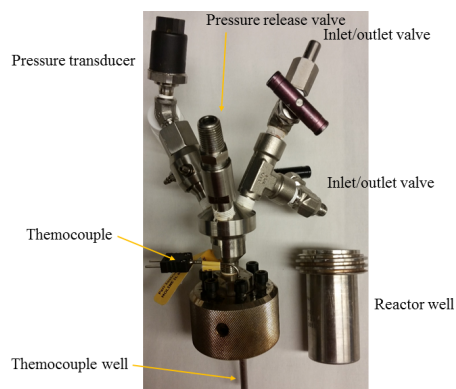
Figure 5.14. Picture of reactor type A with the parts of the reactor labeled.

Reactor B (Hastelloy C) is identical to the type A reactors except that it has an additional attachment on the head. This attachment is an adaptor for a Raman probe that is submerged into the well of the reactor. This attachment is used for *in situ* Raman spectroscopy (Figure 5.15).
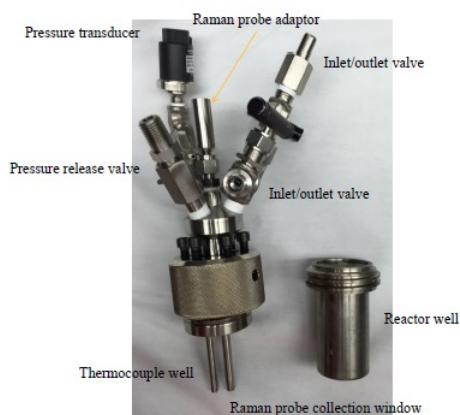
Figure 5.15. Picture of reactor type B with the parts of the reactor labeled.

Materials and Methods

The ligands bis(2-(dicyclohexylphosphino)ethyl)amine (PNP^{Cy}), bis(2-(diisopropylphospino)ethyl)amine (PNP^{iPr}), and bis(2-(diethylphosphino)ethyl)amine (PNP^{Et}) was purchased from commercial sources (98%, Alfa Aesar) or synthesized according to the literature.[73] Catalysts Ru-**2a**,[74] Fe-**2b**,[18] Fe-**2c**[21], Ru-**3**,[75] Ru-**4**,[76] and Ru-**5**[54] were prepared according to a literature procedure. Anhydrous FeBr$_2$ (Alfa Aesar, 98%), anhydrous K$_2$CO$_3$ (Acros, 99%), sublimed KOtBu (Oakwood, 99%), KHMDS (Aldrich, 95%), NaOEt (TCI, 95%) and anhydrous K$_3$PO$_4$ (Aldrich, 98%) were ground with a mortar and pestle before use. Research grade hydrogen (99.9999%), carbon dioxide (99.999%), ultra-high purity hydrogen (99.999%), and carbon monoxide (99.5%) were purchased from

Metro Welding. All catalytic experiments were set up under an oxygen-free atmosphere in a glovebox. All catalytic experiments were conducted in triplicate, and the reported results represent an average of three runs (NMR yields) and a single isolated yield where applicable. Anhydrous *N,N*-dimethylformamide (DMF, Alfa Aesar, 99.8%) as well as the solid reagents *N,N*-diphenylformamide (Aldrich, 99%), *N*-phenylformamide (Alfa Aesar, 98%), *N*-(4-methoxyphenyl)formamide (TCI, >98%), *N*-(2-methylphenyl)formamide (Alfa Aesar, 98%), *N*-(4-bromophenyl)formamide (Aldrich, 97%), *N*-(2-bromophenyl)formamide (Aldrich, 97%), *N*-phenylacetamide (Aldrich, 97%), *N,N*-diphenylacetamide (Enamine, 95%), *N,N*-dimethylbenzamide (Aldrich, 99%), *N*-phenylbenzamide (Alfa Aesar, >98%), $NaBH_4$ (Aldrich, Venpure SF) and 1,3,5-trimethoxybenzene (Acros) were obtained from commercial sources and used without further purification. *N*-Formylmorpholine (Aldrich, 99%), *N*-methylformamide (Aldrich, 99%), and formamide (Acros, 99.5%) were degassed and used without further purification. *N*-(4-(Dimethylamino)phenyl)formamide[77] and *N*-benzyl-2,2,2-trifluoroactamide[78] were prepared according to literature procedures. Amides from Table 5.4, entries 5-10 were synthesized from the corresponding commercially-available acid chloride and *N,N*-diphenylamine (Aldrich, >99%) according to literature procedure.[79] Dimethylamine (Aldrich, anhydrous >99%) was condensed in dry THF using standard Schlenk line techniques to yield a 3.8 M solution of $NHMe_2$ in THF or purchased as a 2M solution in THF (Aldrich, 99%). Anhydrous morpholine (Aldrich) and PEHA (Aldrich, tech. grade) were degassed prior to use. Tetrahydrofuran (THF), dichloromethane (DCM), toluene, NEt_3, and pentane, were purified using an Innovative Technologies (IT) solvent purification system consisting of a copper catalyst, activated alumina, and molecular sieves. Anhydrous ethanol (EtOH, Aldrich), dimethylsulfoxide-d_6 (DMSO-d_6, Cambridge Isotope Laboratories), benzene (C_6D_6, Cambridge Isotope Laboratories), and chloroform ($CDCl_3$, Cambridge Isotope Laboratories) were purchased from the respective supplier and used as received.

Synthesis and Characterization of Fe-PNP^{Cy}H(CO)-BH$_4$ (Fe-2a)
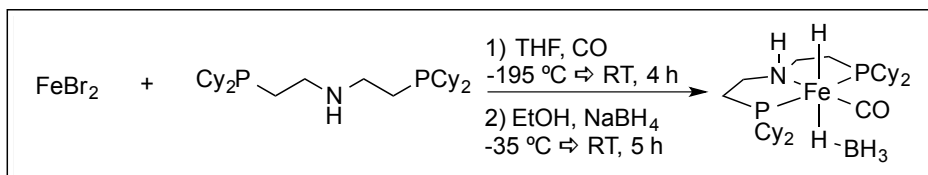
Fe-PNP^{Cy}H(CO)-BH_4 (Fe-2a): Fe-**2a** has been previously reported.^{Error! Bookmark not defined.} Anhydrous FeBr$_2$ (304.3 mg, 1.41 mmol, 1 equiv) and PNP^{Cy} (657.1 mg, 1.41 mmol, 1 equiv) were weighed and transferred into a 50 mL Schlenk tube, followed by 30 mL of anhydrous THF. The Schlenk tube was sealed using a PTFE stopper and shaken for 15 min. Upon formation of a white precipitate, the Schlenk tube was partially submerged in LN$_2$ (–195 °C) until the solution was completely frozen. The Schlenk tube was evacuated and backfilled with CO. The tube was resealed and allowed to thaw to RT on a shake plate. After 4 h, the resulting blue solution was cannula transferred to a 250 mL Schlenk flask equipped with an octagonal magnetic stirbar (5/16 x 1/2 in.) and the solvent was removed *in vacuo*.

Upon removal of THF, 50 mL of anhydrous EtOH was added to the blue solid, and the solution placed in a freezer (–35 °C) for 30 min. To the prechilled solution was added NaBH$_4$ (267 mg, 7.05 mmol, 5 equiv) with vigorous stirring. The blue solution slowly changed color to yellow over a 5 h time period. The solvent was removed, and the solid was extracted in 3 x 50 mL portions of toluene, and the resulting solution was filtered through a thin pad of dried silica (1 x 3 cm) and then concentrated to dryness. The solid was triturated with pentane (3 x 4 mL) and dried *in vacuo* resulting in the title compound as a golden yellow solid (602 mg, 1.06 mmol, 76% yield). Anal. Calcd. for C$_{29}$H$_{58}$BFeNOP$_2$: C, 61.61%; H, 10.34%; N, 2.48%. Found: C, 61.94%, H, 10.28%; N, 2.49%. IR ATR: $\bar{v}$ [cm^{-1}] 2341 (b), 2059 (b), 1900 (s), 1816 (s).

^{1}H NMR (500 MHz, C$_6$D$_6$) δ 3.95 (s, 1H), 2.88 (d, *J* = 12.5 Hz, 2H), 2.65-2.40 (multiple peaks, 3H), 2.27-2.05 (multiple peaks, 3H), 2.01-1.82 (multiple peaks, 5H), 1.81-1.44 (multiple peaks, 24H), 1.43-0.97 (multiple peaks, 15H), –2.95 (bs, 4H), –19.56 (t, *J* = 50.1 Hz, 1H).

^{13}C NMR (100 MHz, C_6D_6) δ 54.34, 40.28 (t, J = 9.3 Hz), 36.77 (t, J = 12.2 Hz), 31.50, 30.48, 29.30, 28.38, 28.29, 28.13 (t, J = 7.3 Hz), 27.86 (d, J = 3.9 Hz), 27.28 (dt, J = 23.2, 5.4 Hz), 26.83, 26.68 , 21.45, CO resonance not observed by ^{13}C NMR; however, the presence of the CO ligand was confirmed by IR spectroscopy.

^{31}P NMR (202 MHz, C_6D_6) δ 91.03 (d, J = 50.1 Hz).

^{11}B NMR (128 MHz, C_6D_6) δ –31.39.

General Procedure for Hydrogenation Reactions

I. Reproducibility as a Function of H_2 Source (Table 5.1)

In a N_2-atmosphere dry box, Fe-**2a** (5.6 mg, 10 μmol, 1.00 mol %) was dissolved in 2 mL THF, and this solution was added to the metal well of a pressure vessel containing K_3PO_4 (53 mg, 0.25 mmol, 25 mol %, 25 equiv relative to Fe) and a micro magnetic stirbar (3 x 10 mm). The *N*-formylmorpholine substrate (115 mg, ~100 μL, 1.0 mmol, 100 equiv relative to Fe) or *N,N*-dimethylformamide (73 mg, ~ 80 μL, 1.0 mmol, 100 equiv relative to Fe) was then added, and the vessel (reactor-type A) was sealed and removed from the dry box. The vessel was connected to the Parr Multiple Reactor System, and the manifold was thoroughly purged with ultra-high purity hydrogen (99.999%) or research grade H_2 (99.9999%). The vessel was then pressurized with 50 bar of ultra-high purity or research grade H_2 at room temperature, and the reaction was heated to 130 ºC with a stir rate of 800 RPM. The heating was conducted using Specview software. After 3 h of heating, the reaction mixture was allowed to cool to room temperature. The pressure vessel was placed in a –84 °C bath (ethyl acetate/LN_2) for 15 min and then carefully vented using a metering valve.

II. Hydrogenation and Optimization of DMF (Table 5.2)
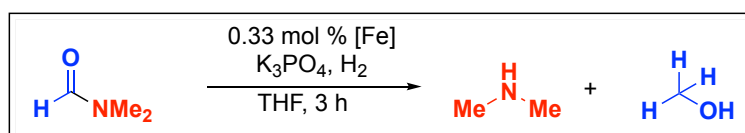
General Procedure for the Hydrogenation of DMF. In a N_2-atmosphere dry box, [Fe] (10 μmol, 0.33 mol %) was dissolved in 2 mL of THF, and this solution was added to the metal

well of a pressure vessel containing the appropriate quantity of base and a micro magnetic stirbar (3 x 10 mm). DMF (230 μL, 3.0 mmol, 300 equiv relative to Fe) was then added, and the vessel (Reactor-type A) was sealed and removed from the dry box. The vessel was connected to the Parr Multiple Reactor System, and the manifold was thoroughly purged with research grade H_2 (99.9999%). The vessel was then pressurized with research grade H_2 at room temperature, and the reaction was heated at the desired temperature with a stir rate of 800 RPM. The heating was conducted using Specview software. After 3 h of heating, the reaction mixture was allowed to cool to room temperature. The pressure vessel was placed in a –84 °C bath (ethyl acetate/LN_2) for 15 min and then carefully vented using a metering valve. THF (0.5 mL) was added through the venting valve of the pressure vessel to wash any residual liquids/solids into the vessel. The vessel was then opened, 1,3,5-trimethoxybenzene (0.178 mmol, 300 μL of 0.593 M solution in DMSO-d_6) was added as a ^{1}H NMR standard, and the contents of the vessel were diluted with DMSO-d_6. Approximately 50 μL of the resulting solution was added to an NMR tube, diluted further with DMSO-d_6. The sample was then analyzed by ^{1}H NMR spectroscopy (see Figure 5.16 for a representative spectrum).

Figure 5.16. Representative spectrum for the determination of yield by NMR. 1,3,5-Trimethoxybenzene used as internal standard.

III. General Procedure for the Hydrogenation of Formamides (Table 5.3)
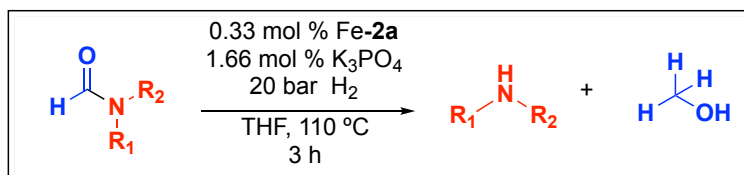
General Procedure A: In a N_2-atmosphere dry box, Fe-**2a** (5.6 mg, 10 μmol, 0.33 mol %) was dissolved in 2 mL THF, and this solution was added to the metal well of a pressure vessel containing the K_3PO_4 (10.6 mg, 50 μmol, 1.66 mol%, 5 equiv relative to Fe) and a micro magnetic stirbar (3 x 10 mm). The amide substrate (3.0 mmol, 300 equiv relative to Fe) was then added, and the vessel (Reactor-type A) was sealed and removed from the dry box. The vessel was connected to the Parr Multiple Reactor System, and the manifold was thoroughly purged with research grade H_2 (99.9999%). The vessel was then pressurized with 20 bar of research grade H_2 at room temperature, and the reaction was heated to 110 ºC with a stir rate of 800 RPM. The heating was conducted using Specview software. After 3 h of heating, the reaction mixture was allowed to cool to room temperature. The pressure vessel was placed in a –84 °C bath (ethyl acetate/LN_2) for 15 min and then carefully vented using a metering valve.

Preparation of samples for NMR analysis: THF (0.5 mL) was added through the venting valve of the pressure vessel to wash any residual liquids/solids into the vessel. The vessel was then opened, 1,3,5-trimethoxybenzene (0.178 mmol, 300 μL of 0.593 M solution in DMSO-d_6) was added as a ^{1}H NMR standard, and the contents of the vessel were diluted with DMSO-d_6. Approximately 50 μL of the resulting solution was added to an NMR tube, diluted further with DMSO-d_6. The sample was then analyzed by ^{1}H NMR spectroscopy (see Figure S3 for a representative spectrum).

General Method for the Isolation of Non-volatile Products: Ethyl acetate (5 mL) was added through the venting valve of the pressure vessel to wash any residual liquids/solids into the vessel. The vessel was then opened, and the contents were further diluted with ethyl acetate (~ 30 mL) and filtered through a silica plug (3.5 x 4 cm). The plug was washed with additional ethyl acetate (~ 80 mL), and the solvent was removed *in vacuo* to yield the pure product, unless otherwise noted. The ^{1}H and ^{13}C{^{1}H} NMR spectra

of the isolated products matched those reported in the literature.

Hydrogenation of _N_-formylmorpholine: General Procedure A was followed using _N_-formylmorpholine (345 mg, 300 μL, 3.0 mmol, 300 equiv relative to Fe). Yield and conversion (>99%) were determined by ^{1}H NMR analysis of CH_3OH.

Hydrogenation of _N,N_-diphenylformamide: General Procedure A was followed using _N,N_-diphenylformamide (592 mg, 3.0 mmol, 300 equiv relative to Fe). Yield (>99%) was determined by NMR analysis of CH_3OH. Isolated yield was based on _N,N_-diphenylamine (506 mg, 2.990 mmol, 99% yield, brown solid).

^{1}H NMR (400 MHz, $CDCl_3$) δ 7.21 (t, _J_ = 8.0 Hz, 4H), 7.02 (d, _J_ = 8.0 Hz, 4H), 6.87 (t, _J_ = 8.0 Hz, 2H), 5.63 (s, 1H).

^{13}C NMR (176 MHz, $CDCl_3$) δ 143.22, 129.47, 121.12, 117.92.

Hydrogenation of _N_-phenylformamide: General Procedure A was followed using _N_-phenylformamide (363 mg, 3.0 mmol, 300 equiv relative to Fe). Yield (>99%) was determined by ^{1}H NMR analysis of CH_3OH. Isolated yield was based on aniline (495.4 mg, 2.880 mmol, 96% yield, brown liquid).

^{1}H NMR (400 MHz, $CDCl_3$) δ 7.17 (t, _J_ = 7.6 Hz, 2H), 6.77 (t, _J_ = 7.6 Hz, 1H), 6.70 (d, _J_ = 7.6 Hz, 2H), 3.64 (s, 2H).

^{13}C NMR (176 MHz, $CDCl_3$) δ 146.47, 129.40, 118.65, 115.20.

Hydrogenation of _N_-(4-methoxyphenyl)formamide: General Procedure A was followed using _N_-(4-methoxyphenyl)formamide (454 mg, 3.0 mmol, 300 equiv relative to Fe). Yield (69%) was determined by ^{1}H NMR analysis of CH_3OH. Isolated yield was based on _p_-methoxyaniline (218 mg, 1.770 mmol, 59% yield, tan solid) upon further purification by column chromatography (4:1 hexanes:ethyl acetate).

^{1}H NMR (400 MHz, CDCl$_3$) δ 6.75 (dd, *J* = 8.7, 1.9 Hz, 2H), 6.65 (dd, *J* = 8.7, 1.9 Hz, 2H), 3.74 (d, *J* = 1.9 Hz, 3H), 3.42 (s, 2H).

^{13}C NMR (176 MHz, CDCl$_3$) δ 152.89, 140.04, 116.52, 114.90, 55.84.

Hydrogenation of *N*-(2-methylphenyl)formamide: General Procedure A was followed using *N*-(2-methylphenyl)formamide (406 mg, 3.0 mmol, 300 equiv relative to Fe). Yield (>99%) was determined by ^{1}H NMR analysis of CH$_3$OH. Isolated yield was based on *o*-methylaniline (302 mg, 2.82 mmol, 94% yield, light brown liquid).

^{1}H NMR (400 MHz, CDCl$_3$) δ 7.07 (m, 2H), 6.75-6.69 (multiple peaks, 2H), 3.60 (s, 2H), 2.19 (s, 3H).

^{13}C NMR (176 MHz, CDCl$_3$) δ 144.64, 130.53, 127.05, 122.40, 118.70, 115.00, 17.46.

Hydrogenation of *N*-(4-bromophenyl)formamide: General Procedure A was followed using *N*-(4-bromophenyl)formamide (601 mg, 3.0 mmol, 300 equiv relative to Fe). Yield (>99%) was determined by ^{1}H NMR analysis of CH$_3$OH. Isolated yield was based on *p*-bromoaniline (495.4 mg, 2.880 mmol, 96% yield, tan solid).

^{1}H NMR (400 MHz, CDCl$_3$) δ 7.06 (d, *J* = 8.2 Hz, 2H), 6.38 (d, *J* = 8.2 Hz, 2H), 3.49 (s, 2H).

^{13}C NMR (176 MHz, CDCl$_3$) δ 145.51, 132.03, 116.77, 110.15.

Hydrogenation of *N*-(2-bromophenyl)formamide: General Procedure A was followed using *N*-(2-bromophenyl)formamide (601 mg, 3.0 mmol, 300 equiv relative to Fe). Yield (>99%) was determined by ^{1}H NMR analysis of CH$_3$OH. Isolated yield was based on *o*-bromoaniline (501 mg, 2.910 mmol, 97% yield, brown liquid).

^{1}H NMR (400 MHz, CDCl$_3$) δ 7.41 (d, *J* = 7.9 Hz, 1H), 7.11 (t, *J* = 7.9 Hz, 1H), 6.77 (d, *J* = 7.9 Hz, 1H), 6.62 (t, *J* = 7.9 Hz, 1H), 4.07 (s, 2H).

^{13}C NMR (176 MHz, CDCl$_3$) δ 144.17, 132.69, 128.44, 119.51, 115.86, 109.43.

Hydrogenation of *N*-methylformamide: General Procedure A was followed using *N*-methylformamide (177 mg, 175 μL, 3.0 mmol, 300 equiv relative to Fe). Yield (12%) was determined by ^{1}H NMR analysis of CH$_3$OH.

Hydrogenation of formamide: General Procedure A was followed using formamide (136 mg, 120 μL, 3.0 mmol, 300 equiv relative to Fe). Yield (1%) was determined by ^{1}H NMR analysis of CH$_3$OH.

Hydrogenation of *N*-(4-(dimethylamino)phenyl)formamide: General Procedure A was followed using *N*-(4-(dimethylamino)phenyl)formamide (493 mg, 3.0 mmol, 300 equiv relative to Fe). Yield (<1%) was determined by NMR analysis of CH$_3$OH.

IV. General Procedure for the Hydrogenation of Acetamide Derivatives (Table 5.4, entries 1-2)
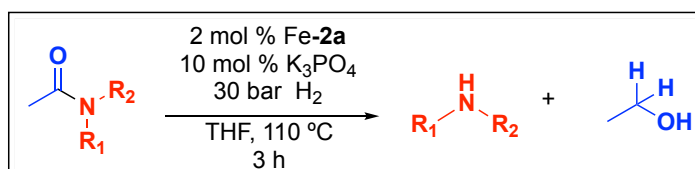
General Procedure B: In a N$_2$-atmosphere dry box, Fe-**2a** (5.6 mg, 10 μmol, 2 mol %) was dissolved in 2 mL THF, and this solution was added to the metal well of a pressure vessel containing the K$_3$PO$_4$ (10.6 mg, 50 μmol, 10 mol%, 5 equiv relative to Fe) and a micro magnetic stirbar (3 x 10 mm). The acetamide substrate (0.5 mmol, 50 equiv relative to Fe) was then added, and the vessel (Reactor type A) was sealed and removed from the dry box. The vessel was connected to the Parr Multiple Reactor System, and the manifold was thoroughly purged with research grade H$_2$ (99.9999%). The vessel was then pressurized with 30 bar of research grade H$_2$ at room temperature, and the reaction was heated to 110 ºC with a stir rate of 800 RPM. The heating was conducted using Specview software. After 3 h of heating, the reaction mixture was allowed to cool to room

temperature. The pressure vessel was placed in a –84 °C bath (ethyl acetate/LN$_2$) for 15 min and then carefully vented using a metering valve.

Preparation of samples for NMR analysis: THF (0.5 mL) was added through the venting valve of the pressure vessel to wash any residual liquids/solids into the vessel. The vessel was then opened, 1,3,5-trimethoxybenzene (0.178 mmol, 300 µL of 0.593 M solution in DMSO-d_6) was added as a ^{1}H NMR standard, and the contents of the vessel were diluted with DMSO-d_6. Approximately 50 µL of the resulting solution was added to an NMR tube, diluted further with DMSO-d_6. The sample was then analyzed by ^{1}H NMR spectroscopy.

General Method for the Isolation of Non-volatile Products: Ethyl acetate (5 mL) was added through the venting valve of the pressure vessel to wash any residual liquids/solids into the vessel. The vessel was then opened and the contents further diluted with ethyl acetate (~ 30 mL) and filtered through a silica plug (3.5 x 4 cm). The plug was washed with additional ethyl acetate (~ 80 mL), and the solvent removed *in vacuo* to yield the pure product, unless otherwise noted. The ^{1}H and ^{13}C{^{1}H} NMR spectra of the isolated products matched those reported in the literature.

Hydrogenation of *N*-phenylacetamide: General Procedure A was followed using *N*-phenylformamide (68 mg, 0.5 mmol, 50 equiv relative to Fe). Yield (>99%) was determined by ^{1}H NMR analysis of EtOH. Isolated yield was based on aniline (41 mg, 0.44 mmol, 88% yield, brown liquid).

Hydrogenation of *N,N*-diphenylacetamide: General Procedure B was followed using *N,N*-diphenylacetamide (106 mg, 0.5 mmol, 50 equiv relative to Fe). Yield (>99%) was determined by ^{1}H NMR analysis of EtOH. Isolated yield was based on *N,N*-diphenylamine (81.2 mg, 0.48 mmol, 96% yield, brown solid).

V. General Procedure for the Synthesis of Benzamide Derivatives

N,N-Diphenyl benzamide derivatives were prepared by modification to a reported procedure.[79] A 500 mL round bottom flask, equipped with a magnetic stir bar, was charged with *N,N*-diphenyl amine (1.1 equiv), NEt$_3$ (1.2 equiv), and anhydrous DCM (50 mL) and the cooled to 0 °C. The appropriate acid chloride (1 equiv) was added dropwise under a N$_2$

atmosphere, and the reaction was then allowed to warm to RT. The reaction was stirred overnight. After 16 h, DCM (50 mL) was added, and the reaction mixture was transferred to a separatory funnel. The organic layer was washed with 1 M HCl (aq) (3 x 100 mL) and NaCl (aq) (1 x 50 mL). The organic layer was dried over MgSO$_4$, and the solvent was removed *in vacuo*. The resulting solid was purified by column chromatography.

N,N-**diphenylbenzamide**[80]: The general procedure for the synthesis of *N,N*-diphenyl benzamide derivatives was followed. Benzoyl chloride (6.680 g, 52.8 mmol, 1 equiv), *N,N*-diphenyl amine (9.832 g, 58.1 mmol, 1.1 equiv), and NEt$_3$ (6.689 g, 66.1 mmol, 1.2 equiv) were used. The product was isolated as a white solid (6.000 g, 21.95 mmol, 42% yield) upon purification by trituration with hexanes.

^{1}H NMR (400 MHz, CDCl$_3$) δ 7.48 (d, *J* = 7.5 Hz, 2H), 7.34-7.17 (multiple peaks, 13H).

^{13}C NMR (176 MHz, CDCl$_3$) δ 170.74, 144.02, 136.21, 130.28, 129.28, 129.21, 127.97, 127.60, 126.45.

4-fluoro-*N,N*-diphenylbenzamide: The general procedure for the synthesis of *N,N*-diphenyl benzamide derivatives was followed. 4-Fluorobenzoyl chloride (2.000 g, 12.61 mmol, 1 equiv), *N,N*-diphenyl amine (2.347 g, 13.87 mmol, 1.1 equiv), and NEt$_3$ (1.684 g, 16.64 mmol, 1.2 equiv) were used. The product was isolated as a white solid (2.388 g, 8.20 mmol, 65% yield) upon purification by column chromatography (6:1 hexanes: ethyl acetate).

^{1}H NMR (400 MHz, CDCl$_3$) δ 7.43 (dd, *J* = 8.5, 5.1 Hz, 2H), 7.26 (t, *J* = 7.6 Hz, 4H), 7.19-6.95 (multiple peaks, 6H), 6.86 (t, *J* = 8.5 Hz, 2H).

^{13}C NMR (176 MHz, DMSO-d_6) δ 168.69, 162.53 (d, *J* = 247.8 Hz), 143.61, 143.39, 132.78 (d, *J* = 3.1 Hz), 131.19 (d, *J* = 8.8 Hz), 129.16, 127.71, 126.54, 119.62, 116.68, 114.87 (d, *J* = 21.8 Hz).

^{19}F NMR (377 MHz, CDCl$_3$) δ −109.11.

4-(trifluoromethyl)-*N,N*-diphenylbenzamide: The general procedure for the synthesis of *N,N*-diphenyl benzamide derivatives was followed. 4-Trifluoromethylbenzoyl chloride (2.000 g, 9.59 mmol, 1 equiv), *N,N*-diphenyl amine (1.785 g, 10.55 mmol, 1.1 equiv), and NEt$_3$ (1.286 g, 12.66 mmol, 1.2 equiv) were used. The product was isolated as a white solid (2.134 g, 6.25 mmol, 65% yield) upon purification by column chromatography (6:1 hexanes: ethyl acetate).

^{1}H NMR (400 MHz, CDCl$_3$) δ 7.47 (dt, *J* = 34.7, 6.4 Hz, 4H), 7.35-6.70 (multiple peaks, 10H).

^{13}C NMR (176 MHz, CDCl$_3$) δ 169.22, 143.38, 139.79, 131.85 (q, *J* = 32.5 Hz), 129.46 (q, *J* = 15.2 Hz), 127.54, 126.93, 125.04 (q, *J* = 3.9 Hz), 125.27 (q, *J* = 272.8 Hz), 121.06, 117.89.

^{19}F NMR (377 MHz, CDCl$_3$) δ −62.99.

4-cyano-*N,N*-diphenylbenzamide: The general procedure for the synthesis of *N,N*-diphenyl benzamide derivatives was followed. 4-cyanobenzoyl chloride (2.000 g, 11.79 mmol, 1 equiv), *N,N*-diphenyl amine (2.195 g, 12.97 mmol, 1.1 equiv), and NEt$_3$ (1.431 g, 14.15 mmol, 1.2 equiv) were used. The product was isolated as a white solid (2.134 g, 6.25 mmol, 63% yield) upon purification by column chromatography (6:1 hexanes: ethyl acetate).

^{1}H NMR (400 MHz, CDCl$_3$) δ 7.57-7.45 (m, 4H), 7.31 (t, *J* = 7.6 Hz, 4H), 7.22 (t, *J* = 7.3 Hz, 2H), 7.15 (d, *J* = 7.8 Hz, 4H).

^{13}C NMR (176 MHz, CDCl$_3$) δ 168.68, 143.04, 140.63, 131.84, 129.60, 129.45, 127.45, 127.08, 118.18, 113.65.

_N,N_-diphenylnicotinamide[81]: The general procedure for the synthesis of *N,N*-diphenyl benzamide derivatives was followed. Nicotinoyl chloride hydrochloride (3.000 g, 16.85

mmol, 1 equiv), *N,N*-diphenyl amine (3.137 g, 18.54 mmol, 1.1 equiv), and NEt$_3$ (8.550 g, 84.25 mmol, 5 equiv) were used. The product was isolated as an orange solid (1.783 g, 6.50 mmol, 39% yield) upon trituration with cyclohexane and subsequent purification by column chromatography (5:1 hexanes: ethyl acetate).

^{1}H NMR (400 MHz, CDCl$_3$) δ 8.64 (s, 1H), 8.51 (d, *J* = 4.0 Hz, 1H), 7.76 (dt, *J* = 8.0, 2.0 Hz, 1H), 7.32 (t, *J* = 7.6 Hz, 4H), 7.25-7.13 (multiple peaks, 7H).

^{13}C NMR (176 MHz, CDCl$_3$) δ 168.28, 150.80, 150.08, 143.30, 136.66, 132.25, 129.49, 127.59, 127.04, 122.96.

4-(methoxy)-*N,N*-diphenylbenzamide[Error! Bookmark not defined.]**:** The general procedure for the synthesis of *N,N*-diphenyl benzamide derivatives was followed. 4-(Methoxy)benzoyl chloride (2.000 g, 11.72 mmol, 1 equiv), *N,N*-diphenyl amine (2.181 g, 12.89 mmol, 1.1 equiv), and NEt$_3$ (1.423 g, 14.06 mmol, 1.2 equiv) were used. The product was isolated as a faint-pink solid (1.833 g, 6.04 mmol, 52% yield) purification by column chromatography (5:1 hexanes: ethyl acetate).

^{1}H NMR (700 MHz, CDCl$_3$) δ 7.44 (d, *J* = 7.0 Hz, 2H), 7.29 (t, *J* = 7.0 Hz, 4H), 7.18 (t, *J* = 7.0 Hz, 2H), 7.14 (d, *J* = 7.0 Hz, 4H), 6.71 (d, *J* = 7.0 Hz, 2H), 3.76 (s, 3H).

^{13}C NMR (176 MHz, CDCl$_3$) δ 170.37, 161.19, 144.46, 131.52, 129.20, 128.16, 127.55, 126.23, 113.22, 55.35.

4-(dimethylamino)-*N,N*-diphenylbenzamide: The general procedure for the synthesis of *N,N*-diphenyl benzamide derivatives was followed. 4-(Dimethylamino)benzoyl chloride (0.500 g, 2.72 mmol, 1 equiv), *N,N*-diphenylamine (0.508 g, 3.0 mmol, 1.1 equiv), and NEt$_3$ (0.331 g, 3.26 mmol, 1.2 equiv) were used. The product was isolated as an off-white solid (0.573 g, 1.81 mmol, 66% yield) upon trituration with hexanes and then recrystallization from ethyl acetate.

^{1}H NMR (400 MHz, CDCl$_3$) δ 7.41-7.34 (multiple peaks, 2H), 7.31-7.21 (multiple peaks, 4H), 7.12 (td, J = 8.0, 3.6 Hz, 6H), 6.44 (d, J = 8.0 Hz, 2H), 2.92 (s, 6H).

^{13}C NMR (176 MHz, CDCl$_3$) δ 170.91, 151.71, 145.14, 131.73, 129.13, 127.55, 125.83, 122.30, 110.51, 40.14.

VI. General Procedure for the Hydrogenation of Amides (Table 5.4, 3-10)
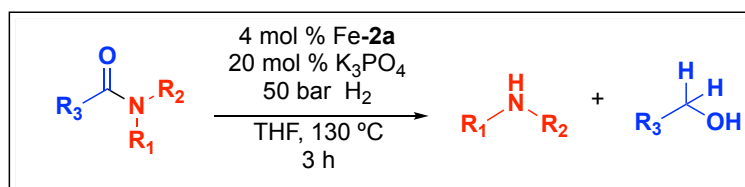
General Procedure C: In a N$_2$-atmosphere dry box, Fe-**2a** (5.6 mg, 10 μmol, 4 mol %) was dissolved in 2 mL THF, and this solution was added to the metal well of a pressure vessel containing the K$_3$PO$_4$ (10.6 mg, 50 μmol, 20 mol%, 5 equiv relative to Fe) and a micro magnetic stirbar (3 x 10 mm). The amide substrate (0.25 mmol, 300 equiv relative to Fe) was then added, and the vessel (Reactor type A) was sealed and removed from the dry box. The vessel was connected to the Parr Multiple Reactor System, and the manifold was thoroughly purged with research grade H$_2$ (99.9999%). The vessel was then pressurized with 50 bar of research grade H$_2$ at room temperature, and the reaction was heated to 130 ºC with a stir rate of 800 RPM. The heating was conducted using Specview software. After 3 h of heating, the reaction mixture was allowed to cool to room temperature. The pressure vessel was placed in a –84 °C bath (ethyl acetate/LN$_2$) for 15 min and then carefully vented using a metering valve.

      Preparation of samples for NMR analysis: THF (0.5 mL) was added through the venting valve of the pressure vessel to wash any residual liquids/solids into the vessel. The vessel was then opened, 1,3,5-trimethoxybenzene (0.178 mmol, 300 µL of 0.593 M solution in DMSO-d_6) was added as a ^{1}H NMR standard, and the contents of the vessel were diluted with DMSO-d_6. Approximately 50 µL of the resulting solution was added to an NMR tube, diluted further with DMSO-d_6. The sample was analyzed by ^{1}H NMR spectroscopy.

      General Method for the Isolation of Non-volatile Products: Ethyl acetate (5 mL) was added through the venting valve of the pressure vessel to wash any residual

liquids/solids into the vessel. The vessel was then opened, and the contents were further diluted with ethyl acetate (~ 30 mL) and filtered through a silica plug (3.5 x 4 cm). The plug was washed with additional ethyl acetate (~ 80 mL), and the solvent was removed *in vacuo* to yield the pure product, unless otherwise noted. The ^{1}H and ^{13}C{^{1}H} NMR spectra of the isolated products matched those reported in the literature.

Hydrogenation of *N,N*-dimethylbenzamide[80]**:** General Procedure C was followed using *N,N*-dimethylbenzamide (38 mg, 0.25 mmol, 25 equiv relative to Fe). Yield (36%) was determined by ^{1}H NMR analysis of benzyl alcohol.

Hydrogenation of *N*-phenylbenzamide: General Procedure C was followed using *N*-phenylbenzamide (50 mg, 0.25 mmol, 25 equiv relative to Fe). Yield (>99%) was determined by ^{1}H NMR analysis of benzyl alcohol.

Hydrogenation of *N,N*-diphenylbenzamide: General Procedure C was followed using *N,N*-diphenylbenzamide (137 mg, 0.25 mmol, 25 equiv relative to Fe). Yield (>99%) was determined by ^{1}H NMR analysis of benzyl alcohol. Isolated yield was based on diphenyl amine (124 mg, 0.248 mmol, 99% yield, brown solid).

Hydrogenation of 4-fluoro-*N,N*-diphenylbenzamide: General Procedure C was followed using 4-fluoro-*N,N*-diphenylbenzamide (73 mg, 0.25 mmol, 25 equiv relative to Fe). Yield (>99%) was determined by ^{1}H NMR analysis of 4-fluorobenzyl alcohol. Isolated yield was based on diphenylamine (39 mg, 0.233 mmol, 93% yield, brown solid).

Hydrogenation of 4-(trifluoromethyl)-*N,N*-diphenylbenzamide: General Procedure C was followed using 4-(trifluoromethyl)-*N,N*-diphenylbenzamide (85 mg, 0.25 mmol, 25 equiv relative to Fe). Yield (>99%) was determined by ^{1}H NMR analysis of 4-(trifluoromethyl)benzyl alcohol. Isolated yield was based on diphenylamine (39 mg, 0.233 mmol, 93% yield, brown solid).

Hydrogenation of 4-cyano-*N,N*-diphenylbenzamide: General Procedure C was followed using 4-cyano-*N,N*-diphenylbenzamide (75 mg, 0.25 mmol, 25 equiv relative to Fe). Yield

(>99%) was determined by ^{1}H NMR analysis of (4-(aminomethyl)phenyl)methanol. Isolated yields were obtained of both diphenylamine (39 mg, 0.233 mmol, 93% yield, brown solid) and (4-(aminomethyl)phenyl)methanol (22 mg, 0.163 mmol, 65% yield, light yellow solid). (4-(Aminomethyl)phenyl)methanol was isolated following a modified procedure to the general method for the isolation of non-volatile products. After flushing the silica plug with ethyl acetate, the top layer of the silica plug was transferred to a round bottom flask. The silica was washed with diethyl ether (~100 mL) and acidified with 1.0 M HCl in diethyl ether. A white precipitate formed upon concentration *in vacuo*, and this material was collected via filtration. The solid was dissolved in diethyl ether (~50 mL), this solution was transferred to a separatory funnel, and the organic layer was washed with sat. K_2CO_3 (aq) (1 x 15 mL) and sat. NaCl (aq) (1 x 15 mL). The organic layer was dried over $MgSO_4$, and the solvent removed *in vacuo*.

(4-(aminomethyl)phenyl)methanol
^{1}H NMR (400 MHz, $CDCl_3$) δ 7.30 (d, *J* = 7.7 Hz, 2H), 7.25 (d, *J* = 7.7 Hz, 2H), 4.63 (s, 2H), 3.81 (s, 2H), 1.85 (bs, 3H).

^{13}C NMR (176 MHz, $CDCl_3$) δ 142.42, 139.93, 127.38, 127.34, 64.93, 46.22.

Hydrogenation of *N,N*-diphenylnicotinamide: General Procedure C was followed using *N,N*-diphenylnicotinamide (69 mg, 0.25 mmol, 25 equiv relative to Fe). Yield (>99%) was determined by ^{1}H NMR analysis of 3-pyridinemethanol. Isolated yields were obtained of both diphenylamine (40 mg, 0.238 mmol, 95% yield, brown solid) and 3-pyridinemethanol (23 mg, 0.213 mmol, 85% yield, colorless liquid). 3-Pyridinemethanol was isolated following a modified procedure to the general method for the isolation of non-volatile products. After flushing the silica plug with ethyl acetate, the top layer of the silica plug was transferred to a round bottom flask. The silica was washed with diethyl ether (~100 mL) and acidified with 1.0 M HCl in diethyl ether. A white ppt formed upon concentration *in vacuo* and this material was collected by filtration. The solid was dissolved in diethyl ether (~50 mL), this solution was transferred to a separatory funnel, and the organic layer was washed with sat. K_2CO_3 (aq) (1 x 15 mL) and sat. NaCl (aq) (1 x 15 mL). The organic layer was dried over $MgSO_4$ and the solvent removed *in vacuo*.

3-pyridinemethanol

^{1}H NMR (400 MHz, CDCl$_3$) δ 8.45 (d, J = 2.1 Hz, 1H), 8.39 (dd, J = 4.7, 1.8 Hz, 1H), 7.69 (dd, J = 7.8, 2.1 Hz, 1H), 7.32-7.12 (multiple peaks, 1H), 4.67 (s, 2H), 4.16 (s, 1H).

^{13}C NMR (176 MHz, CDCl$_3$) δ 148.49, 148.25, 137.00, 135.21, 123.71, 62.35.

Hydrogenation of 4-(dimethylamino)-*N,N*-diphenylbenzamide: General Procedure C was followed using 4-(dimethylamino)-*N,N*-diphenylbenzamide (73 mg, 0.25 mmol, 25 equiv relative to Fe). Yield (<1%) was determined by ^{1}H NMR analysis of 4-fluorobenzyl alcohol.

Hydrogenation of 4-(methoxy)-*N,N*-diphenylbenzamide: General Procedure C was followed using 4-(methoxy)-*N,N*-diphenylbenzamide (76 mg, 0.25 mmol, 25 equiv relative to Fe). Yield (<1%) was determined by ^{1}H NMR analysis of 4-methoxybenzyl alcohol.

Hydrogenation of *N*-Benzyl-2,2,2-trifluoroactamide: General Procedure A was followed using *N*-Benzyl-2,2,2-trifluoroacetamide (567 mg, 3.0 mmol, 300 equiv relative to Fe). Yield (44%) was determined by ^{1}H NMR analysis of 2,2,2-trifluoroethanol

VII. General Procedure for *In Situ* Raman Kinetics (Figure 5.5)

In a N$_2$-atmosphere dry box, Ru-**2a** (21.4 mg, 35 µmol) or Fe-**2a** (19.6 mg, 35 µmol) and K$_3$PO$_4$ (37.1 mg, 175 µmol, 5 equiv relative to Ru-**2a** or Fe-**2a**) were added to the metal well of Reactor B which also contained a micro magnetic stirbar (3 x 10 mm) and a glass cylinder to displace solvent volume toward the Raman probe. THF (7 mL) and DMF (805 µL, 10.5 mmol, 300 equiv relative to Ru-**2a** or Fe-**2a**) were then added, and the vessel was sealed and removed from the dry box. The vessel was connected to the Parr Multiple Reactor System, and the manifold was thoroughly purged with research grade H$_2$ (99.9999%). The vessel was then pressurized to 70 bar with research grade H$_2$ at room temperature. The Raman probe was attached to the instrument. A dark spectrum was acquired at the onset. The reactor was then placed into a preheated block to obtain a reactor internal temperature of 110 °C. Once the reactor's internal temperature was at 110

°C ± 5 °C (after 35 min), Raman spectra were collected for 4 exposures (1 accumulation for 3 s) over a period of 6 min with collections every 1.5 min, at which time spectra were then collected every 3 min until the reaction had reached completion (for Ru-**2a**, an additional 122 spectra were collected over 6.1 h; for Fe-**2a**, an additional 168 spectra were collected over 8.4 h). Savitzky-Golay smoothing (using a 5th order polynomial constructed from 7 points with distortion being removed) and normalization was applied to each spectrum. A background spectrum of THF was also treated with Savitzky-Golay smoothing and normalized before being subtracted from each spectrum. The data was truncated to include the region between 240-1800 cm^{-1}. Baseline correction was applied between endpoints, and peak areas were determined by peak picking for DMF peaks at ~658 cm^{-1} (integration area between 629-687 cm^{-1}) and ~865 cm^{-1} (integration area 852-878 cm^{-1}). A constant factor was subtracted from each spectrum determined from the value of the computed areas after full conversion (–30.06 for peaks at 658 cm^{-1} and –21.25 for 865 cm^{-1}). This removes the constant contribution of noise to the peak areas. Peak areas were converted to concentrations based on a calibration curve constructed at six different concentrations ranging from 0-1.34 M DMF in THF.

VIII. General Procedure for Variable Pressure *In Situ* Raman Kinetics (Figure 5.7)

In a N_2-atmosphere dry box, Fe-**2a** (19.6 mg, 35 µmol) and K_3PO_4 (37.1 mg, 175 µmol, 5 equiv relative to Fe-**2a**) were added to the metal well of Reactor B which also contained a micro magnetic stirbar (3 x 10 mm) and a glass cylinder to displace solvent volume toward the Raman probe. THF (7 mL) and DMF (805 µL, 10.5 mmol, 300 equiv relative to Fe-**2a**) were then added, and the vessel was sealed and removed from the dry box. The vessel was connected to the Parr Multiple Reactor System, and the manifold was thoroughly purged with research grade H_2 (99.9999%). The vessel was then pressurized to either 20, 50, or 70 bar with research grade H_2 at room temperature. The Raman probe was attached to the instrument. A dark spectrum was acquired at the onset. The reactor was then placed into a preheated block to obtain a reactor internal temperature of 110 °C. Once the reactor's internal temperature was at 110 °C ± 5 °C (after 35 min), Raman spectra were collected for 3 exposures (1 accumulation for 3 s) over a period of 10 h with collections every 3 min. Savitzky-Golay smoothing (using a 5th order polynomial constructed from 7 points with distortion being removed) and normalization was applied to

each spectrum. The data was truncated to include the region between 480-1137 cm^{-1}. Baseline correction was applied between endpoints, and peak intensities were determined by peak picking for DMF peaks at ~658 cm^{-1} and ~865 cm^{-1}. A constant factor was subtracted from each spectrum determined from the value of the computed intensities after full conversion. This removes the constant contribution of noise to the peak intensities. The resulting peak intensities were used to compare the reaction progress.

IX. ^{1}H NMR Time Study (Figure 5.8)

In a N$_2$-atmosphere dry box, Fe-**2a** (2.8 mg, 5 μmol) was dissolved in 1 mL THF, and this solution was transferred to a J-Young NMR tube containing the K$_3$PO$_4$ (5.3 mg, 25 μmol, 5 equiv relative to Fe). The tube was capped, and removed from the glovebox. The J-Young tube was connected to a vacuum manifold and submerged in N$_{2(l)}$ until frozen. The J-Young NMR tube was evacuated and backfilled with H$_2$ (X3) (1 bar). The resulting yellow solution was analyzed by ^{1}H NMR spectroscopy and then placed in an oil bath at 100 ºC for the allotted data points.

X. Synthesis of Unknown species (Fe-2a–Morph)[23]

In a N$_2$-atmosphere dry box, Fe-**2a** (49.4 mg, 88 μmol) was dissolved in 3.5 THF , and this solution was transferred to a 25 mL Schlenk flask containing (9.2 mg, 106 μmol, 1.2 equiv relative to Fe) in 0.5 mL THF. The flask was capped, removed from the glovebox and connected to a vacuum manifold. The flask and submerged in N$_{2(l)}$ until the THF solution was frozen. The Schlenk flask was evacuated and backfilled with H$_2$ (X3) (1 bar and then placed in an oil bath at 60 ºC overnight resulting in a red solution. Upon cooling to RT the red solution slowly changed to yellow. The flask transferred into an inert glovebox and the solution was filtered. The solvent was removed *in vacuo* to afford the title product.

XI. DMF Hydrogenation with Fe-2a–Morph (Figure 5.10)

In a N$_2$-atmosphere dry box, **Fe-2a–Morph** (10 μmol, 0.33 mol %) was dissolved in 2 mL of THF, and this solution was added to the metal well of a pressure vessel a micro magnetic stirbar (3 x 10 mm). DMF (230 μL, 3.0 mmol, 300 equiv relative to Fe) was then added, and the vessel (Reactor-type A) was sealed and removed from the dry box. The vessel was connected to the Parr Multiple Reactor System, and the manifold was

thoroughly purged with research grade H_2 (99.9999%). The vessel was then pressurized with research grade H_2 at room temperature, and the reaction was heated at the desired temperature with a stir rate of 800 RPM. The heating was conducted using Specview software. After 3 h of heating, the reaction mixture was allowed to cool to room temperature. The pressure vessel was placed in a –84 °C bath (ethyl acetate/LN_2) for 15 min and then carefully vented using a metering valve. THF (0.5 mL) was added through the venting valve of the pressure vessel to wash any residual liquids/solids into the vessel. The vessel was then opened, 1,3,5-trimethoxybenzene (0.178 mmol, 300 μL of 0.593 M solution in DMSO-d_6) was added as a ^{1}H NMR standard, and the contents of the vessel were diluted with DMSO-d_6. Approximately 50 μL of the resulting solution was added to an NMR tube, diluted further with DMSO-d_6. The sample was then analyzed by ^{1}H NMR spectroscopy (see Figure 5.16 for a representative spectrum).

XII. Hydrogenation of CO_2 to formamides (Table 5.5)

In a N_2-atmosphere dry box, [Fe] catalyst (10 μmol) was dissolved in 2 mL of THF containing the appropriate quantity of amine. The resulting solution was added to the pre-chilled (in the dry box freezer at –33 °C) metal well of a pressure vessel containing K_3PO_4 (10.6 mg, 50 μmol) and an octagonal magnetic stirbar (5/16 x 1/2 in). The vessel was sealed and removed from the dry box. The vessel was pressurized with CO_2 and then immediately with H_2 (50 bar) at room temperature. The reaction was then heated at 95 °C with a stir rate of 800 RPM. After 10 h of heating, the reaction mixture was allowed to cool to room temperature. The pressure vessel was placed in a –84 °C bath (ethyl acetate/LN_2) for 15 min and then carefully vented using a metering valve. THF (0.5 mL) was added through the venting valve of the pressure vessel to wash any residual liquids/solids into the vessel. The vessel was then opened, 1,3,5-trimethoxybenzene (0.178 mmol, 300 μL of 0.593 M solution in DMSO-d_6) was added as a ^{1}H NMR standard, and the contents of the vessel were diluted with DMSO-d_6. 50 μL of the resulting solution was added to an NMR tube, diluted further with DMSO-d_6, and acidified using 12 M HCl to a pH of 2. The sample was then analyzed by ^{1}H NMR spectroscopy. No methanol was detected under these conditions.

XII. Hydrogenation of CO$_2$ to CH$_3$OH with ramp. (Table 5.6)

In a N$_2$-atmosphere dry box, [Fe] catalyst (10 μmol, 0.25 mol %) was dissolved in 2 mL of THF containing the amine (7.6 mmol). The resulting solution was added to the pre-chilled (in the dry box freezer at –33 ℃) metal well of a pressure vessel containing K$_3$PO$_4$ (10.6 mg, 50 μmol) and an octagonal magnetic stirbar (5/16 x 1/2 in). The vessel was sealed and removed from the dry box. The vessel was pressurized with CO$_2$ (0.5 bar) and then immediately with H$_2$ (50 bar) at room temperature. The reaction was then heated using the temperature ramp with a stir rate of 800 RPM. After 20 h of heating, the reaction mixture was allowed to cool to room temperature. The pressure vessel was placed in a –84 ℃ bath (ethyl acetate/LN$_2$) for 15 min and then carefully vented using a metering valve. THF (0.5 mL) was added through the venting valve of the pressure vessel to wash any residual liquids/solids into the vessel. The vessel was then opened, 1,3,5-trimethoxybenzene (0.178 mmol, 300 μL of 0.593 M solution in DMSO-d_6) was added as a ^{1}H NMR standard, and the contents of the vessel were diluted with DMSO-d_6. 50 μL of the resulting solution was added to an NMR tube, diluted further with DMSO-d_6, and acidified using 12 M HCl to a pH of 2. The sample was then analyzed by ^{1}H NMR spectroscopy.

XIII. Two-step Hydrogenation of CO$_2$ to CH$_3$OH. (Table 5.7)

In a N$_2$-atmosphere dry box, Fe-**2a** catalyst (5.6 mg, 10 μmol), and the appropriate [Ru] complex (10 μmol) were dissolved in 2 mL of THF containing the NHMe$_2$ (7.6 mmol). The resulting solution was added to the pre-chilled (in the dry box freezer at –33 ℃) metal well of a pressure vessel containing K$_3$PO$_4$ (10.6 mg, 50 μmol) and an octagonal magnetic stirbar (5/16 x 1/2 in). The vessel was sealed and removed from the dry box. The vessel was pressurized with CO$_2$ (1 bar) and then immediately with H$_2$ (50 bar) at room temperature. The reaction was then heated using to 95 ℃ for 3 h with a stir rate of 800 RPM. After 3 h of heating, the vessel was allowed to cool to room temperature and vented under positive pressure of H$_2$. After a thorough purge with H$_2$, the vessel was re-pressurized with H$_2$ (50 bar) at room temperature and heated at 110 ℃ for 3 h. After a total reaction time of 6 h, the reaction mixture was allowed to cool to room temperature. The pressure vessel was placed in a –84 ℃ bath (ethyl acetate/LN$_2$) for 15 min and then carefully vented using a metering valve. THF (0.5 mL) was added through the venting valve of the pressure vessel to wash any residual liquids/solids into the vessel. The vessel

was then opened, 1,3,5-trimethoxybenzene (0.178 mmol, 300 μL of 0.593 M solution in DMSO-d_6) was added as a ^{1}H NMR standard, and the contents of the vessel were diluted with DMSO-d_6. 50 μL of the resulting solution was added to an NMR tube, diluted further with DMSO-d_6, and acidified using 12 M HCl to a pH of 2. The sample was then analyzed by ^{1}H NMR spectroscopy.

5.5 References

(1) Roose, P.; Eller, K.; Henkes, E.; Rossbacher, R.; Höke, H. In Ullmann's Encyclopedia of Industrial Chemistry; Wiley-VCH, Weinhma, Germany, Amines, Aliphatic: 2000. DOI: 10.1002/14356007.a02_001.pub2.

(2) Jessop, P. G. In The Handbook of Homogeneous Hydrogenation; Wiley-VCH Verlag GmbH: 2006, p 489-511.

(3) Dodds, D. L.; Cole-Hamilton, D. J. In *Sustainable Catalysis*; John Wiley & Sons, Inc.: 2013, p 1-36.

(4) Smith, A. M.; Whyman, R. *Chem. Rev.* **2014**, *114*, 5477-5510.

(5) Yuan, M.-L.; Xie, J.-H.; Zhu, S.-F.; Zhou, Q.-L. *ACS Catal.* **2016**, 3665-3669.

(6) Zell, T.; Milstein, D. *Acc. Chem. Res.* **2015**, *48*, 1979-1994.

(7) Mérel, D. S.; Do, M. L. T.; Gaillard, S.; Dupau, P.; Renaud, J.-L. *Coord. Chem. Rev.* **2015**, *288*, 50-68.

(8) Casey, C. P.; Guan, H. *J. Am. Chem. Soc.* **2007**, *129*, 5816-5817.

(9) Langer, R.; Leitus, G.; Ben-David, Y.; Milstein, D. *Angew. Chem. Int. Ed.* **2011**, *50*, 2120-2124.

(10) Gorgas, N.; Stöger, B.; Veiros, L. F.; Pittenauer, E.; Allmaier, G.; Kirchner, K. *Organometallics* **2014**, *33*, 6905-6914.

(11) Gorgas, N.; Stöger, B.; Veiros, L. F.; Kirchner, K. *ACS Catal.* **2016**, *6*, 2664-2672.

(12) Sui-Seng, C.; Freutel, F.; Lough, A. J.; Morris, R. H. *Angew. Chem. Int. Ed.* **2008**, *47*, 940-943.

(13) Zuo, W.; Lough, A. J.; Li, Y. F.; Morris, R. H. *Science* **2013**, *342*, 1080-1083.

(14) Sonnenberg, J. F.; Lough, A. J.; Morris, R. H. *Organometallics* **2014**, *33*, 6452-6465.

(15) Zuo, W.; Prokopchuk, D. E.; Lough, A. J.; Morris, R. H. *ACS Catal.* **2015,** 301-314.

(16) Zell, T.; Ben-David, Y.; Milstein, D. *Catal. Sci. Technol.* **2015**, *5*, 822-826.

(17) Werkmeister, S.; Junge, K.; Wendt, B.; Alberico, E.; Jiao, H.; Baumann, W.; Junge, H.; Gallou, F.; Beller, M. *Angew. Chem. Int. Ed.* **2014**, *53*, 8722-8726.

(18) Chakraborty, S.; Dai, H.; Bhattacharya, P.; Fairweather, N. T.; Gibson, M. S.; Krause, J. A.; Guan, H. *J. Am. Chem. Soc.* **2014**, *136*, 7869-7872.

(19) Qu, S.; Dai, H.; Dang, Y.; Song, C.; Wang, Z.-X.; Guan, H. *ACS Catal.* **2014**, 4377-4388.

(20) Fairweather, N. T.; Gibson, M. S.; Guan, H. *Organometallics* **2015**, 34, 335-339.

(21) Elangovan, S.; Wendt, B.; Topf, C.; Bachmann, S.; Scalone, M.; Spannenberg, A.; Jiao, H.; Baumann, W.; Junge, K.; Beller, M. *Adv. Syn. Catal.* **2016**, 358, 820-825.

(22) Garg, J. A.; Chakraborty, S.; Ben-David, Y.; Milstein, D. *Chem. Commun.* **2016,** *52*, 5285-5288.

(23) Schneck, F.; Assmann, M.; Balmer, M.; Harms, K.; Langer, R. *Organometallics* **2016**, *35*, 1931-1943.

(24) Fox, D. J.; Bergman, R. G. *Organometallics* **2004**, *23*, 1656-1670.

(25) Jiao, H.; Junge, K.; Alberico, E.; Beller, M. *J. Comput. Chem.* **2016**, *37*, 168-176.

(26) Morrison, A. L.; Long, R. F.; Konigstein, M. *J. Chem. Soc.* **1951**, 952-955.

(27) Kikugawa, Y.; Ikegami, S.; Yamada, S. *Chem Pharm Bull* **1969**, *17*, 98-104.

(28) Szostak, M.; Spain, M.; Eberhart, A. J.; Procter, D. J. *J. Am. Chem. Soc.* **2014**, *136*, 2268-2271.

(29) Kilner, M.; Tyers, D. V.; Crabtree, S. P.; Wood, M. A. W.O. Patent 093208, November 13, 2007.

(30) Ito, M.; Sakaguchi, A.; Kobayashi, C.; Ikariya, T. *J. Am. Chem. Soc.* **2007**, *129*, 290-291.

(31) Magro, A. A. N.; Eastham, G. R.; Cole-Hamilton, D. J. *Chem. Commun.* **2007**, 3154-3156.

(32) Ito, M.; Koo, L. W.; Himizu, A.; Kobayashi, C.; Sakaguchi, A.; Ikariya, T. *Angew. Chem. Int. Ed.* **2009**, *48*, 1324-1327.

(33) Balaraman, E.; Gnanaprakasam, B.; Shimon, L. J. W.; Milstein, D. *J. Am. Chem. Soc.* **2010**, *132*, 16756-16758.

(34) Ito, M.; Kobayashi, C.; Himizu, A.; Ikariya, T. *J. Am. Chem. Soc.* **2010**, *132*, 11414-11415.

(35) John, J. M.; Bergens, S. H. *Angew. Chem. Int. Ed.* **2011**, *50*, 10377-10380.

(36) Miura, T.; Held, I. E.; Oishi, S.; Naruto, M.; Saito, S. *Tetrahedron Lett.* **2013**, *54*, 2674-2678.

(37) Kita, Y.; Higuchi, T.; Mashima, K. *Chem. Commun.* **2014**, *50*, 11211-11213.

(38) John, J. M.; Loorthuraja, R.; Antoniuk, E.; Bergens, S. H. *Catal. Sci. Technol.* **2015**, *5*, 1181-1186.

(39) Coetzee, J.; Dodds, D. L.; Klankermayer, J.; Brosinski, S.; Leitner, W.; Slawin, A. M. Z.; Cole-Hamilton, D. J. *Chem. Eur. J.* **2013**, *19*, 11039-11050.

(40) Coetzee, J.; Manyar, H. G.; Hardacre, C.; Cole-Hamilton, D. J. *Chemcatchem* **2013**, *5*, 2843-2847.

(41) Meuresch, M.; Westhues, S.; Leitner, W.; Klankermayer, J. *Angew. Chem. Int. Ed.* **2016**, *55*, 1392-1395.

(42) vom Stein, T.; Meuresch, M.; Limper, D.; Schmitz, M.; Hölscher, M.; Coetzee, J.; Cole-Hamilton, D. J.; Klankermayer, J.; Leitner, W. *J. Am. Chem. Soc.* **2014**, *136*, 13217-13225.

(43) Cabrero-Antonino, J. R.; Alberico, E.; Junge, K.; Junge, H.; Beller, M. *Chem. Sci.* **2016**, *7*, 3432-3442.

(44) Gunanathan, C.; Milstein, D. *Acc. Chem. Res.* **2011**, *44*, 588-602.

(45) Cantillo, D. *Eur. J. Inorg. Chem.* **2011**, 3008-3013.
(46) Fogler, E.; Garg, J. A.; Hu, P.; Leitus, G.; Shimon, L. J. W.; Milstein, D. *Chem. Eur. J.* **2014**, *20*, 15727-15731.
(47) Gunanathan, C.; Milstein, D. *Chem. Rev.* **2014**, *114*, 12024-12087.
(48) Huff, C. A.; Sanford, M. S. *J. Am. Chem. Soc.* **2011**, *133*, 18122-18125.

(49) Huff, C. A.; Sanford, M. S. *ACS Catal.* **2013**, *3*, 2412-2416.

(50) Rezayee, N. M.; Huff, C. A.; Sanford, M. S. *J. Am. Chem. Soc.* **2015**, *137*, 1028-1031.

(51) Brewster, T. P.; Rezayee, N. M.; Culakova, Z.; Sanford, M. S.; Goldberg, K. I. *ACS Catal.* **2016**, *6*, 3113-3117.

(52) Kuriyama, W.; Matsumoto, T.; Ogata, O.; Ino, Y.; Aoki, K.; Tanaka, S.; Ishida, K.; Kobayashi, T.; Sayo, N.; Saito, T. *Org. Process Res. Dev.* **2012**, *16*, 166-171.

(53) Lagaditis, P. O.; Sues, P. E.; Sonnenberg, J. F.; Wan, K. Y.; Lough, A. J.; Morris, R. H. *J. Am. Chem. Soc.* **2014**, *136*, 1367-1380.

(54) Zhang, L.; Han, Z.; Zhao, X.; Wang, Z.; Ding, K. *Angew. Chem. Int. Ed.* **2015**, *54*, 6186-6189.

(55) Zhang, Y.; MacIntosh, A. D.; Wong, J. L.; Bielinski, E. A.; Williard, P. G.; Mercado, B. Q.; Hazari, N.; Bernskoetter, W. H. *Chem. Sci.* **2015**, *6*, 4291-4299.

(56) Fe-**2b** has been demonstrated for ester hydrogenation (refs 17 and 18). Additionally, a very recent report demonstrated that Fe-**2a** is also effective for ester hydrogenation (ref. 21).

(57) Fe-**2a** offers the additional advantages that it is straightforward to synthesize and exhibits high solubility in our reaction solvent (THF).

(58) These initial conditions were selected based on our studies of DMF hydrogenation with a related Ru pincer catalyst (ref. [50]).

(59) Noyori, R.; Ohkuma, T. *Angew. Chem. Int. Ed.* **2001**, *40*, 40-73.

(60) Hamilton, R. J.; Bergens, S. H. *J. Am. Chem. Soc.* **2006**, *128*, 13700-13701.

(61) Clarke, M. L.; Diaz-Valenzuela, M. B.; Slawin, A. M. Z. *Organometallics* **2007**, *26*, 16-19.

(62) Saudan, L. A.; Saudan, C. M.; Debieux, C.; Wyss, P. *Angew. Chem., Int. Ed.* **2007**, *46*, 7473-7476.

(63) The use of NaOEt, KOtBu, and KHMDS resulted in poor mass balance, suggesting incompatibility between these bases and the DMF substrate.

(64) Catalyst Fe-**2c** has been reported for the hydrogenation of esters (ref 21) and, recently, a small subset of amides (ref 23). To confirm the activity of our samples of Fe-**2c**, we also performed the hydrogenation of methyl benzoate (using 1 mol % of Fe-**2c** and 30 bar H_2 at 60 ºC for 6 h) and benzanilide (using 4 mol % of Fe-**2c**, 20 mol % of K3PO4 and 50 bar H_2 at 110 ºC for 3 h). In our hands, these transformations afforded >99% yield (100 turnovers), and 70% yield (18 turnovers), respectively.

(65) Cabrero-Antonino, J. R.; Alberico, E.; Drexler, H.-J.; Baumann, W.; Junge, K.; Junge, H.; Beller, M. *ACS Catal.* **2016**, *6*, 47-54.

(66) Bornschein, C.; Werkmeister, S.; Wendt, B.; Jiao, H.; Alberico, E.; Baumann, W.; Junge, H.; Junge, K.; Beller, M. *Nat. Commun.* **2014**, *5*, 4111.

(67) Genna, D. G.; Pfund, L. Y.; Samblanet, D. C.; Wong-Foy, A. G.; Matzger, A. J.; Sanford, M. S. *ACS Catal.* **2016**, *6*, 3569-3574.

(68) Cook, A. K.; Schimler, S. D.; Matzger, A. J.; Sanford, M. S. *Science* **2016**, *351*, 1421-1424.

(69) Our Raman set-up requires a larger reaction volume than the standard reaction conditions (7 vs 2 mL) in order to submerge the Raman probe; as such, the concentration of DMF was kept constant between the two volumes, and all other components were scaled appropriately to maintain consistent ratios.

(70) The low reactivity of amides bearing electron donor groups (e.g, Table 5.3 entry 4 and Table 5.4, entry 10) provides preliminary evidence in support of rate limiting hydride transfer with catalyst Fe-**2a**.

(71) For example, see: Cheng, T.-Y.; Brunschwig, B. S.; Bullock, R. M. *J. Am. Chem. Soc.* **1998**, *120*, 13121-1317.

(72) Čechová, L.; Jansa, P.; Šála, M.; Dračínský, M.; Holý, A.; Janeba, Z. *Tetrahedron* **2011**, *67*, 866-871.

(73) Abdur-Rasad, K.; Graham, T.; Tsang, C.; Chen, X.; Guo, R.; Jia, W.; Amoroso, D.; Sui-Seng, C. (Kanata Chemical Technologies, CA). Method for the Production of Hydrogen from Ammonia Borane. US Patent 20,110,070,152, March 24, 2011.

(74) Han, Z.; Rong, L.; Wu, J.; Zhang, L.; Wang, Z.; Ding, K. *Angew. Chem. Int. Ed.* **2012**, *51*, 13041.

(75) Mainz, V. V.; Andersen, R. A. Organometallics **1984**, 3, 675

(76) Mason, R.; Meek, D. w.; Scollary, G. R. Inorg. Chim. Acta, **1976**, 16, L11.

(77) Voss, C.; Scholz, C.; Knorr, S.; Beck, P.; Stein, M. L.; Zall, A.; Kuckelkorn, U.; Kloetzel, P.-M.; Groll, M.; Hamacher, K.; Schmidt, B. *ChemMedChem* **2014**, *9*, 2557.

(78) Barluenga, J.; Álvarez-Gutiérrez, J. M.; Ballesteros, A.; González, J. M. *Angew. Chem. Int. Ed.* **2007**, *46*, 1281.

(79) Pelletier, G.; Bechara, W. S.; Charette, A. B. *J. Am. Chem. Soc.* **2010**, *132*, 12817.

(80) Wei, P.; Bi, X.; Wu, Z.; Xu, Z. *Org. Lett.* **2005**, *7*, 3199.

(81) Deguest, G.; Devineau, A.; Bischoff, L.; Fruit, C.; Marsais, F. *Org. Lett.* **2006**, *8*, 5889.

(83) Rezayee, N. M.; Samblanet, D. C.; Sanford, M. S. *ACS Catal.* **2016**, 6377.

CHAPTER 6: IDENTIFICATION OF A SWITCHABLE CATALYST FOR THE HYDROGENOLYSIS OF AMIDES: INVESTIGATION OF C–O AND C–N BOND SCISSION

The chemistry detailed in this chapter has been made possible with Prof. Melanie S. Sanford. The work described was performed in part of the Center for Enabling New Technologies Through Catalysis and the Carbon Dioxide Activation Center.

6.1 Introduction

The reduction of carboxylic acids and carboxylic acid-derivatives has provided a readily accessible carbon feedstock for both academic and industrial settings.[1,2] Amides are challenging carboxylic acid derivatives to reduce owing to the increased resonance stabilization energy.[1] Traditional use of stoichiometric reductants such as lithium aluminum hydride (LAH) leads, primarily, to the deoxygenated aliphatic amine.[3] Complementary methodologies such as the use of SmI_2 have been disclosed to selectively yield the C–N bond cleaved products (alcohol and amine).[4] Hydrogenation of amides has also posed similar differences in selectivity.[5,6] Often, the selection of hydrogenation catalyst predetermines the product distribution shown in Figure 6.1.[7]

Transition metal catalysts (Ru,[1] Fe,[8,9,10,11] Mn,[12] etc.) selective for C–N bond scission have been widely advanced using a variety of pincer ligands and their mechanisms have been thoroughly investigated. In contrast, catalyst development for amide C–O bond cleavage remains in its infancy despite earlier precedent.[13] To date, only

two catalysts have been reported to yield C–O bond cleaved products shown in Figure 6.1 and both catalysts necessitate the use of highly acidic additives.[13,14,15,16,17,18,19]
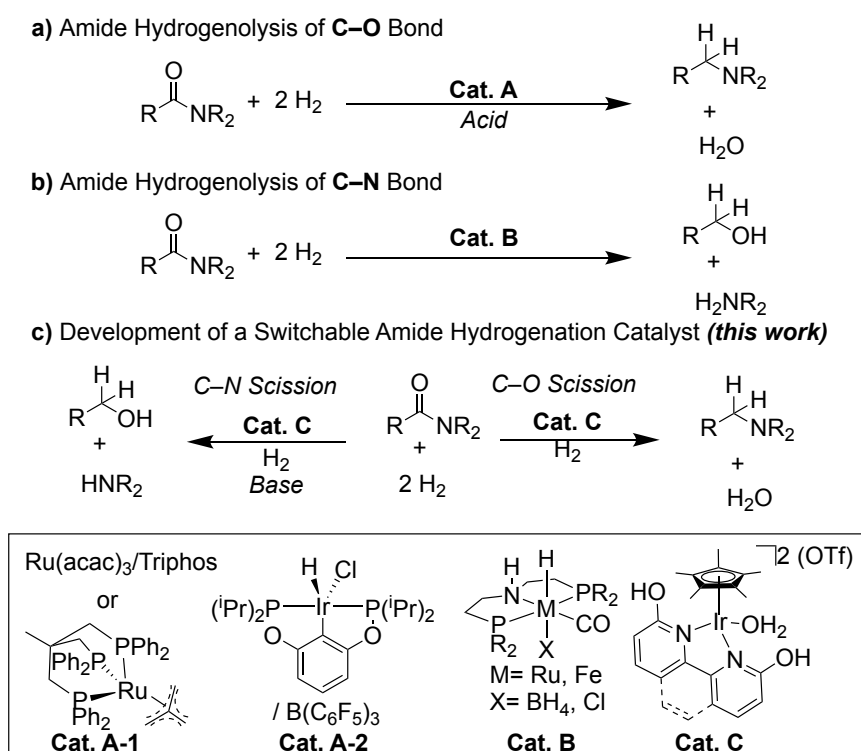
Figure 6.1. Overview of amide hydrogenation.

Seminal works by Cole-Hamilton and co-workers[13,19] reported the use of the tripodal ligand 1,1,1-tris(diphenylphosphinomethyl)ethane (triphos) in conjunction with ruthenium acetylacetonate [Ru(acac)$_3$] to hydrogenate 1° and 2° amides at elevated temperature (>150 °C) to the desired deoxygenated amine. Importantly, the product selectivity (C–O vs. C–N) was determined to be highly dependent on the water content. Despite a thorough mechanistic investigation, the reaction proved irreproducible.[19] Subsequent collaborative studies with the labs of Leitner and Klankermayer revealed that the methanesulfonic acid (MSA) additive yielded reproducible results.[14] Further investigations by the Leitner and Klankermayer labs disclosed a discrete ruthenium precatalyst supported by the κ^3-triphos ligand and a η_4-trimethylenemethane [triphosRu(TMM)] that also required the use of an acidic co-catalyst such as MSA or bis(trifluoromethane)sulfonamide (HNTf$_2$) to hydrogenate amides.[15] Despite these advances, the selectivity of products remains highly substrate dependent. Consequently, catalyst features and reaction conditions governing selectivity remain wholly unexplored.[15]
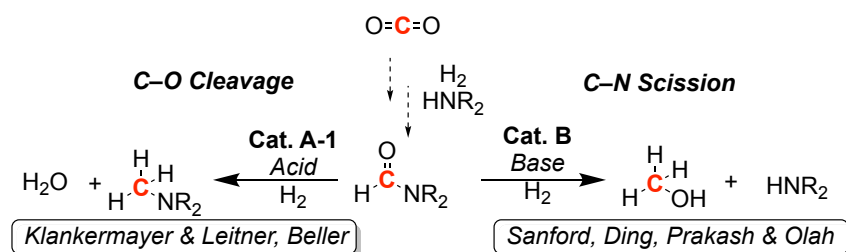
Figure 6.2. Representative divergence in the hydrogenation of formamides.

The quintessential paradigm regarding selectivity is epitomized in the hydrogenation of formamides. Formamides have played a pivotal role as in intermediate in two diverging strategies involving CO_2 reduction shown in Figure 6.2.[20,21,22,23,24] Depending on the selection of catalyst, either the methylated amine (C–O scission)[20,21] or methanol and amine (C–N cleavage)[22,23,24] results from the hydrogenation of the formamide intermediate. The labs of Leitner, and Beller have developed methods for the methylation of amines using CO_2 and H_2 using the ruthenium-triphos system.[20,21] Alternatively, our lab has focused on the hydrogenation of CO_2 to methanol through a formamide intermediate.[22] Both methods demonstrate high selectivity for their respective products(s), however, the origin of the selectivity for the two distinct products of hydrogenation is poorly understood.
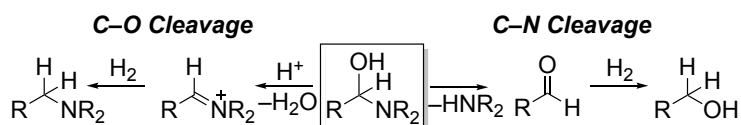
Figure 6.3. Potential origin of selectivity: stability of hemiaminal.

In the effort to design and develop improved catalysts, identifying and investigating the origin of selectivity is essential. We hypothesize that the stability of the resulting hemiaminal intermediate dictates C–O vs. C–N bond scission. Consequently, we propose the mechanism of hydrogenation (acidic or basic) by the transition metal catalyst dictates the product distribution.

To investigate our hypothesis, we sought to hydrogenate amides with catalysts that are active under both acidic and basic conditions. To our knowledge, no such catalyst has been reported. This is primarily due to the incompatibility of the mechanism of hydrogenation under acidic or basic conditions. Reported herein is the development of a proton-switchable iridium complex used for the hydrogenation of amides to yield C–O and C–N bond scission products. Remarkably, this catalyst is active in both acidic and basic

media. In the protonated state, the iridium complex selectively yields C–O bond cleaved products without any additives. Upon treatment of the catalyst with base, a switch in product selectivity is observed yielding C–N bond scission products.

6.2 Results and Discussion
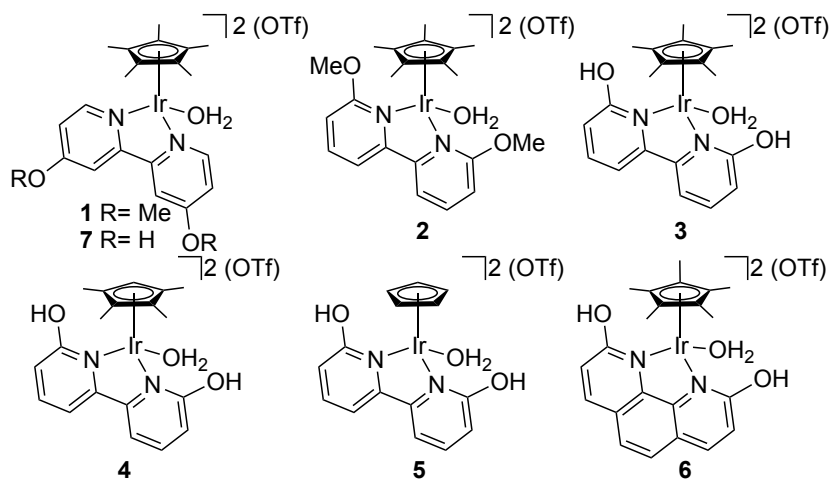
Figure 6.4. Suite of evaluated half-sandwich complexes for the hydrogenation of amides.

Deoxygenation of Amides

We have previously disclosed a hydrogenation catalyst, **1**, for the hydrogenation of esters that operated under Lewis acidic conditions.[25] Based on our hypothesis shown in Figure 6.3, we anticipated that **1** would yield C–O bond scission products. The hydrogenation of 2° amide *N*-(*o*-tolyl)formamide was evaluated using **1**. Gratifyingly, the deoxygenated products *N*-methyl-*o*-toluidine and *N,N*-dimethyl-*o*-toluidine, presumably formed from the hydrogenation of the transamidated product, were obtained without any traces of the C–N bond cleaved product. Excitingly these results exhibit an unexplored class of catalysts for this rare transformation. These results prompted the systematic evaluation of a series of catalysts.

Table 6.1. Catalyst screen and evaluation for the hydrogenation of *N*-(*o*-tolyl)formamide.[a]
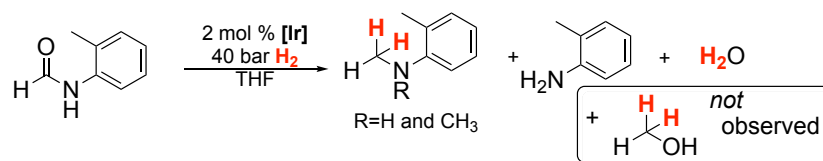
Entry	Cat	Temp. (ºC)	Time (h)	Conversion
1	**1**	100	16	68%
2	**1**	100	3	3%
3	**2**	100	3	3%
4	**3**	100	3	24%
5	**4**	100	3	24%
6	**5**	100	3	2%
7	**6**	100	3	85%
8	**6**	50	3	63%
9	**6**	90	3	80%
10	**6**	110	3	>99%

[a]Conditions: 125 μmol amide, 5 μmol 1-**6**, 1 mL THF, 40 bar H_2. Conversion determined by ^{1}H NMR Spectrosopy.

Previous optimization of these half-sandwich Ir complexes has shown increased catalytic activity with the addition of electron rich supporting ligands for the hydrogenation of carboxylic acids[26] and esters.[25] In order to better evaluate the catalysts, the reaction time was shortened to 3 hours. Under these conditions only a 3% yield was obtained with catalyst **1**. Substitution of the 4,4'-dimethoxybipyridine ligand to more sterically encumbering 2,2'-dimethoxybipyridine, **2**, resulted in comparable activity suggesting minimal steric effects. Following previous trends, the more donating 2,2'-dihydroxybipyridine, **3**, resulted in an increased yield of 24% (12 turnovers). Modification of the sterically bulky Cp* (pentamethylcyclpentadienyl) to the less donating Cp (cyclopentadienyl) ligand led to a dramatic decrease in activity (Table 6.1, entries 4-6). With Cp* identified as one of the optimal ligands, the bipyridine was further modified. After a thorough survey of catalysts, 2,9-dihydroxyphenanthroline supported catalyst, **6**, led to highest yield of 85%. Further optimization of conditions led to quantitative conversion of *N*-(*o*-tolyl)formamide to the deoxygenated products (Table 6.1, entry 10).

      With these optimized conditions in hand, the scope of the deoxygenation was evaluated. Secondary formamides were reduced to the corresponding alkylated amine, however mixtures of mono- and di-alkylation, presumably formed from transamidation,

were observed along with the non-alkylated aniline. 4-chloroformanilide (Table 6.2, entry 1) was hydrogenated to 4-chloro-*N*-methyl aniline and 4-chloro-*N,N*-dimethyl aniline in 45% and 53% yield, respectively. Hydrodehalogenation products were not detected. In order to avoid the formation of mixtures of products, tertiary amides were explored.

Table 6.2. 6-catalyzed deoxygenation of amides. [a]
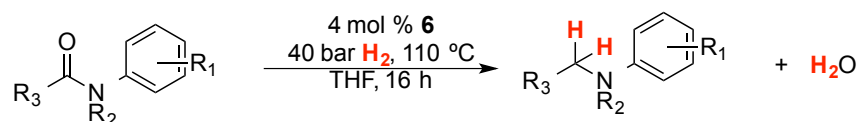
Entry	Substrate	Product	Yield[a]
1		R=H or CH$_3$	45%[b] 53%[cd]
2			46%
3			61%
4			59%
5			90%
6			82%
7			53%
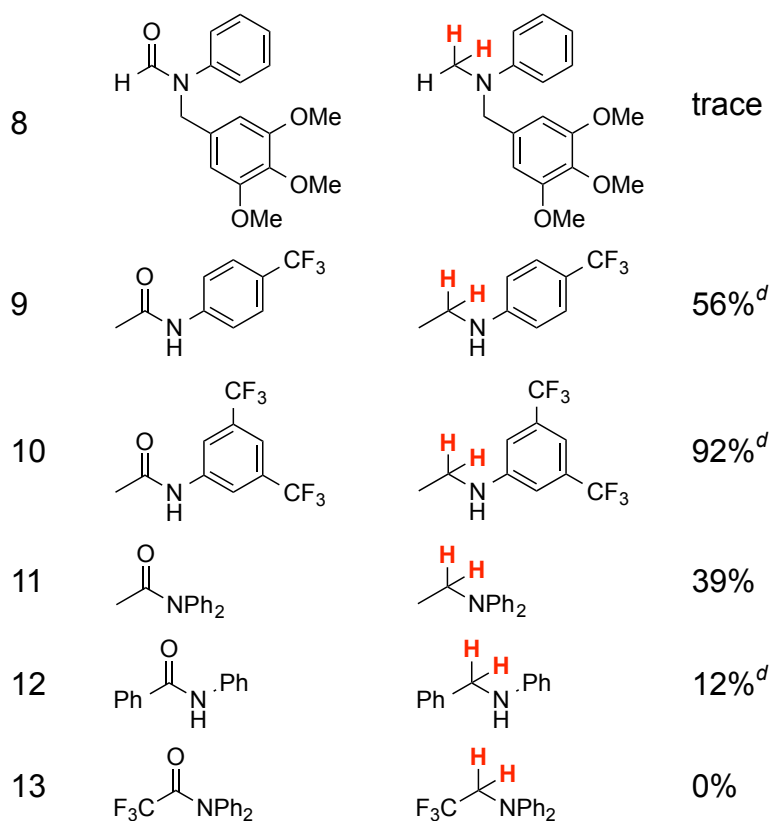
#	Amide	Amine	Yield
8	*N*-formyl-*N*-phenyl 3,4,5-trimethoxybenzylamine	*N*-methyl-*N*-phenyl 3,4,5-trimethoxybenzylamine	trace
9	4-(CF$_3$)phenyl acetamide	*N*-ethyl-4-(CF$_3$)aniline	56%[d]
10	3,5-(CF$_3$)$_2$phenyl acetamide	*N*-ethyl-3,5-(CF$_3$)$_2$aniline	92%[d]
11	acetamide, NPh$_2$	ethyl, NPh$_2$	39%
12	Ph–C(O)–N(H)–Ph	Ph–CH$_2$–N(H)–Ph	12%[d]
13	F$_3$C–C(O)–NPh$_2$	F$_3$C–CH$_2$–NPh$_2$	0%

[a]Conditions: 125 μmol amide, 5 μmol **6**, 1 mL THF, 40 bar H$_2$, 110 °C, 16 h. Yields are isolated yields of the amine product. [b]Yield of monoalkylated product. [c]Yield of dialkylated product. [d]Determined by ^{1}H NMR spectroscopy based on amine.

Gratifyingly, tertiary substrates resulted in a single product. *N*-methylformanilide (Table 6.2, entry 2) resulted in 46% isolated yield of *N,N*-dimethylaniline. *N*-benzyl- substituted aryl formamides were also viable substrates, affording yields of 59-90% (Table 6.2, entries 3-7) of the C–O bond scission products. Importantly, methanol, the C–N bond cleaved product, was not detected by ^{1}H NMR under these conditions. Highest yields were obtained with substrates bearing electron-neutral (Table 6.2, entry 3) or electron-withdrawing (Table 6.2, entries 4-7) substituents. Halogen containing substrates were well tolerated with no evidence for hydrodehalogenation (Table 6.2, entry 5). Addition of bulky substituents on the amine linkage did not hamper activity. This is consistent with our previous study of this class of catalysts for the hydrogenation of esters where the activity was highly sensitive to the substitution of the carbonyl and minimally on the heteroatom. Correspondingly, failed hydrogenation of the highly activated amide, *N,N*-Diphenyltrifluoroacetamide further supports this observation (Table 6.2, entry 13). Further showcasing the steric preference of **6** is entry 7, which bears both amide and ester functionality. The formamide is selectivity hydrogenated in the presence of the ester

providing the *N*-methylated amine 53% yield. These results are particularly noteworthy, as esters are generally considered more susceptible towards reduction.[1,2] To our surprise, substrates bearing methoxy groups (Table 6.2, entry 7) led to only trace products with starting material recovered.

Activated acetamides were also selectively hydrogenated to the deoxygenated product (Table 6.2, entries 9-11). As previously mentioned, bulkier substrates such as benzanilide (Table 6.2, entry 12) led to low yields. Despite the activated nature of the substrates, these results suggest that the C–O bond hydrogenolysis is not a specific consequence of the formamide functionality.

Mechanistic Studies
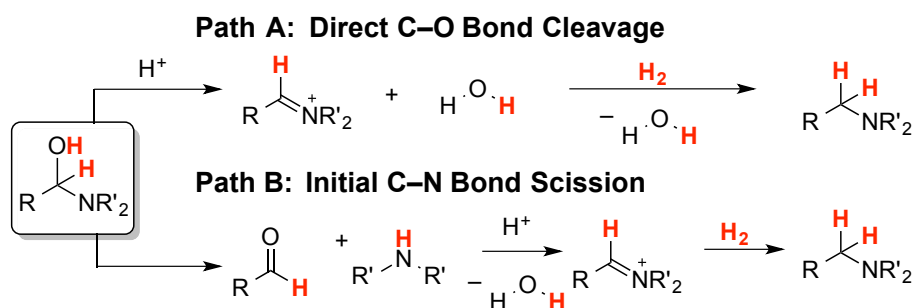
Figure 6.5. Potential pathways for the deoxygenation of amides.

With the scope of the **6**-catalyzed deoxy-hydrogenation evaluated, we investigated the mechanism of this rare transformation. Upon initial hydrogenation of the amide to the hemiaminal, two similar, yet diverging, paths have been proposed for the deoxygenation of amides shown in Figure 6.5. Path A involves the direct elimination of H_2O upon protonation of the hemiaminal to yield the imine/iminium followed by subsequent hydrogenation to the amine. Notably, treatment of hemiaminals with acid to yield the dehydrated product has been well precedented.[27] Alternatively, Path B proposes that the hemiaminal can undergo initial C–N bond scission yielding an aldehyde and amine. These intermediates may undergo an acid-catalyzed Schiff base condensation followed by concomitant hydrogenation to generate the deoxygenated amine product.

As previously noted, two other catalysts have been reported to perform this transformation, both necessitating the use of stoichiometric or sub-stiochiometric Lewis acid additives.[16,17] Studies by Beller *et al.* have implicated Path B as operational using the triphos-Ru(acac)$_3$ system.[16] The acidic additive was shown to perform a pivotal role as a hydrogen-barrowing catalyst to yield the aldehyde and amine after initial C–N bond

scission and hydrogenation.[16] Despite the absence of C–N bond scission products and the omission of the hydrogen-barrowing catalyst, Path B remained a potentially viable pathway. However, this would imply that the rate of condensation of the aldehyde and amine exceeds the **6**-catalyzed hydrogenation of the aldehyde or that **6** acts as both the hydrogenation and hydrogen-barrowing catalyst under 40 bar of H_2.

      In order to distinguish between the two routes proposed in Figure 6.6, a crossover experiment was devised. In this experiment an amide (blue) is hydrogenated in the presence of 1 equivalent of an amine (red). If Path A is operational, the deoxygenated amide (alkylation of blue) should be the sole product. Alternatively, if Path B were functional, alkylation of the amine (red) would be the major product as there is a higher concentration of amine to condense with the resulting aldehyde.
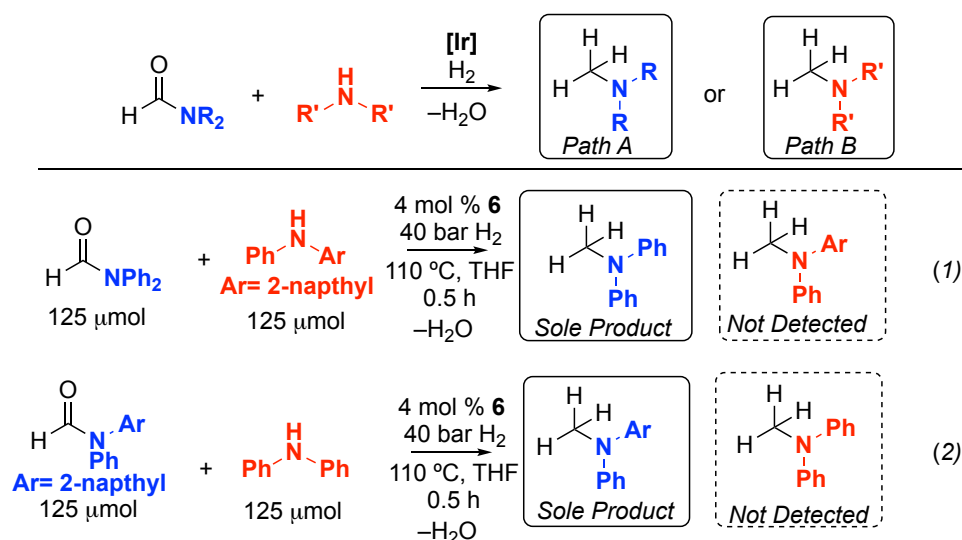
Figure 6.6. Cross-over experiments. *(1)* Hydrogenation of *N,N*-diphenylformamide in the presence of *N,N*-(2-napthyl)phenyl amine. *(2)* Hydrogenation of *N*-2'-napthylformanilide in the presence of *N,N*-diphenylamine.

      In performing this experiment, *N,N*-diphenylformamide (blue) was hydrogenated in an equimolar solution of *N,N*-(2-napthyl)phenyl amine (red) (Figure 6.6, eq. 1). In order to minimize ambiguity from transamidation, the reactions were run for 0.5 h. Under these conditions, only the deoxygenated amide product (blue) was detected by NMR and confirmed by GC-MS. Retention of the C–N bond implicates Path A as the operating mechanism. To confirm that product distribution resulted directly from the mechanism and not as a consequence of thermodynamics, another crossover experiment was conducted where the substitution of the amide and amine were switched (Figure 6.6,

eq 2). No crossover products were detected and the C–N bond was retained, supporting direct H₂O elimination from the hemiaminal.
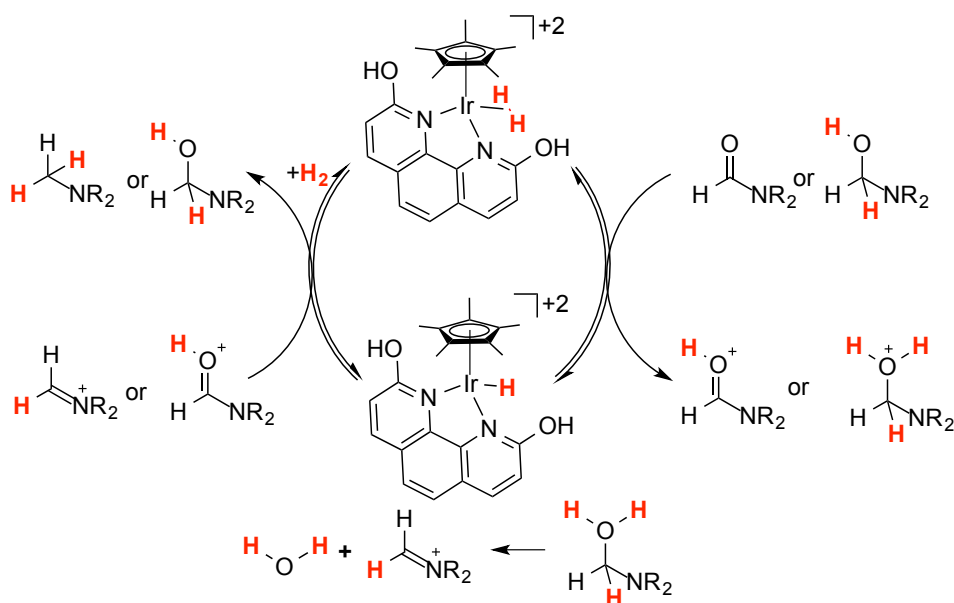
Figure 6.7. Proposed mechanism for the deoxygenation of amides.

We propose a mechanism for hydrogenation based on these studies and previous experiments for the hydrogenation of carboxylic acids[26] and esters[25] with this class of compounds. Importantly, the mechanism proposed in Figure 6.7 is based on speculation and unverified. Initial substitution of the aquo ligand for H_2 yields a dicationic complex bearing an Ir–H_2 σ-adduct. This complex is sufficiently acidic to protonate the carbonyl oxygen of the amide substrate forming an oxonium ion and an iridium hydride complex. The oxonium ion accepts a hydride, to form the hemiaminal intermediate. Under these acidic conditions, the hemiaminal is protonated to eliminate H_2O and the corresponding imine/iminium. Hydride transfer to the resulting imine/iminium yields the deoxygenated product.

Identification of a Switchable Catalyst


68% Yield
Selective C–N Scission
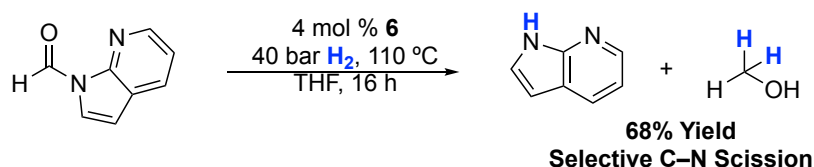
Figure 6.8. **6**-catalyzed hydrogenation of *N*-formyazaindole leading to C–N bond scission.

While recognizing that the mechanism of hydrogenation operated through an acidic mechanism, we were interested in probing compatibility with substrates containing

basic functionalities. *N*-formylazaindole, shown in Figure 6.8 bearing a pyridine moiety, was evaluated as a representative for this class of basic substrates. Interestingly, we were able to hydrogenate *N*-formylazaindole however, we exclusively obtained the C–N bond scission products, methanol and azaindole. The switch in selectivity from C–O bond scission with previous substrates to C–N bond cleavage with *N*-formylazaindole provided an opportunity to investigate the origin of this selectivity

Similar to the case shown in Figure 6.8, variation in selectivity has often been linked to the substrate. A potential oversight may be that substrates bearing basic functionalities have typically resulted in C–N bond scission, despite identical reaction conditions. Since the concentration of substrate is higher than catalyst, the hydrogenation is ultimately occurring under basic conditions. These differences in conditions may ultimately determine the selectivity.

**Table 6.3.** Hydrogenation of *N,N*-diphenylformamide under basic conditions. [a]
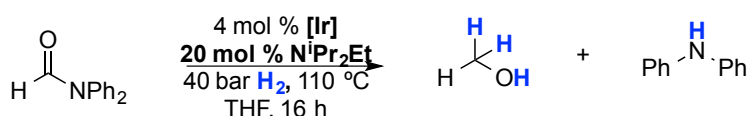
Entry	Cat.	Conversion[a]	Yield
1	**1**	0%	0%
2	**2**	0%	0%
3	**3**	92%	79%
4	**4**	72%	56%
5	**5**	0%	0%
6	**6**	>99%	90%
7	**7**	0 %	0%

[a]Conditions: 125 μmol amide, 5 μmol **1-7**, 25 μmol N^{i}Pr$_2$Et 1 mL THF, 40 bar H$_2$, 110 ºC, 16 h.

To evaluate this hypothesis, hydrogenation of a neutral substrate was examined under basic conditions. Shown in Table 6.3, the hydrogenation of *N,N*-diphenylformamide was evaluated with the addition of base. Under these conditions, catalysts **1**, **2**, and **5** were completely inactive. We hypothesize that, the Ir–H$_2$ σ-adduct is deprotonated by the base, yielding an Ir–H and preventing the activation of the substrate. The absence of substrate activation ultimately precludes hydride transfer. Excitingly,

catalysts **3**, **4**, and **6** remained active for hydrogenation and yielded C–N bond scission products in 79%, 56%, and 90% yield respectively.
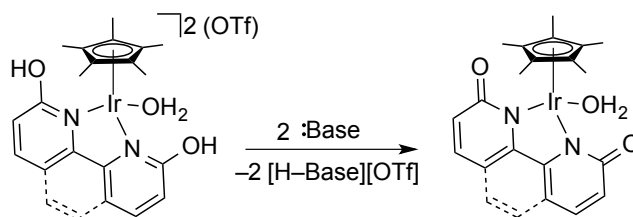
Figure 6.9. Proton-responsive ligand scaffold.

Catalysts **3**, **4**, and **6**, unlike **1** and **2**, contain a protic site that may be intimately involved under basic conditions. These catalysts have been implicated in mechanisms involving ligand-metal cooperativity.[28,29,30,31] Indeed, treatment of these catalysts with base yields a neutral iridium complex shown in Figure 6.9.[28,32] Interestingly, catalyst **7**, which is supported by 4,4'-dihydroxybipyridine (an isomer of **3**), was completely inactive under these basic conditions. These results highlight the importance of the location of the hydroxyl functionality. Proximity of the hydroxyl substitution to the iridium metal center suggests a bifunctional mechanism of hydrogenation.[28,31]
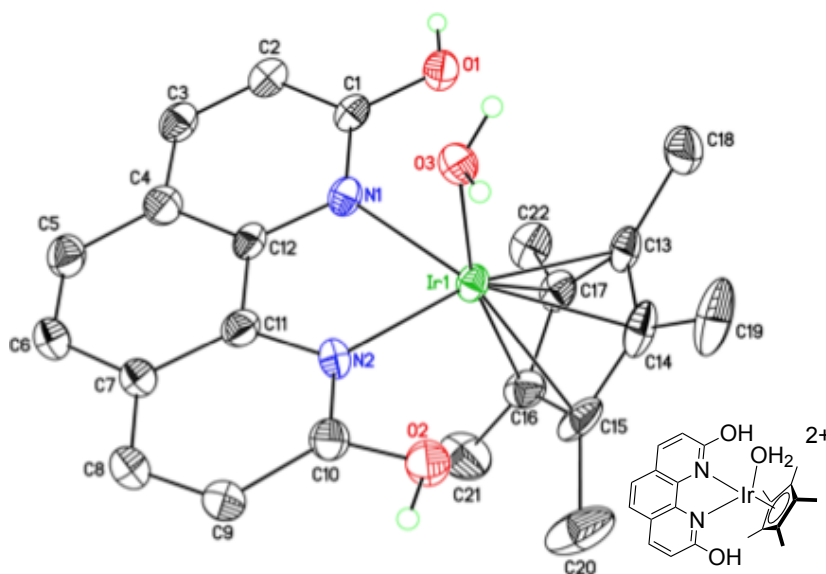
Figure 6.10. ORTEP of drawing of **6**. Thermal ellipsoids are drawn at 50%. Hydrogen atoms, counteranions (OTf), co-crystallized water and THF were omitted for clarity.

Evaluation of the two protic states of **6** under amide hydrogenation conditions leads to distinct major products. Though a potentially viable species, discussion of the monodeprotonated species (cationic) is omitted for simplicity. Under protic conditions, the dicationic **6** leads to C–O bond scission products. Alternatively, under basic conditions, **6** is

presumed to be fully deprotonated to **6**', which leads to C–N bond cleaved products (however the monodeprotonated species). Comparison of the two states demonstrate key structural difference that may be involved in the product selectivity. As shown in Figure 6.10, the dicationic complex **6** adopts a piano-stool geometry with an Ir–O bond length of 2.157(3) Å and Ir–N bond distances of 2.118(3) and 2.124(3) Å. The distance of the Cp* centroid to Ir was calculated to be 1.829 Å. Importantly, the C–O bond lengths of the phenanthroline ligand were found to be 1.311(5) and 1.316(5) Å, indicating that the hydroxyl groups of the ligand remain protonated. Alternatively, the neutral complex **6'**, bears overall longer metal-ligand bond lengths shown with an Ir–O bond distance of 2.200 Å and symmetric Ir–N bond lengths of 2.128 Å.[28] Measurement from the Cp* centroid to Ir disclosed a bond length of 1.871 Å. Shorter ligand-based C–O bonds (1.259 Å vs. 1.311(5) and 1.316(5) Å) are consistent with deprotonation of the hydroxyl groups.[28] Notably, the fully deprotonated dianionic ligand in **6'** is more planar than in **6** and reveals a larger dihedral angle between the centroid of Cp* and the phenanthroline ligand (133.02° for **6'** and 132.04° for **6**). Comparison of the two complexes demonstrates that **6** is the more electrophilic Ir metal center. Furthermore, the increased electron density about Ir in **6'** may lead to a more hydridic Ir–H than in **6**. Coupling the increased hydricity with the bifunctional nature of the deprotonated ligand may implicate an alternative hydrogenation mechanism.
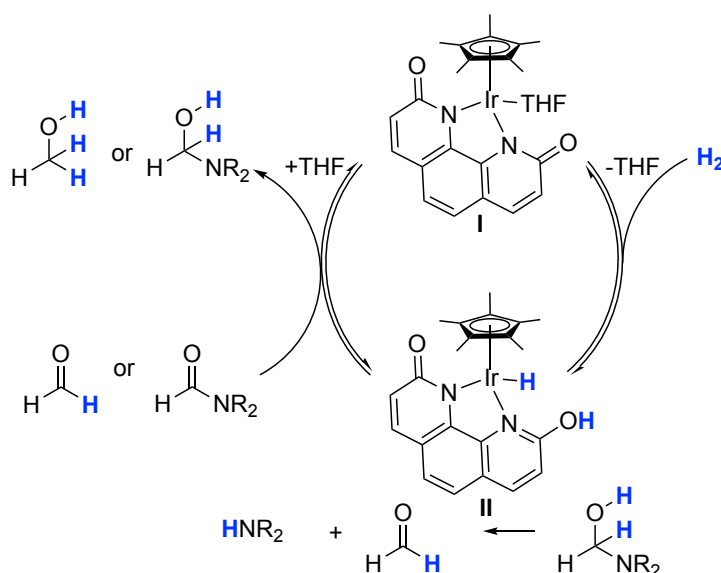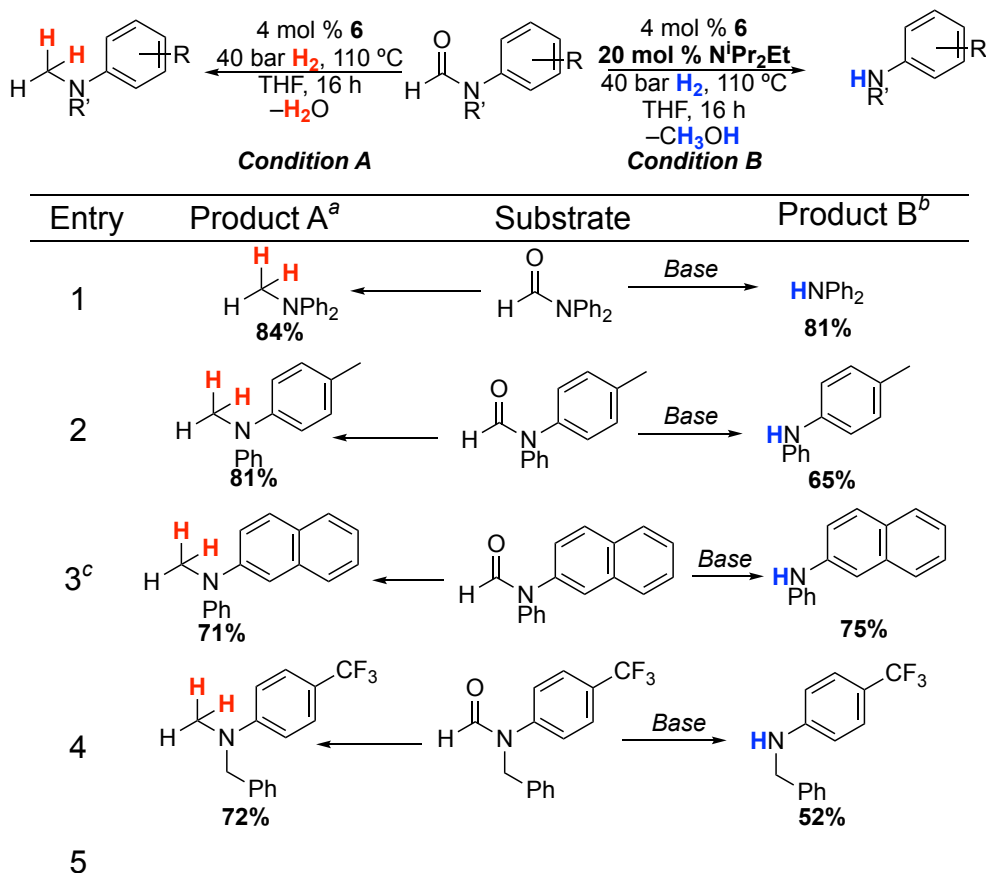

Figure 6.11. Potential catalytic cycle for the hydrogenation of amides yielding C–N bond scission.

A proposed catalytic cycle for the C–N bond scission products is shown in Figured 6.11 (hydrogen bonding networks are omitted for simplicity). The mechanism outlined in Figure 6.11 is speculative and necessitates a detailed mechanistic study. This mechanism is similar to other amide hydrogenation catalysts using ligand-metal cooperativity.[28,29,30,31,32] The proposed Ir intermediates, **I** and **II**, have also been identified as key intermediates in alcohol (de)hydrogenations. Upon deprotonation, H_2 is heterolytically cleaved across the basic pyridone ligand and Ir metal center to yield **II**. Complex **II** activates and reduces the amide substrate *via* a hydrogen-bond-directed hydride transfer with concurrent protonation to yield the hemiaminal and regenerating **I**. The hemiaminal, under these basic conditions, eliminates the amine yielding an aldehyde. Following a second addition of H_2 to form **II**, the aldehyde is hydrogenated to the primary alcohol.

Finally, identification of a single catalyst that is operational via both acidic and basic mechanisms allows for the development of a proton-responsive amide hydrogenation catalyst. Application of **6** for the hydrogenation of amides is outlined in Table 6.4 with two different conditions. Condition A utilizes 40 bar H_2 at 110 ºC in THF and favors the acidic mechanism shown in Figure 6.7. Under these conditions the primary product was the deoxygenated amide. Addition of base, under otherwise identical conditions (Condition B), switched the major product from the C–O bond cleaved amine to the C–N bond scission products.

Hydrogenation of *N,N*-diphenylformamide using **6** under Condition A yielded *N,N,N*-methyldiphenylamine in 84% yield (Table 6.4, entry 1, Condition A). However, in applying Condition B with **6,** methanol and *N,N*-diphenylamine was obtained in 81% yield (Table 6.4, entry 1, Condition B). These results demonstrate that the product selectivity (C–O vs. C–N) is a consequence of the conditions of hydrogenation. This highlights a rare example of a single substrate yielding two distinct classes of products using a single catalyst. *N,N*-diaryl formamides (Table 6.4, entries 1–3) and *N*-benzyl-aryl formamides (Table 6.4, entries 4 and 5) were viable substrates featuring the switchable product distribution ranging in yields from 52–89% yield.

Table 6.4. Scope for the switchable amide hydrogenation catalyst yielding C–O and C–N bond cleavage products. [a]

Condition A: 4 mol % **6**, 40 bar H₂, 110 °C, THF, 16 h, –H₂O

Condition B: 4 mol % **6**, 20 mol % N^iPr₂Et, 40 bar H₂, 110 °C, THF, 16 h, –CH₃OH

Entry	Product A[a]	Substrate	Product B[b]
1	H₂C–NPh₂ (84%)	H(C=O)NPh₂	Base → HNPh₂ (81%)
2	H₂C–N(Ph)(p-tolyl) (81%)	H(C=O)N(Ph)(p-tolyl)	Base → HN(Ph)(p-tolyl) (65%)
3[c]	H₂C–N(Ph)(2-naphthyl) (71%)	H(C=O)N(Ph)(2-naphthyl)	Base → HN(Ph)(2-naphthyl) (75%)
4	H₂C–N(CH₂Ph)(4-CF₃-C₆H₄) (72%)	H(C=O)N(CH₂Ph)(4-CF₃-C₆H₄)	Base → HN(CH₂Ph)(4-CF₃-C₆H₄) (52%)
5			

[a]Conditions: 125 μmol amide, 5 μmol **6**, 1 mL THF, 40 bar H₂, 110 °C, 16 h. Yields are isolated yields of the amine product. [b]Addition of 20 mol % N^iPr₂Et. [c]Conditions A: 0.5 h.

6.3 Conclusions

In summary, this chapter describes the development of a switchable amide hydrogenation catalyst that yields C–O and C–N bond scission products. The difference in selectivity was found to be highly dependent on the conditions of hydrogenation. Catalyst **6** was found to undergo an acidic hydrogenation mechanism that selectively leads to the C–O bond cleaved product. Contrary to previously reported systems,[16] mechanistic studies using **6** reveal that the deoxygenated product arises from the direct elimination of H₂O from the hemiaminal intermediate. The addition of base to the hydrogenation reactions with **6** deprotonates the ligand and activates ligand-metal cooperativity. Through the bifunctional ligand manifold,[28] the catalyst remains an active hydrogenation catalyst that now operates via a basic mechanism. The hydrogenation of amides under the basic conditions primarily lead to the C–N bond cleaved products.

6.4 Experimental

General Procedures

All manipulations were carried out under a nitrogen atmosphere using standard Schlenk line or glove box techniques unless otherwise noted. All high-pressure reactions were carried out using a Parr Model 5000 Multiple Reactor system that includes six 45 mL vessels equipped with flat-gaskets and head mounting valves. The system was operated by a 4871 process controller and SpecView version 2.5 software. All pressures are reported from the SpecView interface at room temperature. NMR spectra were obtained on Varian VNMRs: 400 MHz (400 MHz for ^{1}H; 100 MHz for ^{13}C) or 700 MHz (700 MHz for ^{1}H; 176 MHz for ^{13}C). Chemical shifts are reported in parts per million (ppm) and are referenced to an internal standard. Unless otherwise noted, the NMR yields with formamide substrates were based on methanol (δ = 3.16 ppm, T_1 = 7.2 s) and were quantified using 1,3,5-trimethoxybenzene (δ = 6.02 ppm, T_1 = 2.8 s) as an internal standard in dimethylsulfoxide-d_6 (DMSO-d_6). For each NMR experiment, 4 scans were collected, a 35 s relaxation delay was used, and a pulse angle of 90° was applied.

Reactor Descriptions

Each vessel is 45 mL in volume and is composed of a well (in which the solid and liquid reagents are charged) and a head, which contains various attachments as described below.

The reactors are made of Hastelloy C, and the wells are 7.5 cm tall and 3 cm in diameter. The heads consist of a pressure transducer and two inlet/outlet valves that can connect to a Parr Model 5000 Multiple Reactor system described above, a safety release valve, and a well for a thermocouple (Figure 6.12).
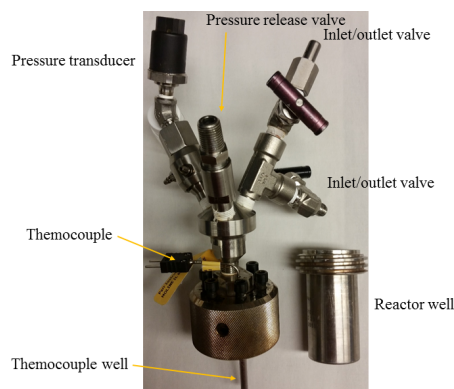
Figure 6.12. Picture of reactor type A with the parts of the reactor labeled.

Materials and Methods

The ligands 4,4'-dihydroxy-2,2'-bipyridine,[33] 6,6'-dimethoxy-2,2'-bipyridine,[34] 6,6'-dihydroxy-2,2'-bipyridine,[35] and 2,9-dihydroxy-1,10-phenanthroline[36] was synthesized according to the literature. Complexes **1-6** were prepared according to a literature procedure.[26] Ultra-high purity hydrogen (99.999%), was purchased from Metro Welding. All catalytic experiments were set up under an oxygen-free atmosphere in a glovebox. All catalytic experiments were conducted in triplicate, and the reported results represent an average of 2 runs (NMR yields) and a single isolated yield where applicable. Aniline (Acros), 4-chloroaniline (Acros), 2-aminobiphenyl (Aldrich), 3,5-bis(trifluoromethyl)aniline (Oakwood), 4-(trifluoromethyl)aniline (Chem-Impex), anhydrous benzaldehyde (Acros), *N*-methylformanilide (Acros), trifluoroacetic anhydride (Aldrich), acetic anhydride (Fisher), formic acid (Fisher), 4-acetoxybenzaldyde (Lancaster Synthesis), 1,2,3,4,5-pentamethylcyclopentadiene (TCI), 1,2,3,4-tetramethyl-1,3-cyclopentadiene (Alfa Aesar),4-tert-butylbenzaldeyde (Aldrich), sodium cyclopentadienylide (2M in THF) (Aldrich), and anhydrous *N,N*-diisopropylethylamine (Aldrich), were obtained from commercial sources and used without further purification. The solid reagents *N,N*-diphenylformamide (Aldrich, 99%), *N*-(2-methylphenyl)formamide (Alfa Aesar, 98%), *N,N*-diphenylacetamide (Enamine, 95%), *N*-phenylbenzamide (Alfa Aesar, >98%), NaBH$_4$ (Aldrich, Venpure SF), *N*-Benzylaniline (TCI), 4-bromobenzaldehyde (Lancaster Synthesis), 3,4,5-trimethoxybenzaldehyde (Mallinckrodt), *N*-phenyl-2-napthylamine (TCI), 4-methyldiphenylamine (ArkPharm), azaindole (Oakwood), *N*-(3,5-

156

bis(trifluoromethyl)phenyl)acetamide (Alfa Aesar), *N*-(4-trifluoromethyl)phenylacetamide (Alfa Aesar), anhydrous $IrCl_3$ (Pressure), $NaHBCN_3$ (Chem-Impex), AgOTf (Oakwood), and 1,3,5-trimethoxybenzene (Acros) were obtained from commercial sources and used without further purification *N*-benzyl-2,2,2-trifluoroactamide,[8] were prepared according to literature procedures. Tetrahydrofuran (THF), dichloromethane (DCM), toluene, NEt_3, and pentane, were purified using an Innovative Technologies (IT) solvent purification system consisting of a copper catalyst, activated alumina, and molecular sieves. Dimethylsulfoxide-d_6 (DMSO-d_6, Cambridge Isotope Laboratories) and chloroform ($CDCl_3$, Cambridge Isotope Laboratories) were purchased from the respective supplier and used as received.

I. Synthesis and Characterization of Amides (Table 6.2, Figure 5.8, and Table 6.4)

General Method A: A 20 mL vial was charged with amine (3 mmol), formic acid (2 mL), and stir bar. The vial was capped and heated to 105 ºC overnight. After the reaction was complete, EtOAc (15 mL) was added and the mixture was washed with water (3x15 mL) and sat. Na_2CO_3 (2x10 mL). The organic layer was dried (Na_2SO_4) and concentrated in vacuo. If necessary, product was purified with column chromotography.

General Method B: A 20 mL vial was charged with Ac_2O (0.5 mL, 5.3 mmol), formic acid (0.2 mL, 5.3 mL), and stir bar. The vial was capped with a septum and heated to 65 ºC. After 1 h, the vial was cooled to RT and the amine (<2 mmol) was added. The resulting mixture was stirred at RT. After 3 h, EtOAc (15 mL) was added and the mixture was washed with water (3x15 mL) and sat. Na_2CO_3 (2x10 mL). The organic layer was dried (Na_2SO_4) and concentrated in vacuo. If necessary, product was purified with column chromotography.

General Method C: A mixture of the aniline (1.2 mmol) and the corresponding benzaldehyde (1 mmol) was dissolved in DMF (5 mL). Acetic acid (0.05 mL) was added to the solution. After 1 h, $NaBH_3CN$ (5 mmol) was added and the mixture was stirred at rt overnight. Then, EtOAc (15 mL) was added and the mixture was washed with water (3x15 mL) and sat. Na_2CO_3 (2x10 mL). The organic layer was dried (Na_2SO_4) and concentrated in vacuo. In another vial, 20 mL vial was charged with Ac_2O (0.5 mL, 5.3

mmol), formic acid (0.2 mL, 5.3 mL), and stir bar. The vial was capped with a septum and heated to 65 ºC. After 1 h, the vial was cooled to RT and the crude mixture was added. The resulting mixture was stirred at RT. After 3 h, EtOAc (15 mL) was added and the mixture was washed with water (3x15 mL) and sat. Na_2CO_3 (2x10 mL). The organic layer was dried (Na_2SO_4) and concentrated in vacuo. If necessary, product was purified with column chromotography.

4-Chloroformanilide (Table 6.2, entry 1): General Method A was followed with 4-chloroaniline (3 mmol), resulting in a gray solid (2.2 mmol, Yield 73%).
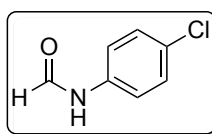
Major isomer

^{1}H NMR (700 MHz, CDCl$_3$) δ 8.35 (s, 1H), 7.77 (s, 1H), 7.49 (d, J = 6.8 Hz, 2H), 7.27 (d, J = 7.0 Hz, 2H).

^{13}C NMR (176 MHz, CDCl$_3$) δ 159.28, 129.94, 129.23, 121.36, 120.14.

***N*-4'-Bromobenzyl-4-chloroformanilide (Table 6.3, entry 5):** General Method C was followed with 4-chloroaniline (1.2 mmol), 4-bromobenzaldehyde (1.0 mmol), resulting in a pink solid (0.45 mmol, Yield 45%).
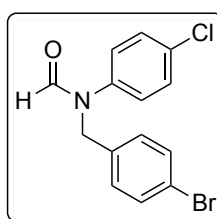
^{1}H NMR (700 MHz, CDCl$_3$) δ 8.48 (s, 1H), 7.40 (d, J = 8.4 Hz, 2H), 7.31 (d, J = 8.7 Hz, 2H), 7.08 (d, J = 8.3 Hz, 2H), 7.01 (d, J = 8.7 Hz, 2H), 4.90 (s, 2H).

^{13}C NMR (176 MHz, CDCl$_3$) δ 162.13, 139.23, 135.39, 133.02, 131.96, 129.99, 129.80, 125.54, 121.79, 48.40.

HRMS: ESI^{+}(m/z): [M+H]$^{+}$ calcd for C$_{14}$H$_{11}$BrClNO: 323.9785; found 323.9785.

N-4'-*tert*-butylbenzyl-3,5-(bistrifluoromethyl)formanilide (Table 6.3, entry 6): General Method C was followed with 3,5-bis(trifluoromethyl)aniline (1.2 mmol), 4-tert-butylbenzaldehyde (1.0 mmol), resulting in a colorless oil (0.60 mmol, Yield 60%).
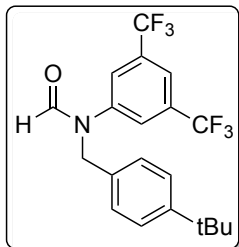

^{1}H NMR (700 MHz, CDCl$_3$) δ 8.64 (s, 1H), 7.76 (s, 1H), 7.56 (s, 2H), 7.34 (d, J = 8.1 Hz, 2H), 7.15 (d, J = 7.7 Hz, 2H), 5.04 (s, 2H), 1.29 (s, 9H).

^{13}C NMR (176 MHz, CDCl$_3$) δ 161.47, 151.13, 142.57, 133.09 (q, J = 33.9 Hz), 132.34, 127.59, 126.87, 126.15, 125.87, 123.55, 53.11, 48.30, 31.19.

^{19}F NMR (658 MHz, CDCl$_3$) δ -63.11.

HRMS: ESI$^+$(m/z): [M+H]$^+$ calcd for C$_{14}$H$_{11}$BrClNO: 323.9785; found 323.9785.

N-4'-Acetoxybenzyl-3,5-(bistrifluoromethyl)formanilide (Table 6.3, entry 7): General Method C was followed with 3,5-bis(trifluoromethyl)aniline (1.2 mmol), 4-acetoxybenzaldehyde (1.0 mmol), resulting in a colorless oil (0.48 mmol, Yield 48%).
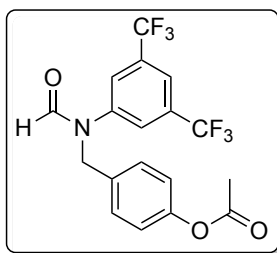
^{1}H NMR (700 MHz, CDCl$_3$) δ 8.61 (s, 1H), 7.75 (s, 1H), 7.57 (s, 2H), 7.22 (d, J = 7.6 Hz, 3H), 7.03 (d, J = 8.3 Hz, 2H), 5.04 (s, 2H), 2.26 (s, 3H).

^{13}C NMR (176 MHz, CDCl$_3$) δ 169.45, 161.72, 150.45, 142.40, 133.33 (q, J = 38.1, 36.0 Hz), 133.06, 129.46, 129.05, 123.42, 122.22, 115.87, 48.06, 21.11.

^{19}F NMR (658 MHz, CDCl$_3$) δ -63.09.

HRMS: ESI$^+$(m/z): [M+Na]$^+$ calcd for $C_{18}H_{13}F_6NO_3$: 428.0692; found 428.0697.

N-3',4',5'-Trimethoxybenzyl-formanilide (Table 6.3, entry 7): General Method C was followed with aniline (3.6 mmol), 3,4,5-trimethoxybenzaldehyde (1.0 mmol), resulting in a colorless oil (0.48 mmol, Yield 48%).
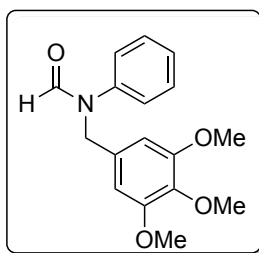

^{1}H NMR (700 MHz, CDCl$_3$) δ 8.52 (s, 1H), 7.35 (d, J = 7.7 Hz, 2H), 7.26 (s, 1H), 7.10 (d, J = 7.8 Hz, 2H), 6.42 (s, 2H), 4.90 (s, 2H), 3.79 (s, 3H), 3.76 (s, 6H).

^{13}C NMR (176 MHz, CDCl$_3$) δ 162.45, 153.35, 141.06, 137.29, 132.45, 129.70, 127.14, 124.36, 104.92, 60.91, 56.12, 49.20.

HRMS: ESI$^+$(m/z): [M+H]$^+$ calcd for $C_{17}H_{19}NO_4$: 302.1387; found 302.1389.

N-Formylazaindole (Figure 6.8): General Method B was followed with 7-azaindole (3 mmol) resulting in a white powder (2.1 mmol, Yield 70%).
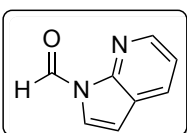
^{1}H NMR (700 MHz, CDCl$_3$) δ 9.82 (s, 1H), 8.35 (d, J = 7.8 Hz, 1H), 7.91 (d, J = 7.8 Hz, 1H), 7.80 (d, J = 4.1 Hz, 1H), 7.26 (dd, J = 7.8, 4.1 Hz, 1H), 6.67 (s, 1H).

^{13}C NMR (176 MHz, CDCl$_3$) δ 157.02, 148.24, 144.71, 129.86, 122.91, 122.15, 120.15, 108.00.

N-4'-tolylformanilide (Table 6.4, entry 2): General Method A was followed with 4-methyldiphenylamine (3 mmol) resulting in a dark brown powder (2.74 mmol, Yield 91%).
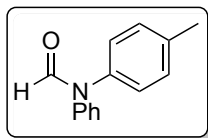
^{1}H NMR (700 MHz, CDCl$_3$) (mixture of two conformers) δ 8.67 (s, 1H), 8.62 (s, 1H), 7.39 (vq, J = 8.4 Hz, 4H), 7.30 (d, J = 7.5 Hz, 3H), 7.24 (d, J = 7.4 Hz, 1H), 7.21 (d, J = 9.7 Hz, 4H), 7.17 (d, J = 8.5 Hz, 3H), 7.16 (s, 1H), 7.07 (d, J = 8.2 Hz, 2H), 2.38 (s, 3H), 2.36 (s, 3H).

^{13}C NMR (176 MHz, CDCl$_3$) (mixture of two conformers) δ 161.85, 161.84, 142.03, 139.93, 139.26, 137.22, 137.04, 136.97, 130.37, 129.94, 129.71, 129.18, 126.91, 126.72, 126.23, 125.90, 125.38, 124.78, 21.16, 21.06.

***N*-2'-napthylformanilide (Table 6.4, entry 3):** General Method A was followed with *N*-phenyl-2-napthylamine (3 mmol) resulting in a dark gray powder (1.88 mmol, Yield 63%).
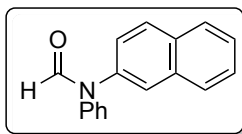
^{1}H NMR (700 MHz, CDCl$_3$) (mixture of two conformers) δ 8.56 (s, 1H), 8.53 (s, 1H), 7.66 – 7.52 (m, 7H), 7.45 (s, 1H), 7.36 – 7.27 (m, 2H), 7.27 – 7.22 (m, 2H), 7.18 (s, 5H), 7.15 – 6.88 (m, 7H).

^{13}C NMR (176 MHz, CDCl$_3$) (mixture of two conformers) δ 161.95, 161.89, 141.87, 139.60, 139.04, 137.08, 133.58, 132.01, 129.88, 129.80, 129.26, 129.11, 128.91, 128.21, 127.99, 127.84, 127.76, 127.72, 127.47, 127.19, 127.15, 126.93, 126.58, 126.34, 126.14, 125.74, 125.50, 125.15, 125.03, 124.70, 124.60, 124.39, 123.72, 123.02.

***N*-Benzyl-4-trifluoromethylformanilide (Table 6.4, entry 4):** General Method C was followed with 4-trifluoromethylaniline (1.2 mmol), benzaldehyde (1.0 mmol), resulting in a colorless oil (0.38 mmol, Yield 38%).
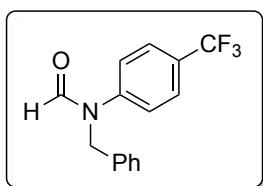
¹H NMR (700 MHz, CDCl₃) δ 8.68 (s, 1H), 7.59 (d, *J* = 7.8 Hz, 2H), 7.29 (t, *J* = 7.1 Hz, 2H), 7.24 (m, 5H), 5.06 (s, 2H).

¹³C NMR (176 MHz, CDCl₃) δ 161.96, 144.10, 136.12, 129.10, 128.84, 127.74, 127.58, 126.87 (q, *J* = 3.6 Hz), 124.74, 123.05, 48.37.

¹⁹F NMR (658 MHz, CDCl₃) δ -62.44.

HRMS: ESI⁺(m/z): [M+H]⁺ calcd for $C_{15}H_{12}F_3NO$: 280.0944; found 280.0952.

N-Benzyl-3,5-(bistrifluoromethyl)formanilide (Table 6.4, entry 5): General Method C was followed with 3,5-bis(trifluoromethyl)aniline (1.2 mmol), benzaldehyde (1.0 mmol), resulting in a colorless oil (0.35 mmol, Yield 35%).
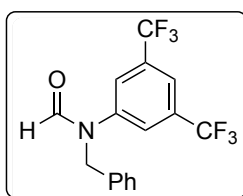
¹H NMR (700 MHz, CDCl₃) δ 8.67 (s, 1H), 7.74 (s, 1H), 7.58 (s, 2H), 7.30 (m, 2H), 7.26 (m, 1H), 7.23 (d, *J* = 7.4 Hz, 2H), 5.08 (s, 2H).

¹³C NMR (176 MHz, CDCl₃) δ 161.50, 142.52, 135.44, 133.11 (q, *J* = 33.9 Hz), 129.21, 128.94, 128.01, 127.75, 127.04, 123.22, 48.42.

¹⁹F NMR (658 MHz, CDCl₃) δ -62.44.

HRMS: ESI⁺(m/z): [M+H]⁺ calcd for $C_{16}H_{11}F_6NO$: 348.0818; found 348.0822.

II. Hydrogenation of Amides (Table 6.2, Figure 5.8, and Table 6.4)

General Hydrogenation, Method A: In a N₂-atmosphere dry box, [Ir] (5 μmol, 4 mol %) was dissolved in 1 mL of THF, and this solution was added to the metal well of a pressure and a micro magnetic stir bar (3 x 10 mm). Amide (125 μmol, 25 equiv relative to Ir) was then added, and the vessel (Reactor-type A) was sealed and removed from the dry box.

The vessel was connected to the Parr Multiple Reactor System, and the manifold was thoroughly purged with ultra-high purity grade H_2 (99.999%). The vessel was then pressurized with H_2 (40 bar) at room temperature, and the reaction was heated at 110 °C with a stir rate of 800 RPM. The heating was conducted using Specview software. After 16 h or 0.5 h of heating, the reaction mixture was allowed to cool to room temperature. The pressure vessel was cooled to RT and then carefully vented using a metering valve. THF (0.5 mL) was added through the venting valve of the pressure vessel to wash any residual liquids/solids into the vessel. The vessel was then opened, 1,3,5-trimethoxybenzene (0.178 mmol, 300 μL of 0.593 M solution in DMSO-d_6) was added as a ^{1}H NMR standard, or the solution was treated with excess NEt_3 and the solvent removed *in vacuo*. The product was isolated with column chromatography.

General Hydrogenation, Method B: In a N_2-atmosphere dry box, **6** (5 μmol, 4 mol %) was dissolved in 1 mL of THF containing 25 μmol NiPrEt, and this solution was added to the metal well of a pressure and a micro magnetic stir bar (3 x 10 mm). Amide (125 μmol, 25 equiv relative to Ir) was then added, and the vessel (Reactor-type A) was sealed and removed from the dry box. The vessel was connected to the Parr Multiple Reactor System, and the manifold was thoroughly purged with ultra-high purity grade H_2 (99.999%). The vessel was then pressurized with H_2 (40 bar) at room temperature, and the reaction was heated at 110 °C with a stir rate of 800 RPM. The heating was conducted using Specview software. After 16 h of heating, the reaction mixture was allowed to cool to room temperature. The pressure vessel was cooled to RT and then carefully vented using a metering valve. THF (0.5 mL) was added through the venting valve of the pressure vessel to wash any residual liquids/solids into the vessel. The vessel was then opened, 1,3,5-trimethoxybenzene (0.178 mmol, 300 μL of 0.593 M solution in DMSO-d_6) was added as a ^{1}H NMR standard, or the solution was treated with excess NEt_3 and the solvent removed *in vacuo*. The product was isolated with column chromatography.
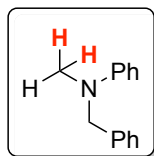
Hydrogenation of 4-Chloroformanilide (Table 6.2, entry 1): General Hydrogenation Method A was applied. The fractions resulting where acidified with 2N HCl in Et_2O resulting in a 45% yield of the monoalkylated amine and 53% yield of the dialkylated.
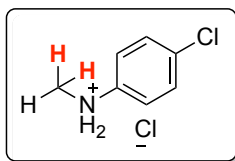
^{1}H NMR (700 MHz, CDCl$_3$) δ 11.26 (bs, 2H), 7.51 (d, *J* = 8.0 Hz, 2H), 7.40 (d, *J* = 7.8 Hz, 2H), 2.99 (s, 3H).

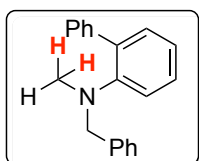^{13}C NMR (176 MHz, CDCl3) δ 136.44, 134.92, 130.49, 123.52, 37.73.

Hydrogenation of *N*-Benzylformanilide (Table 6.2, entry 3): General Hydrogenation Method A was applied resulting in a 61 % yield.

^{1}H NMR (700 MHz, CDCl$_3$) δ 7.34 (t, *J* = 6.6 Hz, 2H), 7.29 – 7.22 (m, 5H), 6.78 (d, *J* = 6.9 Hz, 2H), 6.74 (t, *J* = 6.6 Hz, 1H), 4.56 (s, 2H), 3.04 (s, 3H).

^{13}C NMR (176 MHz, CDCl$_3$) δ 149.86, 139.15, 129.30, 128.68, 126.97, 126.84, 116.63, 112.46, 56.75, 38.64.

Hydrogenation of *N*-Benzyl(2-phenyl)formanilide (Table 6.3, entry 4): General Hydrogenation Method A was applied resulting in a 59 % yield.

^{1}H NMR (700 MHz, CDCl$_3$) δ 7.60 (d, *J* = 7.2 Hz, 2H), 7.41 (t, *J* = 7.7 Hz, 2H), 7.33 – 7.26 (m, 3H), 7.24 – 7.16 (m, 3H), 7.12 – 7.06 (m, 2H), 7.02 (d, *J* = 7.2 Hz, 2H), 3.89 (s, 2H), 2.46 (s, 3H).

^{13}C NMR (176 MHz, CDCl$_3$) δ 151.04, 141.78, 138.64, 135.74, 131.79, 129.30, 128.70, 128.40, 128.26, 128.17, 126.98, 126.75, 122.44, 119.72, 60.38, 40.08.
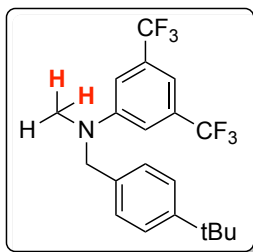
Hydrogenation of *N*-4'-Bromobenzyl-4-chloroformanilide (Table 3, entry 5): General Hydrogenation Method A was applied resulting in a 90 % yield.
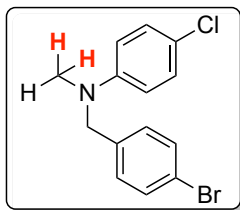
^{1}H NMR (700 MHz, CDCl$_3$) δ 7.44 (d, J = 8.3 Hz, 2H), 7.15 (d, J = 9.0 Hz, 2H), 7.08 (d, J = 8.2 Hz, 2H), 6.62 (d, J = 9.0 Hz, 2H), 4.45 (s, 2H), 3.00 (s, 3H).

^{13}C NMR (176 MHz, CDCl$_3$) δ 147.92, 137.45, 131.67, 128.92, 128.30, 121.59, 120.69, 113.48, 56.19, 38.79.

Hydrogenation of *N*-4'-*tert*-butylbenzyl-3,5-(bistrifluoromethyl)formanilide (Table 6.3, entry 6): General Hydrogenation Method A was applied resulting in a 83 % yield.


^{1}H NMR (700 MHz, CDCl$_3$) δ 7.37 (d, J = 8.1 Hz, 2H), 7.15 (s, 1H), 7.13 (d, J = 7.3 Hz, 2H), 7.07 (s, 2H), 4.59 (s, 2H), 3.10 (s, 3H), 1.32 (s, 9H).

^{13}C NMR (176 MHz, CDCl$_3$) δ 150.62, 150.12, 134.14, 132.43 (q, J = 32.1 Hz), 129.08, 126.43, 125.93, 111.29, 109.32, 55.96, 38.77, 34.66, 31.47.

^{19}F NMR (658 MHz, CDCl$_3$) δ -63.06.

Hydrogenation of *N*-4'-Acetoxybenzyl-3,5-(bistrifluoromethyl)formanilide (Table 3, entry 7): General Hydrogenation Method A was applied resulting in a 61 % yield.
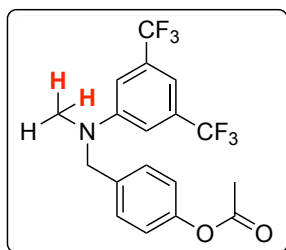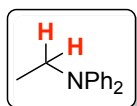
^{1}H NMR (700 MHz, CDCl$_3$) δ 7.20 (d, *J* = 8.1 Hz, 2H), 7.16 (s, 1H), 7.07 (d, *J* = 8.1 Hz, 1H), 7.04 (s, 2H), 4.60 (s, 2H), 3.10 (s, 3H), 2.30 (s, 3H).

^{13}C NMR (176 MHz, CDCl$_3$) δ 169.67, 150.10, 149.96, 134.76, 132.53 (q, *J* = 32.1 Hz), 127.66, 122.21, 111.35, 109.62, 108.41, 55.86, 38.82, 21.28.

^{19}F NMR (658 MHz, CDCl$_3$) δ -63.09.

Hydrogenation of *N,N*-diphenylaceamide (Table 6.2, entry 11): General Hydrogenation Method A was applied resulting in a 39 % yield.

^{1}H NMR (700 MHz, CDCl$_3$) δ 7.25 (m, 4H), 6.99 (d, *J* = 7.8 Hz, 4H), 6.94 (t, *J* = 7.3 Hz, 2H), 3.78 (q, *J* = 7.0 Hz, 2H), 1.22 (t, *J* = 7.0 Hz, 3H).

^{13}C NMR (176 MHz, CDCl$_3$) δ 147.69, 129.22, 121.04, 120.88, 46.38, 12.66.

Hydrogenation of *N,N*-diphenylformamide (Table 6.4, entry 1): General Hydrogenation Method A was applied resulting in a 84 % yield.
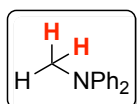
^{1}H NMR (700 MHz, CDCl$_3$) δ 7.30 (m, 4H), 7.06 (m, 4H), 6.99 (m, 2H), 3.35 (s, 3H).

^{13}C NMR (176 MHz, CDCl$_3$) δ 149.13, 129.30, 121.36, 120.55, 40.36.
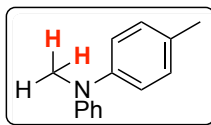
General Hydrogenation Method B was applied resulting in a 81 % yield.

^{1}H NMR (700 MHz, CDCl$_3$) δ 7.27 (m, 4H), 7.08 (m, 4H), 6.93 (m, 2H), 5.70 (s, 1H).

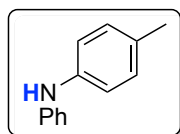^{13}C NMR (176 MHz, CDCl$_3$) δ 143.22, 129.48, 121.12, 117.92.

Hydrogenation of *N*-4'-tolylformanilide: General Hydrogenation Method A was applied resulting in an 81 % yield.

^{1}H NMR (700 MHz, CDCl$_3$) δ 7.26 (t, *J* = 7.6 Hz, 2H), 7.15 (d, *J* = 8.1 Hz, 2H), 7.03 (d, *J* = 7.6 Hz, 2H), 6.95 (d, *J* = 8.1 Hz, 2H), 6.90 (t, *J* = 7.6 Hz, 1H), 3.32 (s, 3H), 2.35 (s, 3H).

^{13}C NMR (176 MHz, CDCl$_3$) δ 149.47, 146.69, 132.16, 130.03, 129.14, 122.69, 119.87, 118.27, 40.45, 20.89.
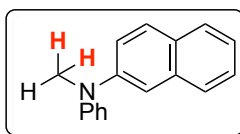
General Hydrogenation Method B was applied resulting in a 65 % yield.

^{1}H NMR (700 MHz, CDCl$_3$) δ 7.27 (m, 2H), 7.11 (m, 2H), 7.03 (m, 4H), 6.90 (m, 1H), 5.61 (s, 1H), 2.33 (s, 3H).

^{13}C NMR (176 MHz, CDCl$_3$) δ 144.04, 140.37, 131.04, 129.97, 129.43, 120.40, 119.01, 116.96, 20.83.

Hydrogenation of *N*-2'-napthylformanilide: General Hydrogenation Method A was applied for 0.5 h, resulting in a 71 % yield.
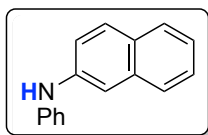

^{1}H NMR (700 MHz, CDCl$_3$) δ 7.76 (d, *J* = 8.1 Hz, 1H), 7.36 – 7.31 (m, 2H), 7.44 (t, *J* = 7.6 Hz, 1H), 7.33 (dd, *J* = 16.0, 8.7 Hz, 4H), 7.24 (d, *J* = 8.7 Hz, 1H), 7.13 (d, *J* = 7.6 Hz, 2H), 7.04 (t, *J* = 7.3 Hz, 1H), 3.44 (s, 3H).

^{13}C NMR (176 MHz, CDCl$_3$) δ 149.19, 146.71, 134.80, 129.41, 129.22, 128.69, 127.66, 126.85, 126.38, 123.83, 122.07, 121.93, 121.52, 114.68, 40.75.

General Hydrogenation Method B was applied for 0.5 h resulting in a 75 % yield.
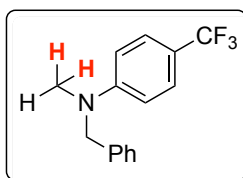
^{1}H NMR (700 MHz, CDCl$_3$) δ 7.75 (d, *J* = 8.4 Hz, 2H), 7.66 (d, *J* = 8.4 Hz, 1H), 7.43 (m, 2H), 7.32 (d, *J* = 8.8 Hz, 3H), 7.23 (d, *J* = 8.8 Hz, 1H), 7.18 (d, *J* = 7.9 Hz, 2H), 7.00 (s, 1H), 5.87 (s, 1H).

^{13}C NMR (176 MHz, CDCl$_3$) δ 142.89, 140.82, 134.60, 129.43, 129.17, 127.64, 126.48, 126.44, 123.48, 121.40, 120.03, 118.25, 111.54.

Hydrogenation of *N*-Benzyl-4-trifluoromethylformanilide: General Hydrogenation Method A was applied resulting in a 71 % yield.
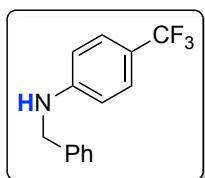

^{1}H NMR (700 MHz, CDCl$_3$) δ 7.44 (d, *J* = 8.6 Hz, 2H), 7.34 (t, *J* = 7.5 Hz, 2H), 7.27 (t, *J* = 7.5 Hz, 1H), 7.22 – 7.18 (m, 2H), 6.74 (d, *J* = 8.6 Hz, 2H), 4.61 (s, 2H), 3.11 (s, 3H).

^{13}C NMR (176 MHz, CDCl$_3$) δ 151.56, 137.89, 128.75, 127.15, 126.47 (q, *J* = 3.7 Hz), 126.41, 125.88, 120.43, 111.17, 56.09, 38.72.

^{19}F NMR (658 MHz, CDCl$_3$) δ -60.85.

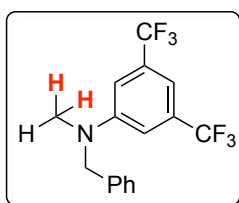General Hydrogenation Method B was applied resulting in a 75 % yield.

^{1}H NMR (700 MHz, CDCl$_3$) δ 7.40 (d, *J* = 8.4 Hz, 2H), 7.37 (m 4H), 7.31 (m, 1H), 6.63 (d, *J* = 8.4 Hz, 2H), 4.40 (m, 1H), 4.38 (d, *J* = 4.3 Hz, 2H).

^{13}C NMR (176 MHz, CDCl$_3$) δ 150.43, 138.42, 128.78, 127.51, 127.35, 126.61 (q, *J* = 3.8 Hz), 125.70, 124.17, 111.95, 47.78.

^{19}F NMR (658 MHz, CDCl$_3$) δ -61.01.

Hydrogenation of *N*-Benzyl-3,5-bis(trifluoromethyl)formanilide: General Hydrogenation Method A was applied resulting in a 72 % yield.

^{1}H NMR (700 MHz, CDCl$_3$) δ 7.36 (t, *J* = 6.8 Hz, 1H), 7.29 (t, *J* = 6.8 Hz, 1H), 7.21 (d, *J* = 7.6 Hz, 2H), 7.17 (s, 1H), 7.07 (s, 2H), 4.62 (s, 2H), 3.13 (s, 3H).

^{13}C NMR (176 MHz, CDCl$_3$) δ 149.87, 137.06, 132.30 (q, *J* = 32.4 Hz), 128.89, 127.47, 126.48, 124.47, 122.92, 111.16, 56.20, 38.73.

^{19}F NMR (658 MHz, CDCl$_3$) δ -63.09.

General Hydrogenation Method B was applied resulting in a 82 % yield.
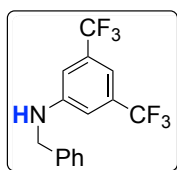
^{1}H NMR (700 MHz, CDCl$_3$) δ 7.41 – 7.30 (m, 4H), 7.17 (s, 1H), 6.97 (d, *J* = 3.3 Hz, 2H), 4.46 (bs, 1H), 4.37 (s, 2H).

^{13}C NMR (176 MHz, CDCl$_3$) δ 148.52, 137.53, 132.40 (d, *J* = 32.8 Hz), 128.91, 127.84, 127.53, 124.28, 111.92, 109.99, 48.00.

^{19}F NMR (658 MHz, CDCl$_3$) δ -63.23.

III. Cross Over Experiment (Figure 6.6)

In a N_2-atmosphere dry box, **6** (5 μmol, 4 mol %) was dissolved in 1 mL of THF, and this solution was added to the metal well of a pressure and a micro magnetic stir bar (3 x 10 mm). Amide (*N,N*-diphenylformamide) (125 μmol, 25 equiv relative to Ir) and amine (*N*-phenyl-2-napthylamine) were then added, and the vessel (Reactor-type A) was sealed and removed from the dry box. The vessel was connected to the Parr Multiple Reactor System, and the manifold was thoroughly purged with ultra-high purity grade H_2 (99.999%). The vessel was then pressurized with H_2 (40 bar) at room temperature, and the reaction was heated at 100 ºC with a stir rate of 800 RPM. The heating was conducted using Specview software. After 0.5 h of heating, the reaction mixture was allowed to cool to room temperature. The pressure vessel was cooled to RT and then carefully vented using a metering valve. THF (0.5 mL) was added through the venting valve of the pressure vessel to wash any residual liquids/solids into the vessel. The products were analyzed by ^{1}H NMR Spectroscopy and GC-MS, yielding *N*-methyl-*N*-phenylaniline as the sole products.

IV. X-Ray Crystallography Experimental Data 6
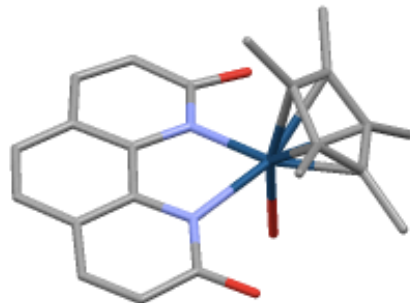
Yellow needles of **6** were grown from a tetrahydrofuran/pentane solution of the compound at –10 ºC. A crystal of dimensions 0.09 x 0.09 x 0.04 mm was mounted on a Rigaku AFC10K Saturn 944+ CCD-based X-ray diffractometer equipped with a low temperature device and Micromax-007HF Cu-target micro-focus rotating anode (λ = 1.54187 A) operated at 1.2 kW power (40 kV, 30 mA). The X-ray intensities were measured at 85(1) K with the detector placed at a distance 42.00 mm from the crystal. A total of 2028 images were collected with an oscillation width of 1.0° in ω. The exposure times were 1 sec. for the low angle images, 3 sec. for high angle. The integration of the data yielded a total of 28334 reflections to a maximum 2θ value of 138.68° of which 6933 were independent and 6887 were greater than 2σ(I). The final cell constants (Table 1) were based on the xyz

centroids of 22797 reflections above 10σ(I). Analysis of the data showed negligible decay during data collection. The structure was solved and refined with the Bruker SHELXTL (version 2016/6) software package, using the space group P1bar with Z = 2 for the formula $C_{32}H_{43}N_2O_{12}F_6S_2Ir$. All non-hydrogen atoms were refined anisotropically with the hydrogen atoms placed in idealized positions. Full matrix least-squares refinement based on F^2 converged at R1 = 0.0329 and wR2 = 0.0844 [based on I > 2sigma(I)], R1 = 0.0333 and wR2 = 0.0847 for all data. Acknowledgement is made for funding from NSF grant CHE-0840456 for X-ray instrumentation.

6.5 References

(1) Smith, A. M.; Whyman, R. *Chem. Rev.* **2014**, *114*, 5477.

(2) Dub, P. A.; Ikariya, T. *ACS Catal.* **2012**, *2*, 1718.

(3) Dodds, D. L.; Cole-Hamilton, D. J. *Sustainable Catalysis*; John Wiley & Sons, Inc.: 2013, p 1.

(4) Szostak, M.; Spain, M.; Eberhart, A. J.; Procter, D. J. *J. Am. Chem. Soc.* **2014**, *136*, 2268.

(5) Magro, A. A. N.; Eastham, G. R.; Cole-Hamilton, D. J. *Chem. Commun.* **2007**, 3154.

(6) John, J. M.; Bergens, S. H. *Angew. Chem. Int. Ed.* **2011**, *50*, 10377.

(7) Werkmeister, S.; Junge, K.; Beller, M. *Org. Process Res. Dev.* **2014**, *18*, 289.

(8) Garg, J. A.; Chakraborty, S.; Ben-David, Y.; Milstein, D. *Chem Commun (Camb)* **2016**, *52*, 5285.

(9) Schneck, F.; Assmann, M.; Balmer, M.; Harms, K.; Langer, R. *Organometallics* **2016**, *35*, 1931.

(10) Rezayee, N. M.; Samblanet, D. C.; Sanford, M. S. *ACS Catal.* **2016**, 6377.

(11) Schneck, F.; Assmann, M.; Balmer, M.; Harms, K.; Langer, R. *Organometallics* **2016**, *35*, 1931.

(12) Papa, V.; Cabrero-Antonino, J. R.; Alberico, E.; Spanneberg, A.; Junge, K.; Junge, H.; Beller, M. *Chem. Sci.* **2017**, *8*, 3576.

(13) Magro, A. A. N.; Eastham, G. R.; Cole-Hamilton, D. J. *Chem. Commun.* **2007**, 3154.

(14) Coetzee, J.; Dodds, D. L.; Klankermayer, J.; Brosinski, S.; Leitner, W.; Slawin, A. M. Z.; Cole-Hamilton, D. J. *Chem. Eur. J.* **2013**, *19*, 11039.

(15) vom Stein, T.; Meuresch, M.; Limper, D.; Schmitz, M.; Hölscher, M.; Coetzee, J.; Cole-Hamilton, D. J.; Klankermayer, J.; Leitner, W. *J. Am. Chem. Soc.* **2014**, *136*, 13217.

(16) Cabrero-Antonino, J. R.; Alberico, E.; Junge, K.; Junge, H.; Beller, M. *Chem. Sci.* **2016**, *7*, 3432.

(17) Yuan, M. L.; Xie, J. H.; Zhu, S. F.; Zhou, Q. L. *ACS Catal.* **2016**, *6*, 3665.

(18) Meuresch, M.; Westhues, S.; Leitner, W.; Klankermayer, J. *Angew. Chem. Int. Ed.* **2016**, *55*, 1392.

(19) Magro, A. A. N.; Eastham, G. R.; Cole-Hamilton, D. J. *Chem. Commun.* **2012**, *48*, 12249.

(20) Beydoun, K.; vom Stein, T.; Klankermayer, J.; Leitner, W. *Angew. Chem. Int. Ed.* **2013**, *52*, 9554.

(21) Li, Y. H.; Sorribes, I.; Yan, T.; Junge, K.; Beller, M. *Angew. Chem. Int. Ed.* **2013**, *52*, 12156.

(22) Rezayee, N. M.; Huff, C. A.; Sanford, M. S. *J. Am. Chem. Soc.* **2015**, *137*, 1028.

(23) Zhang, L.; Han, Z.; Zhao, X.; Wang, Z.; Ding, K. *Angew. Chem. Int. Ed.* **2015**, *54*, 6186.

(24) Kothandaraman, J.; Goeppert, A.; Czaun, M.; Olah, G. A.; Prakash, G. K. S. *J. Am. Chem. Soc.* **2016**, *138*, 778.

(25) Brewster, T. P.; Rezayee, N. M.; Culakova, Z.; Sanford, M. S.; Goldberg, K. I. *ACS Catal.* **2016**, 3113.

(26) Brewster, T. P.; Miller, A. J. M.; Heinekey, D. M.; Goldberg, K. I. *J. Am. Chem. Soc.* **2013**, *135*, 16022.

(27) Barys, M.; Ciunik, Z.; Drabent, K.; Kwiecien, A. *New J. Chem.* **2010**, *34*, 2605.

(28) Kawahara, R.; Fujita, K.-i.; Yamaguchi, R. *Angew. Chem. Int. Ed.* **2012**, *51*, 12790.

(29) Badiei, Y. M.; Wang, W.-H.; Hull, J. F.; Szalda, D. J.; Muckerman, J. T.; Himeda, Y.; Fujita, E. *Inorg. Chem.* **2013**, *52*, 12576.

(30) Hou, C.; Jiang, J.; Zhang, S.; Wang, G.; Zhang, Z.; Ke, Z.; Zhao, C. *ACS Catal.* **2014**, *4*, 2990.

(31) Fujita, K.-i.; Kawahara, R.; Aikawa, T.; Yamaguchi, R. *Angew. Chem. Int. Ed.* **2015**, *54*, 9057.

(32) Wang, W.-H.; Himeda, Y.; Muckerman, J. T.; Manbeck, G. F.; Fujita, E. *Chem. Rev.* **2015**, *115*, 12936.

(33) Norris, M. R.; Concepcion, J. J.; Glasson, C. R. K.; Fang, Z.; Lapides, A. M.; Ashford, D. L.; Templeton, J. L.; Meyer, T. J. *Inorg. Chem.* **2013**, *52*, 12492.

(34) Liao, L.-Y.; Kong, X.-R.; Duan, X.-F. *J. Org. Chem.* **2014**, *79*, 777.

(35) Umemoto, T.; Nagayoshi, M.; Adachi, K.; Tomizawa, G. *J. Org. Chem.* **1998**, *63*, 3379.

(36) Krapcho, A. P.; Sparapani, S. *J. Heterocyclic Chem.* **2008**, *45*, 1167.